



HAL
open science

Molecules and complexes with hydrogen bond: solvation and photoreactivity in cryogenic matrices

Alejandro Gutiérrez Quintanilla

► **To cite this version:**

Alejandro Gutiérrez Quintanilla. Molecules and complexes with hydrogen bond: solvation and photoreactivity in cryogenic matrices. Chemical Physics [physics.chem-ph]. Université Paris Saclay (COMUE), 2016. English. NNT: 2016SACLS561 . tel-01686957

HAL Id: tel-01686957

<https://theses.hal.science/tel-01686957v1>

Submitted on 18 Jan 2018

HAL is a multi-disciplinary open access archive for the deposit and dissemination of scientific research documents, whether they are published or not. The documents may come from teaching and research institutions in France or abroad, or from public or private research centers.

L'archive ouverte pluridisciplinaire **HAL**, est destinée au dépôt et à la diffusion de documents scientifiques de niveau recherche, publiés ou non, émanant des établissements d'enseignement et de recherche français ou étrangers, des laboratoires publics ou privés.

NNT : 2016SACLS561

THESE DE DOCTORAT
DE
UNIVERSITE PARIS-SACLAY
PREPAREE A
UNIVERSITE PARIS-SUD

ÉCOLE DOCTORALE N°572
Ondes et matière

Spécialité de doctorat : Milieux dilués et optique fondamentale

Par

M. Alejandro Gutiérrez Quintanilla

**Molecules and complexes with hydrogen bond: solvation and photoreactivity in
cryogenic matrices**

Thèse présentée et soutenue à Orsay, le 16 décembre 2016 :

Composition du Jury :

Pascale ROUBIN, Professeur des Universités (Université d'Aix Marseille, France), Présidente du Jury

Martin SUHM, Professeur (Georg-August-Universität, IPC, Allemagne), Rapporteur

Xavier MICHAUT, Maître de Conférence (Université Pierre et Marie Curie, France), Rapporteur

Marc BRIANT, Chargé de recherche (CEA-Saclay, France), Examineur

Germán ROJAS LORENZO, Professeur (InSTEC, Cuba), Examineur

Claudine CREPIN, Directrice de Recherche au CNRS (ISMO, France), Directrice de thèse

Titre : Molécules et complexes à liaison hydrogène: solvatation et photoréactivité en matrices cryogéniques

Mots clés : liaison hydrogène, acétylacétone, photoisomérisation, matrices cryogéniques, para-hydrogène, gouttelettes d'hélium

Résumé : La liaison hydrogène est une interaction stabilisante très importante, qui est présente dans de nombreux systèmes moléculaires, des petits clusters d'eau à la molécule d'ADN. L'étude du cas de la Liaison Hydrogène Intramoléculaire (LHI) est d'un intérêt particulier en raison du rôle important de ce type d'interaction dans les processus de transfert d'hydrogène interne, dans la photodynamique et la conformation structurelle. La famille des molécules β -dicarboxyles est un système modèle de LHI unique car il possède relativement peu de degrés de liberté et tous les processus mentionnés précédemment sont clairement présents. L'objectif principal de ce travail est d'étudier le lien entre structure isotopique et électronique des molécules β -dicarboxyles, force de la liaison hydrogène intramoléculaire, sélectivité sur le processus de photoisomérisation et couplage du transfert d'hydrogène avec d'autres mouvements de grande amplitude. Les expériences sont complétées par des calculs de chimie quantique.

Quatre molécules de la famille des β -dicétones (acétylacétone doublement deutérée, 3-chloroacétylacétone, hexafluoroacétylacétone et trifluoroacétylacétone) et une β -dialdéhyde (2-chloromalonaldéhyde) sont étudiées dans des environnements inertes à basse température par spectroscopie électronique et vibrationnelle (FT-IR et Raman). Le néon et le para hydrogène ont été utilisés principalement comme matrices hôtes permettant une analyse spectroscopique claire. Les β -dicarboxyles se présentent sous deux formes tautomères: le céto et l'énol, mais ce dernier prédomine en grande partie en phase gazeuse, et par conséquent, dans les échantillons déposés étudiés. Huit différents conformères énoliques peuvent exister, mais celui avec LHI (énol chélaté) est le plus stable. Ces conformères peuvent être divisés en quatre paires dans lesquelles chaque couple partage la même structure squelettique et ne diffère que dans la conformation hydroxyle. Le conformère énolique fermé a toujours été trouvé comme l'espèce la plus stable dans nos expériences.

L'influence de l'environnement et de la force de la liaison hydrogène sur des variables spectroscopiques comme la largeur de bande, l'intensité et le déplacement spectral sont discutées. On a également trouvé des preuves expérimentales du processus de conversion de spin nucléaire dans la forme énolique fermée de l'acétylacétone doublement deutérée en matrice de para-hydrogène. Différents conformères énoliques ouverts ont été produits dans chaque système après excitation par laser UV. Les conformères énoliques ouverts présentent des ordres d'énergie différents pour chaque analogue halogéné en raison de l'existence d'interactions non covalentes spécifiques, comme le révèlent les calculs théoriques. Néanmoins, dans tous les cas, les conformères produits sont les conformères les plus stables de leurs paires énoliques. Ceci est expliqué par un processus régi par passage tunnel de l'hydrogène hydroxylique, comme observé expérimentalement dans les isotopologues deutérés. A partir des résultats expérimentaux, nous avons proposé un mécanisme général pour expliquer la photo-isomérisation dans ces systèmes.

Par ailleurs, la technique des gouttelettes d'hélium a également été utilisée pour avoir accès à des informations spectroscopiques précieuses (spectres ro-vibrationnels) sur des complexes fortement ou faiblement liés en milieu inerte. Le rôle de l'eau comme espèce donneur ou accepteur de protons dans un complexe peut facilement être modifié par un déséquilibre des forces d'interaction en jeu. Les résultats préliminaires sur le système à liaison hydrogène intermoléculaire propyne-eau dans des gouttelettes d'hélium sont présentés.

Title : Molecules and complexes with hydrogen bond: solvation and photoreactivity in cryogenic matrices

Keywords : hydrogen bond, photoisomerization, vibrational spectroscopy, acetylacetone analogs, matrix isolation, para-hydrogen

Abstract : The hydrogen bond interaction is an important stabilizing interaction present in many kinds of molecular systems, from small water clusters to the big DNA molecule. The study of the specific case of the Intramolecular Hydrogen Bond (IHB) is of special interest because of the important role of this kind of interaction in internal hydrogen transfer processes, photodynamic behavior and structural conformation. The β -dicarbonyl family of molecules is a unique model system with relatively small amount of degrees of freedom and where all the processes just mentioned are clearly present. The main aim of this work is to study the link between the isotopic and electronic structure of β -dicarbonyl molecules (model IHB system) with the strength of intramolecular hydrogen bond, selectivity on the photoisomerization process and coupling of hydrogen transfer with other large amplitude motions. Experiments are supported with quantum chemical calculations.

Four molecules from the β -diketone family (double deuterated acetylacetone, 3-chloroacetylacetone, hexafluoroacetylacetone and trifluoroacetylacetone) and one from the β -dialdehyde (2-chloromalonaldehyde) are studied in low temperature inert environments by means of electronic and vibrational spectroscopy (FT-IR and Raman). Neon and para-hydrogen were mainly used as host matrices allowing clear spectroscopic analysis. The β -dicarbonyl molecules can be present in two tautomeric forms: keto and enol, but the latter largely predominates in the gas phase, and as a consequence, in the deposited isolated samples. Eight different enol conformers can exist, but the one with intramolecular hydrogen

bond (chelated enol) is the most stable. The enol conformers can be divided in four pairs in which each couple shares the same skeletal structure and differs only in the hydroxyl conformation. In the deposited sample of all the molecules under study, the closed enolic conformer was found as the most stable species. The influence of the environment and the hydrogen bond strength on spectroscopic variables like bandwidth, intensity and frequency position are discussed. Experimental evidence of Nuclear Spin Conversion process in para-hydrogen matrix of the closed enol form of double deuterated acetylacetone was also found. Different open enol conformers were produced in each system after UV laser excitation. The open enol conformers show different energy ordering for each halogenated analog because of the existence of specific non covalent interactions, as revealed by theoretical calculations. Nevertheless, in all cases, the produced conformers are the most stable conformers of their enolic pairs. This is explained by a tunneling driven process in the hydroxyl hydrogen, as observed experimentally in deuterated isotopologues. From the experimental results we proposed a general mechanism to explain the photoisomerization in these systems.

On the other hand, helium droplets technique was also used to allow recording valuable spectroscopic information (ro-vibrational spectrum) about strong and weak complexes in inert media. The role of water as donor or acceptor proton species in a complex can easily change by an imbalance of the interaction forces at play. Preliminary results about the intermolecular hydrogen bonded system propyne-water in helium droplets are presented.

To my parents

To my beautiful wife and my *petite Alejandra*

To *Patrick de Pujo*

*Todo es hermoso y constante,
Todo es música y razón,
Y todo, como el diamante,
Antes que luz es carbón.*

José Martí

Acknowledgment

First of all, I would like to thank to all the members of the jury: Pascale Roubin, Germán Rojas Lorenzo, Marc Briant, Martin Suhm and Xavier Michaut, for accepting to be part of this work, specially to the examiners, for their criticisms, opinions and suggestions about the work and the document.

I want to acknowledge the members of my group (MOMA) and the D team, who have shared so many things and patiently listen to my long talks during lunches: Didier Chamma, Wutharath Chin, Valeria Lepère, Anne Zehnacker-Retien, Niloufar Shafizadeh, Katia le Barbus-Debus, Aifan Alata, Pierre Carçabal, Gerard O'Connor, Raphael Thon (former student), Ferial Ben Nasr, Urzula Sczepaniak and Karine Steenkeste (G Team). I also include our colleague M. Jean Pierre Galaup from LAC who was always willing to share a smile, a "coffee", his scientific knowledge and his love for Cuba.

This work would have not been possible without the support of all the technical and administrative team at ISMO, specially: Farah Savina, Catherine Le Bris, Nicolas Tournier, Marc Hilaire, Christophe Lefumeux, Christophe Charrière, Thierry Chamailé, Julian Vincent, Phillippe Dos Santos, Yves Bergougnoux, Sebastian Debest, Olivier Kermoyan, Stephanie Delhaye, Marie Claire Paul, Annie Le Gal, Bernadette Rome, Véronique Veron, Alexis Marié, André Szewc and Frederic Ferreira.

I am very grateful to the French embassy in Cuba for the financial support, the kind attention, its services and for giving me the opportunity to make this dream real. I also thank the *Triangle de la Physique* and *École doctorale Ondes et Matière* (EDOM) for the financial support, and the important guidance. I want also thank to ISMO, Paris Sud-XI University institutions and Île de France CNRS delegation.

I thank my teaching team at Orsay, Céline Dablemont, Nathalie Prud'homme and Emilie Amzallag, who gave me the opportunity to teach in this important university.

I thank my French friends Kevin Charles Jr. and Manu Bernhard, as well as Maurice Monnerville and Vivianne Monnerville for all the moments we shared together. Also, to M. Roland Galliot and Mme. Monique Galliot, as well as *les petites* Océane and Noëlla, who shared more than his home with me.

A big part of this work was developed in two other groups I would like to thank. First, some the members of the Department of General Physics and Spectroscopy at Vilnius University in Lithuania: Valdas Sablinskas, Rasa Platakite (master student), Kestukis Aidas and specially Justinas Ceponkus who shared all his knowledge about matrix isolation and vibrational spectroscopy with me, and showed me the nice and important art of "improvisation" in experimental science. Second, to the members of the LIDyL group at CEA: Jean-Michel Mestdagh, Ephriem Tadesse, Lionel Poisson, Benoit Soep, Marc André Gaveau, Patrick de Pujo and specially

Marc Briant for teaching me how to handle, strictly organize and pay attention to every small detail of a complex experimental setup like helium droplets, and for our talks and the chocolate drinks they included.

Thanks to all the members of my department in Cuba (Radiochemistry) and my institute (InSTEC), for always being curious about this work, and for cover my teaching hours for me. I also thank to Jesús Rubayo Soneira, Rolando Lozada García and Germán Rojas Lorenzo for opening this opportunity and for all the advices.

I am grateful to Gustavo Sánchez Perdomo, Flora Villar Bahamonde, and Romy Sánchez for accepting me as a part of their friends, for sharing their time, their interesting talks and their delicious lunches with me.

I want to thank all the cuban friends in France that supported me during this time, helped me in the difficult moments, and shared the nicer ones: Ernesto Quintas Sánchez, Ariel F. Pérez Mellor, Liss Vázquez Rodríguez, Rolando R. Lozada García, Iván Coto Hernández, Ernesto Martínez Baez, Mykel L. González Martínez, Manuel Antuch and specially Alejandro Rivero Santamaría and Margarita Reyes Roselló who are also part of my family. I would also like to thank Alba Campillo and Cecile Azaiz who are determined to discover the origin of the cuban hapiness.

I am more than proud to say that I had Michele Chevalier and Claudine Crépin-Gilbert as mentors of my PhD thesis. During these four years I had the freedom to learn and to experience by myself in the lab (which included breaking some equipment) under the guidance of these two amazing researchers. I learned more than science, I learned about team work, patience, dedication, love and respect for our work. I learned english, french (I want to believe that) and many others things that I won't ever forget. For all these things, for their patience and for making a place for me in the small family of the MOMA group I will be always grateful to them.

During my PhD I did not only learn about science but also about other cultures, foods, languages, religions, etc. I just want to thank to all the people that kindly shared their time, experience and knowledge with me, that are not directly mentioned here.

This work is also part of the dream of my family, especially my parents, who always supported me and celebrated each small step I have achieved. Thanks to my brother's beautiful family and the cuban friends in Cuba and the rest of world who are also part of my family.

Finally, I could not have finished this important step in my life without the support, the comprehension and the love of my wife, who has waited four long years to celebrate this day with me, and in the last year has shared with me the most beautiful, intriguing and exciting "experimental result" of our lives, our daughter Alejandra.

Table of Contents

Glossary	vii
Introduction	1
Chapter I Hydrogen bonded systems	5
I.1. The hydrogen bond	5
I.1.1. Intramolecular Hydrogen Bond (IHB).....	6
I.1.2. Resonance Assisted Hydrogen Bond (RAHB).....	7
I.2. Systems under study	7
I.2.1. β -diketones.....	8
I.2.2. β -dialdehyde.....	12
I.2.3. Other systems under study	12
I.2.4. Notations	13
Chapter II Experimental and theoretical tools	15
II.1. Matrix Isolation (MI).....	15
II.1.1. A brief history	15
II.1.2. Principles and advantages	16
II.1.3. General techniques	18
II.2. Molecular spectroscopy: Principles.....	21
II.3. Electronic absorption spectroscopy	24
II.4. Vibrational spectroscopy.....	25
II.4.1. Vibrational modes and transitions	25
II.4.2. Infrared spectroscopy.....	26
II.4.3. Raman spectroscopy	29
II.5. Vibrational and electronic spectroscopies in Matrix Isolation.....	31
II.6. The queen of MI: <i>para</i> -hydrogen (pH_2) matrix.....	33
Chapter III Theoretical Methods	37

III.1. Ab initio methods	37
III.2. Basis functions	40
III.3. Density Functional Theory	43
III.4. NCI calculations	45
III.5. Infrared and Raman scattering theoretical calculation	46
III.5.1. Normal modes and frequencies	46
III.5.2. IR and Raman intensities	47
III.6. Electronic absorption spectrum	49
III.7. Relaxed and non-relaxed rotational barriers.....	50
III.8. Tunnel effect and WKB approximation	51
III.9. Theoretical calculations details	52
III.9.1. Geometry optimization and frequency calculations	52
III.9.2. Rotational barriers.....	52
III.9.3. Electronic vertical transitions	53
Chapter IV Experimental Setup	55
IV.1. Chemical Products.....	55
IV.1.1. Quality and physico-chemical properties.....	55
IV.1.2. D, D-Acetylacetone and D-Chloroacetylacetone synthesis	55
IV.2. Matrix isolation experiments	59
IV.2.1. Deposition conditions.....	61
IV.3. <i>Para</i> -hydrogen ($p\text{H}_2$) matrix	62
IV.3.1. Preparation.....	62
IV.3.2. Spectroscopy	63
IV.4. Vibrational and electronic spectroscopies	64
IV.5. UV and IR laser irradiations.....	65
IV.6. Helium nanodroplet experiment.....	66
IV.6.1. Source chamber.....	67

IV.6.2. Pickup chamber.....	67
IV.6.3. Spectroscopy chamber.....	69
Chapter V Acetylacetone (D2)	71
V.1. Theoretical calculations.....	71
V.2. Vibrational spectroscopy of as-deposited samples.....	72
V.2.1. FT-IR spectra.....	72
V.2.2. AcAcD2: CCC conformer.....	74
V.2.3. Monodeuterated isotopologues: CCC(OD) and CCC(CD).....	78
V.2.4. Raman spectra.....	80
V.2.5. Nuclear spin conversion (NSC).....	81
V.3. UV laser irradiation: Isomerization.....	86
V.3.1. UV absorption spectra of acetylacetone in solid neon.....	86
V.3.2. First group of deuterated conformers.....	87
V.3.3. Second group of deuterated conformers in neon matrix.....	93
V.3.4. Monodeuterated open enol conformers in neon.....	94
V.4. Tunneling process.....	96
Chapter VI 3-Chloroacetylacetone	99
VI.1. Theoretical results.....	99
VI.2. Vibrational spectroscopy of as-deposited samples.....	102
VI.2.1. FT-IR spectrum in Ne and $p\text{H}_2$ matrices.....	102
VI.2.1. Raman and FT-IR spectrum in argon matrix.....	103
VI.3. UV laser irradiation.....	105
VI.3.1. Electronic absorption spectra.....	105
VI.3.2. Electronic excitation.....	108
VI.3.3. TCT conformer.....	109
VI.4. Deuterated chloroacetylacetone in $p\text{H}_2$	112
VI.4.1. Deposited sample.....	112

VI.4.2. Open enol conformers.....	113
Chapter VII Hexafluoroacetylacetone	121
VII.1. Theoretical results	121
VII.2. Vibrational spectroscopy of as-deposited samples.....	124
VII.2.1. FT-IR spectrum in Ne and $p\text{H}_2$ matrices.....	124
VII.2.2. Raman spectrum in argon matrix.....	126
VII.3. UV laser irradiation.....	127
VII.3.1. Electronic absorption spectra.....	127
VII.3.2. CTT conformer	130
VII.3.3. TCC conformer.....	134
Chapter VIII Trifluoroacetylacetone	137
VIII.1. Theoretical results	137
VIII.2. Vibrational spectroscopy of as-deposited samples.....	138
VIII.2.1. FT-IR spectrum in Ne and $p\text{H}_2$ matrices.....	138
VIII.2.2. Raman spectrum	139
VIII.3. UV laser irradiation.....	142
VIII.3.1. Electronic absorption spectrum	142
VIII.3.2. Open enol conformers	143
Chapter IX 2-Chloromalonaldehyde	149
IX.1. Theoretical results	149
IX.2. Vibrational spectroscopy of as-deposited samples.....	152
IX.2.1. FT-IR spectrum in Ne and $p\text{H}_2$ matrices.....	152
IX.2.2. Raman spectrum in argon matrix	154
IX.3. UV laser irradiation: Isomerization.....	157
IX.3.1. UV absorption spectra in solid neon	157
IX.3.2. Isomerization	158
IX.3.3. Comparison with malonaldehyde.....	161

Chapter X Propyne-H₂O complex	163
X.1. Propyne monomer	163
X.2. Propyne dimers	167
X.3. Propyne-H ₂ O complex.....	170
X.3.1. Theoretical simulations	171
X.3.2. Experimental results.....	172
Chapter XI Discussion	173
XI.1. Hydrogen bond.....	173
XI.1.1. Geometric and energetic theoretical variables.....	173
XI.1.2. Spectroscopic variables	176
XI.1.3. Environment.....	180
XI.2. Nuclear Spin Conversion	182
XI.3. Open enol conformers production.....	183
Conclusions	187
References	191
Appendix	204

Glossary

A

AM1: Austin Model 1, 11
AO: Atomic Orbitals, 24
ATR: Attenuated Total Reflection, 31

B

B3LYP: Becke and 3 parameter Lee-Yang-Parr functional, 11, 45, 53, 71, 75, 79, 82, 92, 95, 99, 100, 102, 103, 108, 121, 124, 125, 137, 138, 153, 181, 182
BO: Born-Oppenheimer, 38

C

CCD: Charge Coupled Device, 25, 65
CCSD: Coupled Cluster with Single and Double excitations, 3, 11, 49, 165, 166; Coupled Clusters with Single and Double excitations, 43
CICR: Cluster Isolated Chemical Reaction Spectroscopy, 167
CIS(D): Configuration Interaction with Single Excitations and Double Excitations treated with perturbative approach, 49; Configuration Interaction with Singles and Doubles excitations, 49
CID: Configuration interaction with Single and double excitations, 43

E

ELF: Electron Localization Functions, 45
EOM-CCSD: Equation of Motion Coupled Cluster with Singles and Doubles excitations, 49
EPA: Ether-pentane-alcohol mixture, 15
EPR: Electron Paramagnetic Resonance, 15

F

FT: Fourier Transform, 3, 10, 11, 27, 28, 31, 32, 37, 59, 64, 66, 71, 72, 80, 81, 82, 91, 98, 102, 103, 104, 124, 126, 127, 138, 139, 140, 142, 152, 154, 156, 165, 167, 177, 178
FT-IR: Fourier Transform Infrared Spectroscopy, 3, 10, 27, 28, 32, 37, 59, 64, 66, 71, 72, 80, 81, 82, 91, 98, 102, 103, 104, 124, 126, 127, 138, 139, 140, 142, 152, 154, 156, 165, 167, 177, 178
FT-MW: Fourier Transform Microwave spectroscopy, 11

G

GED: Gas Electron Diffraction, 10, 11
GGA: Generalized Gradient Approximation, 44, 45
GM: Gifford-McMahon refrigerator, 18
GMPCS: Grappe Massivement Parallèle de Calcul Scientifique, 52
GTO: Gaussian Type Orbital, 41

H

HENDI: Helium Nanodroplet Isolation Spectroscopy, 66
HF: Hartree-Fock, 38
HF-SCF: Hartree-Fock Self-Consistent Field method, 38, 39, 40, 43, 44
HOMO: Highest Occupied Molecular Orbital, 50, 108
HR: High Resolution, 33

I

IC: Internal Conversion, 9
IHB: Intramolecular hydrogen bond, 6, 7, 11, 152, 173, 174, 175, 176, 178, 179, 181, 182; Intramolecular Hydrogen Bond, 10
INDO: Intermediate Neglect of Differential Overlap, 11
IRC: Intrinsic Reaction Coordinate, 50, 52, 96, 97
ISC: Intersystem Crossing, 9

IUPAC: International Union of Pure and Applied Chemistry, 5

L

LCAO: Linear Combination of Atomic Orbitals, 24, 40

LDA: Local Density Approximation, 44, 45

LUMO: Lowest Occupied Molecular Orbital, 50, 108

M

M06-2X: Minnesota functional from the 06 family, 45, 99, 100, 102, 103, 106, 109, 110, 112, 113, 114, 116, 117, 118, 120, 121, 124, 125, 128, 131, 132, 134, 137, 139, 140, 142, 144, 146, 149, 152, 155, 159, 160, 162, 174, 175, 182

MI: Matrix isolation, 3, 15, 17, 31, 32, 33, 35, 37

MO: Molecular Orbitals, 24

MOCVD: Metalorganic Chemical Vapor Deposition Agents, 7, 10

MP2: Møller-Plesset perturbation theory to second order, 3, 11, 40, 43, 49, 52, 96, 97, 153, 165, 166, 170, 171

N

NCI: Non Covalent Interactions, 3, 37, 45, 46, 100, 101, 122, 123, 138, 151, 152, 175

NMR: Nuclear Magnetic Resonance, 6, 10

P

PES: Potential Energy Surfaces, 37, 46, 47

PM3: Parametrized Model number 3, 11

PT: Pulse Tube refrigerator, 18

Q

QTAIM: Quantum Theory of Atoms in Molecules, 45

R

RAHB: Resonance assisted hydrogen bond, 7, 8; Resonance-assisted hydrogen bond, 174

RDG: Reduce Density Gradient, 152; Reduced Density Gradient, 100

S

STO: Slater Type Orbitals, 40, 41

T

TD-DFT: Time-dependent DFT, 49, 53, 108

TS: Transition State, 47, 50, 52

U

UV: Ultraviolet, 3, 9, 11, 12, 15, 17, 24, 25, 27, 30, 31, 32, 34, 49, 50, 55, 59, 60, 65, 66, 71, 74, 86, 87, 88, 89, 90, 91, 93, 94, 96, 102, 105, 108, 112, 115, 116, 126, 127, 130, 134, 135, 142, 143, 153, 157, 158, 159, 160, 161, 183, 184, 185, 186

V

VPT2: Second order Vibrational Perturbational Theory, 47

W

WKB: Wentzell-Kramers-Brillouin method, 3, 37, 51, 97, 98

Z

ZINDO: Zerner's Intermediate Neglect of Differential Overlap, 49

ZPE: Zero-Point vibrational Energy, 48, 49, 52, 71, 96, 97, 98, 103, 121, 150, 171

Introduction

The hydrogen bond is an important interaction in chemistry which can be described in a very simplified way by a hydrogen atom partially shared between two very electronegative atoms, in the same molecule (intramolecular) or in different molecules (intermolecular). However, this simple description does not completely describe the complexity of the participating forces and their implications [1]. Hydrogen bonds can favor specific conformational structures; they can have a big impact in the thermodynamic properties of the system and can also modify its spectroscopic properties [2]–[4].

A special kind of intramolecular hydrogen bond is the Resonance Assisted Hydrogen Bond (RAHB), in which a π delocalization involving the groups participating in the hydrogen bond enhances the strength of the interaction [5]. The formation of an intramolecular hydrogen bond in a molecule can favor some conformations in respect to the others. In principle, some of these conformations can be selectively produced or destroyed by ultraviolet (UV) irradiation, exciting $\pi \rightarrow \pi^*$ transitions related to the resonant system. **The main aim of this thesis is to study how the electronic and isotopic structure of RAHB systems influences the intramolecular hydrogen bond and the photoisomerization process that can be induced by electronic excitations in this kind of systems.**

β -diketones is a family of molecules existing as two tautomeric forms called *keto* and *enol* forms. Different studies have demonstrated that the less polar enolic form predominates in the gas phase [6]–[9]. The enol form is one of the simplest models of intramolecular RAHB bonded systems. Over the years, several studies have been conducted on this family of molecules, mainly focused on its tautomeric equilibrium, the photoisomerization process and the intramolecular hydrogen transfer [10]–[13].

The simplest member of the β -diketone family is acetylacetone, but several halogenated analogs have been synthesized and are commercially available. Three of these analogs: **hexafluoroacetylacetone**, **trifluoroacetylacetone** and **chloroacetylacetone**, are used in this work as model systems to study the influence of halogen substituents on the intramolecular hydrogen bond and photoisomerization. The importance of the methyl groups on the dynamics and photodynamics of these systems have been previously remarked [14]. For this reason, the smaller **2-chloromalonaldehyde** molecule from β -dialdehyde family, in which the methyl groups are replaced by hydrogen atoms, is also studied. Proton tunneling can also play a key role in the composition of the conformers produced after irradiation [15]. So, deuterated isotopologues of **acetylacetone** and **3-chloroacetylacetone** with deuterated hydroxyl groups are included in this research.

Introduction

It should be taken into account that most of the time the UV photoexcitation of a system in the gas phase do not lead to isomerization, instead photodissociation products are formed [16], [17]. In order to favor the photoisomerization channel, the reaction needs to be usually carried out in a solvent, which can absorb part of the energy of the excited molecule and guide the reaction in the expected direction. This is the case of the β -diketone molecules, where isomerization, guiding to the production of open enol conformers has been only observed in low temperature matrices [15], [18]–[21].

Matrix isolation (MI) technique is considered as the solid phase analog of the gas phase, when weak interacting matrices are used [22]. Because of the low temperatures, only the lowest vibrational levels are populated, making very convenient the use of vibrational spectroscopy in combination with matrix isolation [22]. Different gases can be used as hosts, but the weakly perturbing properties of *para*-hydrogen makes it the *nec plus ultra* solid matrix [23]. The vibrational spectra in *para*-hydrogen generally show very narrow bandwidths [24]. A big advantage in comparison to other matrices is that site effects are generally not observed. Recently, Nuclear Spin Conversion (NSC) process was observed in acetylacetone trapped in solid *para*-hydrogen [14]. The observation of this process highlights the coupling between large amplitude motions *i.e.* methyl torsions and hydrogen transfer. However, NSC has not been studied in any other analog of acetylacetone.

The main questions to address in this work are:

1. How the electronic and isotopic structure of the β -diketone family of molecules influence the intramolecular hydrogen bond and the photoisomerization process?
2. Is there a criterion to define which conformers are more probable to be observed after UV irradiation according to their electronic structure?
3. Does the photoisomerization proceed in a different manner in *para*-hydrogen matrices compared to rare gas matrices?
4. Do we observe the presence of a Nuclear Spin Conversion in the closed enolic form of the halogenated and deuterated analogs of acetylacetone in *para*-hydrogen matrix?

In addition, we want to explore small intermolecular hydrogen bonded complexes with water, in which this molecule can act either as a proton donor or as an acceptor species. The Helium Droplets (HD) technique offers a unique way to study molecular complexes in a very weakly perturbing environment and at very low temperatures, by means of its ro-vibrational spectrum [25]. In contrast to the smaller acetylene-water complex in which water act as a proton acceptor, the propyne-water complex has never been experimentally studied before. The study of this complex can help to answer to the final question addressed in this work:

5. Does water acts as a proton donor or acceptor species in the intermolecular hydrogen bonded complex propyne-water?

In the present work the dynamics (nuclear spin conversion, hydrogen bond) and photodynamics (photoisomerization) of different hydrogen bonded systems are studied with matrix isolation and helium droplets techniques. Neon, argon, nitrogen and *para*-hydrogen are used as hosts in MI. Vibrational (FT-IR and Raman) and electronic spectroscopies are used to characterize the systems under study. Theoretical calculation with DFT and MP2 methods are used to support the experimental results. The photoisomerization process is produced by means of a tunable OPO laser which allows to perform selective UV and IR irradiations.

This thesis is organized as follows: Introduction, eleven Chapters, Conclusions and References. The first chapter, “**Hydrogen bonded systems**” is an extended introduction to the general features of this special kind of systems. The two categories of inter and intramolecular hydrogen bonded system are further discussed. In the latter, the special case of resonance assisted intramolecular hydrogen bonded systems is detailed. After, the molecules under study in this work are introduced including a discussion about *l'état de l'art* of the vibrational and electronic spectroscopies of each of them, photoisomerization and studies on matrix isolation.

The second chapter is named “**Experimental and theoretical tools**”. The aim of this chapter is to introduce first the matrix isolation technique: historical survey, working principle, advantages and disadvantages. After, the theoretical bases of vibrational and electronic spectroscopies are discussed, along with the use of these techniques in combination with matrix isolation. At the end of the chapter, the special *para*-hydrogen matrix is introduced, and its most important properties are discussed.

In the third chapter, “**Theoretical methods**”, the basis of the quantum chemistry methods used to obtain relative energies, geometries, barriers, frequencies (infrared and Raman spectra), description of Non-Covalent Interactions (NCI) and electronic excitations are discussed. This includes a brief discussion on different approaches: Hartree Fock (HF), Density Functional Theory (DFT) and Möller-Plesset Perturbative methods (MP n). Next, the Wentzel-Kramers-Brillouin method (WKB) to estimate tunneling kinetic constants is presented. Finally, the details of the theoretical calculations performed in this work are given.

The fourth chapter is named “**Experimental Setup**”. First, the physico-chemical properties of the molecules under study are given, as well as all relevant details about the chemical synthesis performed. After, all the details of the experimental setups used to obtain the results shown in this thesis are explained. Special attention is given to the *para*-hydrogen matrix setup. Technical details on the FT-IR, Raman and UV

Introduction

spectrometers, as well as the laser sources are given next. At the end of the chapter an extended and detailed discussion on the helium droplet experiment is made.

After, six chapters of “**Results**” are presented. These chapters are mainly dedicated to describe and analyze the experimental (matrix isolation and helium droplets techniques) and theoretical results obtained for six different hydrogen bonded molecules. The first four are analogs of acetylacetone (β -diketone family), these are named: “**Double deuterated acetylacetone**”, “**Chloroacetylacetone**”, “**Hexafluoroacetylacetone**” and “**Trifluoroacetylacetone**”. The fifth molecule is a member of the β -dialdehydes family, smaller than the previous molecules: “**Chloromalonaldehyde**”. All these five molecules are intramolecular hydrogen bonded systems.

The chapter “**Propyne-H₂O complex**” (sixth system), is an extension of the intramolecular hydrogen bonded systems previously analyzed by introducing an intermolecular hydrogen bonded system. The chapter starts with the study of propyne monomer in helium droplets and a brief description in *para*-hydrogen and krypton matrices. Then, the dimers and multimers are analyzed in helium droplets. Finally, the propyne-water complex is examined. An important feature is the comparison with the acetylene-water system which allows to analyze the role of different interactions that favors a water acceptor or donor behavior.

In the chapter “**Discussion**” a general analysis of the three main processes under study in this work is made. First, theoretical and experimental effects of hydrogen bond are discussed through the comparison of the effects of the hydrogen bond in geometric and spectroscopic parameters. Then, comments on the nuclear spin conversion processes in these molecules are made. Finally, the photoisomerization process in β -dicarbonyl systems is analyzed through experimental evidences.

The last chapter, “**Conclusions**” is a summary of the most important results and ideas obtained in this work. In addition, some recommendations are given for future works in this field, either through proposed complementary experiments or as hypothesis to test.

Chapter I Hydrogen bonded systems

The aim of this chapter is to introduce the processes and systems under study in the present work. First, a description of the hydrogen bond with the subsequently development of the definition and its characteristics will be given. After, intra and intermolecular hydrogen bonded systems will be discussed, with a general description of *l'état de l'art* on this subject. This includes both experimental and theoretical results in different systems and physical states, along with different processes like: tautomerism, hydrogen transfer, and photophysics. The advantages of the use of matrix isolation technique in these studies are detailed. We will make emphasis in β -dicarbonyl systems as the central part of this thesis. The singular features of these kinds of intramolecular hydrogen bonded systems are mentioned. Then, we present an insight on the details of each of the molecules and the works already published on them.

I.1. The hydrogen bond

In the first three decades of the XX century great advances were made in the understanding of the nature of the chemical bond, thanks mainly to the revolution of quantum chemistry and spectroscopy but also in thermodynamics and crystallography [26]. Since then, different kinds of interactions and type of bond associated to them were identified. One of the most intriguing and even today not completely understood is the “hydrogen bridge” or “hydrogen bond”. There are many types of combinations but the simplest representation is a hydrogen (H) atom covalently bond to an electronegative atom X and interacting with another electronegative atom Y. This is represented as $X-H\cdots Y$.

According to IUPAC Gold Book a hydrogen bond is: “A form of association between an electronegative atom and a hydrogen atom attached to a second, relatively electronegative atom. It is best considered as an electrostatic interaction, heightened by the small size of hydrogen, which permits proximity of the interacting dipoles or charges. Both electronegative atoms are usually (but not necessarily) from the right part of the second row of the Periodic Table, *i.e.* N, O or F. Hydrogen bonds may be inter-molecular or intramolecular. With a few exceptions, usually involving fluorine, the associated energies are less than 20 - 25 kJ mol^{-1} (5 - 6 kcal mol^{-1})” [27].

However, this definition is not complete and lacks of rigor in some aspects (*e.g.* the range of energies), but is an acceptable general description. A few years ago, in 2011, a multidisciplinary commission from the IUPAC

HYDROGEN BONDED SYSTEMS

proposed a new definition with six criteria (with six general common characteristics, and 9 footnotes) to consider an interaction as a hydrogen bond [3], [28]. The criteria includes: forces intervening, geometry of the bond, infrared and NMR (Nuclear Magnetic Resonance) signatures and Gibbs free energy. We mention the two most relevant to our work:

1. The X-H...Y angle is usually straight (180°) and the closer the angle is to 180° , the stronger the hydrogen bond and the shorter the H...Y distance.
2. The length of the X-H bond usually increases on hydrogen-bond formation leading to a redshift in the infrared X-H stretching frequency and an increase in the infrared absorption cross section for the X-H stretching vibration. The greater the lengthening of the X-H bond in X-H...Y, the stronger the H...Y bond. Simultaneously, new vibrational modes associated with the formation of the H...Y bond are generated.

The new short definition is as follows: "The hydrogen bond is an attractive interaction between a hydrogen atom from a molecule or a molecular fragment X-H in which X is more electronegative than H, and an atom or a group of atoms in the same or a different molecule, in which there is evidence of bond formation." [3].

Vibrational spectroscopy is a very suitable technique for the study of hydrogen bonded systems. The interaction directly affects the force constant of the intervening modes, changing its frequency position. The intensity and bandwidth of involved modes are also sensible to the formation of a hydrogen bond interaction [29].

In principle the hydrogen bond can be formed between (minimum) two groups in one molecule or between groups of different molecules. These two possibilities are called *intramolecular* and *intermolecular* hydrogen bonds.

I.1.1. Intramolecular Hydrogen Bond (IHB)

The intramolecular hydrogen bond plays an important role in the stabilization of the structure of many molecules, *e.g.* the DNA double helix, peptides, among others. It is more common between O-H and N-H donor groups and C=O, C \equiv N and π electronic clouds acceptor groups. But, many other possible donor-acceptor combinations exist [5], [30].

According to G.C Pimentel and Andrew L. McClellan [2], the intramolecular H-bonds differ from intermolecular H-bonds in two things: "... First, they form only under specific, stringent spatial requirements; second, their formation does not create molecular association.". The spatial requirements make for example that the X-H...Y angle usually deviates from 180° in intramolecular H-bonds. The second condition is related to the fact that in most of the cases the intramolecular H-bond does not significantly affects the

physical properties of the molecule compared to a similar molecule without H-bond. An important characteristic is that the vibrational spectroscopic parameters such as intensity, position (frequency) and bandwidth are not greatly affected by change of solvent or concentration [31].

I.1.2. Resonance Assisted Hydrogen Bond (RAHB)

The resonance assisted hydrogen bond can be found (for IHB) in molecules in which the donor and acceptor groups are separated by a conjugated chain. The donor and acceptor groups (*e.g.* C=O and O-H) can also participate in the resonance system, extending the conjugation [5]. As a consequence, there is a synergistic reinforcement of the hydrogen bond and the π -delocalization, leading to a stronger hydrogen bond compared to other classical systems. In this kind of hydrogen bonded systems some kind of intramolecular hydrogen transfer can be present depending on the strength of the interaction. This effect is mainly due to the presence of a resonant structure which facilitates the transfer.

I.2. Systems under study

Deuterated and halogenated analogs of acetylacetone and malonaldehyde are studied in this thesis. Acetylacetone family of compounds are commonly applied in transitions metal coordination chemistry as bidentate ligands [32], in heterocyclic compounds synthesis as building blocks [33] and as Metalorganic Chemical Vapor Deposition agents (MOCVD) [34]. On the other hand, these molecules are a good model systems to study intramolecular hydrogen bond, hydrogen transfer [35]–[38], keto-enolic tautomerism [7], [9], [39], [40] and photo-isomerization [15], [18], [41]–[44]. Both families of molecules can be classified as β -dicarbonyl, in which the generic structure is shown in Figure I.1. Their main physico-chemical properties are resumed in Table IV.1 in Section IV.1.1.

The aim of the next section is to introduce the molecules under study as well as a bibliographic review focused in the physico-chemical processes previously mentioned. The research works already made in the electronic and vibrational spectroscopies of these systems are also discussed.

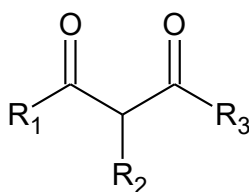


Figure I.1: Schematic representation of the β -dicarbonyl family. R₁ and R₃ represent different functional groups like: CH₃, CF₃ and H, while R₂ represents: H and Cl (for the molecules under study in this thesis).

I.2.1. β -diketones

I.2.1.1. Acetylacetone and isotopologues

Acetylacetone ($C_5H_8O_2$) is the simplest and more representative molecule of the β -diketones family. There are a lot of information about this molecule and its physico-chemical behavior. We start this section with a summary of the most important literature about the processes analyzed in this work. At the same time, this molecule will allow us to introduce some common characteristics of the β -diketone family.

β -diketone molecules is a family of ketones which has two carbonyl groups separated by a carbon atom (in β position) in the skeleton. This configuration is known as *keto* tautomer. There is a second possible configuration, which is in thermodynamic equilibrium with the *keto* structure: the *enol* tautomer. In this form one of the original hydrogens of the α carbon is bonded to one of the oxygen atoms forming a hydroxyl group, the vacant left is completed with a double bond. Both structures are shown in Figure I.2. The equilibrium established between the two possible configurations is called in chemistry “tautomerism”, which is a special kind of structural isomerism.

As we can observe in Figure I.2 the enolic form is stabilized by an internal hydrogen bond, only a small amount of the *keto* form is present in the gas phase [7], [45]. The keto-enol tautomerism can be strongly affected by the environment [46] (*e.g.* polarity of a liquid solvent) but the prevailing form of the isolated molecule is chelated enol. For a long time there was some controversy about the symmetry of the chelated enol form between the C_{2v} and the C_s symmetry [47]. Finally, many experimental and theoretical works have supported the C_s symmetry [8], [9], [48], [49]. The enol tautomer of this molecule (and all β -diketones) is a clear example of a RAHB system. The alternate double bonds can have a high degree of delocalization favoring the hydrogen transfer and making stronger the hydrogen bond.

Theoretically, eight stable enolic isomers are found: the chelated enol form, and seven open conformers¹ [41], [42], [50]. They are obtained by rotations around three bonds, two CC bonds and one CO bond as shown

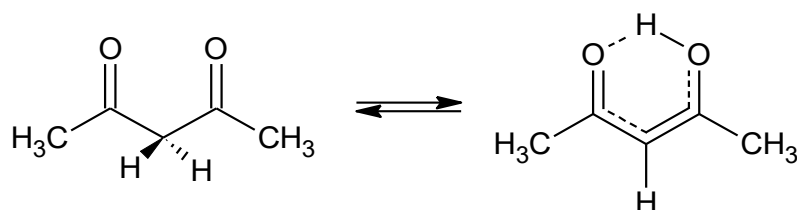


Figure I.2: Tautomeric equilibrium in acetylacetone, between keto (left) and enol (right) forms.

¹ “conformer” is used here to refer to enolic rotational isomers. This term will be used from now on.

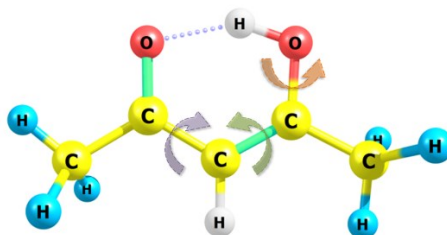


Figure I.3: CCC enol conformer of acetylacetone. Hydrogen atoms exchanged with deuterium are marked in white. Each colored arrow defines one of the possible rotations in order to produce a new conformer. Double bonds are coloured in light green

in Figure I.3, and are denoted XYZ, where letters X, Y and Z stand for C or T depending on the *cis* or *trans* positions of the groups around the C-C, C=C and C-O bonds, respectively. The chelated enol (CCC) is the most stable form, the only one with a hydrogen bond and the only one observed in the gas phase. In cryogenic matrices, it is also the most stable but several open conformers can be produced by UV irradiation [15], [18], [21], [41], [51].

The highly stabilizing hydrogen bond interaction in the CCC form prevents isomerization in the electronic ground state and an electronic excitation is required to access to the open forms. It has been suggested, from experiments and theoretical calculations, that this occurs through the excitation of the molecule to the S_2 level *via* a π - π^* transition. Non-radiative processes like Internal Conversion (IC) and Intersystem Crossing (ISC) between $S_2/S_1/T_2/T_1$ states lead the system to the T_1 state, where fragmentation (in gas phase) or isomerization (in cryogenic matrix) can occur [15], [42], [52]–[54].

Photo-isomerization of acetylacetone in matrices was probed in previous works by electronic and vibrational spectroscopy. Different kinds of matrices were used in order to test the influence of the environment in this photophysical process, among them: N_2 , Ne, Ar, Xe and hydrogen hosts (normal hydrogen n - H_2 , normal deuterium n - D_2 and *para*-hydrogen p - H_2) [15], [18], [41], [43], [51]. The stabilization of different open conformers depends on the host. Previous studies in our group showed that in Ne and p - H_2 matrices, only the CTC, TCC and TTC conformers, in which the OH group is in the *cis* conformation, were observed after 266 nm laser irradiation [15]. In n - H_2 and n - D_2 , TCT (OH in *trans* conformation) was also detected. This conformer was also observed in Ar, Xe and N_2 matrices [41], [43]. Furthermore, CTT was stabilized in N_2 and Xe [43], [51]. Consequently, it was proposed that CTT and TCT conformers were not observed in p - H_2 and Ne because of a fast tunneling process of the hydrogen in the OH group converting CTT and TCT into CTC and TCC respectively [15].

Surprisingly very few studies are related with the effect of the exchange of an H atom by another atom (D or F for example) [35], [37] although this change, deuteration in particular, could give information on the various physico-chemical properties of the molecule.

HYDROGEN BONDED SYSTEMS

The double deuterated acetylacetone has been previously studied in pure solid, liquid and gas phases through FT-IR spectroscopy and neutron scattering [55]–[59]. All these works report studies on the chelated enol form (CCC), and none of them on the open enol conformers.

I.2.1.2. 3-Chloroacetylacetone

3-Chloroacetylacetone ($C_5O_2ClH_7$), hereinafter chloroacetylacetone, is one of the simplest halogenated analogs of acetylacetone. In this molecule the alpha hydrogen (olefinic hydrogen, see Figure I.3) is substituted by a chlorine atom. In Figure I.1 $R_1=R_3=CH_3$ and $R_2=Cl$. Even when this is one of the cheapest halogenated analogs of acetylacetone and is widely employed as a metal ligand, not many works focused on its spectroscopic behavior has been published. In fact, in the bibliographic search we made, only one study using matrix isolation technique was found, but with an analytical purpose [60].

The main optical spectroscopic study on this molecule has been focused on its vibrational spectrum (IR and Raman) in gas, solid and liquid phases (pure or in solvents like CCl_4) [56], [61]–[63]. Regarding the tautomeric equilibrium, it has been found that in liquid phase the content of enol tautomer is higher than in acetylacetone [10]. But, this trend could not be confirmed for the gas phase through gas electron diffraction (GED), because enol content found is near to 100% (within the error margin) in both cases [6]. Theoretical calculations and infrared spectrum suggest that geometry of the skeleton and the conjugated ring enol tautomer is planar, with both methyl groups in *sync* position compared to oxygen atoms [6], [62], [63]. The intramolecular hydrogen bond in the enol conformer has also been examined from its vibrational and NMR spectra and by quantum chemistry calculations [38], [57], [61]. These studies concluded that the IHB in chloroacetylacetone is stronger than in acetylacetone and the other halogenated β -diketones molecules analyzed in this work. Some authors explain this effect by means of the steric repulsion of the chlorine atom that pushes the methyl groups, resulting in a decrease of the H bond length [62]. Finally, no reports on the photochemical behavior of this molecule were found.

I.2.1.3. Hexafluoroacetylacetone

Hexafluoroacetylacetone ($C_5O_2F_6H_2$) is a halogenated analog of acetylacetone in which the methyl groups (CH_3) are substituted by perfluoromethyl groups (CF_3). In Figure I.1, $R_1=R_3=CF_3$ and $R_2=H$. This analog is very volatile and is often used in MOCVD [64]. After acetylacetone, hexafluoroacetylacetone is one of the best studied β -diketones regarding its structure, spectroscopy and photochemical behavior.

Initial studies carried out by Andreasen *et al.* [65] and Iijima *et al.* [66] using GED suggest a structure near to the C_2 or C_{2v} symmetries. But, a more recent research carried out by Evangelisti *et al.* in supersonic jets

coupled with a Fourier Transform microwave spectrometer (FT-MW) concluded that in gas phase the molecule has a C_s symmetry [67]. Theoretical calculations done by Burk and Koppel with PM3 and AM1 methods [68] and by Buemi at B3LYP/6-31G** [69] also supports the presence of an asymmetric structure. Tayyari *et al.* found similar results with DFT methods and different functionals and Pople's basis set. In their article they try to explain the geometrical parameters obtained in GED by Andreasen *et al.* by assuming a superposition of two equivalent unsymmetrical structures of the enol tautomer. Finally, Chatterjee *et al.* made X-Rays diffraction experiments and high level quantum calculation with Coupled Cluster (CCSD) and correlation consistency basis sets, obtaining the C_s symmetry as the most stable equilibrium configuration [70]. All these works also show a weakening of the IHB compared to acetylacetone.

The vibrational spectrum of this analog has been previously obtained in gas, liquid and solid phases [56]. The electronic spectrum in the gas and liquid phases is also known [71]. Nagashima *et al.* made an extension of these works by obtaining the infrared and UV absorption spectra in argon matrix [72]. They also studied the photophysics of the molecule in this matrix by means of broadband UV irradiation, which allows them to produce and stabilize a new enol conformer. To date, this is the only work developed in cryogenic matrices. Similar to acetylacetone, UV irradiation in the gas phase and in supersonic jets leads to photofragmentation or photodissociation instead of isomerization [16], [73], [74]. The absence of fluorescence suggests very fast non-radiative process that dominates the dynamics of the molecule after electronic excitation.

1.2.1.4. Trifluoroacetylacetone

Trifluoroacetylacetone ($C_5O_2F_3H_5$) has an intermediate structure between acetylacetone and hexafluoroacetylacetone. In Figure I.1, $R_1 (R_3)=CF_3$, $R_3 (R_1)=CH_3$ and $R_2=H$. Because of its asymmetry, it can have in principle two different conformations if the hydroxyl group is in the CH_3 or the CF_3 side. Similar to the case of chloroacetylacetone the amount of research work out of its function as a ligand [75] or as a precursor in organic synthesis [76], is not numerous.

The structure of this molecule has been analyzed from experimental and theoretical approaches. One of the first attempts to describe its structure was made by Andreasen *et al.* using information from GED experiments [65]. The geometry they proposed is based in a C_{2v} symmetry for the internal "ring". In their structure the enolic proton is in the plane almost in line with the oxygen atoms, and the methyl and perfluoromethyl groups are in a staggered position regarding the ring plane. A similar structure but with some degree of asymmetry for the ring and a *sync* position for the CF_3 was obtained by Gordon *et al.* using INDO (Intermediate Neglect of Differential Overlap) molecular orbital theory [77]. Subsequent works using DFT and MP2 theoretical methods and vibrational or microwave experimental information have supported

the asymmetric structure, with almost C_s symmetry, and with the hydroxyl group in the CF_3 side in the most stable isomer [69], [78]–[81].

The infrared and Raman spectra of this analog have already been studied by Tayyari *et al.* and Raissi *et al.* in solution and gas phase [56], [79]. The infrared study in argon matrix was carried out by Minoura *et al.*, following the works previously made by this group (Nagashima's group) in acetylacetone and hexafluoroacetylacetone. In their study, they confirmed the C_s structure previously proposed, and performed UV irradiation like in acetylacetone and hexafluoroacetylacetone. Four open enol conformers were observed during and after irradiation [20]. Like in hexafluoroacetylacetone and acetylacetone UV irradiation in the gas phase provokes fragmentation instead of isomerization [16]. The study made by Nagashima's group in argon is the only one we found in matrix isolation for the fluorinated analogs.

I.2.2. β -dialdehyde

I.2.2.1. 2-Chloromalonaldehyde

2-Chloromalonaldehyde ($C_3O_2ClH_3$, hereinafter chloromalonaldehyde) is a halogenated derivative of malonaldehyde, the smaller β -dialdehyde. In Figure I.1, $R_1=R_3=H$ and $R_2=Cl$. We chose to study this molecule because malonaldehyde needs to be synthesized in the lab and is very unstable. On the other hand, chloromalonaldehyde is commercially available. But, despite being commercially available, only three publications were found about this molecule in the Web of Science search engine. Even data about its physico-chemical properties is scarce. The three publications found are all theoretical studies. In these articles, chloromalonaldehyde is used as a model system to test different theoretical methodologies in order to describe hydrogen transfer in the electronic ground state [82]–[84]. So, no experimental or theoretical spectroscopic data was found.

I.2.3. Other systems under study

Two other hydrogen bonded systems are also studied in this work: glycolaldehyde molecule and propyne-water complex.

Glycolaldehyde ($C_2O_2H_4$) is the smallest molecule with an intramolecular hydrogen bond. This molecule has called the attention of the astrochemical community because it is one of the largest

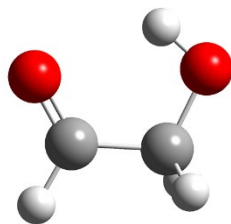


Figure I.4: Glycolaldehyde molecule. The smallest organic molecule with intramolecular hydrogen bond.

organic molecules found in the interstellar media [85]. The vibrational spectroscopy of this molecule has been previously studied in gas phase, supersonic jets and matrix isolation technique [86]–[89].

On the other hand, propyne (C_3H_4) is the second molecule of the alkyne family (after acetylene), which it is characterized by the presence of at least one triple bond (unsaturated hydrocarbon). This molecule is a prolate symmetric top system. The infrared spectroscopy of propyne molecule has been studied in the gas phase, supersonic jets and helium droplets [25], [90], [91]. In the case of propyne-water complex no experimental work was found in our bibliographic research.

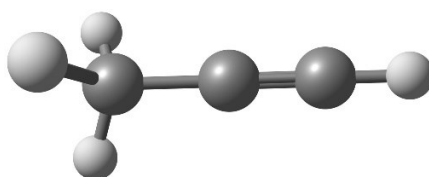


Figure I.5: Propyne molecule. The second member of the alkyne family.

I.2.4. Notations

Through this work the following notations will be used: AcAcH8, AcAcD2 and AcAcD1 to name fully hydrogenated, double deuterated and monodeuterated acetylacetone, respectively. There are two AcAcD1, distinguished by the notations AcAcD1(CD) and AcAcD1(OD), depending on the position of deuterium atom. For halogenated analogs the next acronyms are used: AcAcCl, AcAcF6 and AcAcF3 for chloroacetylacetone, hexafluoroacetylacetone and trifluoroacetylacetone respectively. Chloromalonaldehyde is denoted as MaCl. When multiple isotopologues are discussed at the same time, the specific conformers of the corresponding species will be noted XYZ(H8), XYZ(D2), XYZ(D1) (or XYZ(CD) and XYZ(OD)) and XYZ-Cl(D), with X, Y and Z standing for C or T. The two asymmetric forms of trifluoroacetylacetone are denoted as XYZ(CO) and XYZ(OH) depending on the side the CF_3 group is placed (carbonyl or hydroxyl group).

Chapter II Experimental and theoretical tools

This chapter is mainly dedicated to the theoretical basis and characteristics of the techniques used in this thesis. Emphasis is made in the advantages and disadvantages of each one. A brief historical survey about the development of these techniques will start each section. The first part is dedicated to matrix isolation (MI). In the case of spectroscopy, a general theoretical background will be first given, allowing after to go in some of the details of electronic and vibrational absorption spectroscopies. Then, the advantages of the use of the combined techniques (MI-electronic and MI-vibrational spectroscopy) will be mentioned and explained. Finally, the special case of the *para*-hydrogen matrix as a quantum host will be discussed. The principles of the Helium droplets technique are not included in this chapter; they are included along with the technical details in chapter IV.

II.1. Matrix Isolation (MI)

II.1.1. A brief history

The study of molecular systems at very low temperatures starts at the very beginning of the XX century in parallel with the development of cryogenic techniques and gas liquefaction. Some of the first works were done using cold solutions of nitrogen or special mixtures like Ether-Pentane-Alcohol mixture (EPA) [92]. These first studies were mainly focused on UV and EPR (Electron Paramagnetic Resonance) studies of intermediate species [22], [93].

The great revolution in this field starts at the beginning of the second half of the XX century with the development of the “Matrix isolation” technique, thanks to the progress made in cryogenic techniques. The early works of George Pimentel and George Porter [94], [95] in 1954 recognizes them as the founding fathers of this technique. Since then, several groups all around the world started to use it, producing an enormous amount of papers in different branches of spectroscopy. This development could not be possible without the work of many important researchers considered as the milestones in this field, some of them: L. Andrews, M. Rasänen, B. Nelander, V. Bondybey, W. Weltner, F. Legay, Marilyn Jacox and George Pimentel, among many others.

II.1.2. Principles and advantages

But, how works this technique? The original principle is to trap the molecule under study (guest) in a solid crystal (host) at very low temperatures², and then to study the system with a suitable spectroscopic technique. The sample is usually obtained by deposition of a gas mixture (guest/host) on a cold window inside a cryostat. As example of the processes usually studied with this technique we find: determination of reaction intermediates, generation of reactive species, characterization of weak molecular complexes, conformational studies, among others [96]–[99]. The technique has many general advantages, some of them are [22], [93]:

1. When “inert” hosts are used (*e.g.* rare gases, nitrogen) relatively small interaction between the host and the guest molecule can be achieved, *i.e.* small perturbation of the guest molecule.
2. Unstable species (*e.g.* radicals, ions, isomers, etc.) can be produced (*in situ* or during deposition process) and trapped in the matrix over long periods, which allows their study by means of conventional spectroscopic techniques.
3. Spectroscopic studies are simplified because the ground vibrational level is generally the only one thermally populated and rotation is hindered in most of the cases.
4. Low temperatures make easier to study quantum tunneling driven process (thermal energy is minimized) when the barrier is high enough.
5. Low barrier processes (activation energy of a few kJ/mol) can be studied as well in a controlled environment.

Despite the many advantages just mentioned before, some important limitations need to be taken in to account, among these [100]:

1. The molecule under study (or its precursors) should be relatively volatile or at least able to resist heating, laser ablation or any other process necessary to put it in the gas phase without decomposition.
2. The system is not in thermodynamic equilibrium, so no thermodynamic data can be usually obtained
3. Matrix effects can affect the number, position and shape of the bands in the spectrum:
 - a. **Matrix shift.** It is caused by the host-guest interaction (even if it is small). It is matrix dependent and it is important in interacting matrices like N₂

² The temperature depends on the host used for deposition. As a general rule one third of the triple point temperature should be used for the host gas, to obtain a crystal of high optical quality (good transparency and low scattering).

- b. **Trapping site effects.** Different trapping sites can lead to different host-guest interactions. Also, it can activate modes due to the breaking of the symmetry or even remove mode degeneracy. This effect can be detected by the annealing process³, changes in deposition conditions or by comparison of different spectra from different matrices.
- c. **Aggregation.** Presence of dimers or multimers⁴. Very common in MI experiments, can be revealed by examining the effect of varying concentration in different samples.
- d. **Impurities.** Interaction of the guest molecule with undesired impurities for example from residual air trapped in the matrix (N₂, CO₂, H₂O) or from photolysis products.⁵
- e. **Molecular rotation.** Usually hindered or prevented by the host, is only observed with very small molecules.

It should be pointed out that some of the matrix effects just mentioned as disadvantages can be sometimes very useful or even the purpose of the experiment, *e.g.*: formation of dimers (point 3.c), or the shift in the position and change in intensity of some modes (point 3.a) caused by the use of different matrices, can help in the process of assignment.

In the case of photolysis studies, there is an important factor to take into account: cage effect. This effect occurs when a molecule is fragmented by UV-Vis light absorption (inside a matrix) and the fragments cannot escape from the surrounding host rigid cage. So, unstable fragments are trapped inside and recombine again to form either the original molecule (in the initial or a new conformation), or new molecules. This can be an advantage if isomerization or production of new stable species is desired, or it can be a disadvantage if fragments (radicals, ions, etc.) want to be formed and stabilized.

There are other advantages and disadvantages, mainly related to the work with unstable and intermediate species, which are not mentioned here but that can be consulted in books and reviews on the subject [22], [93], [101].

Nowadays, the technique is commonly used in many laboratories in combination with different kind of classical spectroscopies like EPR, IR, Raman, UV, Fluorescence, but also in more complex experiments like NMR (Nuclear Magnetic Resonance), VCD (Vibrational Circular Dichroism), pump-probe spectroscopy, photon-echo, among others [102]–[104].

³ It is the process of warming a solid material for several minutes and then cooling it down.

⁴ Group of monomers held together with non-covalent interactions

⁵ We need to remark this is a limitation present in most of the techniques used for spectroscopic studies, not only in MI. But, it could be important in MI if a careful technical work is not done.

II.1.3. General techniques

Despite its simple working principle, many important details need to be considered to successfully carry out an experiment in matrix isolation. Some of them will be mentioned next.

The main goal in cryogenics is to achieve a low temperature and to maintain it over a long period of time with a fair stability. There are different kinds of cryostats if we take into account the methods used to cool down the system. Nevertheless, these can be divided in two main groups: helium bath and closed cycle helium cryostats [105]. The former uses a bath of a cryocooler (usually helium) to maintain the desired temperature, either in static way or with a continuous flow from a vessel. But, in the case of low temperatures (< 10 K), its use requires employing liquid helium relatively often (even when recycling helium devices have been developed), which is very expensive. Also, the work with it can be cumbersome. Nevertheless, many labs still use this design.

On the other hand, closed cycle helium cryostats are based in thermodynamic cycles, *e.g.* Joule-Thompson, Stirling, Brayton, pulse tube refrigerator (PT) and Gifford-McMahon (GM) [106], [107]. When low temperatures (< 10 K) want to be achieved, GM and PT cryostats are more suitable. The PT cryostat reduces considerably vibrations in the system, but is a more expensive and delicate equipment than the GM one.

Nowadays, the two stages GM cryostat is commonly used in setups when stable temperatures under 10 K (more important, 4 K) are desirable and vibrations are not a determinant factor. This cryostat uses a compressor filled with gaseous helium and coupled to a rotary head that allows the expansion/contraction of the gas at different places [108], [109]. Usually, the closed cycle helium compressor is more expensive at the beginning but its price is compensated with the fact that maintenance needs to be done after 10000 hours and gas changed after 5 years or more depending on the setup [22].

Other factors to take into account when a cryostat is chosen are: minimum temperature achievable, cooling power, stability of the temperature, geometry and vibrations. As an example, the specific data of the Gifford-McMahon cryostat used in setup #2 (see Figure IV.4) in this thesis is shown in Table II.1. Finally, hybrid cryostats that mix some of the methods already mentioned are also employed when lower temperatures (< 2 K) want to be attained.

In cryogenic systems any source of heat should be avoided. Heat conduction between the metallic walls of the cryostat and the internal cold head is diminished working at very low pressures between $10^{-5} - 10^{-7}$ mbar⁶

⁶ In fact, the pressure can be less than 10^{-7} mbar because cryopumping takes place.

(this also guaranties to maintain at very low levels possible sources of impurities). Convection process is also decreased by this mean.

Table II.1: Gifford-McMahon cryostat specifications (used in Setup #2 in this thesis, see section IV.2.)

Lowest Temperature ⁷	Temperature Range	Temperature Stability	Cooling power	Cool down Time ⁸
$< 3.5 \text{ K}$ At the cold plate	$\sim 3.5 < T < 60 \text{ K}$ (stable)	$\pm 20 \text{ mK}$	1.5W at 4.2 K	$< 2h$ From 300 to 4.2 K

On the other hand, if a very good heat conduction is desired *e.g.* between the coldest stage (cold finger) and the internal window, indium foils have to be used. Heat transmission by radiation is decreased by using a radiation shield of a very good thermal conductivity and heat reflective material like OFHC (Oxygen-free high thermal conductivity copper) that covers the cold head, leaving only small holes for the optical beam pathway, pumping and gas input/output.

Deposition of the samples is made onto a sample holder of good thermal conductivity that is in contact with the cold finger (Figure II.1). The sample holder can be metallic (use for reflection) or made of ionic salts (CaF_2 , CsI, etc.), diamond, sapphire, etc. (use for transmission). Many kinds of gases are used as host, depending mainly on the purpose and conditions of the experiment, and its availability. Some general properties are

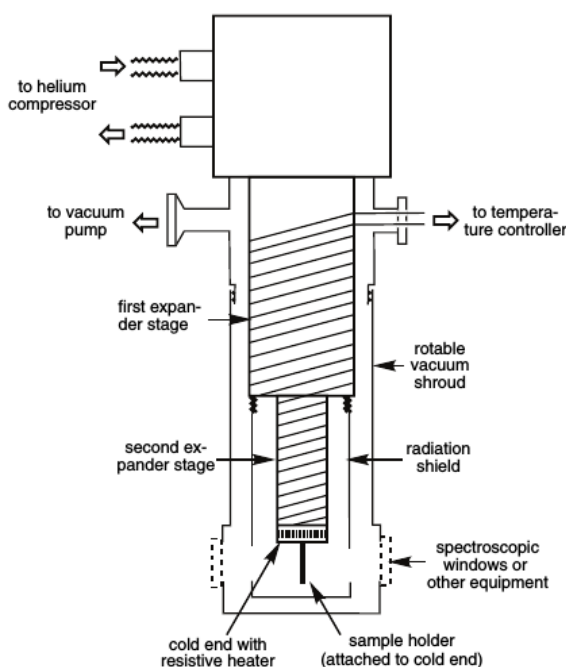


Figure II.1: Scheme of a closed-cycle cryostat (from references [93]) Copyright © 2004 by John Wiley & Sons, Inc. All rights reserved.

⁷ Minimum stable temperature guaranteed by the manufacturer, a lower temperature is achieved in practice (2.8 K)

⁸ This parameter greatly depends of the specific heat capacity of the material used in the cryogenic head and their mass.

EXPERIMENTAL AND THEORETICAL TOOLS

desirable and were discussed by Pimentel in one of his first papers [110]: inertness, rigidity, good transparency¹⁰, volatility, and we can add a high degree of purity of the gas, and high thermal conductivity. The final choice depends on all these factors. For example, if a very non interactive host wants to be used, Ne and pH₂ are the best choices, but their price, the technical requirements for its production and the difficulties to achieved temperature below 9 K, make them less available for many labs. Another example is that in some cases instead of a non-interactive matrix (noble gases) a very reactive one is desired, like CO or H₂O. Some physical properties of the host gases used in this thesis are shown in Table II.2 (taken from references [23], [111]–[113]).

Other important parameters that need to be controlled are the host to guest ratio (usually between 1/100 and 1/10000 ratio), the flux of the deposition (depends also if continuous or pulsed technique is used), and the deposition temperature.

Table II.2: Physical properties of host gases used in this work (sources from NIST [111] and references [23], [112], [113])

	Ne	Ar	N ₂	H ₂	He*	
Crystal lattice	<i>fcc</i>	<i>fcc</i>	<i>fcc</i> (T<35K)	<i>fcc</i> and <i>hcp</i> ¹¹	-	
Lattice constant (Å)	4.462	5.316	5.661	5.338	-	
Λ¹²	0.07	0.05	NF	0.28	0.48 (³ He) 0.43 (⁴ He)	
Polarizability (Å³)	0.39	1.63	1.76	0.80	0.21	
Triple point	T (K)	24.6	83.8	63.15	13.95	2.18 [†]
	P (bar)	0.43	0.69	0.14	0.072	0.0504 [†]
Sublimation temp. (K) at 10⁻⁶ torr	9	31	NF	NF	-	

*Helium only solidifies under high pressures (>250 bar), so, values corresponding to its solid are not included here.

† Helium has no Triple point. These values correspond to its λ point, the pressure/temperature point where gas, and liquid helium (I) and (II) phases coexist.

NF: not found

¹⁰ This property is not only related to the light absorption of the gas but to the thickness and crystallinity of the sample also, in order to avoid light scattering.

¹¹ The *hcp* phase is the most stable. The *fcc* phase formed under a non-equilibrium process can be converted to *hcp* after annealing at T>4 K

¹² The *de Boer* parameter $\Lambda = \frac{h}{\sigma(m.\epsilon)^{1/2}}$ (where σ and ϵ are the Lennard-Jones parameters and m the mass of the atom or molecule) is a measure of the atom's deviation from classical behavior. Values near to 1 indicate the behavior of a quantum solid.

II.2. Molecular spectroscopy: Principles

To summarize the basic principles of molecular spectroscopy in a few pages is a difficult task. So, the main ideas and equations that described the behavior of a molecular system interacting with light will be given in the best logical way.

The first step is to know how light interacts with matter. Three processes can occur when light interacts with a molecule: absorption, induced emission and scattering. The discussion that follows is mainly dedicated to absorption processes.

Generally speaking, any kind of molecular spectroscopy is based in some general rules from quantum physics. First, the energy states of an isolated molecule are discrete. Second, the total energy (leaving out the translation kinetic component) of a molecule can be decomposed in the sum of contributions corresponding to different kinds of degrees of freedom¹³, that can be coupled between them in a greater or lesser extent (neglected here), and each of them is quantized as mentioned before, leading to the next expressions for the energy and the wavefunction¹⁴:

$$E_T \cong E_e + E_v + E_r \quad (\text{II.1})$$

$$\psi_t \cong \varphi_e \times \varphi_v \times \varphi_r \quad (\text{II.2})$$

Where E_T is the total energy, E_e is the electronic energy, E_v is the vibrational energy and E_r is the rotational energy. For the wavefunction ψ_t in equation (II.2) each component is defined by the same subscript used for the energy. We remark that coupling between different contributions is important in many systems (and cannot be always neglected) and is subject of study of many research groups.

Third, transitions between energy levels are conducted through “quantum of energy” and are more probable when the Bohr condition is satisfied:

$$\Delta E = E_2 - E_1 = h \cdot \nu \quad (\text{II.3})$$

Where E_2 is the final state, E_1 is the initial state, h is the Planck constant and ν is the frequency of the photon.

¹³ The contributions are usually classified according to the difference in energy between the energy levels of the states, and their physical nature.

¹⁴ In the expression (II.1) the Born-Oppenheimer approximation (see section III.1.) is applied and the ro-vibrational coupling is neglected.

EXPERIMENTAL AND THEORETICAL TOOLS

The three rules already mentioned are not enough if practical applications want to be done. But first, we need to know how probable is a transition to occur and how to relate theoretical magnitudes with experimental ones.

For the first question, the semi-classical analysis of the interaction of a resonant monodimensional periodic electromagnetic wave (of electric field E_x^0) with a quantum system of two stationary states leads to the next expression for the probability P ¹⁵ of finding the system in the excited state m after an irradiation time t [114]:

$$P = \frac{1}{\hbar^2} \left[\int_{-\infty}^{+\infty} \varphi_m^* \mu_x \varphi_l dx \right]^2 \cdot [E_x^0]^2 \cdot t \quad (II.4)$$

Where $\hbar = \frac{h}{2\pi}$ is the reduced Planck constant, μ_x is the electric dipolar moment, φ_m and φ_l are the initial and final state, which according to equation (II.2) can be decomposed in electronic, vibrational and rotational components.

The important conclusions from equation (II.4) are that the probability of transition directly depends on: the time of irradiation, the intensity of the radiation ($[E_x^0]^2$) and the integral factor which is known as *transition dipole moment* (denoted hereafter as d_{lm}). The last factor is the most important in the following analysis because it takes into account the intrinsic characteristics of the system. For example, through the symmetry of each term (wavefunctions and operator) we can know when the value of the integral equals zero, and consequently which transitions are allowed to occur (selection rule).

The processes of induced absorption, induced emission and spontaneous emission were analyzed by A. Einstein in the first half of the XX century. He demonstrates from thermodynamics principles that the induced absorption coefficient B_{lm} and the induced emission coefficient B_{ml} are equal for non-degenerated states¹⁶, and related to the transition dipole moment as next [115]:

$$B_{lm} = \frac{2\pi}{3\hbar^2} \cdot [d_{lm}]^2 \quad (II.5)$$

Using this expression, we can finally relate experimental and theoretical magnitudes through the next equation:

¹⁵ This equation is only valid under the assumption that the probability has a small value, which implies that the time of the perturbation is much smaller than the inverse of the others terms (a): $t \ll 1/a$. Otherwise, the probability will be higher than 1, which is absurd, from the mathematical definition of probability (normalization).

¹⁶ If degeneracy (g) of the states is included the relation between the absorption coefficients is $\frac{B_{lm}}{B_{ml}} = \frac{g_m}{g_l}$ which is a more general expression (g_m : degeneracy of upper state, g_l : degeneracy of lower state)

$$D = \frac{Nh}{c} \cdot \nu_{lm} \cdot B_{lm} = \frac{4\pi^2 N}{3\hbar c} \cdot \nu_{lm} \cdot [d_{lm}]^2 \quad (II.6)$$

Where N is the number of particles and c is the speed of the light. The experimental magnitude D is named *integrated intensity* and is defined as:

$$D = \int \frac{\varepsilon(\nu)}{0.434} d\nu \quad (II.7)$$

Where $\varepsilon(\nu)$ is the molar attenuation coefficient, which depends on the frequency. At the same time, this coefficient is related to another important equation in practical spectroscopy, the Beer-Lambert-Bouguer law:

$$A(\nu) = -\log \frac{I_1(\nu)}{I_0(\nu)} = \log \frac{1}{T} = \sum_{i=1}^N \varepsilon_i(\nu) c_i l \quad (II.8)$$

Where $A(\nu)$ is the absorbance, $I_0(\nu)$ is the light intensity of the source, $I_1(\nu)$ is the light intensity after crossing the sample, T is the Transmittance, c_i is the concentration of the i absorbing species and l the sample length crossed by the light. Log is in 10 basis.

This equation relates the amount of light absorbed by a molecular system with non-specific variables like concentration and path length in the sample, and intrinsic properties of the molecule like the attenuation coefficient. Moreover, it allows, within its limits of validity, making quantitative determination of the absorbing species.

Up to this point, we have already discussed about two of the main characteristics of an absorption band: its position (given by Bohr condition, Eq. (II.3)) and its intensity (related to d_{lm} Eq. (II.6) and Eq. (II.7)). But, there is a third important characteristic to mention: the bandwidth. The width of a band is always finite and different from a delta function profile which is the ideal profile. This is due to some factors that can increase the bandwidth *e.g.*: the excited state lifetime (related to the Heisenberg's uncertainty relation) known as *natural width* and the collisional broadening (gas phase) that includes different cases and can also affects the excited state lifetime [116]. The effect of these factors is known as *homogeneous broadening* and it is described by a Lorentzian profile. In addition, there is also an *inhomogeneous broadening* which is related mainly to Doppler effect in the gas phase and to the presence of different environments in condensed phase. The result is the absorption or emission of light at different frequencies around a nominal value. Inhomogeneous broadening can dominate band broadening in the condensed phase. Finally, we should take into account that inter and intramolecular interactions are a very important source of broadening, *e.g.* hydrogen bond and complex formation.

II.3. Electronic absorption spectroscopy

The energy required to excite or induce a transition between electronic levels (E_e) is usually located in the ultraviolet (UV) and visible (Vis) regions of the electromagnetic spectrum. So, the UV-Vis spectroscopy studies transitions between these types of levels.

The electronic levels of a molecular system are closely related to the definition of *molecular orbitals* (MO) in analogy to the *atomic orbitals* used for atoms. The square of these MO can give the probability to find the electrons in the spatial regions. The most extended representation is the Linear Combination of Atomic Orbitals (LCAO) first used by L. Pauling [26] and J. Lennard-Jones [117] at the end of 1920's, and subsequently developed by Mulliken and Hund [118]. These MO are linear combinations (in the mathematical sense) of the *atomic orbitals* (AO) of the atoms present in the molecule. There are as many MO as AO that are used to create them, and they have a specific order in energy for each molecular system. Given the nature of the MO we can have bonding, antibonding and non-bonding orbitals. The electrons occupy the MO following the Hund's rule of maximum multiplicity and the Pauli's exclusion principle.

An electronic transition will take place between occupied and non-occupied orbitals. If we develop the equation (II.4) assuming that there is no dependence between each contribution we will have:

$$d_{lm} = \int_{-\infty}^{+\infty} \varphi_m^* \mu \varphi_l dq = \int_{-\infty}^{+\infty} \psi_m^* \mu_e \psi_l dq_e \int_{-\infty}^{+\infty} \chi_m^* \chi_l dq_v \int_{-\infty}^{+\infty} \phi_m^* \phi_l dq_s \quad (II.9)$$

Where the total wavefunction has been separated in the electronic orbital ψ , vibrational χ and electronic spin ϕ components¹⁷, and we take into account that the dipole moment only acts over the electronic variables. If we look at equation (II.9) the probability of an electronic transition to occur is related to the symmetry of the MO's involved. But, the multiplicity of the states also determines the probability of the transition, last integral in equation (II.9). In this sense it can be demonstrated through the orthonormality property, that only transition between states of the same multiplicity are theoretically possible e.g. singlet-singlet, triplet-triplet.

An electronic excitation usually involves the change of vibrational states: $\varphi_0(n_0, v_0) \rightarrow \varphi_1(n_1, v_{1,2,3...})$, where n is the electronic quantum number and v is the vibrational quantum number. This change can be one of the main responsible of the shape of the band (or vibronic distribution) of an electronic excitation. The intensity of each vibronic transition is proportional to the square of the overlap integral between the vibrational wave functions of the two states that are involved in the transition. This refers to the second

¹⁷ The rotational degree of freedom has not been included in this discussion

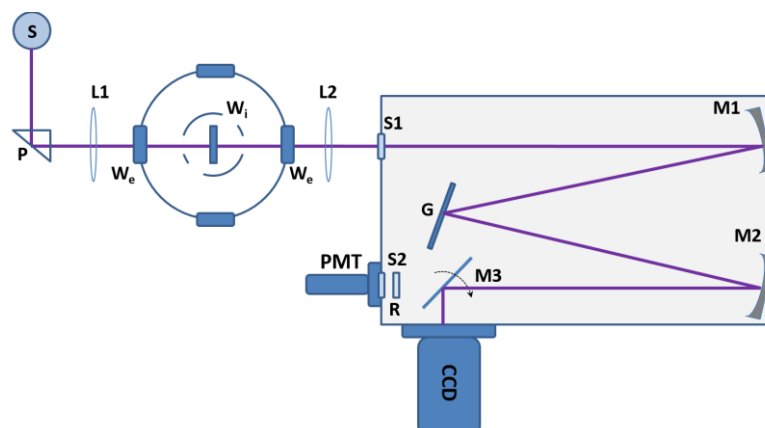


Figure II.2: Scheme of a UV-Vis spectrometer. S: deuterium lamp (source), P: prism, L1 and L2: Lenses, W_e and W_i : external and internal windows in the cryostat, S1 and S2: input and output slit, M1 and M2: mirrors, M3: movable mirror, G: grating, R: optical retarder, PMT and CCD: Photomultiplier tube and CCD camera (detectors)

integral in equation (II.9), also known as the *Franck-Condon factor* (FC). The previous result is explained by the Franck-Condon principle which is based on the assumption that during an electronic excitation the nuclear geometry and its momentum do not change (because of different temporal scales for each motion), also known as *vertical excitation*. Then, depending on the potential energy curve of the lower and upper state different distributions of the vibronic band intensities are obtained.

In practice a UV-Vis spectrum is usually obtained through a dispersive equipment. In Figure II.2 the scheme used in our lab is shown.

In this configuration, there is a light source (tungsten filament, deuterium lamp, Xenon lamp, etc.) in which the light is produced, passing then through the sample where absorption can occur. The light transmitted enters through the slit of the monochromator where a dispersive optical element (prism, gratings) chooses a narrow band wavelength that is finally analyzed by a suitable detector (photomultiplier or a CCD camera¹⁸). The scan of the chosen wavelength by the dispersive element and its corresponding intensity gives the final spectrum. Care should be paid to the resolution and sensibility of the equipment (which are not independent) depending on the standard need for each experiment.

II.4. Vibrational spectroscopy

II.4.1. Vibrational modes and transitions

Vibrational transitions imply transitions between vibrational levels corresponding to a single normal mode or linear combinations of them. Let's continue by defining first the meaning of "normal mode". Any overall

¹⁸ Charge Coupled Device

EXPERIMENTAL AND THEORETICAL TOOLS

nuclear movement of a molecule can be described by a specific set of motions called normal modes. These can be seen as a minimum set of vectors whose linear combinations describe or span the entire space or range of motions¹⁹. The number of normal modes for a molecule of N atoms equals $3N - 6$ ($3N - 5$ for linear systems), which is related to the number of non rotational or translational degrees of freedom. These normal modes have different energies and a defined symmetry. The energies are quantized and the levels are described by the quantum number " ν ".

The difference in energy between vibrational levels is in the domain of the infrared electromagnetic radiation, and it is in the order of $0.2\text{-}55 \text{ kJ}\cdot\text{mol}^{-1}$ ($20\text{-}4600 \text{ cm}^{-1}$) for fundamental transitions. Even at values of temperature near to normal temperature (293.15 K), the Boltzmann distribution indicates that the ground state is the most populated. This implies that most of the transitions start from it, but transitions from higher levels can be also observed in less extent due to their lower population (these are called "hot bands").

II.4.2. Infrared spectroscopy

As mentioned before the selection rules that determine the possibility for a transition to occur are related to the value of the integral of the transition dipole moment. The analysis of the symmetry of the eigenfunctions from the solution of the Schrödinger equation yields that only transitions between states with different symmetries are allowed (if the product of the three symmetries of the two wavefunctions and of the dipole includes the symmetric representation)²⁰. The harmonic potential imposes that only $\Delta\nu = 1$ is allowed [119]. This result does not agree with experimental observations like the presence of overtones $\Delta\nu = 2, 3, \dots$ and the dissociation limit of the molecular system. The problem is the assumption of a harmonic potential to describe the vibration, which is not the case in most of the instances. A more general and correct approach is to assume an anharmonic potential either through an analytical equation (like the Morse potential) or a Taylor expansion around the equilibrium geometry. A deeper analysis of the transition dipole moment integral shows that there is an important variable to take into account. If the dipolar moment operator is developed around the geometry of equilibrium with a Taylor series, we will find that the transition intensity depends on the variation of the dipole moment of the molecule with the vibration coordinate around the equilibrium point $\left(\frac{\partial\mu}{\partial Q}\right)$ [120].

The infrared radiation is classified in three main groups according to the type of transition involved and the electromagnetic range [120]:

¹⁹ The normal modes are the eigenvectors (or eigenfunctions) of the Schrödinger equation for a harmonic potential

²⁰ Normal modes in molecules with no symmetry, belonging to the C_1 point group, are always infrared actives.

1. Near-infrared (13000-4000 cm^{-1}): It is the region of overtones of high frequency stretching vibrations and combinations bands.
2. Mid-infrared (4000-400 cm^{-1}): It is the most important region because most of the fundamentals bands of organic compounds (and some inorganic also) are placed in it. Most of the studies are done in this region.
3. Far-infrared (400-10 cm^{-1}): It is the region of low frequency vibrations and some pure rotational transitions.

The infrared spectrum is a good signature to distinguish each molecule. This is mainly due to the dependence of the frequency, the intensity and the bandwidth of the infrared bands on the bond type, the reduced mass, and the geometrical configuration of the chemical groups in the molecule. The analysis of the spectrum starts with the identification of bands corresponding to active modes. In addition, when analyzing an infrared spectrum there are other factors to take into account [31], [121]:

1. Physical state of the sample (*e.g.* solids: site effects in matrices, gases: ro-vibrational structure)
2. Possible presence of overtones, hot bands and combinations or difference bands ($\nu_1 \pm \nu_2$)
3. Forbidden or very low intensity transitions
4. Degenerated transitions (True and accidental)
5. Fermi resonance: $\nu_1 \approx \nu_2 + \nu_3$ (or any other kind of resonance)

All these factors can be predicted by theoretical calculations (inclusion of anharmonic potentials are needed for some of them). But, these calculations are not always possible because of practical reasons (see Section III.5.).

Some of these factors are more easily recognized than the others, but a careful assignment requires a good knowledge of the system, the way in which the spectrum was obtained and of course experience from the researcher.

Infrared spectra can be obtained through the use of dispersive spectrometers (which were the first developed) or Fourier Transform spectrometers. IR dispersive spectrometers have a similar principle to the one already explained in UV spectrometers, and actually they are not almost in use. Fourier Transform infrared spectrometers (aka FT-IR) are based on the mathematical technique that gives it its name. The basic working principle is related to the Michelson interferometer, in which one mirror is moving while the other is fixed. The general scheme of the one used by our Nicolet 670/870 spectrometer is shown in Figure II.3.

EXPERIMENTAL AND THEORETICAL TOOLS

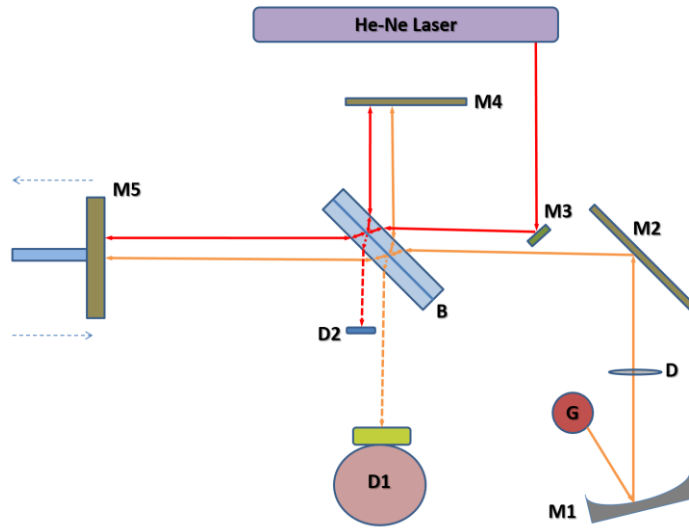


Figure II.3: Michelson interferometer in FT-IR spectrometer. G : IR source, M1 : mirror, D: diaphragm, M2 and M4: fixed mirrors for IR, M3: fixed mirror for He-Ne laser, B: beam splitter, M5: movable mirror at constant speed, D1: IR detector D2: He-Ne laser detector

The basic operation of a Michelson interferometer consists to record the light intensity as a function of the displacement of the movable mirror. The light intensity is then a function of the wavenumber $\bar{\nu}$ and optical path length difference δ (related to the position of the mobile mirror). Considering perfect mirrors and beamsplitter, the functional dependence of the intensity for a monochromatic light, will be of the type:

$$I(\delta) = S(\bar{\nu})(1 + \cos 2\pi\bar{\nu}\delta) \quad (\text{II.10})$$

If we consider a polychromatic source, we can write:

$$I(\delta) = \int_0^{+\infty} S(\bar{\nu})(1 + \cos 2\pi\bar{\nu}\delta) d\bar{\nu} \quad (\text{II.11})$$

We can realize that we have a constant intensity factor and a variable one that depends on the beam path, which has indeed the information of the interferogram. So, the constant factor can be subtracted without affecting the final interpretation and we have:

$$I^*(\delta) = \int_0^{+\infty} S(\bar{\nu}) \cos 2\pi\bar{\nu}\delta d\bar{\nu} = \text{Re} \left(\int_{-\infty}^{+\infty} S(\bar{\nu}) e^{i2\pi\bar{\nu}\delta} d\bar{\nu} \right) \quad (\text{II.12})$$

It can be seen that in this equation $I^*(\delta)$ is nothing more than the Fourier Transform (FT) of $S(\bar{\nu})$. So, if we apply the inverse FT to $I^*(\delta)$ we can pass to the wavenumber domain $S(\bar{\nu})$, where we have:

$$S(\bar{\nu}) = \int_{-\infty}^{+\infty} I^*(\delta) e^{-i2\pi\bar{\nu}\delta} d\delta \quad (\text{II.13})$$

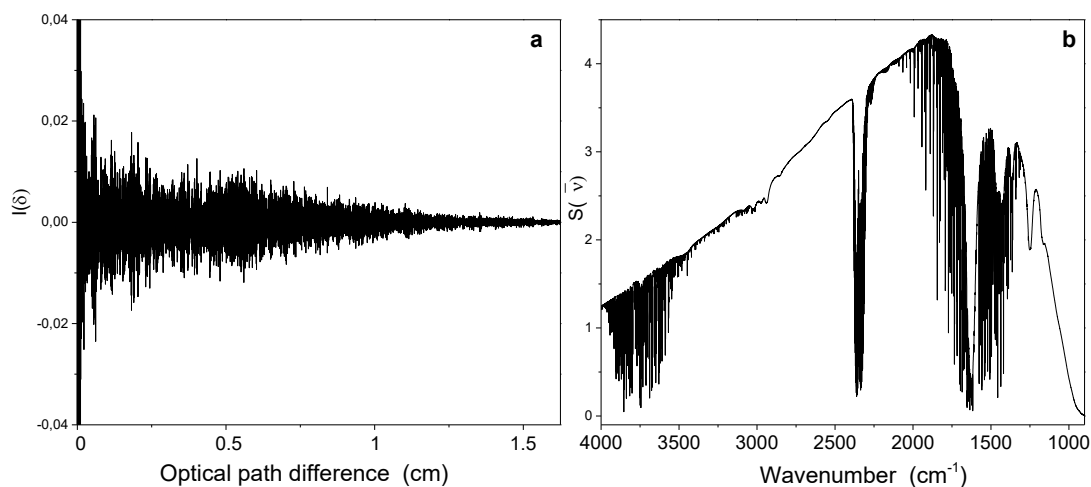


Figure II.4: Interferogram and corresponding single beam spectrum obtained after applying the Fourier transform

In practice there is an infrared detector (photoelectric, bolometer, pyroelectric) that obtains $I^*(t)$ and a computer that transforms the signal in $I^*(\delta)$. This is possible thanks to the fact that the value of the optical path length difference δ (due to the mobile mirror at constant speed) in function of time is controlled by the interference pattern of a He-Ne laser (632.82 nm) coupled to the system. In the last and more important step the inverse Fourier transform is computed (Figure II.4).

If a single-beam spectrum is obtained for the sample and a background, the spectrum can be represented in Transmittance or in Absorbance forms if desired. They are used to eliminate background components in the spectrum and they allow making quantitative determinations through the Beer-Lambert-Bougués equation (see Eq. (II.8)).

II.4.3. Raman spectroscopy

The first important point about Raman spectroscopy is that it involves light inelastic scattering process and so is not an absorption technique. In principle, two kinds of light scattering can take place: elastic (Rayleigh or normal) where the frequency of the incident and scattered photons is the same and inelastic (or anomalous) where these values differed (Figure II.5). The last one, discovered by C.V. Raman and his student K. S. Krishnan in 1928, is the base of the Raman spectroscopy.

Raman dispersion has two components: Stokes ($\Delta\nu = \nu_f - \nu_i = 1$) and anti-Stokes ($\Delta\nu = \nu_f - \nu_i = -1$), where ν_f and ν_i are the vibrational quantum numbers corresponding to the final and initial vibrational states involved in the transition (Figure II.5). The Stokes bands are more intense than their anti-Stokes pair, because the probability of finding the system at the beginning in a vibrational state different from the ground state is small, even at normal temperatures (as it was previously discussed).

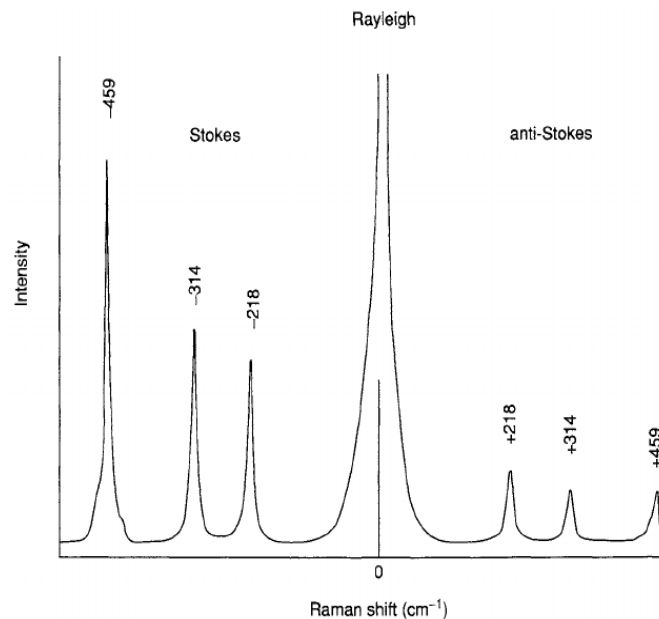


Figure II.5: Different scattering bands. Raman spectrum of CCl₄ (488.0 nm excitation) Taken from reference [122]. Copyright © 2003, 1994 Elsevier Science (USA)

Two important practical features of the Raman scattering are: the frequency of the incident photon must be high for the effect to be observed, and this is why UV-Vis-NIR (~200-1064 nm) sources are usually employed. Second, the Stokes bands are around 5 orders of magnitude less intense than the Rayleigh band, because the probability of the process to occur is low. This makes necessary the use of powerful sources like lasers.

The mechanism of interaction between light and the system in infrared and Raman is different. Theoretically, Raman scattering can easily be explained through a semi classical treatment (even when the quantum description is more rigorous). In this approach, we take into account the change of the polarizability during the vibration of the molecule which is interacting with the electric field of an electromagnetic radiation. The induced electric dipole moment μ generated under these conditions can be expressed as:

$$\mu = \alpha \cdot E \tag{II.14}$$

Where α represents the polarizability and E is the electric field. According to the classical theory the oscillating dipole will emit in all directions with the same frequency and with an intensity proportional to the square of its maximum value $\alpha^2 E^2$. If the electric field around the molecule is expressed in function of time and frequency, and the polarizability is developed in the form of a Taylor function with the normal coordinate Q exercising small periodical displacements, the next expression is obtained [122], [123]:

$$\mu = \alpha_0 E_0 \cos 2\pi\nu t + \left(\frac{\partial\alpha}{\partial Q}\right)_0 \frac{Q_0 E_0}{2} [\cos 2\pi(\nu - \nu_m) \cdot t + \cos 2\pi(\nu + \nu_m) \cdot t] \tag{II.15}$$

Where α_0 is the maximum value of the polarizability, E_0 is the maximum value of the electric field, ν_m is the frequency of the vibration and Q_0 is its maximum displacement. The first term in equation (II.15) corresponds to the Rayleigh dispersion (ν) and the second one to Raman scattering ($\nu - \nu_m$ and $\nu + \nu_m$). We can observe that Raman scattering only occurs when there is a change in the polarizability of the molecule with a change in the normal coordinates $\left(\frac{\partial\alpha}{\partial Q}\right)_0$.

From a practical point of view dispersive and FT spectrometers have been developed, and nowadays both types are commonly used (contrary to IR). The FT spectrometers have the common advantages mentioned before for IR. But, they are mainly limited to lower frequency sources in the NIR region (> 700 nm), out of the UV-Vis zone where the sensibility is higher²¹. The excitation line must be far from the absorption lines of the molecule to avoid fluorescence emission that could make difficult to obtain the spectrum. Nevertheless, because fluorescence is wavelength dependent it can be avoided by simply changing the excitation wavelength, if possible.

Despite these disadvantages, Raman spectroscopy is a very useful technique that is usually applied as a complement of IR spectroscopy. Different selection rules are applied to IR and Raman, so, the intensity of the transitions is not the same for each technique. In many cases, transitions that are not allowed in one of them can be observed in the other. Moreover, Raman is the technique of choice for samples in aqueous solutions where classical IR technique does not work (unless special ATR²² technique is used) because of strong absorption of water. Finally, the range of 50-4000 cm^{-1} is easily accessible for most of Raman equipment without the need to change beamsplitter, optical windows, and detectors as needed in IR. This is due to the fact that excitation and detection are made within a common spectral region supported by the optical devices previously mentioned (*e.g.* for a 4000 cm^{-1} transition and a 785 nm source, detection of the Stokes shift is made around 1144 nm) [122].

II.5. Vibrational and electronic spectroscopies in Matrix Isolation

Infrared spectroscopy was the first technique used in conjunction with MI because of its practical simplicity, economy and the vast amount of structural and dynamical information that it can offer [94].

There are, however, many other advantages in the use of vibrational spectroscopy with MI. Some of them are:

²¹ The relationship between Raman scattering intensity and the wavelength is of the type $1/\lambda^4$ [122]

²² Attenuated Total Reflection

EXPERIMENTAL AND THEORETICAL TOOLS

1. At low temperatures only the ground state is populated, assuring that all the molecules are in the same state and minimizing the presence of hot bands.
2. Line bandwidths are very narrow compared to solid and liquid states, so, bands are better defined (higher spectral resolution).
3. Low guest to host ratio can be used, decreasing (if desired) the interaction between guest molecules placed in different sites (big guest to guest distance, and host screening).
4. Atomic (rare gases) and homonuclear gases are almost transparent in the 20- 60000 cm^{-1} spectral region (also good for UV-Vis experiments), so there is not host interference in the spectrum.

The same advantages mentioned before applies also for Raman spectroscopy, except the third one. Homonuclear molecules can be used as host for Raman experiments (fourth advantage), but it should be taken into account that they actually have Raman absorption. On the other hand, even if the number of publications involving Raman spectroscopy in MI are less than with IR, many interesting studies has been published [124], [125]. The principal drawback is the low sensitivity of Raman spectroscopy. Remember that in MI the amount of sample is usually small ($\sim 1-100$ ppm).

In general, sensitivity in practical Raman experiments was mainly affected, at the beginning, by the lack of powerful laser sources. Another, important factor was the cost of Raman equipment and the relatively slow development of the setups (compared to FT-IR). Nevertheless, nowadays these drawbacks have been overtaken. The main factor to take into account in MI experiments is the need of the use of rather concentrated samples (compared to the guest to host ratios usually use) thus making necessary to pay attention to the possible presence of multimers [122], [124]. Also, a good crystalline sample is desirable in order to avoid possible light scattering from the matrix itself. Finally, the warming of the sample due to the high power laser need to be taken into account.

Electronic spectroscopy was also one of the first to be applied in conjunction with MI, largely due to its high sensitivity [22]. In addition, these techniques share the same advantages than infrared spectroscopy when used with MI. It has been used in the identification of radicals [126], different conformers [51], new stable products [127], among others. On the other hand, absorption and emission (fluorescence and phosphorescence, excitation spectrum) techniques are both available in MI, expanding the amount of information that can be obtained from the ground and excited states. Nevertheless, when the absorption technique is used, the bands can be in some cases relatively large (because of the electron-phonon coupling) limiting its power of distinction between different species.

II.6. The queen of MI: *para*-hydrogen (pH₂) matrix

Despite all the advantages already mentioned about the use of MI with vibrational spectroscopy and rare gases as host matrices, there was the opinion for a long time that the high resolution (HR) limit was not accessible. Even when bands are very narrow in rare gas matrices compared to condensed phases (solid, liquid), they are not narrow enough for HR spectroscopy, because of homogenous and inhomogeneous broadening. This was the case until 1989 when the group of T. Oka published the first paper demonstrating the opposite: HR is possible in MI!²³ [24]. The responsible was a new kind of matrix already known since a long time ago, but rediscovered for its use in MI: *para*-hydrogen²⁴. And it is not the only interesting property of this new matrix [128].

But, what is *para*-hydrogen? If the nuclear spin and the symmetry of the nuclear wavefunction are taken into account, two different isomers of the hydrogen molecule can be identified: *ortho*-hydrogen (symmetric), with unpaired spin $I = 1$ and odd rotational quantum number J ; and *para*-hydrogen (antisymmetric), with paired spin $I = 0$ and even rotational quantum number J ²⁵. A schematic representation from Silvera [129] is shown in Figure II.6. *Para*-hydrogen is the most stable species at low

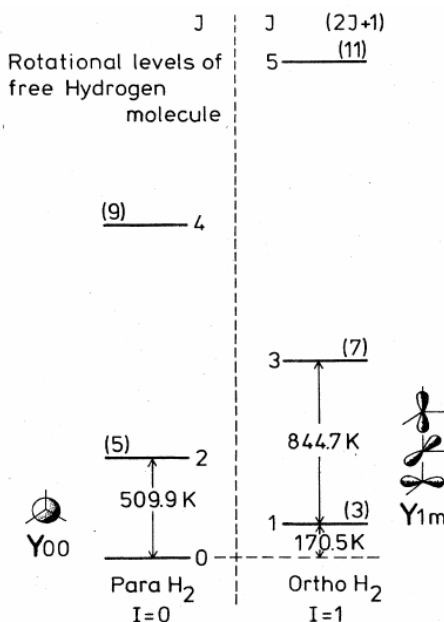


Figure II.6: Ortho and para-hydrogen (Reprinted figure with permission from ref. [129]. Copyright (1980) by the American Physical Society).

²³ Actually, Oka and co-workers refer to transition bands from hydrogen in the matrix. Only in small molecules (such as methane and water) which can rotate in the matrix a HR spectrum has been obtained.

²⁴ *Para*-hydrogen was theoretically proved to exist by F. Hund and W. Heisenberg in 1927, and experimentally found by Paul Harteck and Karl Friedrich Bonhoeffer in 1929. Its properties were subsequently studied during the period 1955-1988 by different groups.

²⁵ The usual nomenclature is "*para*" for the species with the lower value of I and "*ortho*" for the higher one.

EXPERIMENTAL AND THEORETICAL TOOLS

temperature. But, due to entropic reasons (higher multiplicity of the triplet state) and the relative small energetic difference between both spin isomers (170.5 K), $p\text{H}_2$ is only 25% in a hydrogen sample at normal temperature. In principle, this ratio dramatically changes when the system is subjected to low temperatures, but the conversion kinetics is very slow. Nevertheless, the use of paramagnetic catalysts (Fe_2O_3 , rare earth metals, chromic oxide and nickel compounds) greatly increases the rate of conversion and practical amount that can be obtained ($p\text{H}_2 > 99.99\%$). The process is made in two steps: first, condensation of hydrogen over the catalyst, and second, conversion of *ortho* to *para*-hydrogen. These two processes are not completely separated in time, conversion occurs during condensation, when hydrogen starts to be in contact with the catalyst.

Why is *para*-hydrogen so special? As mentioned before, *para*-hydrogen molecule is present in a singlet state ($I = 0$), its angular momentum equals zero ($J = 0$) at low temperatures²⁶. Since the single molecule rotational wavefunction are the spherical harmonics $Y_{jm}(\theta, \phi)$ all $p\text{H}_2$ molecules will be in the spherically symmetric Y_{00} state, and all $o\text{H}_2$ in the p -like state Y_{1m} (only $J = 1$ is populated at low temperatures) [129]. This has two important implications: first and more important, the $p\text{H}_2$ molecule has an isotropic charge distribution. The lack of multipoles provokes that the interaction with other molecules is even smaller than for rare gases (through dispersion forces). Second, because of the spherical distribution it solidifies in close packed structures (like rare gases, see). Another significant property is the large zero-point motion (ZPM) it has (see de Boer parameter). Because of this large value, it is considered as a “quantum solid”, having large near neighbor distance (3.783 Å) and root-mean-square vibration relative to lattice constant (0.18, for comparison Ne: 0.09 and Ar: 0.05 at 0 K) [23]. In addition, solid $p\text{H}_2$ has a large thermal conductivity when the amount of $o\text{H}_2$ is low, larger than in rare gases [129]. In conclusion, the general structural picture of the crystal is a “soft” close-packed solid formed by molecules acting like spheres, with very small capacity of interaction.

Regarding its spectroscopic behavior, *para*-hydrogen solids present some similarities to rare gas solids. First, it absorbs in the UV region, but in the vacuum zone (109.05 nm) far from the 180-700 region where most of the photo-physical studies takes place. Second, it also absorbs in the IR region (group of bands around 4850-4300 cm^{-1} , see Section IV.3.2.), but again far from the main zone where fundamental transitions occur (3700-20 cm^{-1}). In fact, as we will see in section IV.3.2. the IR absorption allows obtaining critical information about its quality (amount of $o\text{H}_2$) and the amount of solid formed. Also, it allows making very interesting studies about energy transfer between the solid host and the guest molecule [130].

²⁶ The energy difference between $J = 0$ and $J = 2$ is around 510 K, so only $J = 0$ is populated at low temperatures.

There are three main drawbacks of $p\text{H}_2$: first, the need to work at very low temperatures (<4 K), which is only achievable for some expensive kind of cryostats. Second, the use of a second cryostat (< 20 K) for $o\text{H}_2 \rightarrow p\text{H}_2$ conversion. These two are technical issues. The third drawback (or better said precaution) is the amount of $o\text{H}_2$ present in the matrix. The $o\text{H}_2$ molecule has a permanent quadrupole moment that allows it to interact with any impurity present in the sample. Paulson and Anderson have observed in different systems such as HF and formic acid, that multiples bands can be present for each mode depending on the amount of $o\text{H}_2$ surrounding the molecule [131]. In addition, they found that the broadening observed in some molecules in $p\text{H}_2$ cannot only be explained by homogeneous broadening and some kind of inhomogeneous broadening mechanism should exist [131]. These studies were done with 99.99% of $p\text{H}_2$ purity, the effect dramatically increase when increasing the amount of $o\text{H}_2$. Because of this the amount of $o\text{H}_2$ should be kept as low as possible if a good spectrum wants to be obtained.

Many interesting works have been published in this field since 1989, and mainly since 1998 when Tam and Fajardo demonstrated the possibility of obtaining in a fast way big and nice crystalline $p\text{H}_2$ matrices with the Rapid Vapor Deposition (RVD) method [132]. A more detailed, well written and complete explanation of the use of *para*-hydrogen in MI can be found in the chapter 6 of reference [133]. A summary of the work done by Mario E. Fajardo in this field along with an excellent review of other works will be found there.

Chapter III Theoretical Methods

Nowadays, the analysis of experimental spectroscopic data is frequently supported by theoretical calculations. For example, in the case of FT-IR MI spectroscopy a frequency calculation of the system can help in the assignment of experimental spectra (and in many cases is the only information). The computation facilities we have today and the use of software packages allow performing quantum chemical simulations to almost everyone with a minimum background in quantum chemistry. Nevertheless, a good understanding of the theory behind the simulation not only contributes to the analysis of the obtained results but also gives the tools to choose the best conditions to perform it (method, basis set, functionals, etc.).

In this chapter a general explanation of quantum chemical calculations is presented. First, the foundations of quantum chemical calculations will be detailed: Schrödinger's equation, basis set, Hartree-Fock (HF) and Density Functional Theory (DFT) approaches. Secondly, an approach to analyze Non Covalent Interactions (NCI) is presented with its advantages. After, details about optimization method, frequency calculation with IR and Raman intensities, and electronic vertical excitations will be discussed. The characteristics of a scan of the Potential Energy Surfaces (PES) and reaction paths are explained after. Then, a brief description about the Wentzel-Kramers-Brillouin method (WKB) for the estimation of the tunnel effect ratio will be given. All the type of calculations mentioned in this section are implemented in Gaussian09 suite [134], software used for the calculations performed in this work. The details of these calculations are given at the end of the chapter.

III.1. Ab initio methods

In the most common non-relativistic formulation of quantum mechanics, the description of a non-relativistic particle in a field is made by the Schrödinger equation:

$$i\hbar \frac{\partial}{\partial t} \Psi(r, t) = \hat{H} \Psi(r, t) = \left[\frac{-\hbar^2}{2\mu} \nabla^2 + V(r, t) \right] \Psi(r, t) \quad (\text{III.1})$$

Where $\Psi(r, t)$ is the wavefunction that describes the system, \hat{H} the Hamiltonian operator, μ the reduced mass of the system, ∇^2 the Laplacian operator, $V(r, t)$ is the potential function and r represents the coordinates of the particle in the reference frame. If the spatial and temporal variables are separated, we can obtain time-independent and time evolution equations:

THEORETICAL METHODS

$$\left[\frac{-\hbar^2}{2\mu} \nabla^2 + V(r) \right] \Psi(r) = E \Psi(r) \quad (\text{III.2})$$

$$\Psi(t) = \Psi(0) \cdot e^{\frac{-iEt}{\hbar}} \quad (\text{III.3})$$

The solution of equation (III.2) gives access to the quantum stationary states $\Psi(r)$ (eigenfunctions) of the system and their corresponding energies E (eigenvalues). But, only for small systems like the hydrogen atom (one particle, the electron in the field of the nucleus) a direct analytical solution can be found²⁷. In principle, the wavefunction contains all the physical information about the system, and it is composed by an orbital part (spatial: radius and angular functions) and a spin component to take into account this intrinsic property of quantum particles. This is known as a *spin-orbital* function.

In the case of a multielectronic atom, several electrons are in the field of the nucleus, and are interacting together. The main approximation to solve this problem is the use of the self-consistent field, in which one electron “feels an average” potential exerted by the other electrons. This is one of the basis of the Hartree-Fock method, which is discussed in the next paragraphs.

In the case of molecules, the problem is much more complicated because of the presence of several nuclei surrounded by electrons. This leads to the use of additional approximations, the most important one being the Born-Oppenheimer (BO) approximation. In a few words it is based on the fact that the electrons “instantaneously” adapt their motions to nuclear motion (fast relaxation). In this frame electronic and nuclear wavefunctions can be separated and we can work only with the electronic part, leaving the nuclear coordinates as parameters. It has been demonstrated that electronic and nuclear degrees of freedom cannot be always decoupled (in degenerated electronic states, *e.g.*: Jahn-Teller effect, conical intersections, internal conversion, etc.) [135], [136]. But, in the cases analyzed in this thesis (ground state of neutral organic molecules) the approximation works very well.

The first well intended approach to solve the Schrödinger equation under BO approximation was given by Hartree in 1927, and explained in an easier physical ground by J.C. Slater and J.A. Gaunt (1928). Finally, J.C. Slater and V. Fock (1930) independently proposed to expand the method by the inclusion of an antisymmetric wavefunction (to take into account the fact that the electrons are fermions). This is the well-known Hartree-Fock (HF) or Hartree-Fock Self-Consistent Field method (HF-SCF). HF relies in the *variational principle* that states that the energy of any trial wavefunction is always greater or equal to the energy obtained for the true wavefunction of the system. Starting from an initial approximate wavefunction to

²⁷ The main issue for bigger system is the many-body problem arising when more than one electron is present.

describe the molecule, an iterative process can be used to improve this function following the decrease of the energy. The general algorithm is as follows: in HF-SCF an initial guess wavefunction (Slater determinant²⁸ to account for antisymmetry property in fermions, like the electrons) is used to construct the Fock operator²⁹ \hat{f}_i (Eq. (III.4)) and to solve a one electron Hamiltonian (Eq. (III.5)).

$$\hat{f}_i = -\frac{1}{2}\nabla_i^2 - \sum_{A=1}^M \frac{Z_A}{r_{iA}} + V_{HF}(i) \quad (\text{III.4})$$

$$\hat{f}_i \psi_i = \epsilon_i \psi_i, i = 1, 2, \dots, N \quad (\text{III.5})$$

In which we have changed to atomic units (from now on). The first term is the kinetic energy, the second one the nucleus-electron potential (Z_A is the charge of the nucleus A , r_{iA} is the distance between electron i and nucleus A , for M nuclei) and the last term is the Hartree-Fock potential describing the mean field produced by the other electrons. In this last term there are a *Coulomb* and an *Exchange* contribution integrals depending on the spin-orbitals of a j electron but also on the i electron (this is why an iterative procedure needs to be used, the operator itself depends on the spin-orbital wavefunction it is applying on) [137]. The *Coulomb* integral describes the classical repulsion between two charge clouds, and the *Exchange* two-electron integral has not classical analog and describes the correlated motion of electrons with parallel spin (in the single determinantal approximation)³⁰. When we solve the equation (III.5) we subsequently obtain the eigenvectors (spin-orbitals) ψ_i and its corresponding energy ϵ_i (eigenvalues) for each electron.

The solution gives a new set of wavefunctions that can be used in a new cycle until a controlled parameter (mean field potential or electronic density) does not change in a predefined threshold value. The main problem with HF is that it does not describe well the electron correlation, specifically the one originated by non-parallel spin electrons³¹ [137]. The original method was subsequently improved trying to solve this last inconvenient. Since then, more accurate approaches known as Post Hartree-Fock methods were developed, some examples are: Configuration Interaction (CI) and Coupled Clusters (CC) methods which basically share (in different ways) a multideterminantal approach to describe the real wavefunction [138]. Møller-Plesset (MP n) perturbative method at different orders n (the most common being $n=2$) is another post-HF method

²⁸ It is a mathematical way to construct the total wavefunction of a multi-fermionic system and satisfied the antisymmetry property taking advantages of the properties of determinants. Because electrons are fermions the exchange of two of them have to change the sign of the total wavefunction.

²⁹ In practice the method is described in a matricial form, which is more suitable for computational calculation.

³⁰ The functional form of these two operators can be seen in reference [137].

³¹ The problem arises from the use of a single Slater determinant description of the wavefunction.

THEORETICAL METHODS

commonly used. Because of its importance and its use in this thesis work, the MP n method will be described a little bit more.

Møller-Plesset perturbation theory is not a variational method. Instead, it is based on the Rayleigh-Schrödinger perturbational theory. In this approach, the total Hamiltonian of the system is divided in two parts: a zero-order Hamiltonian \mathcal{H}_0 (taken as the sum of one-electron Fock operators of the HF-SCF) which has known eigenfunctions and eigenvalues, and a small perturbation \mathcal{H}_1 which is indeed the variable related to the corrections of the energy [137]:

$$\mathcal{H} = \mathcal{H}_0 + \lambda\mathcal{H}_1 \quad (\text{III.6})$$

The eigenvectors $\Psi(r)$ and eigenvalues ε of \mathcal{H} are then represented in a Taylor series in λ (ordering parameter). Then, the first steps include the use of orthonormality relations between the eigenfunctions, substitution of the developed series of $\Psi(r)$ and ε in equation (III.6) and equalization of common terms in λ . After some mathematical treatments the corresponding values of the n^{th} -order energy terms in the Taylor expansion are found. The first two terms are equal to the HF energy, so to improve this value we must use at least the second order-energy correction $E_i^{(2)}$ [137], [139].

Depending on the amount of terms n used in the expansion the method takes the name MP n . The MP2 method is the most employed because of the increasing computational effort for higher order and slow improvement in accuracy for calculated parameters [140]. Nevertheless, MP3 and MP4 are used and implemented in many quantum chemical packages. Analytical energy gradients and second derivatives are available for MP2, which speed up calculations. So, MP2 is a good choice for ground states calculations with high accuracy and speed if some electronic correlation wants to be directly taken into account.

III.2. Basis functions

As we already mentioned molecular orbitals (MO) are formed from linear combinations of atomic orbitals in the LCAO approximation (see section II.3.). But, first these atomic orbitals need to be defined in the best “mathematical” way. The construction of atomic orbitals is based in the form of the solution of the wavefunction for the hydrogen atom, in which an angular (spherical harmonics) and a radial function (that includes an exponential decay dependence) are present.

These orbitals are called Slater type orbitals (STO) and even if they are a very good approximation to the description of hydrogenic orbitals they have a big limitation. There is no analytical solution for the integrals in which there is a radial decay of the type e^{-r} . In order to overcome this issue, Boys (1950) proposed the

use of Gaussian radial decays e^{-r^2} whose integral have analytical solution [141]. In that frame, the general functional form of a normalized Gaussian type orbital (GTO) in atom-centered Cartesian coordinates is [138]:

$$\phi(x, y, z; \alpha, i, j, k) = \left(\frac{2\alpha}{\pi}\right)^{\frac{3}{4}} \left[\frac{(8\alpha)^{i+j+k} i! j! k!}{(2i)! (2j)! (2k)!}\right]^{\frac{1}{2}} x^i y^j z^k e^{-\alpha(x^2+y^2+z^2)} \quad (\text{III.7})$$

Where x , y and z are the Cartesian coordinates; α is an exponent that controls the width of the GTO; i , j and k are non-negative integers values. The first and second expressions (in parenthesis and brackets) are a normalizing factor; the third part (Cartesian pre-factors) defines the angular dependence and the last part defines the radial decay. Trying to recover the good description of STO, Pople proposed to describe one STO by a linear combination of GTO (computationally more efficient). This scheme is known as “contracted”.

A general mathematical representation of the contracted basis set used to construct a molecular orbital is [142]:

$$\psi = Y_{lm} \sum_i C_i \sum_j C_{ij} e^{-\xi_{ij} r^2} \quad (\text{III.8})$$

Where Y_{lm} function gives the correct angular symmetry to the orbital; e^{-r^2} is called Gaussian primitive function; C_{ij} and ξ_{ij} are the contraction and exponent coefficients respectively (read from a database), and C_i is the molecular orbital coefficient which need to be optimized during the SCF calculation using the variational principle.

One of the best examples is the basis set proposed by Pople, Stewart and Hehre in 1969, name STO-MG, and where M (2 to 6) represents the number of gaussian functions that describe one STO. For example, STO-3G means that each STO orbital of each atom in the molecule is represented by 3 gaussian functions. They also found that the optimum combination of speed and accuracy was achieved for M=3: the STO-3G (known as “minimal” or “single- ζ ” basis set) [138]. In this basis set there is only one basis function defined for each type of orbital (from the core to the valence type of electrons). More flexibility can be gained if we describe core and valence orbitals through different basis functions. These are called “split-valence” or “valence-multiple ζ ” basis sets, and usually represent the core orbital by a single “contracted” basis function while the valence orbitals are split into many functions [138]. An example is the Pople’s basis sets, e.g.: 3-21G, 4-31G and 6-311G (there are more). In this case the nomenclature is a guide to the contraction scheme, let’s give an example with 6-311G. The first number (6) indicates the number of primitives used for the contracted core functions. The other numbers (311) indicate the number of primitives used in the valence functions. In the case of 311 there are five primitives in total with three contractions. The number denotes the number

THEORETICAL METHODS

of primitives forming each contraction. If there are two numbers (*e.g.* 4-31G) it is called valence-double- ζ basis, if there are three (*e.g.* 6-311G) is called valence-triple- ζ basis. Pople's basis sets are called also "segmented" basis sets because the primitive used for one basis function are not the same for another with the same angular momentum.

On the other hand, there exists the so called "general" contraction. In this scheme the same set of primitives is used in all contracted basis functions, with different coefficients. It is more computationally efficient, reducing in this way the amount of calculation time. An example is the Dunning basis set, which uses the *cc-VXZ* nomenclature (*correlation consistent* Valence X Zeta), in which X can be double (D), triple (T), and so on.

Additional flexibility to these sets can be achieved by the use of polarization and diffuse functions. In the first case a specific number of higher angular primitives are added to the original basis set, *e.g.* *p* functions for H, or *d* functions for C. The addition of these functions gives the wavefunction more flexibility to change its shape and describe bonds. In Pople's basis set the polarization functions are indicated by one or two " * ", if functions are added to second (and beyond) row elements or to H and He also (*e.g.* 6-31G**) ³², respectively. In Dunning basis set they are indicated by the *p* letter (from *polarized*), *e.g.* *cc-pVTZ*. On the other hand, diffuse functions are primitives with small exponents that allow the description of the shape of the wavefunction far from the nucleus. They are also called "augmented" basis set, and are suitable to describe anions, Rydberg states, van der Waals interactions, hydrogen bonds [138], etc. In Pople's basis set the addition of diffusion functions is indicated by one "+" if they are only added to non H atoms or by two "++" if hydrogens are also included (6-31G++). In the case of Dunning's basis set they are marked at the beginning by "aug" name, *e.g.* *aug-cc-pVTZ*.

Finally, before the next section, it is worth to mention that one of the next four approximations will be always one of the sources of problems to take into account in *ab initio* calculations [142]:

1. Born-Oppenheimer approximation (validity)
2. Omission of relativistic effects (in the Hamiltonian)
3. Incomplete electronic correlation
4. Use of an incomplete basis set

The quantum chemical calculation presented in this work were done in the range of validity of the Born-Oppenheimer approximations and with a big basis set (6-311++G(3df, 3pd)). Taking into account that no heavy atoms are present in the set of molecules studied in this thesis, the relativistic effects can be

³² Nowadays because many different polarization functions can be added, it is more common to explicitly indicate the type of function used, *e.g.*: 6-31G(3df, 3pd). In that case the first group in the parenthesis is the functions added to non-first row elements, and the second the one added to H and He.

neglected. In this case, the main source of deviation from a good description of the geometry, the energy and the frequency calculations should be a good description of the electronic correlation.

III.3. Density Functional Theory

Ab initio methods can give very good results for properties of molecular systems (*e.g.* geometry, etc.) if the correct method and basis set are chosen. The main practical drawback is the high computational cost they demand: memory, disk space, computer processor time. For example HF scales as N^4 , MP2 as N^5 , CISD (Configuration interaction with Single and Double excitations) as N^6 and CCSD (Coupled Clusters with Single and double excitations) as N^6 where N is the number of two-electron integrals [143]. One way to overcome this problem is employing semi-empirical methods. In this case some of the integrals are parameterized and are not calculated, but consequently higher errors are obtained in general. In between *ab initio* and semi-empirical methods we have the Density Functional Theory (DFT) method.

DFT is based on the fact that the energy of a system can be determined from the electronic density (ρ) instead of the wavefunction. This was demonstrated for non-degenerated ground states in two theorems by W. Kohn and P. Hohenberg in 1964. The extension for degenerated ground states was made by Levy some years later [144]. The possibility of practical applications of DFT arrived after the publication of the Kohn-Sham method in 1965 [145]. This method is similar to HF-SCF procedure. First they recognized that the total ground-state energy of an n -electron interacting system can be written as:

$$E[\rho] = E_K[\rho] + J[\rho] + V_{Ne}[\rho] + E_{XC}[\rho]$$

Where $E_K[\rho]$ is the total electron kinetic energy, $J[\rho]$ electron-electron potential, $V_{Ne}[\rho]$ the electron-nucleus potential and $E_{XC}[\rho]$ the exchange-correlation energy. The density is obtained from the N orthonormal spin-orbitals functions $\Psi_i(r)$ as³³ [139]:

$$\rho(r) = \sum_{i=1}^N |\Psi_i(r)|^2 \quad (\text{III.9})$$

And the spin-orbital functions are obtained through the Kohn-Sham (KS) equations³⁴:

$$\left\{ -\frac{1}{2}\nabla^2 - \sum_{A=1}^M \frac{Z_A}{r_{A1}} + \int \frac{\rho(r_2)}{r_{12}} dr_2 + V_{XC}(r_1) \right\} \Psi_i(r_1) = \varepsilon_i \Psi_i(r_1) \quad (\text{III.10})$$

³³ These spin-orbital functions are developed in linear combinations of basis functions like in Hartree-Fock.

³⁴ They are similar to the Hartree-Fock equations except for the term $V_{XC}(r_1)$.

THEORETICAL METHODS

Where 1 and 2 represent two different electrons, Z_A is the charge of the A nucleus, r_{A1} the distance between nucleus A and electron 1, $\rho(r_2)$ is the electron density at 2, r_{12} the distance between electrons 1 and 2, ε_i are the KS orbital energies of the electron orbitals $\Psi_i(r_1)$ and $V_{XC}(r_1)$ is the exchange-correlation potential which is defined as:

$$V_{XC}[\rho] = \frac{\delta E_{XC}[\rho]}{\delta \rho} \quad (\text{III.11})$$

Like in HF-SCF this set of equations is solved iteratively and self-consistently, since V_{XC} depends on the density (which depends on $\Psi_i(r_1)$). First, we need to define an initial guess density function (superposition of atomic electron densities or from a previous HF calculation). Then, the exchange-correlation functional $V_{XC}[\rho]$ is calculated by assuming an approximated form of $E_{XC}[\rho]$, in which its functional dependence on the electron density is expressed as an interaction between the electron density and an “energy density” $\varepsilon_{XC}[\rho(r)]$ [138]:

$$E_{XC}[\rho] = \int \rho(r)\varepsilon_{XC}[\rho(r)]dr \quad (\text{III.12})$$

The simplest is the Local Density Approximation (LDA) in which the real inhomogeneous system is divided into infinitesimal volumes, and the electron density in each of the volumes is taken to be constant. The energy density has as property that it can be divided as the sum of the two components: exchange and correlation. Once the form of $E_{XC}[\rho]$ and consequently $V_{XC}[\rho]$ are known, the Kohn-Sham equations are solved and a new set of spin-orbitals obtained. From this new set of orbitals, we can compute the electronic density function and repeat again the process until its value does not changes in a predefined amount. If we know the forms of the exchange-correlation potential V_{XC} and energy E_{XC} we can obtain the exact energy of the system. In practice, the form of the exchange-correlation functional is unknown.

Several functionals have been proposed until today and every year many studies are still published in this field. Some of these functionals were developed by parameterizing a function to reproduce experimental results in the best way, while others were constructed from fundamental quantum mechanics principles. So, the choice of the functional is essential to get a good description of the system or the expected property to compute. Better approximations compared to LDA have been proposed, for example generalized gradient approximation (GGA), meta-GGA and hybrids functional. GGA and meta- GGA methods includes the gradient of the density in the first case and additionally the second derivatives of the density and the kinetic energy for the second case. These terms include more degrees of freedom and increase the knowledge of the

behavior of the density, increasing the accuracy compared to results that can be obtained with LDA approximation [146].

Nowadays, hybrid functionals are very popular when computing molecular properties like geometry, frequency spectrum, polarizability, thermochemistry, etc. These functionals mix HF exchange and DFT exchange-correlation functional with weight coefficients. As an example of these functionals, we can mention the well-known B3LYP (Becke and 3 parameter Lee-Yang-Parr) functional [147]–[150], and the Minnesota family of functionals [151]. B3LYP functional has been used for a long time in organic molecules to compute thermochemistry properties and spectroscopic data as well [150]. Its performance is surprisingly good compare to other functionals, and it is why it is the most used functional till the date. On the other hand, Minnesota family are hybrid meta-GGA functionals. They are very good for thermochemistry and kinetics parameters. In particular, the M06-2X functional is very suitable when non covalent interactions (*e.g.* hydrogen bonds) are present [146] and has shown a good description of geometry and frequency in halogenated molecules.

The main advantage of DFT over *ab initio* methods is its reduced computational time and “good accuracy” when determine thermochemical properties, optimized geometries, frequency calculations, among other properties. Nevertheless, it should be kept in mind that if a high degree of accuracy on some properties like the optimized geometry or the energy (just to mention two) want to be achieved post-HF methods are more adequate.

III.4. NCI calculations

Non covalent interactions are characterized by small perturbations of the electron density of different interacting groups. These kinds of interactions are usually theoretically studied by means of topological methods focused on the electronic density. Example of those methods are: QTAIM (Quantum Theory of Atoms in Molecules) [152], [153] and ELF (Electron Localization Functions) [154], [155]. Nevertheless, these methods are not always suitable to detect the presence of such weak interactions [156]. A relatively new alternative to these methods is the NCI technique [157]. NCI is based on the analysis and graphical interpretation of the electronic density (ρ) and its derivatives (second eigenvalue λ_2 of the Hessian³⁵ of ρ)³⁶ and the reduced density gradient $s(\rho)$ defined as [157], [158]:

³⁵ Square matrix of second-order partial derivatives of a scalar function

³⁶ In the topological approach of bonding theory, the Laplacian of the density is usually decomposed into the contributions along the three particular axes of maximal variation. These are also the three eigenvalues, λ_i , of the density Hessian matrix, such that $Tr[\nabla^2\rho] = \lambda_1 + \lambda_2 + \lambda_3$, $\lambda_1 < \lambda_2 < \lambda_3$. The sign of λ_1 and λ_3 are well known

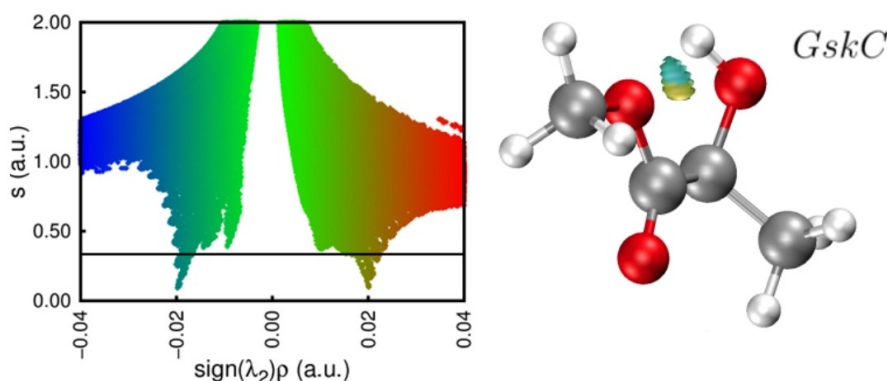


Figure III.1: Example of the visualization of an NCI calculation (Adapted with permission from ref. [160]. Copyright (2015) American Chemical Society). Left: Graph of $s(\rho)$ vs $\text{sign}(\lambda_2) \cdot \rho$. Right: Molecule under study and 3D NCI isosurface. A hydrogen bond interaction is shown, weaker non covalent interactions appears at lower values of ρ .

$$s = \frac{|\nabla\rho|}{2(3\pi^2)^{1/3} \cdot \rho^{4/3}} \quad (\text{III.13})$$

The procedure to reveal the presence of weak interactions focuses on regions far from the nuclei, where weak inter and intramolecular interactions manifest themselves from singularities of the electron density [159]. These singularities appear because of the perturbation of the electronic clouds of the interacting groups, which influence the density and its related properties. From a practical point of view, the NCI method rest on the visualization of singularities with low reduced density gradient placed at low values of density. The interaction can be visualized by means of the graph $s(\rho)$ vs $\text{sign}(\lambda_2) \cdot \rho$ and the NCI isosurface, which allows to observe in which region the interaction takes place. A typical example is shown in Figure III.1 [160] The sign of λ_2 is included because it helps to distinguish between attractive and repulsive interactions (*e.g.* steric repulsion). The first are characterized by negative values of λ_2 while the second by positive values.

III.5. Infrared and Raman scattering theoretical calculation

III.5.1. Normal modes and frequencies

In a vibrational calculation, the first goal is to obtain the symmetry and frequency values of the normal modes of vibration. The most important point to take into account is that the geometry of the molecule must be (first) optimized at the same level of theory and with the same basis set³⁷ that will be used to make

depending if we are in a maximum, a minimum or another region. But, the sign of λ_2 in regions out of minima or maxima varies depending on different variables [153].

³⁷ The optimized geometry corresponds to a minimum in the PES of the system, and the minimum found depends on the method and basis set used. If a different method and/or basis set is used for the frequency calculation (compared to the optimization) the computation might not be made in the real corresponding minimum, and false results are obtained.

the frequency calculation. The algorithm requires diagonalization of the Hessian matrix of the system, related to the second derivatives of the potential in respect to nuclei displacements (force constants), and as a consequence the result gives the normal modes and their frequencies [146]. This implies the use of a harmonic potential to describe the vibration. The frequency calculation is in fact mandatory because depending on the frequency values we can determine if our optimized structure is a minimum or a transition state (TS). For the first one, real positive values are obtained, while in the second one frequency is imaginary (the lowest frequencies).

It is well known that the harmonic potential does not reproduce many features of the vibrational behavior of quantum systems, *e.g.*: overtones, combination bands, etc. Some fundamental vibrations are also badly described. This is mainly due to the fact that the real potential energy surface (PES) is not a harmonic function. If we want to obtain a better description of the potential curve of the system, anharmonic terms need to be added to the original harmonic function. When an anharmonic potential is used, overtones, combinations bands, as well as a better description of the frequencies can be obtained. But, the computation of n^{th} order derivative of the potential demands a lot of calculation power, and sometimes they are very long or impossible to do. This will also depend on the basis set size as well as the level of theory or method used [138], [161]. Different algorithms have been developed like the VPT2 (Second order vibrational perturbational theory) used in Gaussian software, to obtain the anharmonic vibrational properties [162].

An economic (in time), different and very extend way to adjust the harmonic frequencies is the use of direct scaling factors. In this procedure, the obtained harmonic frequencies are multiplied by a constant factor to correct their position. These factors are published for different combinations of methods and basis sets, and are obtained after comparison with a set of standard molecules for which their frequencies are well known [146]. Generally, the dependence on the basis set is weak, and similar scaling factors can be used when we pass from a small basis set to a bigger one. But, attention must be paid to the fact that in order to obtain more reliable frequency values we need to include polarization functions in the basis set [163].

Nevertheless, even when good results are obtained for many systems, attention should be paid in systems with highly anharmonic modes (*e.g.*: OH localized stretching modes), and to the fact that not all modes are corrected in the same way (region dependence of the scaling factor) [146].

III.5.2. IR and Raman intensities

The second step of a vibrational calculation is to determine the Raman and IR intensities for each mode. In the case of IR, the intensity of a band is proportional to $\left(\frac{\partial \mu}{\partial Q_i}\right)^2$. So, we can determine the intensity through

THEORETICAL METHODS

the first derivative of the dipole moment with respect to the normal coordinate. The evaluation can be made from analytical formulae (available for some methods) or from numerical evaluation, which is more computationally demanding³⁸. The intensity of each transition is usually calculated in the harmonic approximation, but anharmonic intensity calculations are also possible [164].

In the case of Raman, the intensity of the transition can be evaluated through the change of the electronic cloud polarization with respect to the nuclei displacements [146] or the numerical differentiation of analytical dipole derivatives with respect to an electric field (both implemented in Gaussian09). Programs like Gaussian actually compute the Raman scattering activity (S_i^R):

$$S_i^R = g_i(45\bar{\alpha}_i^2 + 7\beta_i^2) \quad (\text{III.14})$$

Where g_i is the degeneracy of the vibrational mode i , and $\bar{\alpha}_i$ and β_i are the mean and anisotropy values of the polarizability derivative tensor $\left(\frac{\partial\alpha}{\partial Q_i}\right)$. In order to obtain the absolute differential Raman scattering cross section, directly proportional to Raman intensities (I_i^R), equation (III.15) derived by Polavarapu should be used [165], [166]:

$$I_i^R = C \cdot \frac{(\omega_0 - \omega_i)^4}{\omega_i \cdot \left(1 - e^{-\frac{hc\omega_i}{kT}}\right)} \cdot S_i^R \quad (\text{III.15})$$

Where, ω_0 is the laser excitation wavenumber, ν_i is the calculated wavenumber of the i th mode (both in cm^{-1}), h , k , c and T are Planck and Boltzmann constants, speed of light and temperature. In the original derivation C equals $\frac{2\pi^2 h}{45c}$, but some groups use it as variable parameter to better fit the entire spectrum [167], [168].

In addition to the vibrational spectrum the other important information obtained from frequency calculations is the zero-point vibrational energy (ZPE). This corresponds to the minimum energy of the molecular system at 0 K and is obtained through the sum of the wavenumbers (ω_i) of all normal modes in their ground vibrational state ($v = 0$):

$$E_{ZPE} = \frac{1}{2}hc \sum_i \omega_i \quad (\text{III.16})$$

³⁸ The dipole moment is evaluated from quantum chemical methods and the dipole moment derivatives are calculated by numerical differentiation.

The ZPE is added to correct the energies obtained through electronic calculation where the system is placed at the bottom of the potential well, which does not have a real physical meaning.

Finally, a few words about the methods and basis set. It is known that MP n methods yield good values for the relative energies (because of the good description of correlation) and less accurate values for vibrational frequency calculations compared to DFT [169][170]. So, if we take also into account that the latter requires less computational effort (meaning less time), it is not strange to think in DFT as our primary choice for a common frequency calculation. An important fact to take into account is that in order to obtain reliable results, basis set bigger than 6-31G* need to be used [140].

III.6. Electronic absorption spectrum

As we already saw in Section II.3. an electronic excitation involves the transition between electronic states of a quantum system. Electronic transitions can proceed as “vertical” transitions or as “adiabatic” transitions. In the first case the nuclear geometry and its kinetic energy do not change (Franck-Condon principle), and the system can be found in a non-equilibrium geometry of the excited state. In the second case, the system is able to adapt to the new conditions of the excited state, which means that it can be found in the closest local optimized geometry. Both kinds of transitions can be theoretically described by different methods, but we will only describe those concerning vertical transitions.

There are different approaches used to compute vertical transitions, among them ZINDO, TD-DFT, CIS(D) and EOM-CCSD. ZINDO (Zerner's Intermediate Neglect of Differential Overlap) is a semi-empirical method specially parameterized to reproduce UV spectrum of organic molecules [171]. It is very fast but the obtained values can have considerable errors [172]. CIS(D) is a size-consistent double correction to CIS [173]. It can be considered as an excited state analog of the ground state MP2 method. Its main drawback is that it does not work well in systems whose ground and excited states cannot be described by a single-configuration reference wavefunction. EOM-CCSD (*Equation of Motion Coupled-Cluster with Single and Double excitation*) is a variation of the Coupled Cluster method which allows to describe many-configurational wavefunctions within a single-reference formalism. This method can be computationally expensive and is mainly use in small systems [174]. On the other hand, TD-DFT method is an extension of DFT to treat excited states. It is based on the time-dependent Kohn-Sham equations, derived from the time-dependent Schrödinger equation. Like in DFT, the accuracy of the method is related to an appropriate description of the exchange and correlation contributions. The method does not work well in the study of Rydberg states, double excited states, charge-transfer states and large π system [146]. Also, Wiberg *et al.* found that there is not a big

THEORETICAL METHODS

dependence on the choice of the functional when hybrid functionals are used [175]. They also suggest that the 6-311++G** basis set is flexible enough to obtain reliable results. The error of the method for valence-excited states is within 0.5 eV of experimental value [146]. Finally, it should be pointed out that UV spectra cannot be rigorously calculated as the energy gap between the HOMO/LUMO orbitals because these are computed for the ground state.

III.7. Relaxed and non-relaxed rotational barriers

Energy barriers are defined as the path followed by the system when it goes from an initial stable configuration to another one, passing through an intermediate state known as transition state (TS). In principle there are many pathways to overcome the barrier³⁹ that separated both states, whether one or another is favored depends on the physical process involved and the characteristics of the system (Some of the pathways mixed rotational and vibrational motions).

In quantum chemistry a scan is a process in which the change of configuration is done by changing at least one coordinate. In a “relaxed” scan, each step is defined by the controlled change of that internal coordinate (we can say that this is the scanning coordinate) while the rest of the internal variables are free to adjust in order to minimize the energy of the system. The system will then follow a minimum energy path.

A similar way to compute a relaxed energy barriers, is the use of an Intrinsic Reaction Coordinate calculation, also known as IRC [176]. This method is primary intended to check the configuration of a transition state. In this case we need to know *a priori* the transition state, it means, the configuration of the system at the point of maximum energy in the barrier (it can be obtained in different ways, one of them is a transition state optimization algorithm). Then the system evolves following a “reaction coordinate” in the backward and forward directions. If the initial transition state is the “real” one the final states will coincide with the ones previously expected. In the process, an equivalent “relaxed scan” is made.

Another possibility is to scan the same internal coordinate and calculate directly the energy of the system in each step without further optimization of the other coordinates (Single point calculation). This is called a “non-relaxed” scan. It is adapted to processes in which a variable (scanned variable) changes faster than the others.

³⁹ In fact, the barrier changes depending on the pathway taken to go from one state to the other

III.8. Tunnel effect and WKB approximation

The tunnel effect is one of the clearest differences between classical mechanics and quantum physics. In this one a particle can go through a potential energy barrier without surmounting the potential hill (as needed in the classical framework). In the quantum limit there is always a small probability to find the particle on the other side of the barrier.

There are different ways to estimate the probability of tunneling through a barrier for a quantum system [177]. One of them is to solve the Schrödinger equation and to obtain the probability of finding the particle at a distance r , and compare it to the barrier width. To solve the Schrödinger equation is not always an easy task, even with numerical methods, so approximated methods are commonly used instead.

The Wentzel-Kramers-Brillouin method (also known as WKB) is used to find approximate solutions to linear differential equations with spatially varying coefficients, which is the case of the Schrödinger equation [178]. When this method is applied to the Schrödinger equation, with a potential curve $V(x)$ an approximate solution is obtained for the wavefunction and consequently for the transmission coefficient or permeability of the barrier. The permeability is associated with the probability of tunneling to occur and it can be represented as [178]:

$$P(\varepsilon) = \frac{1}{1 + e^{2\theta(\varepsilon)}} \quad (\text{III.17})$$

In which:

$$\theta(\varepsilon) = \frac{1}{\hbar} \int_{x_1}^{x_2} \sqrt{2\mu[V(x) - \varepsilon]} dx = \frac{1}{\hbar} \int_{x_1}^{x_2} f(x, \varepsilon) dx \quad (\text{III.18})$$

This allows us to obtain the tunnel constant rate as:

$$k_{WKB} = \omega_0 \cdot P(\varepsilon) \quad (\text{III.19})$$

In this equation we have a term that represents the number of times that the particle (of reduced mass μ) tries to pass the barrier, ω_0 (in Hz), and another term representing the probability $P(\varepsilon)$ of this event to occur for a given kinetic energy ε of the particle. In expression (III.18) we use the calculated form of the barrier $V(x)$ to obtain $f(x, \varepsilon)$ and integrate between the limits x_1 and x_2 , which are defined by the turning points where $V(x) - \varepsilon = 0$.

THEORETICAL METHODS

The advantage of the method is that we only need to know the form of the potential energy curve, and there is no need to solve the Schrödinger equation. Despite this advantage, it should be clear that the method is an approximation and no precise quantitative results are obtained but only orders of magnitude.

III.9. Theoretical calculations details

All the calculations presented in this work were run in the GMPCS cluster (Grappe Massivement Parallèle de Calcul Scientifique) at Orsay, Université de Paris-Saclay, using Gaussian09 software [134]. GaussView 5 and Chemcraft [179] software were used to prepare input jobs and visualize output results. NCIPLOT software [157], [180] was used to perform the non covalent interaction study. In this case the output was visualized with VMD program.

III.9.1. Geometry optimization and frequency calculations

Geometry optimizations were performed for all molecules and all isomers (keto and eight enol forms) of each β -dicarbonyl molecule followed by frequency calculations. In all the steps we used DFT level of theory with B3LYP [148], [181] or M06-2x [151] functionals and 6-311++g(3df,3pd) basis set. M06-2X functional was mainly used for halogenated analogs, in which it has a better performance compared to B3LYP, as checked by our calculation. A very tight convergence criteria and ultrafine (-96032 in M06-2X) optimization grids were also used. Vibrational frequencies were obtained by means of harmonic approach. Anharmonic values were also obtained for deuterated acetylacetone and 2-chloromalonaldehyde. For the presented harmonic spectra, different scaling factors were used for each molecule. The values were optimized to fit the theoretical results to the experimental values taking into account the interaction between the host and the molecule.

III.9.2. Rotational barriers

Rotational barriers between *cis* and *trans* positions of OH/OD in open enol conformers of acetylacetone were obtained through relaxed scans, using CCOH/CCOD, respectively, dihedral angle as variable parameter, with 10 and 15 degrees steps. Frequency calculations were performed for initial, final and transition states (TS) in order to account for the Zero Point Energy corrections (ZPE). Each TS structure was optimized through a Berny optimization algorithm [182]–[184], and confirmed through an Internal Reaction Coordinate (IRC) calculation. Calculations related to the barrier were done at the MP2 level of theory using the same basis set as mentioned before.

III.9.3. Electronic vertical transitions

The energy of the vertical transitions was determined by means of the TD-DFT method [185] as implemented in the Gaussian 09 suite of programs. First, the ground state of each conformer in each analog was previously optimized and verified through a frequency calculation. Very tight convergence criteria and ultrafine optimization grids were used. Both calculations were performed at the same level of theory of the TD-DFT calculation. A B3LYP/6-311++G(3df, 3pd) level of theory was used in all cases. After, the optimized geometry was used to compute the vertical transitions energies and oscillator strength of the first five valence excited states using TD-DFT.

Chapter IV Experimental Setup

In this section all the relevant details from experimental setups and synthesis procedures used during the thesis will be mentioned and explained. First, various properties of the molecules under study are presented and the methodology followed for deuteration synthesis of acetylacetone and 3-chloroacetylacetone is described. Second, the three experimental setups used for matrix isolation experiments, two for IR and UV experiments at Orsay and one for Raman experiments at Vilnius, will be presented. Emphasis will be made in the *para*-hydrogen experimental setup used at Orsay because of its importance and special experimental conditions. Then, the optical equipment used during this work is described along with its characteristics. Finally, helium nanodroplet experiment is explained along with the specific conditions used in our setup.

IV.1. Chemical Products

IV.1.1. Quality and physico-chemical properties

The chemical products used in this work as well as some of their more important physico-chemical properties are listed in the Table IV.1.

All the chemical products were used without further purification. For the matrix isolation experiments, each product was stored in a glass (or stainless steel in some cases) reservoir. In the case of liquids, each sample was degassed with freeze-pump-thaw cycles (using liquid nitrogen) after insertion in the reservoir.

IV.1.2. D, D-Acetylacetone and D-Chloroacetylacetone synthesis

Double deuterated acetylacetone (AcAcD₂) was prepared, in general, following synthesis steps published in Dea Kin-Kin doctoral thesis [186]. Roughly, synthesis consists in refluxing, under dry conditions, a mixture of acetylacetone (C₅O₂H₈) and deuterated water (D₂O) for approximately 4 hours at 80-90°C.

We placed 2:10 mL acetylacetone/D₂O volume in a 50 mL glass balloon, with a magnetic bar. The balloon was then connected to a Graham condenser (Liebig condenser was also employed). A three-way adapter, closed in one of its outputs, was placed at the end of the condenser and a vacuum distilling adapter filled

EXPERIMENTAL SETUP

with sodium sulfate⁴⁰ (Na_2SO_4) was connected to the other output (this is an original distillation glassware adapted to our purpose). The temperature and mixing speed of the sample was controlled by a hot plate magnetic stirrer. Sand and oil baths were employed to make a homogeneous and better thermal contact. The scheme of the equipment used is presented in Figure IV.1.

Once the refluxing finished and room temperature equilibrium attained, organic and aqueous phases were extracted and put into a beaker. Then, sodium chloride (NaCl) was added to favor phase separation. Next, the sample was placed in a funnel which allows making phases separation by decantation (the organic phase has lower density). In order to eliminate possible water impurities in the final product we add a small quantity of sodium sulfate and extract the liquid sample with a pipette. The sample was finally stored in the glass reservoir used in the experiments.

A first qualitative test to evaluate deuteration was made through the comparison of the gas phase spectra of deuterated and non-deuterated acetylacetone (Figure IV.2). The comparison between both spectra and the ones published by Ogoshi [55], confirms the success of the deuteration. Attained yield for exchange (deuteration) with non-methyl hydrogens was in general around 90%, value deduced from IR spectra in neon matrix⁴¹. This value includes double (D2) and mono (D1)⁴² deuteration, with a yield of AcAcD_2 always above 65%.

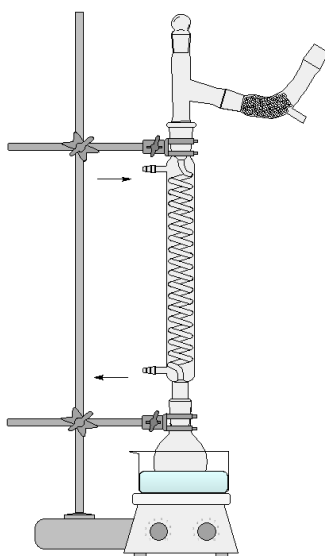


Figure IV.1: Reflux equipment for acetylacetone deuteration. See the text for description.

⁴⁰ To prevent atmospheric water to enter inside the reaction balloon.

⁴¹ This value is relative to the final (total) amount of sample, not to the initial amount of acetylacetone used in the synthesis

⁴² Incomplete deuteration regarding non-methyl hydrogens only

Table IV.1: Physico-chemical properties of compounds under study. The values without references were taken from Aldrich, VWR, Merck and NIST on-line websites.

Molecule	Supplier (Purity)	Molar mass (g/mol)	Vapor pressure (mbar)	Melting Point (°C)	Boiling Point (°C)
Acetylacetone⁴³	Fluka (99.5%)	100.12	8 / 20°C ^a	-23.2	137.9
3-Chloroacetylacetone	Aldrich (97%)	134.56	15 / 20°C	-15	156.0
1,1,1,5,5,5-Hexafluoroacetylacetone	Aldrich (98%)	208.06	NF	NF	69.9
1,1,1-Trifluoroacetylacetone	Aldrich (98%)	154.09	NF	NF	106.9
2-Chloromalonaldehyde	Acros (95%)	106.51	NF	NF (Solid at room Temp.)	NF
Glycolaldehyde*	Aldrich ⁴⁴	60.05	0.26 / 34.5°C ^b	80-90	NF
Propyne	Aldrich (≥97%)	40.06	273 / -49°C	-103.0	-23.2

*In its solid form this compound is found as a dimer.

NF: Not found

Boiling Point and Melting Point are given at 1 bar. ^a Taken from reference [187], ^b taken from reference [188]

⁴³Physico-chemical properties of deuterated acetylacetone are not available

⁴⁴ Purity not given by the manufacture

EXPERIMENTAL SETUP

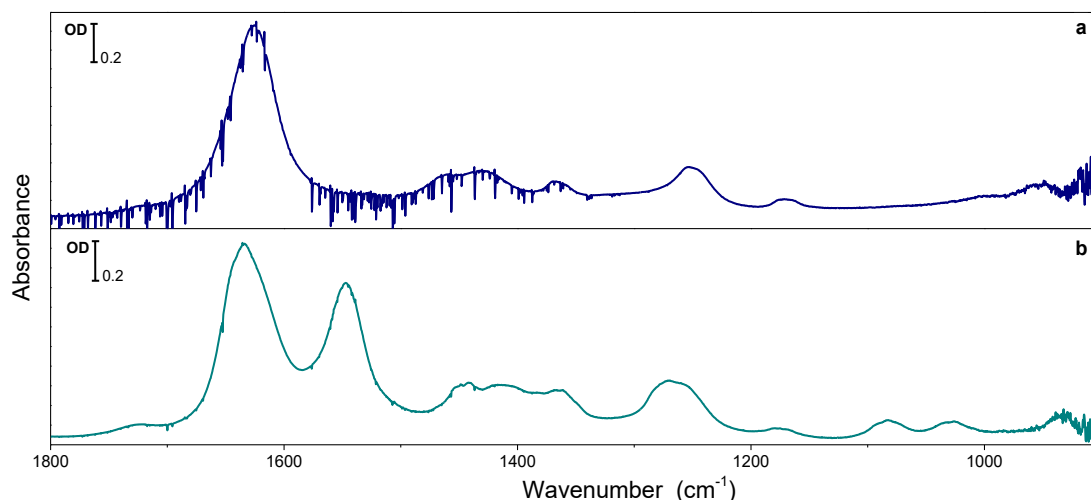


Figure IV.2: Gas phase IR spectra of (a) Acetylacetone 3 torr and (b) deuterated acetylacetone 5 torr, in a glass cell of 20 cm long. Negative bands correspond to non-compensated atmospheric water.

IR bands coming from non-deuterated acetylacetone (AcAcH₈) and the two monodeuterated isotopologues (AcAcD₁) of this compound (taking into account only the two labile hydrogen positions marked with a white color in Figure I.3) can be observed in the spectra. Na₂SO₄ (>99.5%) was purchased at Merck and D₂O (99.9%) and NaCl (>99%) at Sigma-Aldrich.

Exactly the same procedure was followed for the deuteration of chloroacetylacetone. In this case because only one hydrogen atom can easily exchange (the OH hydrogen atom), determination of the degree of deuteration was easier than in Acetylacetone. The obtained yield was over 80%.

At the end of each synthesis the final product was stored in a glass reservoir, connected to a vacuum line and degassed with freeze-pump-thaw cycles. In this way deuteration quality was maintained over long periods (months).

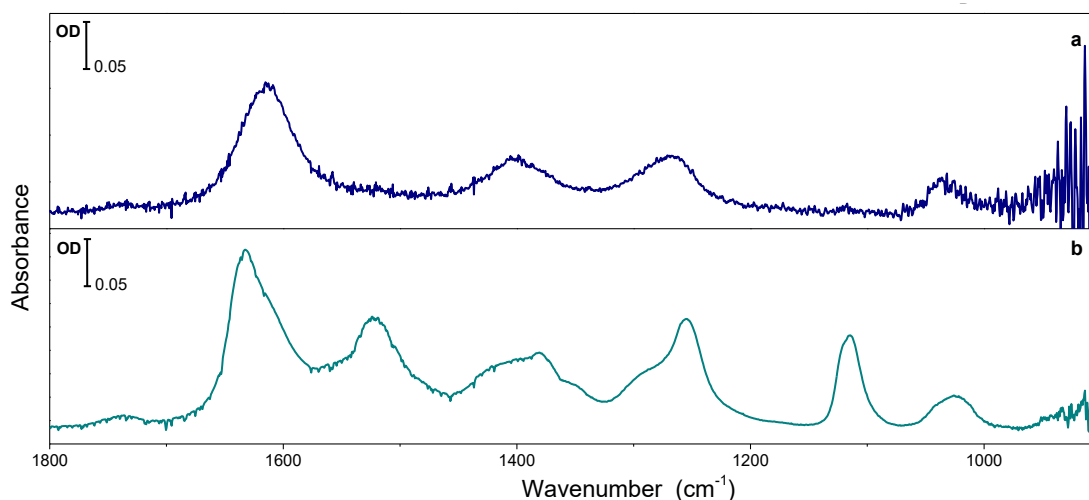


Figure: Gas phase IR spectra of (a) chloroacetylacetone 1 torr and (b) deuterated chloroacetylacetone 1 torr, in a glass cell of 20 cm long.

IV.2. Matrix isolation experiments

FT-IR matrix isolation experiments were done using two different guest/host gas preparation methods, in two different experimental setups available in our lab in Orsay. The main difference between both methods is that in the first one the sample and the host gas were pre-mixed and stored in a buffer volume. While in the second method sample and host gas were mixed directly in the line during the deposition process.

In the first experimental setup in Orsay (Setup #1, see Figure IV.3), the sample and the host gas (around 1-2/1300 torr pressure ratio) were mixed first in a special stainless steel preparation line (first method). The sample vapor was first introduced in the line and after the host gas. Then, the mixture arrived through a 6 mm Swagelok tube to the cryostat chamber where it is deposited onto a Cesium Iodide (CsI) or sapphire internal window (depending on the spectroscopic technique). A variable leak controller Granville-Phillips connected to the line was used to regulate the flow. In this work, deposition times varied from 30 to 40 min, and the deposition rate was around 10 mmol h^{-1} . The internal window (attached to the cold head) was cooled between 7.2 and 8.8 K in a closed cycle He cryostat (APD Cryogenics Inc.), 7K being the lowest possible temperature achieved by our setup at the copper support of the window.

The base of the cryostat is fixed to an optical table, and the internal head is free to turn around its axis. This allows placing the internal window in front of the deposition tube or one of the two optical lines: one for laser irradiation or electronic spectroscopy and the other for FT-IR spectroscopy. The cryostat is pumped by

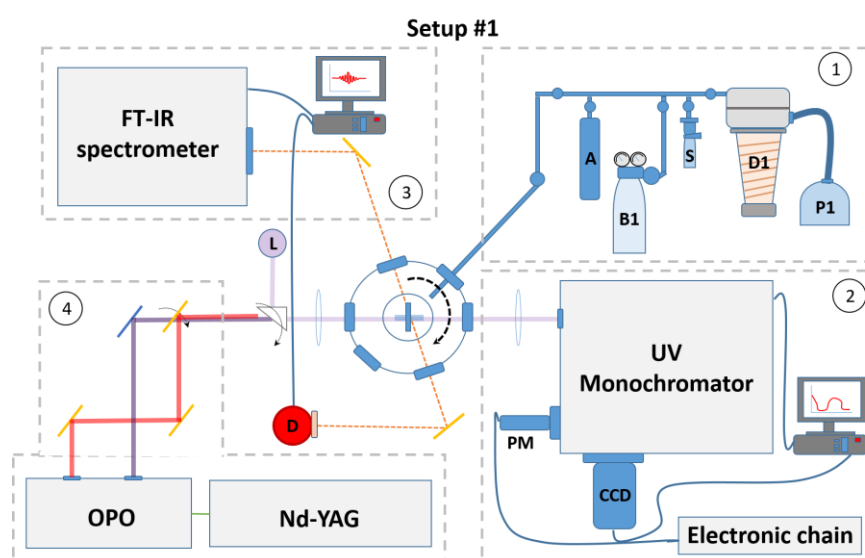


Figure IV.3: Matrix isolation setup for premixed host/guest sample (Setup #1). Zones: 1. Preparation line, 2. UV detection setup (includes lamp source L), 3. IR setup (includes detector D), 4. UV and IR laser system. The cryostat is placed in the middle (blue circles, in axial view), with the external and internal windows. L: deuterium lamp (UV source), D: MCTA detector for IR, A: buffer volumen, S: molecule container, B1: host gas bottle, D1: diffusion pump, P1: primary pump. More details in text. The cryostat is pumped at the bottom by a turbomolecular pump.

EXPERIMENTAL SETUP

a turbomolecular pump (Oerlikon, Leybold vacuum, Turbovac 50) directly attached to the vacuum chamber. This experimental setup was used for all UV experiments and in some of the IR experiments in neon (Messer 5.0) matrices.

The second experimental setup (Setup #2), which employs the second preparation method, was mainly used for $p\text{H}_2$ matrices because the storage of this gas with the required ortho/para quality presents some difficulties⁴⁵. In this case the experimental setup includes two closed cycle helium cryostats: one for the ortho/para-hydrogen conversion process (Air Products, Displex), discussed in section II.6. and the other for the sample deposition (ICE: Innovative Cryogenic Engineering, He Compressor: Sumitomo F-50). Both cryostats are connected through a stainless steel line (Figure IV.4). Two Swagelok microvalves allow controlling the host gas flux and the amount of vapor from the sample entering the line (6 mm Swagelok tube). The mixture of gases arrived directly in front of the internal diamond window, which is attached to the second stage of the cold head of the cryostat. Like in the other setup, the base of the cryostat is fixed to the optical table, and the cold head can rotate around its axis to choose between two optical lines. This setup was also used for some neon and nitrogen (Air Liquide6.0) matrices. In these cases, the first cryostat was maintained at higher temperatures (40 K for Ne, 60 K for N_2) and it was employed to reduce the amount of possible impurities (mainly water). The sample to host gas ratio is not easy to determine *a priori*, due to the lack of precise control over the continuous mixing process. Optimal conditions for deposition of each molecule were set after multiple trials. Matrix quality was verified through the infrared spectrum of the

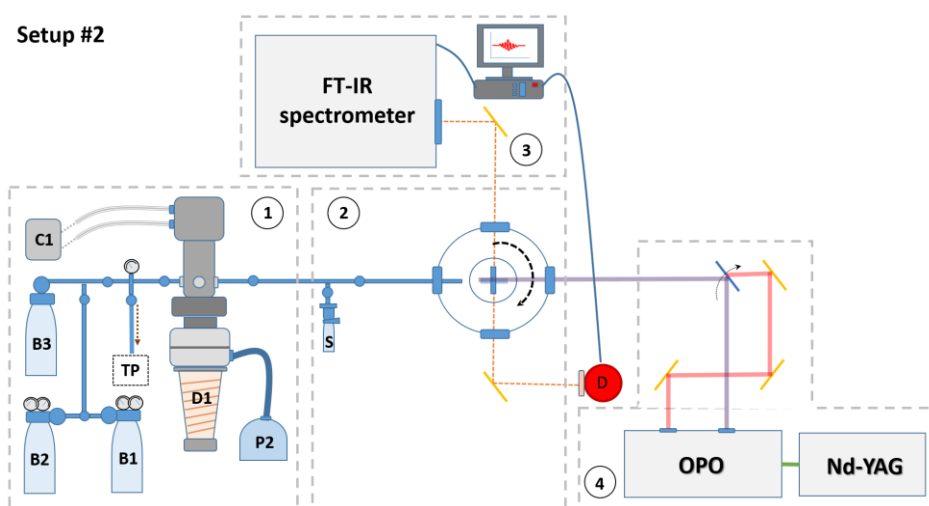


Figure IV.4: Matrix isolation setup (Setup #2). Zones: 1. Ortho-para conversion setup, 2. Main cryostat (for deposition), 3. IR setup (detector D is out), 4. UV and IR laser system. More details in text. S: molecule container, P1 and P2: primary pumps, D1: diffusion pump, C1: compressor, B1: hydrogen bottle, B2: bottle for other host gas (Ne or N_2), B3. Buffer volumen for hydrogen used during the experiment, TP: Turbomolecular pump.

⁴⁵Any ferromagnetic impurity should be avoided in the reservoir and in the best cases the 99.99% *para*-hydrogen purity cannot be kept even for short periods.

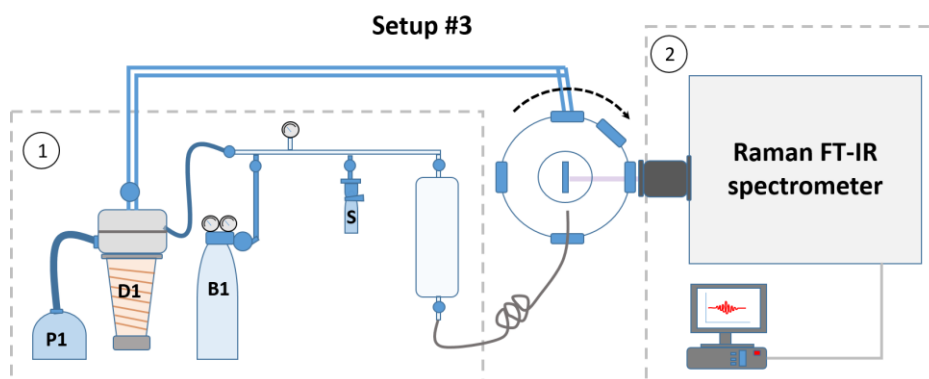


Figure IV.5: Matrix isolation setup used for Raman studies in Vilnius (Setup #3). Zones: 1. Preparation line and vacuum system, 2. Raman setup. The cryostat is placed in the middle (blue circles, in axial view), with the external and internal windows. The dashed arrow indicates that the lower part of the cryostat can rotate.

deposited sample. For non $p\text{H}_2$ matrices, we did not find significant differences in the matrix quality when both methods were used.

In this setup the main cryostat was pumped by a turbomolecular pump (Oerlikon, Leybold vacuum, Turbovac 600C, pumping speed for H_2 : $570 \text{ l}\cdot\text{s}^{-1}$), which allows reaching pressures below 10^{-6} mbar at 293 K. The pump was directly attached to the vacuum chamber of the cryostat to get a better pumping efficiency (very important in the case of $p\text{H}_2$). The $p\text{H}_2$ converter was pumped by a diffusion pump (CIT Alcatel).

Raman and infrared studies in argon matrix (Messer 5.0) were carried out at Vilnius University. The matrix isolation experimental setup (Setup #3) from the group of Valdas Sablinskas and Justinas Ceponkus was used. The experimental setup and working principle is very similar to the one described before in Setup #1: one preparation line for the mixture of gases with multiple entries (made in glass, different from the stainless steel used in the previous cases) connected to a cryostat which is attached to a closed cycle helium compressor (Leybold Hareus RW2), see Figure IV.5. These experiments were conducted at temperatures between 9 and 35 K with guest/host ratio over 1/100 and 1/200. All Raman experiments were carried out with argon as host gas. Deposition times were between 1 and 2 hours, with deposition rates around $10 \text{ mmol}\cdot\text{h}^{-1}$. Concentration was higher than in IR experiments to optimize the small scattering signal for Raman spectra. For Raman measurements, samples were deposited on an aluminum mirror cooled down to 9 K temperature in the closed cycle helium cryostat.

IV.2.1. Deposition conditions

Deposition conditions varied from one molecule to the other, mainly because of the vapor pressure of each compound. For the second deposition method (in Setup #2), cooling baths (ice/water for 0°C , ice/water/ NaCl for -18°C , and N_2 /Ethanol for lower temperatures) were used in some cases to properly adjust the vapor

EXPERIMENTAL SETUP

pressure through the temperature of the sample. The mixtures were always deposited at the lowest temperature reached by each cryostat except for nitrogen matrix⁴⁶ for which 18 K was set as deposition temperature.

For all the molecules (except 2-chloromalonaldehyde) the first deposition method was employed in the Setup #1 and Setup #3. Second deposition method was always used in the Setup #2. In the case of 2-chloromalonaldehyde the second method was the only used in all experiments, because of its low vapor pressure. The reservoir containing the molecule, connected to the deposition line, was completely open in order to collect the maximum amount of molecules: the low vapor pressure of this molecule is entrained by the host gas flow.

The amount of water in the matrices obtained in the Setup #2 were higher than in Setup #1. There are two lines from normal water in *p*H₂ matrix which are mainly observed in the 1700-1500 cm⁻¹ region: one related to ν_2 at 1631.6 cm⁻¹, and a multiplet related to H₂O-*o*H₂ near 1593.7 cm⁻¹. The relative intensity of the bands in this multiplet give an idea of the amount of *o*H₂ in the system and allows to follow its decrease in time through nuclear spin conversion. A very comprehensive work about the assignment of normal and deuterated water in *para*-hydrogen can be found in reference [189]. A similar work was previously developed for water and its isotopologues in neon by Forney *et al.* [190]. In this thesis, water bands will be marked with a “w” in the spectra or by specifying the water isotopologue in the case of deuterated samples.

IV.3. *Para*-hydrogen (*p*H₂) matrix

IV.3.1. Preparation

As we mentioned before the first step to work with a *para*-hydrogen matrix is to obtain this spin isomer gas with a good quality. In our setup the *ortho* to *para*-hydrogen conversion is done in two stages: first, condensation of normal hydrogen (Messer: H₂ 5.6) into a conversion cell completely filled with a catalyst (Fe₂O₃ powder: Sigma-Aldrich 99 %) and maintained at temperatures between 17-20 K. Second, once the proper amount of gas is condensed (around 0.3-0.4 bar) it is left inside the cell for 1 to 2 hours at 14.5-20 K, promoting the conversion. We used a cryostat with a Displex compressor for this purpose. The cold head of the cryostat used in Setup #1 (described before) was also used for *p*H₂ conversion in many experiments.

⁴⁶ This matrix is very fragile, and can easily be broken when very low temperatures are used (T < 10K)

IV.3.2. Spectroscopy

Homonuclear diatomic molecules do not absorb in the infrared region, because there is no change in the dipole moment when the molecule vibrates. But, distortions of the electron distribution (due to collision in the gas phase, or to anisotropic environments in solids) can induce infrared spectral bands. The study of pressure-induced absorption in gaseous hydrogen shows that quadrupole interaction is responsible for most of the intensity of the S ($\Delta J = 2$) band and small part of the Q ($\Delta J = 0$) branches⁴⁷. The assignment of the observed bands was done by Gush *et al.* [191]:

1. Bands corresponding to quadrupolar interactions are observed in the spectrum. Both rotational groups, the $S(0)$ ($J = 0 \rightarrow J = 2$) transition for $p\text{H}_2$ and $S(1)$ ($J = 1 \rightarrow J = 3$) transition for $n\text{H}_2$, show weak single transition $S_1(0)$ and $S_1(1)$, and much stronger double transition of the type $Q_1(J_1) + S_0(J_2)$, $J_{1,2} = 0, 1$. Bands associated to rotational and double transitions involving ortho molecules decrease rapidly in intensity when concentration of $p\text{H}_2$ increases. In pure solid $p\text{H}_2$ the bands become very sharp and double transitions $Q_1(0) + S_0(0)$ show a complex structure. The Q_Q and $S(1)$ bands completely disappear.
2. In the spectrum of pure $p\text{H}_2$, weak double transitions like $2S(0) = S_1(0) + S_0(0)$ in which one molecule executes a ro-vibrational transition and the second one a purely rotational transition in the ground vibrational state, are better observed.

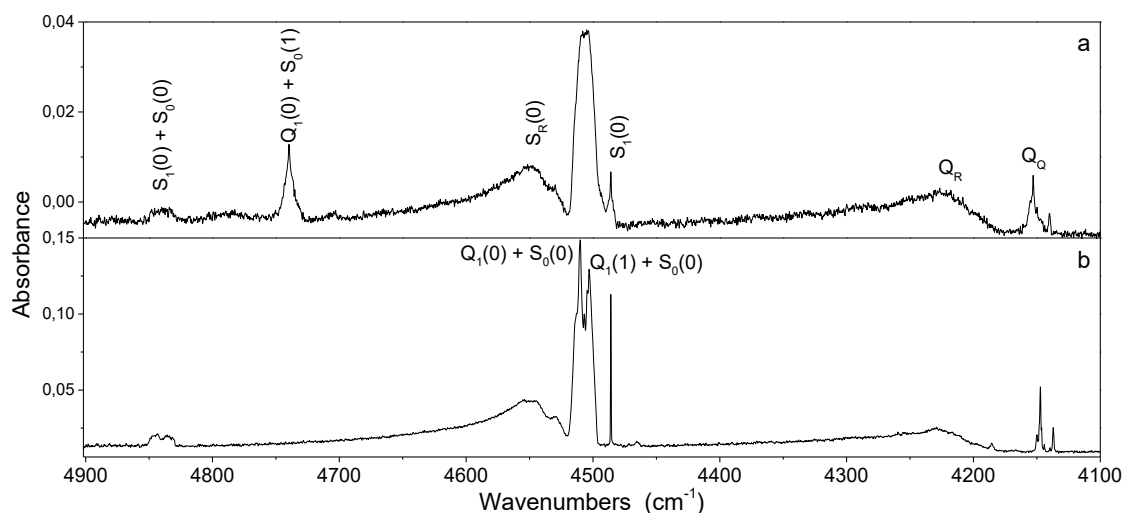


Figure IV.6: Infrared spectra of solid hydrogen in the 4900-4400 cm⁻¹ region for two different $p\text{H}_2$ fractions, (a) 95% and (b) >99.9% Ortho/para-hydrogen ratio can be estimated from the intensity and shape of the bands present in the spectrum (see text).

⁴⁷ The Q band has three components: Q_Q , Q_R and Q_P . The last two are interpreted as summation and difference tones $\nu_0 \pm \nu_k$, where ν_0 denotes the vibrational frequency of the hydrogen molecule and $h\nu_k$ is the continuum of kinetic energies of the relative motion of the absorbing molecule and its nearest neighbors [191].

EXPERIMENTAL SETUP

3. Broad bands like $S_R(0)$ and $S_R(1)$ are interpreted as combinations of molecular rotations and crystal lattice vibrations (phonons)

The thickness of the samples can be evaluated directly from the spectrum looking at the interference pattern of the baseline [192]. A more accurate measurement can be done by determining the intensity of the $S_1(0) + S_0(0)$ or the $Q_1(0) + S_0(1)$ bands. Tam and Fajardo have done a calibration of the intensity of these two bands versus the total sample thickness (d_{total}), for example: $\int A_{Q(0)+S_0(0)} d\tilde{\nu}/d_{total} = 82 \text{ cm}^{-1}$ [192]. Thickness between 0.2-0.5 mm were obtained.

On the other hand, the control of the $p\text{H}_2$ quality can be done in a first approximation through the semblance of the solid $p\text{H}_2$ infrared spectrum (Figure IV.6). The absence of the $Q_1(0) + S_0(1)$ transition (4740 cm^{-1}), as well as a good definition of the $Q_1(0) + S_0(0)$ (4495 to 4520 cm^{-1}) and $S_1(0) + S_0(0)$ (4825 to 4855 cm^{-1}) transitions bands indicates that the $o\text{H}_2/p\text{H}_2$ ratio is over 99.9%. A quantitative measure of the $o\text{H}_2$ fraction (F_0) can be obtained by integrating the $Q_1(0)$ band and then use the expression given by Tam and Fajardo: $(1/l) \int A. d\tilde{\nu} = bF_0 + (a - b)F_0^2$, where l is the thickness of the sample. In the limit of low $o\text{H}_2$ concentrations we can approximate the expression to the first linear term and calculate the fraction using the value of 30 cm^{-1} for constant b .

IV.4. Vibrational and electronic spectroscopies

Infrared spectra in neon, *para*-hydrogen and nitrogen were acquired using a standard FT-IR spectrometer (Nicolet Nexus 670/870) and a liquid nitrogen-cooled MCT (HgCdTe: Mercury Cadmium Telluride) detector. The equipment uses a Globar (SiC: Silicon Carbide) infrared source and a KBr beamsplitter. This optical setup allows us to work in the mid infrared region (650 - 5000 cm^{-1}). All spectra were recorded in transmission mode⁴⁸ and usually with a 0.5 cm^{-1} resolution level. The higher resolution of the spectrometer (0.125 cm^{-1}) was used in some experiments (it will be specified in the caption of the spectrum when used). The number of accumulated scans typically varied from 256 to 1024. The IR beam path was purged with dry air, but atmospheric CO_2 and H_2O were not completely removed or kept at constant levels, and can be observed in some spectra. A background spectrum was obtained before the experiments, when the cryostat was equilibrated at the working temperature. Spectra were recorded using "Omnic 7.3" software to control the spectrometer.

⁴⁸ The IR light passes through the sample and the transmitted component is measured by the detector

The FT-IR spectra in argon matrix were acquired with a Bruker IFS 113 spectrometer, using a Globar source. KBr beamsplitter and MCT detector. 256 scans and a 0.50 resolution level were used in these experiments.

Raman spectra were recorded using a Bruker Multiram Fourier Transform spectrometer. A diode laser operating at 785 nm was used at maximum 500 mW energy for the Raman excitation. Laser irradiation in all experiments resulted in 2 K temperature rise (from 9 K before irradiation to 11 K at the end of measurement) of the sample during the measurement. This temperature is much lower than Argon matrix diffusion temperature (35 K), thus no annealing effect is expected during spectra recording. Ti-Si avalanche diode detector was used for the scattered light detection. Typically, Raman spectra were measured at 0.75, 1.0 and 2.0 cm^{-1} resolution and 1000-2000 interferograms were averaged (total measurement time *ca.* 30 min.). Spectra were collected in 150 – 4000 cm^{-1} Raman shift range.

Ultraviolet spectra were acquired using a 0.6 m JobinYvon grating monochromator and a CCD camera (Andor DH720). We used a deuterium lamp (34500-60000 cm^{-1}) as light source for these studies. In these experiments a sapphire window was used as internal window for deposition of the sample.

External windows from the cryostats were changed depending on the type of study done: CaF_2 (Calcium Fluoride) for ultraviolet and CsI (Cesium Iodide) for infrared measurements (see Table IV.2). The values shown in Table IV.2 are approximate. Transmission is not constant in all the range shown for each material. In the case of sapphire, the minimum cutoff value depends of the amount and kind of dopants it has. The values for optical properties are also an average in the wavenumbers range.

Table IV.2: Optical properties of internal and external windows used in the matrix isolation setups (from reference [193])

	Diamond	CaF_2	CsI	Sapphire
Setup	#2 (internal)	#1 & #3	#1 & #3	#1 (internal)
Transmission range (cm^{-1})	45000-10	66000-1200	33000-150	66000-1600
Refractive index	2.40	1.40	1.74	1.75
Reflectance loss per surface	17%	2.8%	7.3%	7.3%

IV.5. UV and IR laser irradiations

UV and IR induced isomerization experiments in cryogenic matrices were performed using an Optical Parametric Oscillator (OPO) nanosecond laser from Continuum, which was pumped by the 355 nm line of a

EXPERIMENTAL SETUP

tripled Nd:YAG laser, with 10 Hz repetition rate. The pulse energies were in the range of 1–6 mJ. Laser bandwidth for UV and IR wavelengths were around 7 cm^{-1} in both cases. Irradiation times typically varied from some minutes to several hours. The laser source is quite far from the cryostat (in the next room) and optical lenses are used to obtain an irradiation spot almost covering all the deposition window. Laser irradiation was stopped during measurements of FT-IR spectra.

IV.6. Helium nanodroplet experiment

Helium nanodroplet experiment is a less standard setup compare to matrix isolation technique. This is the reason why a more detailed explanation of the experimental setup will be done, even if the obtained results are not the central part but a complement of this thesis.

Helium nanodroplets are formed under very specific conditions. These have been discussed in a deep manner in many reviews on the subject [194]–[198]. Here, we will describe the particularities of the experimental setup used by us, called GOUTTELIUM, which was designed to perform ro-vibrational spectroscopy in helium droplets using the HENDI technique (Helium Nanodroplet Isolation Spectroscopy) [199]. The experimental setup is divided in three chambers where different processes take place: the *source chamber*, the *pickup chamber*, and the *spectroscopy chamber*. These are shown in Figure IV.7.

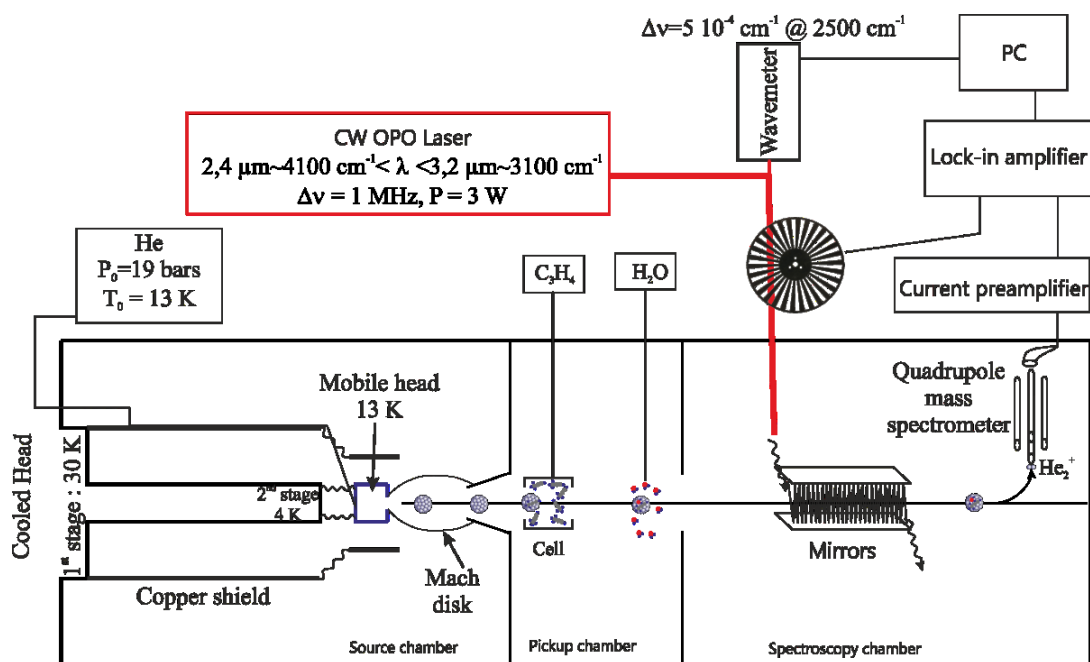


Figure IV.7: Scheme of the experimental setup GOUTTELIUM. The setup is divided in three chambers: Source chamber, pickup chamber and spectroscopy chamber. Pressure and temperature conditions shown in the first chamber, and pickup scheme correspond to propyne experiments, as example.

IV.6.1. Source chamber

The process starts with the precooling of helium gas (6.7⁴⁹) with a two stages Gifford-McMahon cryocooler (Sumitomo Heavy Industry, SRDK-408D2-F50H) operating at *ca* 4 K, before it enters into a reservoir. Under standard operating conditions, the reservoir temperature was at 10.8 K for glycolaldehyde and 13 K for propyne-water experiments (± 0.05 K regulation accuracy) and the helium backing pressure was 8 and 19 bars in each case. From this reservoir, the formation of the liquid nanodroplets is possible due to the expansion of the precooled helium through a nozzle of 5 μm diameter (in a continuous mode).

The supersonic expansion allows the condensation of the helium gas in small liquid droplets of a few thousands of atoms with a log-normal size distribution [197]. The purity of the helium gas is very important in order to avoid the blocking of the nozzle because of the condensation of other compounds in it. The nozzle and the reservoir mentioned above are carried by a mobile head. The latter is connected with OFHC copper breads (to enable heat conduction from the cryocooler to the head) to the first stage (shield) and the second stage (reservoir and nozzle) of the cryocooler. It is important to notice that the beam of nanodroplets should be correctly aligned with the input and output entries of each chamber to maximize the signal at the end. The mobile head allows aligning the nozzle with respect to the series of diaphragms which define the beam axis.

The source chamber is pumped by a 2400 $\text{L}\cdot\text{s}^{-1}$ (for He) magnetic turbo molecular pump (Edwards, STP-XA2703W) backed by a 35 $\text{m}^3\cdot\text{h}^{-1}$ scroll pump (Edwards, XDS35i). Under usual operating conditions, the source chamber is maintained at a pressure of 10^{-5} mbar (uncorrected for helium).

Once the nanodroplets are formed, a skimmer of 1 mm diameter connecting first and second chambers is used to select the central part of the expansion zone. The final temperature of the droplets is around 0.4 K.

IV.6.2. Pickup chamber

In the second chamber the so called *pickup* process takes place. In this process the molecule under study, is introduced inside the nanodroplet through collision. In order to achieve this collision, the molecule must be in the gas phase. In the case of liquid and solid samples with low vapor pressure the use of special techniques like heating or laser ablation is required. Different pickup setups were used for glycolaldehyde and propyne-water experiments. In the first case, glycolaldehyde dimer (solid powder) was heated at 80-90 °C in an external reservoir. The gas vapor was introduced in the pickup chamber through a tube ended in a steel

⁴⁹ In this notation the purity of the gas is expressed as follows: the first digit represents the number of nines in the percentage value and the other digit represents the last digit of the percentages value. In our case it will be: 99.99997%.

EXPERIMENTAL SETUP

needle which was pointing at a right angle to the nanodroplets pathway, allowing the cross of both beams. The gas line was heated from the reservoir to the needle to avoid condensation of glycolaldehyde on the inner surface of the line. In this configuration, the number of molecules introduced in each nanodroplet is controlled through the heating temperature of glycolaldehyde and consequently the vapor pressure.

In the propyne-water complex experiment two pickup systems were used, one for each molecule. In the case of propyne, which is a gas, the molecule can be easily introduced through a pickup cell. The cell is a stainless steel cylinder connected to the gas bottle and open at both ends with two small concentric holes to allow the passage of the droplets beam through it. Water vapor was introduced by using the same needle system used for glycolaldehyde. The amount of water was controlled through the opening of a micro valve connected to an external reservoir containing the sample. The helium droplet beam first crosses the propyne cell, depositing one molecule by collisional capture. The amount of molecules of each compound introduced in the droplet was changed by adjusting its partial pressure. Once both species are picked-up in the same droplet, they have enough mobility to migrate within the droplet and to form the complex. It should be pointed out that the obtained spectrum at the end is a superposition of contributions coming from clusters carrying $(\text{propyne})_m\text{-(water)}_n$ combinations (m and n starting at 0), and that the dominant species is controlled via the procedure just mentioned before. As the pick-up process is random and without memory it follows a Poisson distribution:

$$P_k(\langle m \rangle) = \langle m \rangle^k \cdot \frac{e^{-\langle m \rangle}}{k!} \quad (4.1.1)$$

where k is the exact number of molecules per cluster and $\langle m \rangle$ the average number of molecules per cluster. This property will be used later to determine the stoichiometry of the complexes at the origin of a particular absorption band.

The pickup chamber is pumped by a $1250 \text{ L}\cdot\text{s}^{-1}$ magnetic turbomolecular pump Edwards, STPA-1603C) backed by a 35 m^3 scroll pump (Edwards, XDS35i). When injecting propyne molecules only, the pressure in this chamber is *ca* 4.2×10^{-7} mbar (3×10^{-7} mbar without propyne). When water molecules are injected, the pressure reaches 10^{-6} mbar. In the case of glycolaldehyde the pressure was around 3×10^{-6} mbar during injection of the molecule, and 5.8×10^{-7} mbar without the molecule.

The doped helium droplet beam exits the pickup chamber through a diaphragm of 2 mm diameter and enters next into the spectroscopy chamber.

IV.6.3. Spectroscopy chamber

In the third chamber the molecule or the complex trapped in the helium nanodroplet interacts with a Continuous Wave IR-OPO laser (Lockheed-Martin Aculight ARGOS 2400-SF-15). The laser is tunable between 2.4 and 3.2 μm and has a spectral resolution of 1 MHz ($3.10^{-5} \text{ cm}^{-1}$). A CaF_2 plate is placed near the laser output and reflects 4% of the photon flux. The front reflection on this plate is sent to a wavemeter (Bristol, 621A-IR) whereas the back reflection is sent to a powermeter (Coherent, thermopile PM10). The remaining laser light enters into the spectroscopy chamber through a CaF_2 window after passing through a chopper (see Figure IV.7). The IR laser power is typically 1.5 W after the chopper. An external power supply is used as remote control to tune the IR laser over a 2.5 cm^{-1} range with steps that can be chosen down to $2 \times 10^{-4} \text{ cm}^{-1}$.

The experimental procedure is as follow. When the IR laser matches the frequency of a normal mode of the molecule (around 3000 cm^{-1}) this one will be ro-vibrationally excited. The deexcitation mechanism releases the energy to the environment, value that exceeds the binding energy between helium atoms in the cluster (5 cm^{-1}) and produces the evaporation of the droplet reducing its size. In order to increase the interaction probability between the IR laser and the nanodroplet beam a multipass mirror (two rectangular and parallel gold mirrors) is coaxially located in the way of the molecular beam. This configuration allows multiple reflection of the IR beam (around 30) to interact with the droplets along its transit trough the cell. At the end of the chamber (15 cm downstream the interaction region) the acquisition is performed. In the setup a quadrupole mass spectrometer (MKS, Microvision Plus 100D) is used to follow the change of the helium dimer signal. The detection works as follows: just before the quadrupole mass analyzer the droplet is ionized by electronic impact (energy around 70 eV, and electron emission of 1 mA). The energy of the electron beam is higher than the helium ionization potential (21 eV). The excess energy provokes the explosion of the droplet releasing helium atoms, dimers and multimers. The quadrupole is set on the helium dimer mass/charge window as the dimers are characteristic of the existence of the clusters. Dimers do not exist at room temperature and then, do not participate to the signal background. The amount of dimer formed after ionization is proportional to the size and amount of droplets that arrives at the quadrupole. The process enables to detect helium nanodroplets depletion as a function of the laser wavelength. Since very small depletions are expected, a lock-in amplifier (synchronized with the chopper of the laser mentioned above) is coupled to the output signal of the mass spectrometer. At the end, after the numerical treatment of the experimental data the resolution reaches $0.003\text{-}0.004 \text{ cm}^{-1}$.

The spectroscopy chamber is pumped by another $1250 \text{ L}\cdot\text{s}^{-1}$ magnetic turbomolecular pump (Edwards, STPA-1603C) backed by a 35 m^3 scroll pump (Edwards, XDS35i). A liquid nitrogen trap allows removing

EXPERIMENTAL SETUP

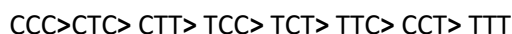
condensable gases. Under usual operating conditions, the pressure in the spectroscopy chamber is *ca* 7×10^{-8} mbar.

Chapter V Acetylacetone (D2)

The study of deuterated acetylacetone is presented first because it follows directly the previous work on AcAcH8 done in our lab and it will clarify the role of tunneling effect in the stabilization of the open enol conformers produced after UV laser irradiation. This will allow us to interpret the results obtained in the halogenated analogs, which are presented later. In this section, the studies performed with FT-IR on double deuterated acetylacetone in neon matrices are presented. Some preliminary results obtained in *para*-hydrogen matrix are also included in some sections.

V.1. Theoretical calculations

Optimization and frequency calculations were performed for all the conformers and keto tautomer with B3LYP/6-311++G(3df,3pd) level. The results show that all deuterated enolic conformers have a planar structure (carbonated skeleton and CCOD dihedral), similar to non-deuterated conformers [15]. The stability order for the open enol conformers in deuterated isotopologues is the same as in the case of non-deuterated acetylacetone:



Energies relative to the CCC conformer for AcAcD2 (CCC(D2)) are reported in Figure V.1. They differ from those of AcAcH8 by no more than 0.2 kJ/mol in the different isotopologues, corresponding to the deuteration effect on the Zero Point Energy (ZPE) contribution, not large enough to perturb the order of stability. We should take into account that this difference is smaller than the error of the method, which is around 4 kJ/mol. So, in practice the energies are the same. We can remark that as in the case of acetylacetone the keto isomer is the most stable after the chelated enol.

Vibrational frequencies and intensities for the keto isomer and conformers were computed in order to identify the IR absorption bands of each of them and to obtain the aforementioned ZPE values. The whole set of theoretical data is reported in the Appendix. The most distinct feature in the case of AcAcD2 conformers is the presence of OD stretching modes near 2790-2760 cm^{-1} for the open conformers, whilst the same mode for the CCC form is 500 cm^{-1} downshifted. This frequency range is especially important to check the formation of open conformers under laser irradiation.

ACETYLACETONE (D2)

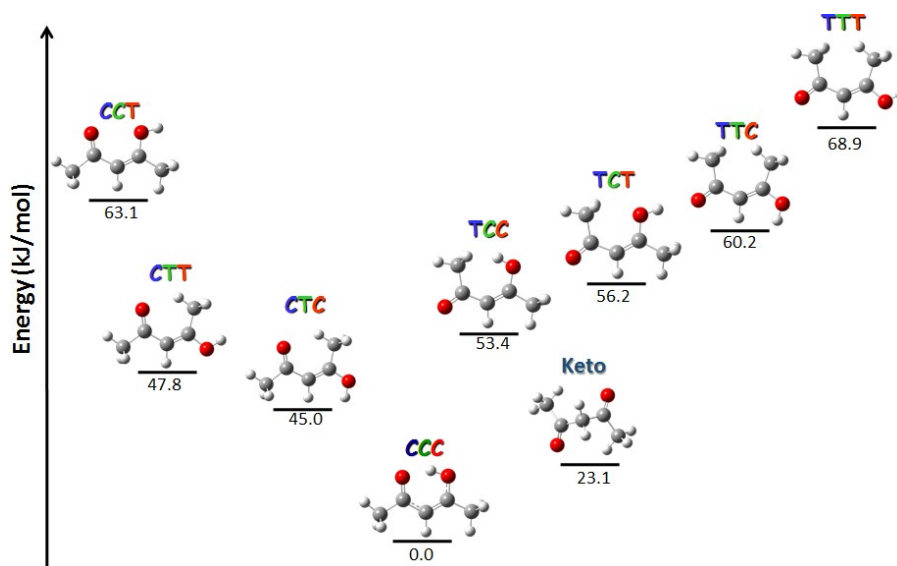


Figure V.1: Schemes and relative energies (kJ/mol) of open enol conformers and keto isomer compared to the CCC conformer, in AcAcD2. Zero Point Energy is included in each reported value.

V.2. Vibrational spectroscopy of as-deposited samples

V.2.1. FT-IR spectra

As previously mentioned in Section IV.1.2, the yield of the synthesis is not 100%; so, our samples contain deuterated and non-deuterated acetylacetonone. Figure V.2 shows in the left panel the spectra of AcAcH8 (a) and of the deuterated species (b) in neon matrices at 7.6 K. The latter is obtained after subtraction of the bands of AcAcH8 (a) from the original spectrum of the deuterated as-deposited sample. The calculated spectrum of CCC(D2) in the harmonic approximation is displayed in panel (c) for comparison. Calculated frequency is scaled by a factor of 0.981. Frequencies obtained in the anharmonic approximation are reported in Table V.1, together with the scaled harmonic frequencies. The agreement between the theoretical spectrum (c) and the experimental one (b) for the most intense bands is very good, and we conclude that AcAcD2 in its chelated enol form is the main structure observed in the experimental spectrum (b). Nevertheless, there are several bands which do not correspond to CCC(D2) (zoom of 1340 - 1470 cm^{-1} region in Figure V.2, right panel). When comparing experimental and theoretical spectra for double deuterated and monodeuterated conformers, we found that these bands correspond to the CCC forms of the monodeuterated species AcAcD1, *i.e.* AcAcD1(CD) and AcAcD1(OD).

Similarly to the case of the non-deuterated molecule, we observe the keto tautomer in the deposited samples, assigning to it two weak vibrational bands at 1717.2 and 1185.4 cm^{-1} . Theoretical calculations

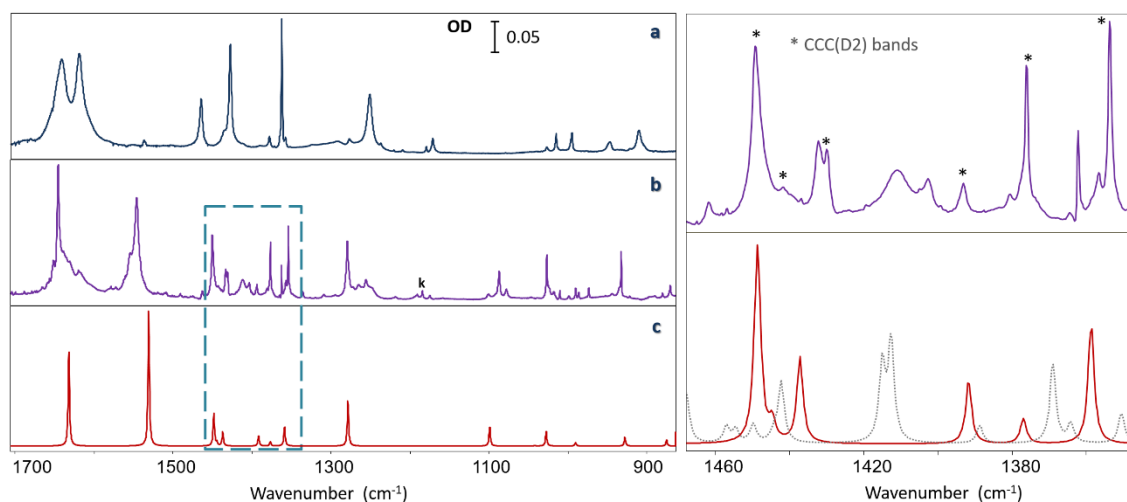


Figure V.2: Left: a) As deposited acetylacetone (AcAcH8) in neon, b) As deposited deuterated acetylacetone in neon (after subtraction of residual AcAcH8 bands), and c) Calculated spectrum of CCC(D2) (red) and convoluted spectra (grey) of CCC(OD) and CCC(CD) monodeuterated isotopologues (harmonic frequency calculation with a 0.981 scaling factor). Right: Zoom on the 1340-1470 cm^{-1} region. * denotes bands assigned to AcAcD2 in the zoomed region, the other bands are assigned to AcAcD1 (see Figure V.6). The theoretical spectrum is shown using a convolution with a Lorentzian profile of 2 cm^{-1} bandwidth. *k* denotes keto band.

suggest that these frequencies are very close from one isotopologue to another (see Appendix). The amount of keto tautomer is very low (approximately 1%), just as with the AcAcH8 isotopologue. This result shows that the keto-enol equilibrium is not significantly perturbed by deuteration.

Some preliminary experiments were performed in *para*-hydrogen matrix. The spectra of the CCD2 conformer in *p*H₂ and neon are shown in Figure V.3. Each spectrum was obtained after a weighted subtraction of two different spectra belonging to different AcAcD2 samples, in which the ratio between the deuterated

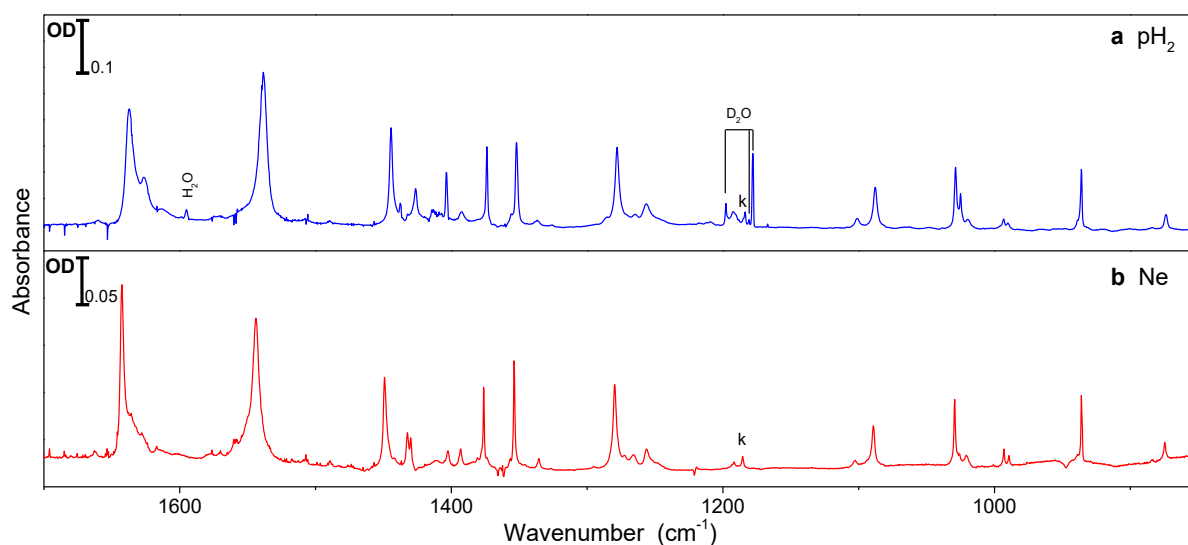


Figure V.3: Infrared spectra (after subtraction of AcAcH8 and AcAcD1 isotopologues) of double deuterated acetylacetone in (a) *para*-hydrogen and (b) neon matrices. Bands corresponding to water isotopologues are identified in *para*-hydrogen. *k* keto bands.

ACETYLACETONE (D2)

isotopologues (AcAcD2/AcAcD1) was different⁵⁰. This procedure allows to decrease (almost eliminate) bands from monodeuterated isotopologues. AcAcH8 spectrum (previously obtained) was also subtracted, leaving at the end bands coming mainly from AcAcD2. The frequencies and the relative intensities between the bands in both matrices experience only small changes. Water bands can be found in *para*-hydrogen matrix and not in neon because different samples and setups were used in each case (Setup #1 for neon and Setup #2 for *p*H₂).

V.2.2. AcAcD2: CCC conformer

The spectra subtraction process previously mentioned allows to distinguish the bands from AcAcD2 to those from monodeuterated isotopologues. The list of bands assigned to double deuterated CCC in both matrices and the calculated bands of CCC(D2) are reported in Table V.1.

The agreement is good for both calculations (harmonic and anharmonic) even if the scaling factor underestimates the effect of the anharmonicity for the highest frequencies. The comparison of both methods can be observed in Figure V.4 through a dispersion graph. Only the OD stretching mode which is the most anharmonic and the most perturbed by the H bond, is not very well reproduced.

There is not a big improvement of the anharmonic calculations compared to scaled harmonic ones. We will see that the same result was obtained for the open enol conformers of this molecule produced after UV irradiation. So, from now on only scaled harmonic frequencies will be used in the discussions.

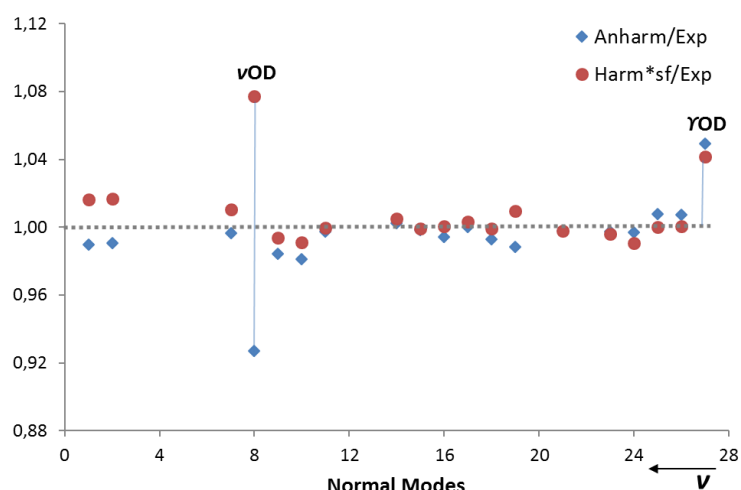


Figure V.4: Dispersion graph of the anharm/experimental and harm*scaling factor/experimental frequency ratios for different assigned modes of the CCCD2 conformer. Experimental values are taken from neon. The scaling factor used is 0.981. The abscissa goes from high (left) to low (right) frequencies. The fourth and the last mode (highest deviation) correspond to the OD stretching and out of plane bending.

⁵⁰ Samples with different synthesis yield.

Vibrational spectroscopy of as-deposited samples

Table V.1: CCC(D2) conformer assignment. Experimental frequencies of the chelated enol form of AcAcD2 in neon and *para*-hydrogen matrices, compared to experimental values obtain by Tayyari *et al.* [58] in gas phase, calculated harmonic and anharmonic frequencies [B3LYP/6-311++G(3df,3pd)] (cm⁻¹). Intensities (km/mol) obtained in the harmonic approximation.

Assignment ^a	Experiment			Theoretical		
	Ne	<i>p</i> H ₂	Tayyari (Gas)	harmonic* <i>sf</i> ^b	anharmonic	Intensity
v_aCH₃ (CO side)	3034 ^c		3018	3083.2	3003.2	10
v_aCH₃ (OD side)	3027 ^c	3015		3078.3	2998.7	9
v_aCH₃ (OD side)			2970	3031.5	2949.3	5
v_aCH₃ (CO side)		2971		3029.5	2954.3	6
v_sCH₃ (OD side)	2951 ^c	2935	2940	2980.5	2928.5	8
v_sCH₃ (CO side)		2928		2976.4	2951.5	3
vCD	2304.5	2299	2300	2328.7	2297.0	1
vOD	2000 ^c	1991 ^d	2027	2158.3	1857.1	259
v_a(C=C + C=O)	1641.8	1637.2	1633	1631.7	1616.5	263
v_s(C=C + C=O) + δOD	1544.2	1538.5	1544	1530.6	1515.2	374
δ_aCH₃(OD side)	1449.4	1444.6	1448	1448.3	1436.7	87
δ_aCH₃(CO side)	1429.3	1426.3	1448	1436.9	1432.6	39
δ_sCH₃(OD side)	1392.7	1392.9		1391.5	1390.5	28
δ_sCH₃	1376.1	1374.0	1365	1376.8	1368.0	11
δ_sCH₃(CO side)	1354.0	1352.3	1365	1358.5	1354.1	54
v_sC-C-C=C-C ring breath	1279.5	1278.0	1273	1278.4	1270.3	126
δOD	1088.6	1087.9	1082	1098.9	1076.0	52
ρCH₃(OD side)	1029.5	1028.7	1025	1027.5	1027.4	34
πCH₃ (CO side)	1020.6	1019.8		1027.2	1020.9	7
ρCH₃(+ δOD)	993.9	993.6		990.2	991.5	10
vC-CH₃(CO side) + ρCH₃	936.3	936.1	936	927.8	933.4	25
Δ ring + ρCH₃	874.9	873.8	880	874.9	881.8	17
δCD	831.1	830.2		831.6	837.1	0.5
γOD	706.1	707.8	707	735.5	740.9	38

^amain characteristic motions; **v**, stretching; **δ**, in plane bending; **γ**, out of plane bending; **ρ**, in plane rocking; **π**, out of plane rocking; **Δ**, in plane ring deformation; **s**, symmetric; **a**, asymmetric

^b*sf*: scaling factor (0.981)

^c Broad bands

^d Very broad band (the center is not well defined)

V.2.2.1. OD and CD stretching modes assignment

The OH and CH stretching modes have never been observed for AcAcH8 in cryogenic matrices, or at least no clear assignment has been done for them. It is expected that their corresponding deuterated analogs should be shifted in frequency compared to the non-deuterated molecule because of the change in mass⁵¹. In the spectra obtained in this work in neon and *para*-hydrogen matrices, the CD stretching band was found near 2300 cm⁻¹ (see Figure V.5). In previous studies of deuterated acetylacetonone in the gas phase, the authors suggest the presence of the OD stretching band around 2025 cm⁻¹ [55], [58], [200]. A closer look at this frequency region was required to find a possible assignment for it: a weak and broad band around 2000 cm⁻¹ could correspond to ν_{OD} (see Figure V.5). The large red shift of ν_{OD} is due to the internal hydrogen bond. In fact, it induces an inversion in the energy ordering of CD and OD stretching modes, observed experimentally and theoretically (see Figure V.5 and Table V.1).

It is known that for most of molecules the position of the OH/OD stretching mode allows easy the discrimination between non-deuterated and deuterated isotopologues. However in AcAcH8, despite its high intensity, the OH band is difficult to observe experimentally because it spreads over hundreds of wavenumbers due to the high delocalization of the hydrogen atom in the hydrogen bond, as suggested by the previous works in the gas phase at room temperature [55], [58]. It is expected that the bandwidth should decrease significantly in the low temperature matrices [200], however it remains very large even at lowest temperature, as proton delocalization is still high even in the cryogenic matrices. This fact makes the observation of the band very difficult and its maximum position cannot be determined accurately. In

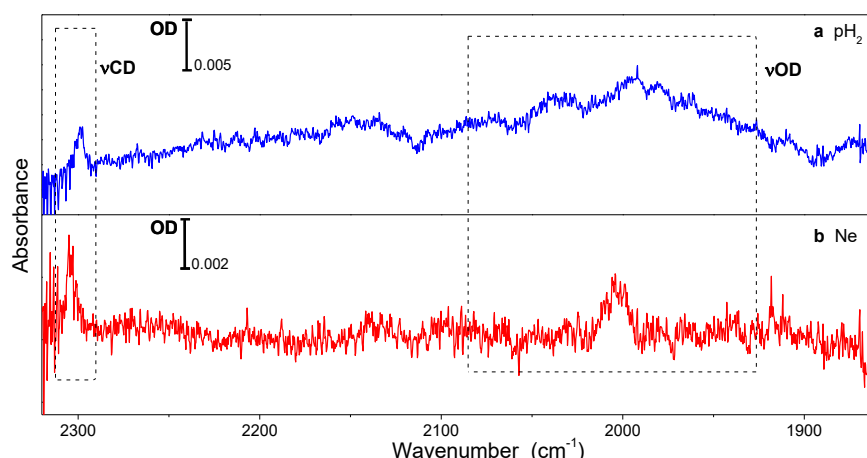


Figure V.5: 1850-2320 cm⁻¹ region of deposited deuterated acetylacetonone in (a) *para*-hydrogen and (b) neon. OD and CD stretching bands for AcAcD2 isotopologue are assigned.

⁵¹ In the simple mechanical model for an harmonic oscillator the frequency of a mode is obtained as: $\nu_i = \frac{1}{2\pi} \sqrt{\frac{k_i}{\mu_i}}$, where k_i is the force constant of the bond (or bending angle), and μ_i is the reduced mass of the group of atoms involved in the vibration.

particular, the OH stretching band of AcAcH8 was not clearly observed neither in neon nor in *para*-hydrogen matrices at 4 K[15].

At first sight most of the bands of AcAcD2 in Figure V.2 are narrower than those of AcAcH8. The decrease of the bandwidth for OH normal modes upon a H-D exchange was expected [201] and it can be explained [201]. The proton transfer between the oxygen atoms at low temperature occurs by tunnel effect through the barrier. The tunneling probability decreases with the increasing mass of the tunneling particle (see section III.8.). This factor decreases the kinetic tunneling constant and the proton transfer process when hydrogen is exchanged by deuterium, making more localized the OD modes (reducing delocalization of the proton), and consequently reducing its bandwidth. In both isotopologues, the stretching and especially the bending modes of the OH/OD group contribute to several normal modes of the molecule. This could explain in part, the global broadening of bands in CCC(H8) compared to CCC(D2). Table V.2 reports FWHM of the main assigned lines of CCC(D2) and CCC(H8) in neon, with a short description of the modes in order to directly compare both isotopologues. The OH/OD stretching modes are not included in Table V.2 because, as it was written above, $\nu_{\text{OH}}\text{-CCC(H8)}$ was not observed. Thus, as we observe the $\nu_{\text{OD}}\text{-CCC(D2)}$ band (Figure V.5), it should be narrower than the $\nu_{\text{OH}}\text{-CCC(H8)}$ band.

Table V.2: Bandwidths in neon for some bands of the CCC conformer of AcAcH8[9] and AcAcD2. Only bands where a measurement of FWHM was possible are shown. The assignment is set according to reference [9], and pairing modes was made taking into account the most relevant motions involved in each mode. Position and width are in cm^{-1} . *nm*: measurement was not possible.

Assignment ^a	AcAcH8		AcAcD2	
	Position	Width	Position	Width
$\nu_s(\text{C}=\text{C} + \text{C}=\text{O})$	1642.0 ^b	16	1641.8	2.5
$\nu_s(\text{C}=\text{C} + \text{C}=\text{O}) + \delta\text{OH}$	1619.7 ^b	11	1544.2	5.7
$\delta_s\text{CH}_3(\text{OH side})$	1465.1	4.6	1449.4	2.0
$\delta_s\text{CH}_3$	1435.8	6.6	1429.3	1.3
δCH_3	1428.1	4.3	1376.1	0.8
$\delta_s\text{CH}_3(\text{OH side})$	1378.6	2.6	1392.7	1.6
$\delta_s\text{CH}_3(\text{CO side})$	1362.9	1.5	1354.0	0.9
δOH	1297.2	78	1088.6	2.3
$\nu_s\text{C-C-C}=\text{C-C}$ ring breath	1251.4	7.3	1279.5	2.9
$\delta\text{CH}_{\text{olefinic}}$	1171.5	3.3	831.1	<i>nm</i>
$\rho\text{CH}_3(\text{OH side})$	1015.8	1.8	1029.5	1.3
$\rho\text{CH}_3(\text{CO side})$	995.2*	1.4	993.9	1.0
γOH	947.9	5.5	706.1	1.1
Δ ring + ρCH_3	910.6	6.3	874.9	1.3

^a main characteristic motions; ν , stretching; δ , in plane bending; γ , out of plane bending; ρ , in plane rocking; π , out of plane rocking; Δ , in plane ring deformation; s , symmetric; a , asymmetric

^b bands with shoulders

ACETYLACETONE (D2)

The bandwidths of the modes of the deuterated sample in *para*-hydrogen are not included in the comparison because the experiments need to be repeated, using different sample concentration and with a lower amount of water, in order to eliminate these effects.

V.2.3. Monodeuterated isotopologues: CCC(OD) and CCC(CD)

It should be noted that AcAcD1 is always present in the samples as CCC forms of AcAcD1(OD) and AcAcD1(CD). We were able to obtain the spectrum of AcAcD1 in neon (Figure V.6) by subtracting spectra of samples with different deuteration ratios and to assign a few bands of the monodeuterated isotopologues. It appears that the ratio between isotopomers AcAcD1(OD) and AcAcD1(CD) is roughly the same in all the samples, close to 50/50 (a precise measurement is not possible).

The band assignment to a particular isotopomer is complicated because AcAcD1(OD) and AcAcD1(CD) have many modes with very similar frequencies. Nevertheless, we were able to identify some bands for each isotopologue using the theoretical spectra (Figure V.6 b and c). These bands suggest that similarly to AcAcD2 and AcAcH8, those corresponding to AcAcD1(OD) are narrower than those of AcAcD1(CD). Additional bands can be tentatively assigned to each isotopologue following this remark. The experimental frequencies compared to calculations are reported in Table V.3. Considering that AcAcD2 and AcAcD1(OD) in one hand, and AcAcH8 and AcAcD1(CD) in the other hand have similar bandwidths we conclude that the α hydrogen (olefinic hydrogen) does not have a wide impact in the band broadening.

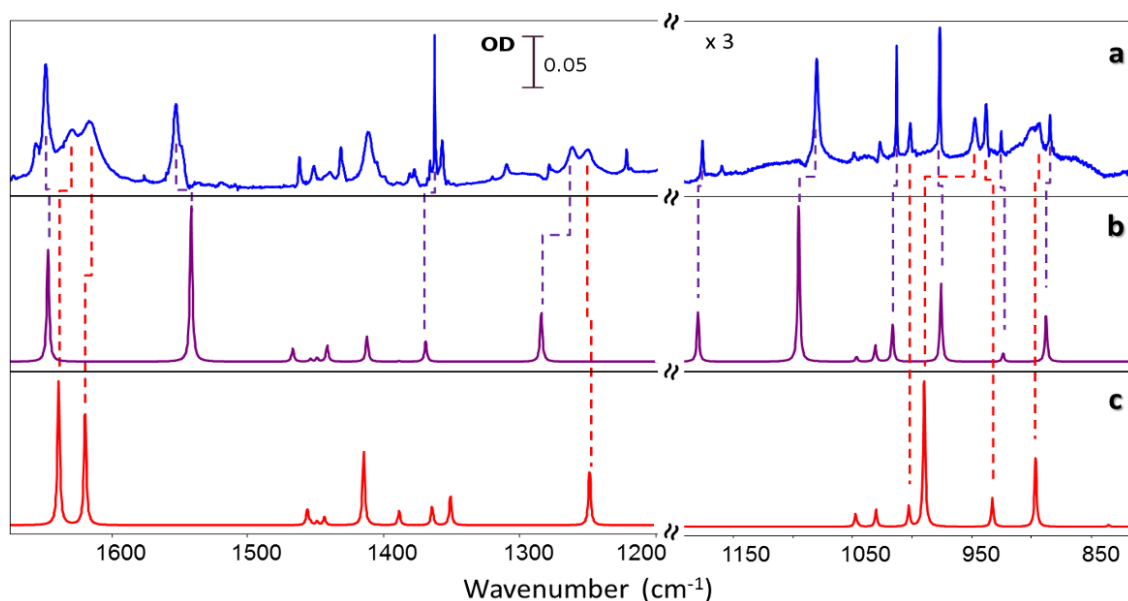


Figure V.6: a) IR spectrum of monodeuterated isotopologues (obtained after removing AcAcD2 and AcAcH8 from the original spectrum); IR theoretical spectra— Lorentzian bandwidths of 2 cm^{-1} -in the scaled harmonic approximation of CCC forms of b) AcAcD1(OD) and c) AcAcD1(CD) isotopologues. Zoom(x3) below 1200 cm^{-1} for a better comparison. Assignment is shown with dashed colored lines for some of the most important bands.

Table V.3: Experimental frequencies (cm^{-1}) of the chelated enol form of AcAcD1(OD) and AcAcD1(CD) conformers in neon, compared to calculated harmonic and anharmonic frequencies [B3LYP/6-311++G(3df,3pd)]. Experimental bandwidths [W (cm^{-1})] and intensities obtained in the harmonic approximation (km/mol) are also reported. nm: measurement was not possible.

CCC(OD)					CCC(CD)				
Assignment ^a	CCC-OD Exp.	W	Theo. Harm.*sf ^b (Anharm.)	Int.	Assignment ^a	CCC-CD Exp.	W	Theo. Harm.*sf ^b (Anharm.)	Int.
$\nu_a(\text{C}=\text{C} + \text{CO})$	1648.7	3.9	1641.9 (1625.5)	273	ν CD	2306.8		2328.7 (2296.2)	1
$\nu_s(\text{C}=\text{C} + \text{CO}) + \delta\text{OD}$	1552.7	4.7	1536.7 (1517.1)	384	$\nu_a(\text{C}=\text{C} + \text{CO})$	1630.5	14	1634.0 (1608.6)	355
$\delta_a\text{CH}_3(\text{OH side}) + \delta\text{CH}$	1461.2	nm	1462.1 (1454.2)	32	$\nu_s(\text{C}=\text{C} + \text{CO}) + \delta\text{OH}$	1616.8	18	1614.6 (1603.9)	283
$\delta_a\text{CH}_3(\text{CO side})$	1431.2	nm	1436.9 (1427.8)	21	$\delta_a\text{CH}_3(\text{OH side}) + \delta\text{OH}$	1451.2	nm	1451.5 (1446.9)	38
$\delta_a\text{CH}_3(\text{OH side})$	1404.5	nm	1407.7 (1399.8)	64	$\delta_a\text{CH}_3(\text{CO side}) + \delta\text{OH}$	1439.7	nm	1438.9 (1427.8)	20
$\delta_s\text{CH}_3(\text{CO side})$	1361.7	0.8	1364.6 (1361.4)	50	$\delta\text{OH} + \nu_s$ (carbon skeleton)	1411.3	7.7	1410.1 (1397.8)	180
ν_s (carbon skeleton) + (δOD)	1261.4	8.5	1279.7 (1260.7)	119	$\delta_s\text{CH}_3$ (OH side)	1380.7	nm	1384.1 (1365.8)	35
δCH	1175.0	1.7	1175.6 (1170.2)	21	$\delta_s\text{CH}_3$ (CO side)	1356.6	3.0	1359.9 (1358.9)	45
δOD	1079.9	3.5	1091.4 (1039.3)	66	ν_s (carbon skeleton) + δOH	1249.1	10.2	1244.3 (1232.1)	135
πCH_3 (CO side)	1027.0	nm	1027.4 (1025.0)	7	πCH_3 (CO side)	1027.0	nm	1027.2 (1024.3)	8
ρCH_3 (OD side)	1013.0	0.8	1013.0 (1013.7)	16	ρCH_3	1048.9	nm	1044.4 (1041.4)	6
ρCH_3 (CO side) + δOD	976.7	1.1	972.4 (978.9)	33	ρCH_3	1001.6	1.8	999.7 (1001.4)	10
Δ ring + ρCH_3	925.2	0.8	920.6 (923.3)	4	Δ ring + ρCH_3	938.2	2.4	929.8 (933.0)	14
Δ ring + $\rho\text{CH}_3(\text{CO side})$	884.1	1.5	884.7 (890.5)	20	Δ ring + ρCH_3 (CO side)	893.9	nm	893.7 (907.3)	32
γCH	777.5	nm	786.6 (792.9)	8	γOH	947.4	3.6	986.9 (986.2)	70
γOD	706.1	nm	732.4 (734.1)	50					

^a main characteristic motions; ν , stretching; δ , in plane bending; γ , out of plane bending; ρ , in plane rocking; π , out of plane rocking; Δ , in plane ring deformation; s, symmetric; a, asymmetric;

^b sf: scaling factor (0.981)

V.2.4. Raman spectra

Raman spectrum was recorded in argon matrix as a complementary source of information to FT-IR for deposited samples. For example, bands corresponding to methyl groups are very intense in Raman, in contrast to infrared. Argon matrix was used for this experiment because the minimum temperature achieved by the cryostat with the excitation laser on (in Setup #3 in Vilnius) was not low enough to perform neon matrix experiments. In this case, FT-IR spectra were also obtained in argon matrix (and compared with the literature) to directly compare the results of both techniques in the same matrix. In addition, the comparison with theoretical Raman spectra, and between the non-deuterated and the deuterated isotopologues can corroborate our assignment.

The experimental and calculated CCC Raman spectra of acetylacetonone and the double deuterated isotopologue are shown in Figure V.7. No treatment has been done on the experimental spectra, and a broad scattering background can be observed. But, this does not affect the analysis of the spectra, which is clear. In the case of deuterated acetylacetonone because the yield of the synthesis was very good and sensitivity of Raman is smaller than in FT-IR, the non-deuterated and monodeuterated isotopologues are not observed.

In both cases the match between experimental and theoretical spectra is quite good, confirming the presence of the CCC conformer. The assignment is shown in Table V.4. It is interesting to note that in both

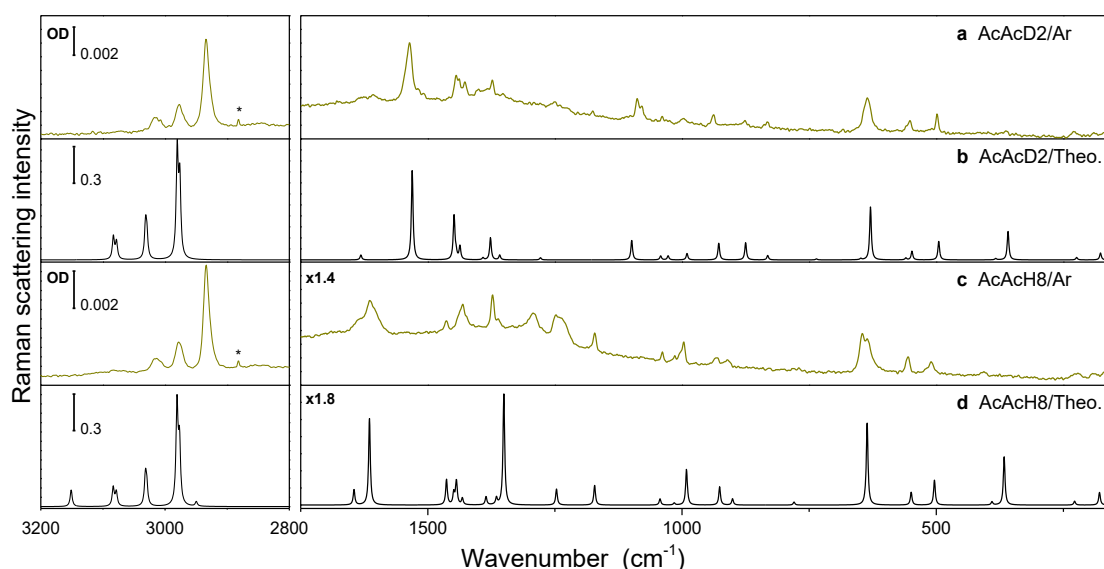


Figure V.7: Experimental and theoretical (b3lyp/6-311++G(3df,3pd)) Raman spectra of double deuterated acetylacetonone (AcAcD2) and acetylacetonone (AcAcH8) in argon matrix. AcAcD2 (a) experimental and (b) theoretical; AcAcH8 (c) experimental and (d) theoretical. A scaling factor of 0.981 is used on the harmonic theoretical spectra. Raman intensity is given in arbitrary units. * background

isotopologues the theoretical predicted band at 375 cm^{-1} in Raman (with medium intensity) is not observed experimentally. This band corresponds to one of the two normal modes associated with the approach of the oxygen atoms, which facilitates the proton tunneling transfer.

The FT-IR spectrum for the double deuterated molecule was also obtained in argon matrix and its assignment is included in Table V.4. It should be pointed out that infrared bands in argon are broader than in neon and *para*-hydrogen, and sites effects can be observed, making less reliable the accuracy of the assignment.

Unlike the double deuterated analog, the results obtained for acetylacetone in argon can be directly compared to those reported by Nagashima *et al.* [41] using FT-IR and Lüttschwager [202] using Raman spectroscopy. These are included in Table V.4 for comparison. We want to remark that there is a previous work on the Raman spectrum of acetylacetone in argon matrix done by Mohacek *et al.* [203]. We decided to obtain and analyze again the Raman spectrum in argon, not only to compare with the double deuterated isotopologue, but also because we do not agree with the conclusions drawn by Mohacek *et al.* In their work they claim to have trapped the “TS2” transition state (C_{2v} symmetry) in which both methyl groups are in *anti* position regarding the oxygen atoms. We do not agree with this conclusion and we conclude that only the CCC stable structure is present in the deposited sample in argon, like in the other matrices.

V.2.5. Nuclear spin conversion (NSC)

Experimental evidences of nuclear spin conversion on acetylacetone were previously observed in *para*-hydrogen matrix⁵² by Lozada *et al.* [14]. Some of the infrared bands of the deposited sample presented two components which evolved with time with a characteristic constant of 0.042 h^{-1} . The intensity of one of the components decreases while the other increases. The origin of these two components is associated with the presence of two nuclear spin states (from the hydrogen of methyl groups) which are coupled by symmetry reasons to the torsion of the methyl group. Each torsional level is split in two states of *A* and *E* symmetries because of tunneling between the 3 equivalent wells of the torsional potential. The *A* state is related to the totally symmetric nuclear spin wavefunction ($I = 3/2$) and the *E* state to the non-symmetric spin wavefunction ($I = 1/2$). In the case of a slightly hindered rotor, there could be a large splitting between *A* and *E* states. The population transfer between these two states is very slow because it implies a nuclear spin conversion process. When the temperature decreases very fast to low values (like in the matrix deposition

⁵² Para-hydrogen is an ideal matrix for the studies of NSC because the inhomogeneous broadening is reduced and large amplitude motions and rotations are preserved for small molecules.

Table V.4: CCC conformer assignment of acetylacetonone and acetylacetonone (D2) in argon matrix. Experimental Raman frequencies (cm^{-1}) obtained for AcAch8 are compared to those of Lüttschwager with 1 mm He-jet [202] and to those obtained by Nagashima *et al.* [41] using FT-IR in argon matrix. Calculated harmonic frequencies [B3LYP/6-311++G(3df,3pd)] (cm^{-1}) are included for each isotopologue. Infrared intensities (km/mol) and Raman scattering activities ($\text{\AA}^3/\text{a.m.u.}$) were obtained in the harmonic approximation. A scaling factor (sf) of 0.981 is used for the frequencies.

Assignment	Acetylacetonone					Acetylacetonone (D2)					Assignment		
	Frequency			Intensity		Frequency			Intensity				
	Experimental			Theoretical Harm.*sf	Ram.	IR	Experimental			Theoretical Harmonic*sf		Ram.	IR
	Raman		IR				Raman	IR					
Our work	Lüttschwager	Nagashima											
vCH	3083	3088		3151	59	3			3083	65	10	vCH ₃ as (CO side)	
vCH ₃ as (CO side)				3084	64	12	3017	3015.8	3078	50	9	vCH ₃ as (OH side)	
vCH ₃ as (OH side)	3013	3013	3015	3079	48	9			3031	96	5	vCH ₃ as (OH side)	
vCH ₃ as (OH side)				3032	96	5	2977	2977.7	3029	60	6	vCH ₃ as (CO side)	
vCH ₃ as (CO side)	2978	2978	2979	3029	60	6			2980	283	8	vCH ₃ s (OH side)	
vCH ₃ s (OH side)				2981	315	17	2934	2933.4	2976	205	3	vCH ₃ s (CO side)	
vCH ₃ s (CO side)	2934	2937	2933	2977	191	5			2329	23	1	vCD	
vOH				2950	14	358			2158	12	259	vOD	
vCO + vC=C (as) + δ OH	1635	1639	1636	1645	9	372	1630	1636	1632	4	263	vCO + vC=C (as)	
vCO + vC=C (s) + δ OH	1614	1621	1616	1615	47	269	1536	1536	1531	70	374	vCO + vC=C (s) + δ OD	
δ_a CH ₃ (OH side)	1463	1466	1462	1463	12	61	1444	1443.8	1449	5	7	δ_a CH ₃ (CO side)	
δ_a CH ₃ (CO side)				1449	5	7	1438	1437.0	1448	27	87	δ_a CH ₃ (OD side)	
δ_a CH ₃ (OH side)				1444	4	10			1444	4	9	δ_a CH ₃ (OD side)	
δ CH ₃ (OH side) + δ CH ₃ (CO side)				1443	8	14	1427	1426.4	1437	9	39	δ_a CH ₃ (CO side)	
δ CH ₃ (OH side) + δ CH ₃ (CO side)	1431	1436	1432	1432	3	131	1401	1402	1392	1	28	δ_s CH ₃ (OD side) umbrella	
δ_s CH ₃ (OH side) umbrella	1373	1376	1374	1386	3	13	1373	1372.3	1377	15	11	δ CH ₃ (OD side) + δ CH ₃ (CO side)	

$\delta_s\text{CH}_3(\text{CO side})$ umbrella	1360		1360	1365	3	64									
δOH	1293	1293	1280	1350	46	84	1353	1359.4	1359	3	54	$\delta\text{CH}_3(\text{OD side}) + \delta\text{CH}_3(\text{CO side})$			
$\nu_s\text{C-C-C=C-C}$ ring breath	1248	1250		1247	6	142	1262		1278	1	126	$\nu_{as}\text{C-C}$			
δCH	1172	1172	1174	1172	7	16	1088	1088.8							
$\pi\text{CH}_3(\text{OH side})$	1039	1042	1024	1043	2	1	1080	1078.6	1099	9	52	δOD			
$\pi\text{CH}_3(\text{CO side})$				1027	0.01	8	1039		1042	2	1	$\pi\text{CH}_3(\text{OD side})$			
$\rho\text{CH}_3(\text{OH side})$	1014	1017	1013	1015	1	10		1028.3	1027.5	2	34	$\rho\text{CH}_3(\text{OD side})$			
$\rho\text{CH}_3(\text{CO side})$	997	996	996	991	9	14		1024.0	1027.2	0.01	7	$\pi\text{CH}_3(\text{CO side})$			
γOH				988	0.5	65	997		990	3	10	$\rho\text{CH}_3(\text{CO side})$			
			958				938	937.6	928	6	25	ρCH_3 both			
ρCH_3 both	931	931	921	926	4	3	876	875.2	875	6	17	$\Delta + \rho\text{CH}_3(\text{CO side})$			
$\Delta + \rho\text{CH}_3(\text{CO side})$	912	913		901	1	37	832		832	1	0.5	δCD			
γCH				780	1	32		716.7	736	0.3	38	γOD			
Πs		611		640	0.2	0.2			648	0.3	0.6	Πs			
Δ	646						636	634.6	629	12	14	Δ			
	634	640		636	13	13	559	559.4	560	0.4	16	γCD			
Πas	555	551		549	2	0.4	552		548	2	0.2	Πas			
$\delta\text{CH}_3\text{-C-O}$	510	508		504	3	11	498		495	3	10	$\delta\text{CH}_3\text{-C-O}$			
δ carbonated skeleton	406	397		390	0.3	3			383	0.2	3	δ carbonated skeleton			
δ carbonated skeleton				366	4	7	363		359	3	7	δ carbonated skeleton			
$\delta\text{C-C=C}$	223	215		228	0.2	3	230		224	0.2	3	$\delta\text{C-C=C}$			
$\tau\text{CH}_3(\text{OH side})$	192	185		179	0.5	0.04	190		177	0.4	0.06	$\tau\text{CH}_3(\text{OD side})$			
$\tau\text{CH}_3(\text{OH side})$		149		147	0.1	0.004			146	0.1	0.01	$\tau\text{CH}_3(\text{OD side})$			
$\tau\text{CH}_3(\text{OH side})$		103		118	0.2	1			117	0.2	1.2	$\tau\text{CH}_3(\text{OD side})$			
$\tau\text{CH}_3(\text{CO side})$		61		28	0.2	0.1			28	0.2	0.08	$\tau\text{CH}_3(\text{CO side})$			

^a main characteristic motions; ν , stretching; δ , in plane bending; γ , out of plane bending; ρ , in plane rocking; π , out of plane rocking; Δ , in plane ring deformation; τ , torsion; Π , ring torsion; s , symmetric; a , asymmetric

ACETYLACETONE (D2)

process) the population of the states of both symmetries differ from the Boltzmann distribution, and the population transfer can be observed. In the case of acetylacetonone the torsion of the methyl groups is coupled to the hydrogen transfer process because of the symmetry of methyl groups in the CCC geometry.

One of the methyl groups is found to evolve in a torsional potential with very low barrier (methyl CO side), *i.e.* a large splitting is expected. Johnson *et al.* have studied the tunneling splitting of the double deuterated isotopologue of acetylacetonone in the solid phase [59]. They observe a decrease in the tunneling splitting of the less hindered methyl group (methyl in CO side)⁵⁴ compare to the non-deuterated molecule, which is explained by a decrease in the hydrogen transfer upon deuteration of the hydroxyl hydrogen.

We look for evidences of NSC in the double deuterated molecule in *para*-hydrogen matrix. Samples were left at least 8 days after deposition to check for any signal of temporal evolution in the bands of the CCC conformer. A clear change in the relative intensity of some of the bands was observed. The most obvious one is observed in the region around 708 cm⁻¹ corresponding to the OD out of plane bending (shown in Figure V.8). In fact, in AcAcD₂ the largest shift between the components was observed for the OH out of plane bending mode (11 cm⁻¹).

The bands at 707.8 and 709.2 cm⁻¹ were fitted with a Lorentzian profile, and the area of the theoretical curves was used to follow the change of the integrated intensity. The dependence of the intensity over time for the 709.2 cm⁻¹ band is given in Figure V.9. transfer and the methyl rotation. The OD modes greatly affects

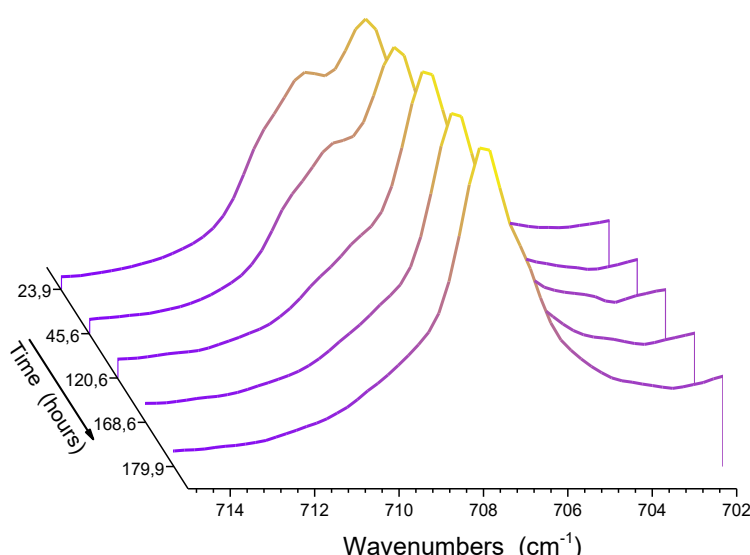


Figure V.8: Temporal evolution after deposition in *p*H₂ of a group of band in the 715-702 cm⁻¹ region (YOD mode).

⁵⁴ In acetylacetonone the methyl group from the hydroxyl (OH) side is more hindered, the tunneling splitting should be very small (4.0×10^{-3} cm⁻¹ in solid phase according to Johnson), then only NSC from the methyl group CO side is observed (0.36 cm⁻¹, solid phase, in AcAcD₂ the value is 0.27 cm⁻¹).

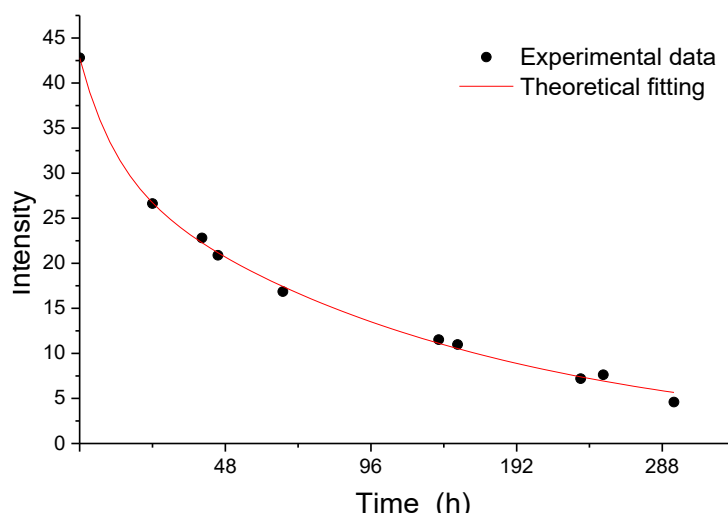


Figure V.9: Evolution over time of the intensity of the 709.2 cm^{-1} band for the CCC conformer of double deuterated acetylaceton in *para*-hydrogen matrix. Black points correspond to experimental data and red line correspond to a biexponential fitting.

the hydrogen transfer (because they are directly involved in this coordinate), affecting then the splitting of the torsional levels of the CH_3 rotor. The big influence of these modes in torsional levels of the methyl groups was demonstrated in AcAch8, in which the largest shift was also observed for the OH out of plane mode [14].

The experimental values were fitted with exponential decay functions. The best fit was obtained when the experimental curve is described by two different exponential decays (see Figure V.9). The description with two exponential functions suggest that different processes are taking place, one with a fast kinetic (0.087 h^{-1}) and the other with a slower one (0.0087 h^{-1}). The value obtained for the fast kinetic in the deuterated molecule is in the order of magnitude found for AcAch8 (0.042 h^{-1}). A similar behavior regarding the processes in place was observed for the CH_3F molecule [204]. But, the kinetics was different, $k_1 = 0.13 \text{ h}^{-1}$ and $k_2 = 0.022 \text{ h}^{-1}$ (the sample was observed for 30 h). Lee *et al.* associate the two observed process to a change (decreasing over time) in the amount of oH_2 molecules interacting with the guest molecule and accelerating the NSC. In that case, the kinetics depends on the quality of the *para*-hydrogen matrix.

We want to remark that the shift between the less stable (*E*) and most stable (*A*) component in the deuterated isotopologue (1.4 cm^{-1}) is much lower than the value for non-deuterated acetylaceton (10.5 cm^{-1}) for the mode in questions. The results obtained by Johnson *et al.* [59] suggest that the *A-E* splitting in the ground state is reduced by 25% in AcAcD2. The effect of the OH bending excitation ($\nu = 1$ in γ_{OH} mode) does not increase a lot this splitting, contrary to the excitation of γ_{OH} in AcAch8 [14]. It is another consequence of the reduced hydrogen transfer in AcAcD2 compared to AcAch8.

V.3. UV laser irradiation: Isomerization

UV irradiation of matrix samples doped with acetylacetone induces the photo-isomerization of the enolic form and the production of open enol conformers. In previous studies done in our group at Orsay with AcAcH8 isolated in neon and *para*-hydrogen matrices, it was shown that the produced open conformers can be separated in two groups: a first one, reduced to CTC, growing from CCC upon irradiation at 266 nm and disappearing in a prolonged irradiation, and a second group, including mainly TCC with a very weak amount of TTC, growing slower upon the same irradiation [15]. A similar behavior is expected with AcAcD2 isolated in neon matrices. With the OPO laser as the UV irradiation source, it is possible to excite acetylacetone in a broad range of UV wavelengths.

In the case of AcAcD2, we did experiments mainly in neon, but we will also present preliminary results in *para*-hydrogen. Generally, we observed different behaviors according to the different wavelengths used in the 250-280 nm range. But in any case, new bands are growing while the CCC conformer is disappearing.

The spectra are complex but these bands can be classified in two groups of open enol conformers. A clear assignment was possible in each group based on two additional processes: (i) the relative intensities of the new bands change in time without irradiation, meaning that the spectra contained the signature of stable and meta-stable conformers; (ii) IR laser irradiation performed after UV irradiation affects differently the produced conformers.

In order to precise the efficiency of the UV irradiation on the various conformers of acetylacetone, we recorded first the UV absorption spectra of acetylacetone isolated in solid neon. These spectra helped in the choice of the excitation wavelengths to induce photo-isomerization.

V.3.1. UV absorption spectra of acetylacetone in solid neon

The UV absorption of AcAcH8 (CCC form) in neon matrices is shown in Figure V.10, left panel - black line. Electronic absorption spectra of acetylacetone in different matrices were already published [205], but not in solid neon. The CCC absorption band position is slightly redshifted from the gas phase [206] with a maximum of absorption at 265 nm in Ne (262.7 nm in the gas phase). The maximum of the band was also found around 265 nm in N₂ and was redshifted in Ar and Xe (maximum around 270 nm) [43]. All these results indicate a weak effect of the matrix on the electronic structure of acetylacetone.

We benefit from the previous study of photo-isomerization of AcAcH8 in neon [15] to use the best experimental conditions to get samples with almost only one conformer trapped. The spectra obtained for CTC and TCC conformers is displayed in Figure V.10, left panel (red dots and blue dashed lines respectively).

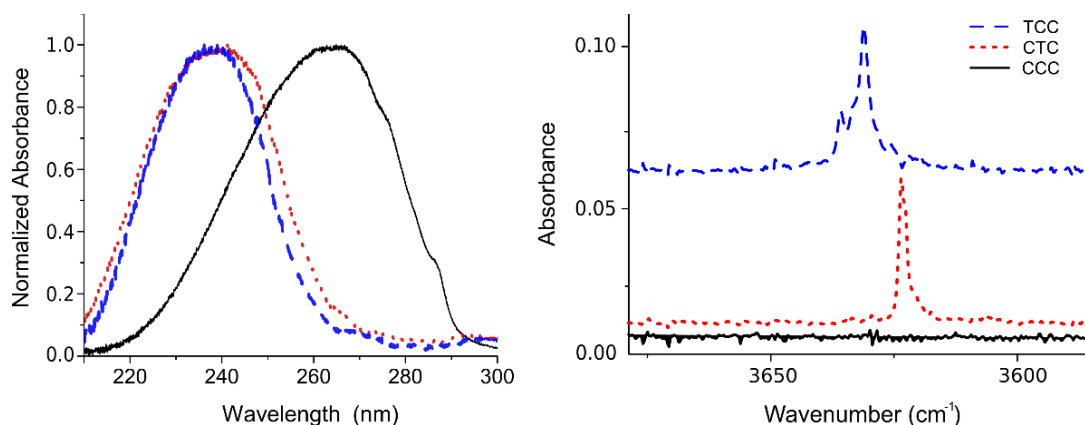


Figure V.10: Left: Electronic absorption spectra of acetylacetone (AcAcH8). CCC (black solid line), first group (CTC) (red dots) and second group (mainly TCC) (blue dashed) of conformers; Right: IR spectra corresponding to each group. The open conformer spectra are obtained combining different weighted spectra in order to get separated spectra for each conformer.

In the spectra shown in Figure V.10, the CCC conformer spectrum was subtracted from the open enol conformer spectra for better clarity, and spectra were normalized.

The three conformers have broad absorption bands. The UV absorption spectra of CTC and TCC are very close (maxima around 240 nm and 237 nm respectively). The IR spectra of the same samples in the frequency range of free OH stretching modes are displayed in the right panel of Figure V.10 to confirm the assignments: CCC—black solid (no free OH), CTC—red dots and TCC—blue dashed lines. Theoretical calculations on the electronic states of AcAcH8 (CR-EOMCCSD(T) method) [205] reported a difference of only 7 nm in the electronic absorption of CTC and TCC, whereas a blue shift of 19 nm was calculated between CTC and CCC: these estimations are in good agreement with the present results in Ne.

The UV absorption spectra of deuterated acetylacetone should be very similar to those of AcAcH8, because of the small perturbation due to deuteration. This assumption was confirmed by recording the absorption spectrum of AcAcD2/Ne after deposition to get the electronic absorption spectrum of the CCC form. We use then the clear results obtained with AcAcH8 to choose the UV wavelengths for the photo-isomerization experiments.

V.3.2. First group of deuterated conformers

V.3.2.1. Neon matrix

In order to obtain mostly the first group, the deposited sample was irradiated in the red part of the CCC absorption band, at 280 nm, far from the maximum of absorption of the other conformers and especially that of CTC (see Figure V.10). In Figure V.11 the simultaneous decrease of CCC with the increase of the two

ACETYLACETONE (D2)

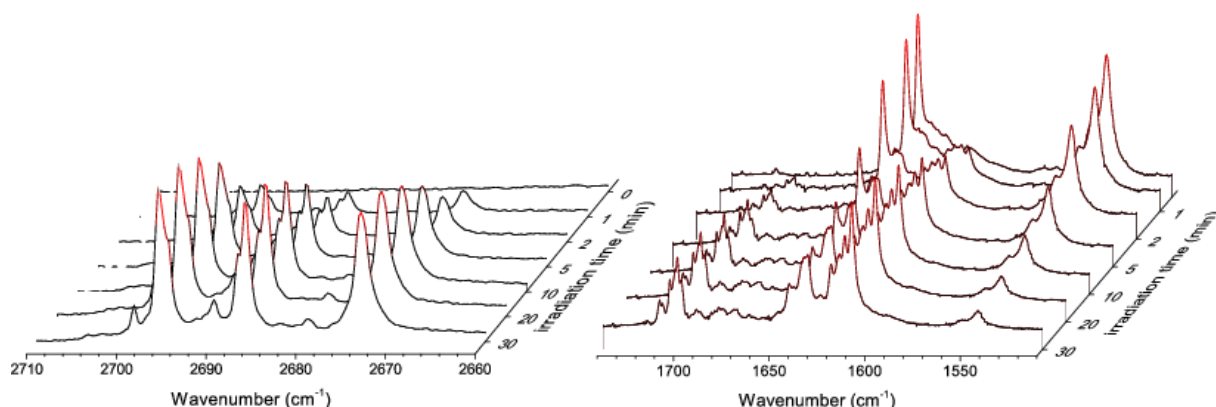


Figure V.11: Evolution of deuterated acetylacetonone IR spectra under 280 nm laser irradiation (from the back to the front). Left: OD stretching region of non-chelated conformers (zoom 14x). Right: C=O and C=C stretching region. The first group of conformers is mainly produced but a small amount of second group is also observed in the spectra.

different groups of conformers can be observed. These groups differ by their kinetics, in the same way as in AcAch8/Ne experiments [15]. When CCC is almost depleted, the first group is predominant. Its spectrum is reproduced in Figure V.12. The second group will be discussed in the next section. It should be pointed out before continuing, that samples with different AcAcD2/AcAcD1 ratios were used during the experiments (for both groups). Because of this, AcAcD1 bands can be easily observed in some spectra. Their assignment is discussed in section V.3.4.

Figure V.12, panel (a), shows the most relevant regions of the IR spectrum of the first group in a neon matrix. The bands coming from CCC and from the second group have been subtracted from the original spectrum. Theoretical spectra of CTC(D2) and CTT(D2) are also reported in Figure V.12 (top panel) for comparison. They allow the assignment of most of the intense bands to these two species. Bands in the 2660-2710 cm^{-1} region (Figure V.12, left) correspond to the OD stretching modes of the deuterated isotopologues. Their number should give an idea of the number of produced conformers. However, because of the mixture of double and mono deuterated isotopologues, these OD modes could belong to AcAcD2 and AcAcD1(OD) open conformers. Moreover, some bands in the spectrum exhibit a doublet structure which comes from site effects. Such doublets are also observed in non-deuterated conformers trapped in solid neon. The presence of different sites was confirmed by annealing process. The site structure is more pronounced in the spectra of modes involving significantly OD motion, *e.g.* OD stretching modes and OD in-plane bending modes (group of doublets near 950 cm^{-1}).

Surprisingly, when leaving the sample in the dark, an evolution in the spectrum of open conformers is observed: some bands increase while others decrease. The corresponding difference spectrum is displayed in Figure V.12, panel (b). This change is attributed to an interconversion between CTT and CTC conformers.

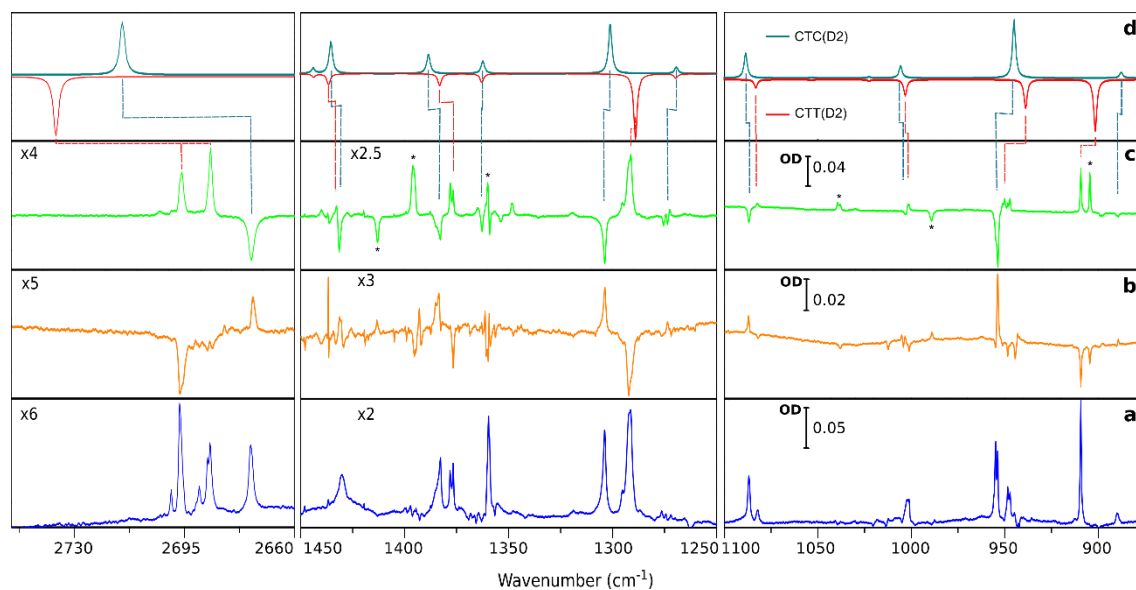


Figure V.12: a) IR spectra of the first group of conformers (bands from CCC and from the second group are subtracted from the original spectrum), b) Difference IR spectrum between the sample just after UV irradiation and 68 h later (kept in the dark), c) Difference IR spectrum of the sample between after and before IR laser irradiation at 5235 cm^{-1} , d) IR theoretical spectrum in the harmonic approximation (scaled by 0.981) of CTC(D2) (blue) and CTT(D2) (red) conformers (Lorentzian bandwidths of 2 cm^{-1}). The positive/negative directions are set in order to compare to panel b). Zooms in the left and middle panels refer to the optical density of the right panel.

The process is very slow, with a kinetic rate estimated at 10^{-7} s^{-1} from experimental measurements. This result gives an important information about conformers stability but also a confirmation of the attribution of the lines of the most stable conformer (CTC with the lowest energy, see Figure V.1). One can notice that the spontaneous CTT \rightarrow CTC interconversion depends on the site where CTT(D2) is trapped, as can be seen in Figure V.12, panel (b).

It is known from previous studies on small organic compounds (including acetylacetone) that interchange between two rotational conformers (around a single bond) could be induced by irradiation with infrared laser matching its wavelength to the absorption of corresponding mode in the molecule [51], [207], [208]. Trivella *et al.* observed that in acetylacetone IR irradiation did not affect the CCC conformer but selective IR irradiation on the OH stretching fundamentals induced changes in the CTC/CTT and TCC/TCT pairs of conformers [43]. The interconversion was matrix dependent: not observed in Ne and Ar matrices, observed only in the CTC/CTT pair in Xe and observed in both pairs in N_2 .

In order to confirm and complete our previous assignment, IR laser irradiation experiments with the laser frequency in the range of the OD stretching first overtone were performed. In our lab, the excitation source available (OPO laser) has no emission below 3700 cm^{-1} , so, it cannot be used to excite the OD fundamentals. In this case, OD overtones bands were chosen to test the photoisomerization process induced by vibrational excitation. The region of the first OD overtones was not recorded in the IR absorption spectra. We found

ACETYLACETONE (D2)

and assigned them by scanning the OPO laser frequency in the region predicted by the anharmonic calculations. The CTC \leftrightarrow CTT interconversion is effectively observed when the laser is in resonance with the first overtone. The effect of IR irradiation at 5235 cm^{-1} is displayed in Figure V.12, panel c. In this case, CTC bands are depleted while those of CTT increase in intensity. An irradiation at 5280 cm^{-1} produces the CTT \rightarrow CTC interconversion, making the process reversible. Furthermore, after IR irradiation at 5235 cm^{-1} , CTT converts back to CTC once the IR laser is turned off, similarly to what happens after UV irradiation. The overtones of the three main OD stretching bands of Figure V.12, panel (c) are obtained and the values are reported in Table V.5, in comparison with theoretical estimations calculated within the anharmonic approach. These experiments proved that the three OD bands (Figure V.12 a, left panel) belong to AcAcD2 open conformers - one to CTC(D2) and two to CTT(D2) -, and not to the monodeuterated isotopologue. The anharmonicity constants ξ_{ii} ⁵⁵ are also given in Table V.5. A relatively constant experimental value ($\sim 56.5 \text{ cm}^{-1}$) is obtained for all the conformers, indicating that the same perturbation of the O-D oscillator occurs in the four different configurations.

Table V.5: Experimental and theoretical frequencies (cm^{-1}) of the first overtones (ν_{OD} modes) in AcAcD2 open enol conformers in neon. Anharmonicity constants determined from experimental and theoretical (in parenthesis) values are also included.

Isomer	$\nu_{\text{anharmonic}}/\text{cm}^{-1}$ (Theoretical)	$\nu_{\text{anharmonic}}/\text{cm}^{-1}$ (Experimental)	Anharmonicity constant / cm^{-1}
CTC	5255	5235	57 (79)
CTT	5279	5260 5280	56 (88)
TCC	5230	5243	58 (99)
TCT	5289	5280	55 (93)

Combining the information from all the experiments and theoretical calculations, we conclude that the conformers produced in the first group are CTC(D2) and CTT(D2). Experimental frequencies and calculated values for CTC(D2) and CTT(D2) conformers are summarized in Table V.6. One can notice that there is no obvious narrowing of the CTC bands from AcAch8 to AcAcD2, even on the OH/OD stretching bands (bandwidths of 1.7 cm^{-1} in AcAch8 and 1.5 cm^{-1} in AcAcD2). The large bandwidth difference is observed only between the chelated enol conformers allows to conclude that highest influence of deuteration is on intramolecular hydrogen bond properties.

⁵⁵ ξ_{ii} is defined by: $2\nu_{i \rightarrow i+1} - \nu_{i \rightarrow i+2} = 2 \xi_{ii}$ [162]

The first group of open conformers was reduced to CTC in the case of AcAcH8 trapped in neon. A fast CTT→CTC interconversion was assumed to explain the absence of CTT, in comparison with the behavior of irradiated AcAcH8 in other matrices where CTT was observed. This assumption is confirmed by the deuteration effect: the tunneling process at play in the CTT→CTC interconversion is slower in the case of AcAcD2, allowing the detection of CTT in solid neon.

V.3.2.2. *para*-hydrogen matrix

Preliminary UV irradiation experiments were also carried out in *para*-hydrogen matrix at 3K. The first results allow us to identify the presence of two open enol conformers after irradiation at 280 nm (see Figure V.13). These conformers correspond to the CTC(D2) and CTT(D2) conformers already discussed in the first group of bands in neon.

Contrary to neon, in *para*-hydrogen no spontaneous evolution was observed in the intensity of the bands after producing the open enol conformers (18 h after irradiation). The IR irradiation over the overtones of OD stretching modes was also performed, but no change was induced by irradiation.

Nevertheless, these results are not conclusive. First, IR irradiation was done just once without a good knowledge of the overtones frequencies which are not the same for *para*-hydrogen and neon. Second, in the sample used for pH₂ experiments there are some amount of water (as remarked for the CCC spectrum, Figure V.13), which can interact with the acetylacetone (D2) molecule and change the dynamic behavior of the system. New tests need to be done to get rigorous conclusions.

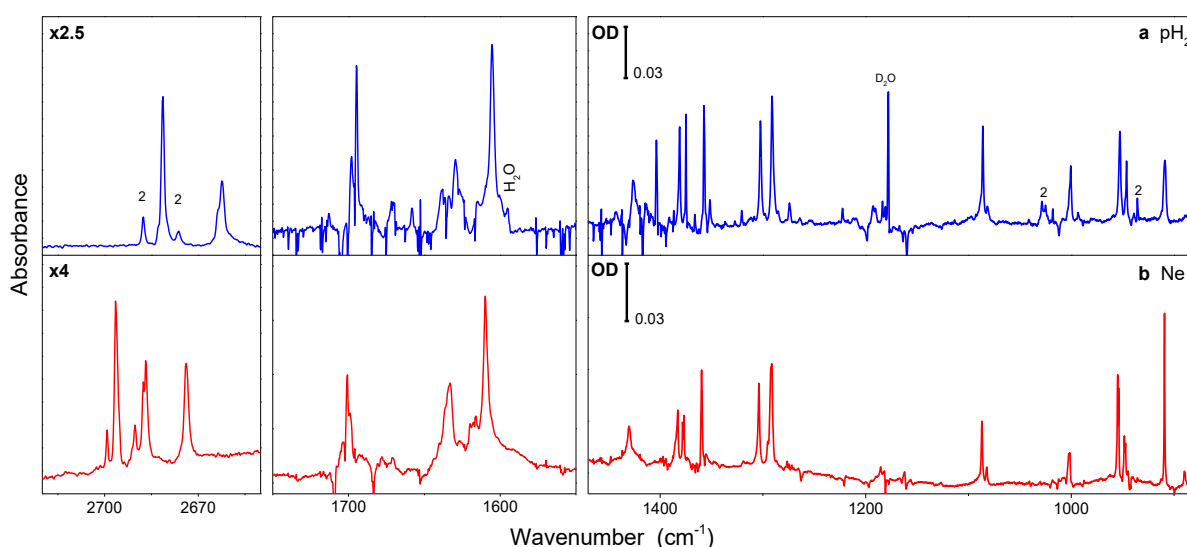


Figure V.13: FT-IR spectra of the first group of conformers in (a) *para*-hydrogen and (b) neon. Negative lines are mainly due to bad environmental water compensation and subtractions of the CCC conformer. Water bands (isotopologues) in trapped in pH₂ are identified in the spectrum. Bands belonging to a second group of conformers are identified with a “2”.

ACETYLACETONE (D2)

Table V.6: First group of conformers: experimental frequencies (cm^{-1}) in neon and *para*-hydrogen compared to theoretical frequencies (cm^{-1}) [B3LYP/6-311++G(3df,3pd)]. Theoretical values in scaled harmonic (0.981) approximation (and anharmonic approximation). Intensities (km/mol) obtained in the harmonic approximation.

Assignments ^a	Experimental		Theoretical		
	Ne	ρH_2	CTC	CTT	Int.
vOD	2696.5 ^b 2686.8 ^b	2682		2727.4 (2684.0)	53
vOD	2674.3	2663.6	2706.4 (2672.1)		29
vCD	2273	2269		2299.3 (2264.7)	4
vCD	2247	2245	2266.0 (2227.6)		12
$\nu_a(\text{C}=\text{C} + \text{CO})$	1707.7	1698.4	1701.6 (1701.4)		170
$\nu_a(\text{C}=\text{C} + \text{CO})$	1698.8	1694.9		1699.3 (1694.4)	171
$\nu_s(\text{C}=\text{C} + \text{CO})$	1632.9	1632.0		1617.7 (1603.3)	481
$\nu_s(\text{C}=\text{C} + \text{CO})$	1610.0	1605.5	1597.1 (1566.1)		545
$\delta_a\text{CH}_3(\text{OD side})$	1433.1	1426.8		1431.9 (1427.7)	41
$\delta_a\text{CH}_3(\text{OD side})$	1431.4		1431.0 (1418.0)		80
$\delta_s\text{CH}_3(\text{OD side})$	1382.8	1381.1	1357.7 (1378.4)		49
$\delta_s\text{CH}_3(\text{OD side})$	1376.7	1375.0		1378.8 (1373.0)	46
$\delta_s\text{CH}_3(\text{CO side})$	1359.8		1358.1 (1351.7)		30
$\delta_s\text{CH}_3(\text{CO side})$	1359.8	1357.2		1358.5 (1352.7)	34
$\delta_s\text{CH}_3 + \nu(\text{C}-\text{CH}_3)(\text{OD side})$	1304.1	1302.5	1296.0 (1288.8)		122
$\delta_s\text{CH}_3 + \nu(\text{C}-\text{CH}_3)(\text{OD side})$	1292.5 ^b 1291.2 ^b	1291.1		1285.0 (1275.3)	251
$\nu(\text{C}-\text{CH}_3)$ (CO side)+ $\nu(\text{C}-\text{O})$ +δCH_3	1273.5		1265.4 (1249.6)		16
$\nu(\text{C}-\text{CH}_3)$ (CO side)+ $\nu(\text{C}-\text{O})$ +δCH_3	1273.5	1274.3		1265.7 (1258.9)	17
$\rho\text{CH}_3(\text{CO side})$	1087.0	1086.1	1085.2 (1079.6)		63
$\rho\text{CH}_3(\text{CO side})$	1082.7	1081.7		1079.8 (1078.2)	18
ρCH_3 (OD side)	1001.3	1001.5	1002.6 (999.1)		30
ρCH_3 (OD side)	1001.3	1000.6		1000.1 (994.6)	35
$\rho\text{CH}_3(\text{CO side}) + \delta\text{OD}$	954.9 ^b 953.8 ^b	952.8	942.0 (934.5)		145
$\rho\text{CH}_3(\text{CO side}) + \delta\text{OD}$	948.4 ^b 947.2 ^b	946.2		935.8 (936.6)	64
δOD	909.4	909.1		898.7 (901.1)	113
$\delta\text{OD} + \delta\text{CD}$	890.1 ^b 889.4 ^b		884.9 (886.1)		14
	708.7			708.9 (707.1)	12
	680.7		694.0 (699.3)		20

^amain characteristic motions; ν , stretching; δ , in plane bending; γ , out of plane bending; ρ , in plane rocking; π , out of plane rocking; Δ , in plane ring deformation; s , symmetric; a , asymmetric

^bbands with doublets due to sites effects

V.3.3. Second group of deuterated conformers in neon matrix

After depletion of the CCC conformer upon irradiation at 280 nm, the samples were irradiated at 260 nm to enhance the production of the second group of conformers. At 260 nm, the absorption of the second group is lower than that of the first one while the CCC can still absorb and react. The second group is the only one growing under 260 nm irradiation.

The IR spectrum of the second group is shown in Figure V.14, panel (a). Two strong bands are observed in the OD stretching region. One decreases while the other increases in the dark (Figure V.14, panel b). Consequently, they are assigned to two conformers prone to interconversion process, similarly to the CTT/CTC pair. Kinetics of this process is slow: the kinetic constant is estimated around 10^{-6} s^{-1} , which is one order of magnitude larger than for the CTT/CTC pair.

IR laser irradiation in the range of OD stretching overtones was also performed, similarly to the experiments with the first group, and the same behavior was observed, *i.e.* the reversible conversion of one species to the other (Figure V.14, panel c). The overtones frequencies are reported in Table V.5.

Combining the information coming from all the experimental and theoretical data, we conclude that the second group is formed by TCC(D2) and TCT(D2). The theoretical spectra of these two conformers are reported in Figure V.14, panel (d) for comparison. Experimental frequencies and calculated values for

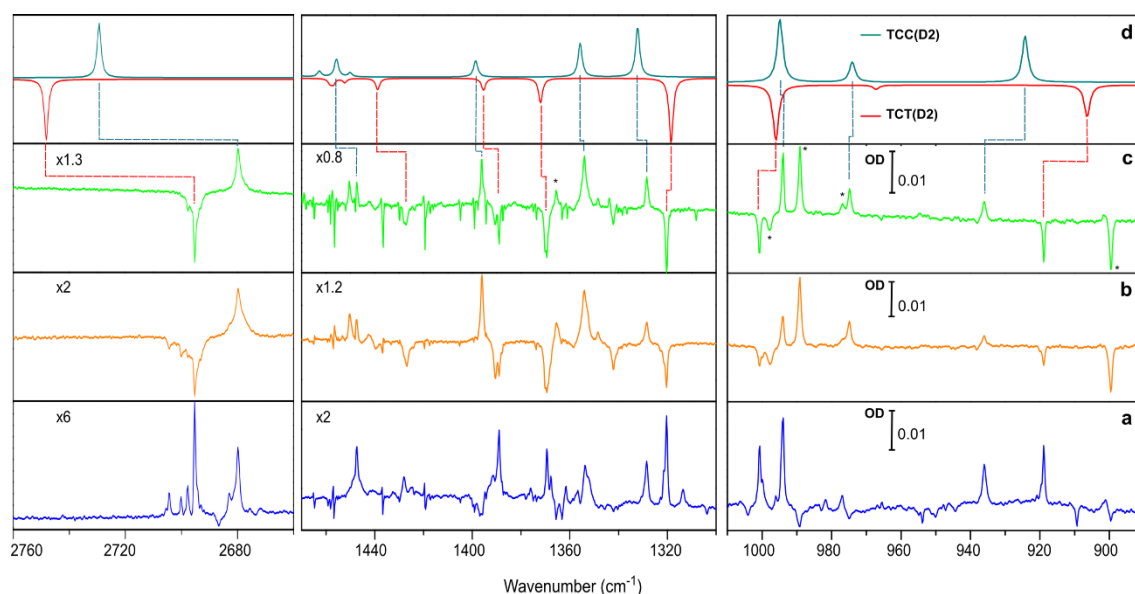


Figure V.14: a) IR spectra of the second group of conformers (negative bands come from non-compensated subtraction of first group and H8 conformers), b) Difference IR spectrum between the sample just after UV irradiation and 72 h after (kept in the dark), c) Difference IR spectrum of the sample after and before IR laser irradiation at 5280 cm^{-1} , d) IR theoretical spectrum in the harmonic approximation (scaled by 0.981) of TCC(D2) and TCT(D2) conformers (The positive/negative directions are set in order to compare to panel b). Zooms in the left and middle panels refer to the optical density of the right panel.

ACETYLACETONE (D2)

conformers assigned to the second group are summarized in Table V.7. Importantly, the TCT conformer in AcAcD2/Ne samples is clearly detected while it was not observed in AcAcH8/Ne samples. As in the case of the first group, there is a slow quantum tunneling of the deuterium, compared to the measurement time scale, whereas the tunneling of hydrogen was too fast in AcAcH8 to be observed.

In the present experiments, there is no evidence of the TTC conformer which was detected in a very low amount in AcAcH8/Ne. As the bands were very weak, if TTC(D2) exists, its bands cannot be clearly distinguished from bands coming from the different conformers of AcAcD1. So, no conclusion can be stated for TTC(D2).

In addition to the experiments previously discussed, we performed a supplementary irradiation at 250 nm after the irradiation at 260 nm in order to excite more efficiently the second group. This last irradiation induces a change inside the second group: TCT bands increase and TCC bands decrease. We do not see any increase of the bands associated with other conformers. It suggests that the TCT/TCC production ratio depends on the energy of the system in the excited S_2 state and/or on the initial geometry of acetylacetonone in this state. Consequently, the measured TCT/TCC ratio in Ne depends on the UV irradiation wavelength just after UV irradiation and then evolves in time. Because of the fast TCT→TCC conversion in the case of AcAcH8, this kind of process cannot be explored with the fully hydrogenated isotopologue. On the other hand, TCT was also observed in more perturbative matrices (Ar, Xe, N₂, n-H₂ and n-D₂) where it can be stabilized by interactions with the host. In these cases, matrix effects must play a role in the observed molecular processes. We want to note that a second group of bands was observed in *para*-hydrogen matrix. But, not enough amount was produced because of technical issues. Matrix evaporations occurred when irradiating at low wavelength, in the two experiments conducted. So, no confident assignment could be done.

V.3.4. Monodeuterated open enol conformers in neon

The assignment of AcAcD1 open conformers is very difficult, due first to their low concentration compared to AcAcD2 conformers, and second to the mixture of AcAcD1(CD) and AcAcD1(OD) conformers. In addition, the effects of IR overtone irradiation and conformer interconversion in the AcAcD1(OD) are also less marked. Nevertheless, we assigned several bands to the first group of AcAcD1(OD) isotopologue (**CTT**: 904.5, 1155.7, 1361.0, 1395.2 cm⁻¹; **CTC**: 989.3, 1038.1, 1165.2, 1412.9 cm⁻¹) and only one to AcAcD1(CD) isotopologue (**CTC**:

Table V.7: Second group of conformers: experimental frequencies (cm^{-1}) in Ne compared to theoretical frequencies (cm^{-1}) [B3LYP/6-311++G(3df,3pd)]. Theoretical values in scaled harmonic (0.981) approximation (and anharmonic approximation). Intensities (km/mol) obtained in the harmonic approximation.

Assignments ^a	Experimental	Theoretical		
		TCC	TCT	Int.
ν OD	2695.4		2737.3 (2689.2)	56
ν OD	2679.8	2714.8 (2661.9)		52
$\nu_a(\text{C}=\text{C} + \text{CO})$	1681.8	1683.9 (1686.3)		232
$\nu_a(\text{C}=\text{C} + \text{CO})$	1678.0		1684.3 (1685.3)	175
$\nu_s(\text{C}=\text{C} + \text{CO}) + \delta\text{OD}$	1664.1		1650.3 (1646.3)	363
$\nu_s(\text{C}=\text{C} + \text{CO}) + \delta\text{OD}$	1635.4	1617.2 (1614.0)		397
$\delta_a\text{CH}_3(\text{OD side})$	1447.5	1451.2 (1451.2)		36
$\delta_a\text{CH}_3(\text{CO side})$	1427.2		1434.3 (1424.2)	22
$\delta_s\text{CH}_3(\text{OD side})$	1396.1	1394.2 (1407.8)		33
$\delta_s\text{CH}_3(\text{OD side})$	1389.2		1391.0 (1401.2)	23
$\delta_s\text{CH}_3(\text{CO side})$	1369.4		1367.7 (1360.3)	48
$\delta_s\text{CH}_3(\text{CO side})$	1354.1	1351.5 (1342.4)		67
ν (carbon skeleton) + $\delta_s\text{CH}_3$	1328.6	1328.0 (1319.2)		101
ν (carbon skeleton) + $\delta_s\text{CH}_3$	1320.2		1314.3 (1303.9)	126
$\nu_s \text{C}-\text{CH}_3 + \rho\text{CH}_3$ (CO side)	1224.1	1211.0 (1202.8)		68
$\nu_s \text{C}-\text{CH}_3 + \rho\text{CH}_3$ (CO side)	1222.6		1208.8 (1200.4)	118
$\rho\text{CH}_3(\text{OD side}) + \delta\text{OD}$	1098.0	1095.5 (1093.3)		41
$\rho\text{CH}_3(\text{OD side}) + \delta\text{OD}$	1097.1		1093.8 (1092.3)	36
$\rho\text{CH}_3(\text{CO side})$	1000.8		992.9 (993.2)	44
$\rho\text{CH}_3(\text{OD side})$	994.1	991.7 (990.3)		55
ρCH_3 (CO side)	977.0	970.9 (970.3)		18
$\delta \text{CD} + \delta \text{OD}$	936.2	921.3 (903.8)		40
δOD	919.0		903.5 (908.7)	25
δCD	847.6		845.2 (853.1)	47

^a main characteristic motions; ν , stretching; δ , in plane bending; ν , out of plane bending; ρ , in plane rocking; π , out of plane rocking; Δ , in plane ring deformation; s , symmetric; a , asymmetric

ACETYLACETONE (D2)

1181.0 cm^{-1}). In the second group we were also able to assign some bands of AcAcD1(OD) isotopologue (**TCT**: 899.6, 998.0, 1192.7, 1263.1 cm^{-1} ; **TCC**: 974.8, 989.2, 1264.1, 1365.7 cm^{-1}). Other bands are observed but a straightforward assignment is not possible.

Before finishing this section, we want to note that keto tautomer did not increase its amount during any UV irradiation performed in the experiments. The production of keto tautomer could be done by two mechanisms: first, from direct relaxation of the electronic excited enol conformer which implies a big rearrangement of the structure (including proton transfer). Second, from a recombination process after photo-fragmentation. No fragments were observed after UV laser irradiation in the experiments performed. Lozada *et al.* observed for AcAch8 in neon and $p\text{H}_2$ that the amount of keto tautomer increases when irradiating at 248 nm for 6 hours [209]. The increase of this tautomer was small compared to open enol conformers (and accompanied of fragmentation), even when they are higher in energy (see Figure V.1). Nevertheless, we did not perform such a long irradiation at wavelength lower than 250 nm, so, the comparison with AcAch8 is not straightforward.

V.4. Tunneling process

CTT \rightarrow CTC and TCT \rightarrow TCC interconversion processes are assumed to be due to proton tunneling because of the significant deuteration effect we observed. The tunnel effect is very important at low temperatures and it has been found in several small organic molecules and complexes [210], [211]. Relaxed scan (and Internal Reaction Coordinate) calculations were performed in order to estimate the rotational barriers for the processes under study. The theoretical heights of the barriers, ZPE included, for both pairs of conformers and both isotopologues (AcAch8 and AcAcD2) are reported in Table V.8. ΔZPE is the difference in ZPE energies obtained for the transition state and the trans conformer XYT (CTT or TCT); ω_0 is the calculated OH/OD rotation frequency (γOH mode) at MP2 level.

A first conclusion is that these barriers are too high compared to thermal energy (6.7×10^{-2} kJ/mol at 8 K) to be overpassed thermally, supporting the tunneling assumption. As indicated by the values reported in Table V.8, the differences in rotational barrier heights between both isotopologues are small, confirming also that the different heights do not govern the different behaviors of AcAcD2 and AcAch8. The two barriers (IRC calculation) are drawn in Figure V.15 in the case of double deuterated isotopologues. They are found very similar (height and width), the barrier is slightly lower between TCT and TCC than between CTT and CTC.

The experimental kinetic constants k related to the tunneling rates were estimated for each pair from the evolution after 68h of the intensities of some characteristic bands assigned to each conformer. We can compare them with the theoretical values obtained within the WKB semiclassical approximation [178]. This methodology has been successfully used in the description of other systems, but gives only an order of magnitude of the kinetic rate [212], [213].

Table V.8: Theoretical rotational barrier (in kJ/mol and cm^{-1}), ZPE difference (ΔZPE in kJ/mol) and frequency ω_0 of the OH/OD rotational mode (Hz) at MP2 level for the pairs of observed conformers, experimental and calculated tunneling rates, k (s^{-1}).

		CTT \rightarrow CTC		TCT \rightarrow TCC	
		AcAcH8	AcAcD2	AcAcH8	AcAcD2
Barrier height	(kJ/mol)[‡]	23.8	24.5	21.4	22.1
	[cm^{-1}]	[1989.5]	[2048.0]	[1788.9]	[1847.4]
ΔZPE	(kJ/mol)	2.8	2.1	2.5	1.8
ω_0	(Hz)	1.17×10^{13}	8.69×10^{12}	1.09×10^{13}	8.29×10^{12}
Tunneling rate constant(k)					
Experimental value		-	5×10^{-7}	-	3×10^{-6}
Theoretical value		2×10^{-1}	2×10^{-7}	1	3×10^{-6}

[‡] ZPE included

The calculated values are reported in Table V.8 together with the estimated experimental values. A difference of six orders of magnitude in the values of the theoretical rates between non deuterated and deuterated isotopologues is found in each pair. The barriers are quite similar and the major difference comes

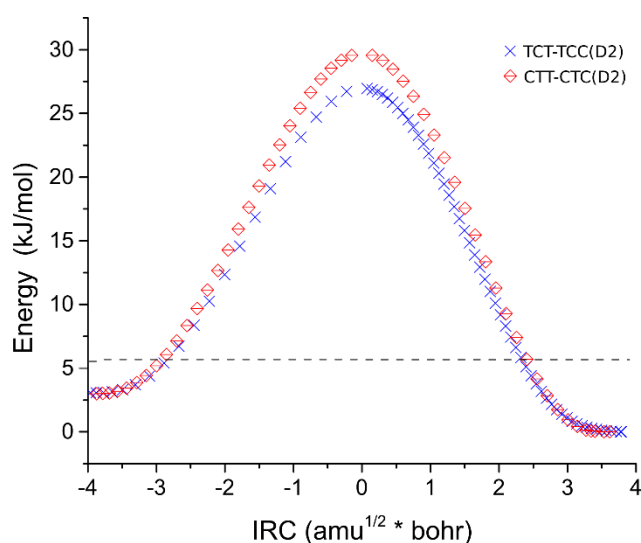


Figure V.15: Calculated CTT \rightarrow CTC and TCT \rightarrow TCC (from the left to the right) theoretical barriers, through IRC method. The dashed line represents approximately the kinetic energy of the particle (deuterium atom), estimated as $\Delta ZPE = ZPE(trans) - ZPE(TS)$ (different for each pair -see Table V.8).

ACETYLACETONE (D2)

from the reduced masses and ΔZPE values in the two isotopologues. The orders of magnitude of k obtained for the non-deuterated molecules highlight a fast tunneling process, in the timescale of seconds, and fully explain the absence of XYT(H8) conformers in the FT-IR spectra recorded more than few seconds after the laser irradiation [15]. Deuteration totally changes the XYT lifetimes. Theoretical values for deuterated pairs describe very well the slow process observed. We obtain a very good agreement for both pairs of conformers, despite the WKB approximation and the fact that the matrix is not taken into account. It seems that the effect of the neon matrix in this process is negligible. Generally, the presence of the matrix slows down the isomerization, but it depends both on the host and the guest [212], [214]. Theoretical estimations open in fact a puzzling matrix effect: whereas tunneling rate constants are larger for TCT \rightarrow TCC than for CTT \rightarrow CTC, TCT is found easier stabilized by a cryogenic lattice than CTT (TCT is observed in Ar, *n*-H₂ and *n*-D₂ and not CTT). This could be related to the fact that in the TCT/TCC pair, the OH group stays in the vicinity of methyl groups, while it is only the case in the less stable CTT conformer of the CTT/CTC pair (see Figure V.1): the geometries of two methyl groups are slightly modified in the TCT \rightarrow TCC process, while only one is involved in the CTT \rightarrow CTC tunneling and the global modification of the molecule can be more perturbed by the matrix in the former case than in the latter.

Chapter VI 3-Chloroacetylacetone

Chloroacetylacetone is the only halogenated analog of acetylacetone studied in this work with a substitution on the α hydrogen. This allows us to directly evaluate the influence of an electronegative substituent in the hydrogen bond strength and the photo-isomerization process. First, theoretical and experimental results obtained for chloroacetylacetone are presented. Then, some preliminary results of the monodeuterated analog, including photoisomerization, are also discussed.

VI.1. Theoretical results

Open enol conformers and keto tautomer structures were optimized at M06-2X level of theory. This new functional was chosen instead of B3LYP because it is parametrized to describe non covalent interactions and works well with organic halogenated molecules [151]. In fact, a better description of the experimental vibrational spectra was obtained with M06-2X compared to B3LYP for all the halogenated molecules studied in this work. The energies relative to CCC as well as their structure are shown in Figure VI.1. The energy values are corrected with the Zero-Point Energy of each conformer and tautomer.

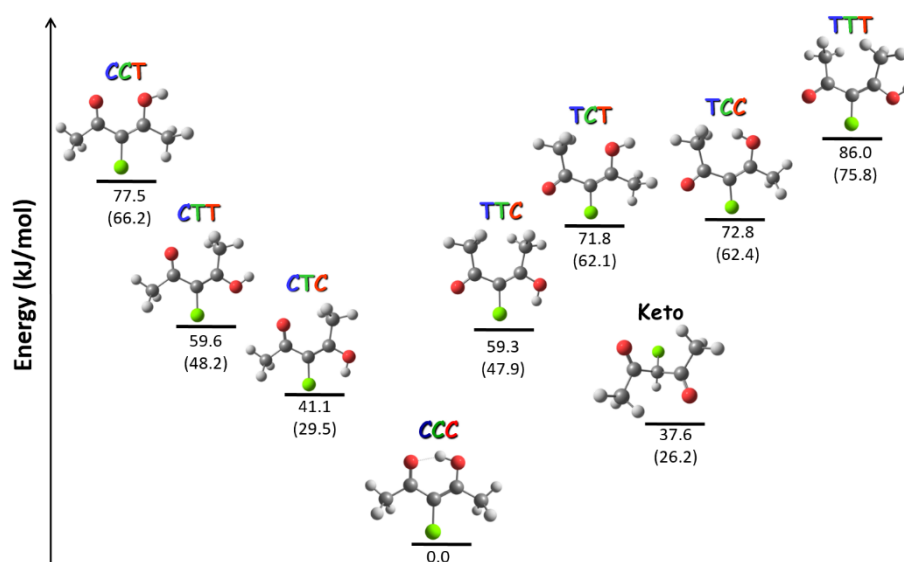


Figure VI.1: Structure and relative energies (kJ/mol) of open enol conformers and keto isomer compared to the CCC conformer, in AcAcCl at M06-2X/6-311++G(3df,3pd). B3LYP values are included in parenthesis. Zero Point Energy is included in each reported value.

3-CHLOROACETYLACETONE

The same trend was obtained with B3LYP functional, being the only difference the TCC-TCT pair of conformers, who have almost the same energy within the error of the methods.

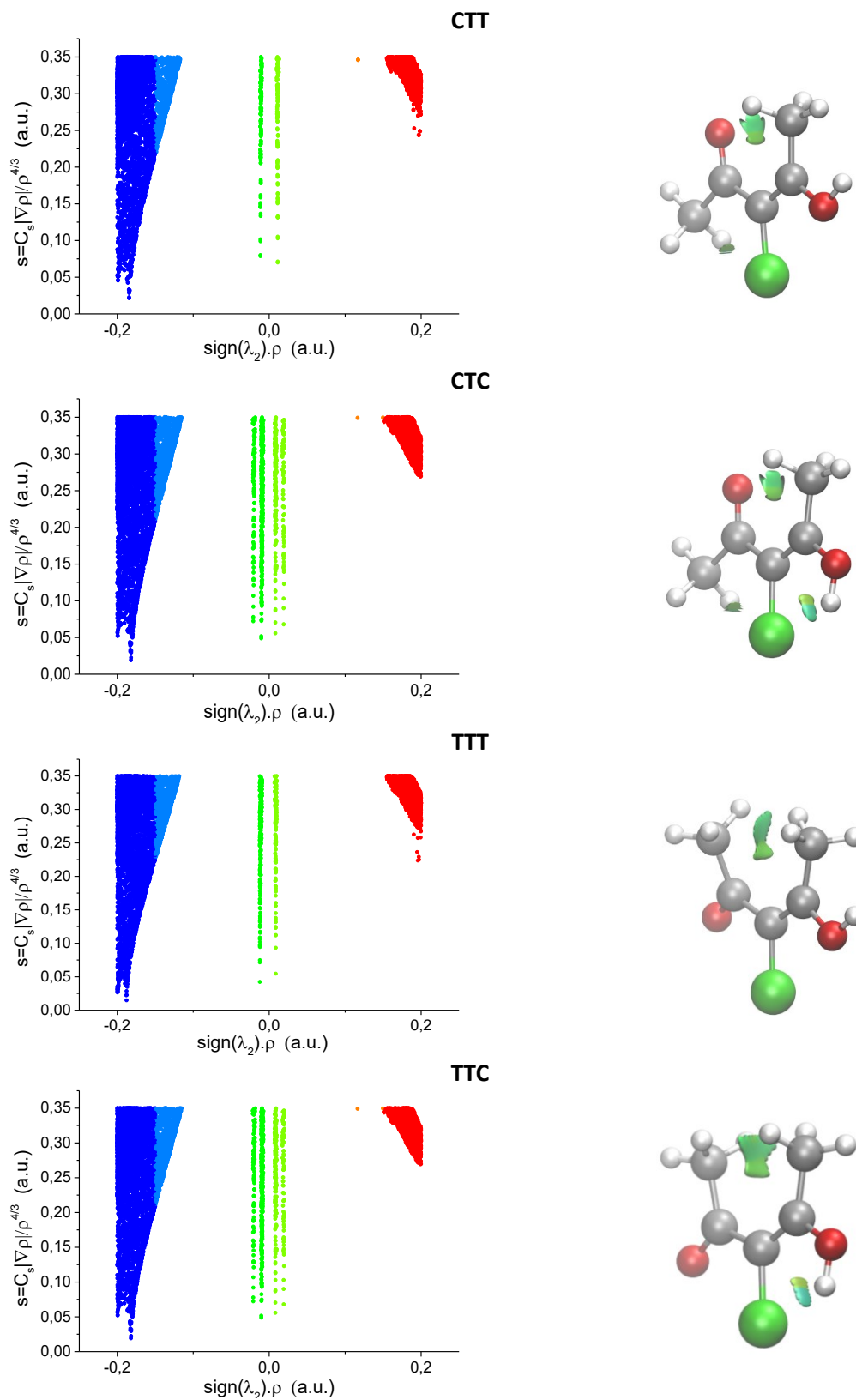
A unique feature of this system compared to acetylacetone and the other analogs studied in this thesis is that the methyl groups of the CCC conformer are symmetric (both have eclipsed configuration with respect to oxygen atoms). This geometry was also found by Tayyari *et al.* [62] and Belova *et al.* [6] in previous theoretical calculations. No other minima were found when methyl orientations differ from the eclipsed configuration. In addition, geometry optimization and frequency calculations for the C_{2v} were done. The results show that this molecular symmetry corresponds to a first order transition state. In addition, it seems that the open enol conformers try to maintain the eclipsed configuration of the methyl groups when no steric repulsion are present. This configuration is even preserved in the methyl groups from OH side in CTC and CTT conformers. In acetylacetone the original *anti* position of the methyl group is also preserved, but, this is a logical result if we take into account that it favors the interaction of one of the methyl hydrogens and the carbonyl oxygen (compare Figure VI.1 and Figure V.1).

The planar structure of the carbonated skeleton is preserved in all the conformers except TTC and TTT. In these two conformers, the steric repulsion of the methyl hydrogens breaks a bit the symmetry of the molecule. In comparison to acetylacetone, methyl groups in chloroacetylacetone are closer and feel a higher repulsion (*e.g.* TTC, $\text{CH}_3\cdots\text{CH}_3$ distance, AcAcH8: 3.25 Å, AcAcCl: 3.04 Å).

The energy order of the conformers in the case of chloroacetylacetone has some changes compared to acetylacetone⁵⁶. The most evident is the decrease in relative energy of the TTC conformer compared to the order in acetylacetone. CTC is still the most stable conformer, but the energy difference with its pair (CTT) has increase. Both, CTC and TTC have a XTC configuration which implies that the hydrogen from the hydroxyl group is pointing to the chlorine atom. This configuration favors a $\text{Cl}\cdots\text{H}$ non-covalent attractive interaction. NCI calculations were performed for all the conformers to search for this kind of interactions. The results from these calculations are shown in Figure VI.2. The left panel shows a plot of the reduced density gradient (RDG) versus the gradient for two pairs of conformers. The presence of attractive non-covalent interactions is revealed by low negative values of RDG (s) at low negatives values of density ($\rho < |0.05|$). The region in which these interactions take place can be seen in the right panel as isosurfaces on the molecule. A light blue color in the isosurface indicates the presence of an attractive non-covalent interaction. We can observe that an additional stabilizing non-covalent interaction in the $\text{Cl}\cdots\text{HO}$ moiety is found in both CTC and TTC

⁵⁶ Geometry optimization and frequency calculations with the M06-2X were also performed for acetylacetone, obtaining the same energy order for the conformers and a similar relative energy (< 3 kJ/mol overall) compared to B3LYP.

Figure VI.2: NCI calculation for the CTT-CTC and TTT-TTC pairs. Left: Graph of reduced density gradient (s) versus density multiplied by the sign of λ_2 (see section III.4.) . Right: Isosurface of s at 0.35; light blue corresponds to non-covalent interactions and green color corresponds to steric repulsion.



3-CHLOROACETYLACETONE

compared to their corresponding XTT couples.

VI.2. Vibrational spectroscopy of as-deposited samples

VI.2.1. FT-IR spectrum in Ne and pH_2 matrices

As we mentioned in section I.2.1.2, there are no reports on this molecule using matrix isolation technique except for the report of Coleman III focus in the keto tautomer [60]. In Figure VI.3 the spectra of the deposited sample in neon and *para*-hydrogen are shown. Theoretical calculation of the CCC conformer for the C_s symmetry with the M06-2X and B3LYP functionals (6-311++G(3df, 3pd)) are shown for comparison.

In contrast to deuterated acetylacetone the bandwidths in chloroacetylacetone are in overall larger than in acetylacetone (it will be discussed in section XI.1.2.2). In addition, we observe that the number and relative intensities of the bands do not completely correspond to the theoretical spectrum. Some of these bands marked with an * in Figure VI.3, show no evolution after UV laser irradiation, and can be related to impurities in the sample (98% of purity according to the manufacturer). Even without considering these bands there are more bands than expected in both matrices. Nevertheless, the experimental result is in better agreement with the M06-2X functional than with the B3LYP one and seems to confirm the presence of the CCC conformer in the deposited sample. As mentioned in the previous section, we made optimization and

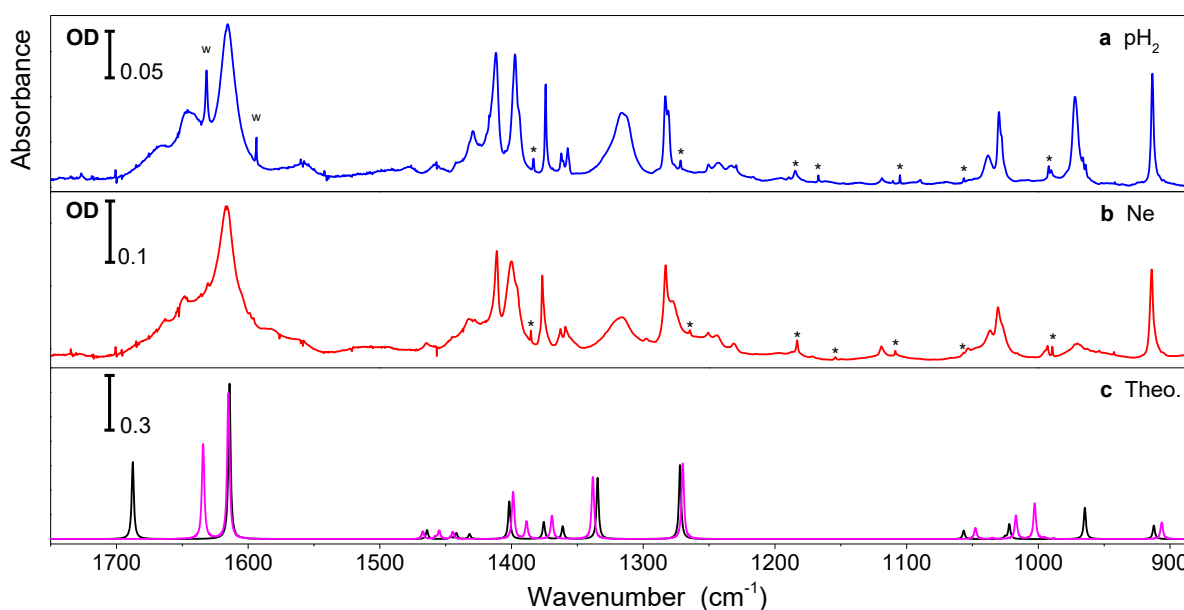


Figure VI.3: Infrared spectra of the deposited sample in (a) neon and (b) *para*-hydrogen matrices. (c) Theoretical spectra of the CCC conformer in the C_s symmetry with M06-2X (black line) and B3LYP (magenta line) functionals. * impurities. 0.977 scaling factor for M06-2X and 0.988 for B3LYP.

frequency calculations for the C_{2v} structure and methyl rotamers. None of these structures was found to be a minimum. Neither their frequency spectra nor the one from the other enol conformers nor keto tautomer match better than the spectrum of the methyl symmetric C_s structure. Looking for anharmonic effects, anharmonic frequency calculations were performed at B3LYP/6-311++G(df,pd)⁵⁷ for the C_s symmetry, but no improvement was obtained.

The hydrogen transfer barrier was determined from the difference of the theoretical energy of the C_{2v} and C_s structures, without ZPE and including the ZPE. In the case when ZPE is included, the value of the lower energy mode is discarded in both structures, to remove the imaginary value of the C_{2v} structure. The obtained values are shown in Table VI.1. The importance of the ZPE in the barrier calculation is clear, as noted by Broadbent *et al.* in acetylacetone [48]. Lozada *et al.* have also computed the barrier in acetylacetone. They found a value of 9.8 kJ/mol at B3LYP/6-311++G(3df,3pd) without including ZPE. Taking into account the use of different functionals, we can at least estimate that the two systems have similar barriers for hydrogen transfer process.

Table VI.1: Hydrogen transfer barrier determined from the difference in energy of the C_{2v} and C_s structures.

	$C_{2v} - C_s$ (kJ/mol)
Without including ZPE	10
ZPE included without lowest frequency mode	0.5

As mentioned before, no clear assignment of the keto tautomer was done. If there is any band from this specie, it can be confused with bands from impurities. In addition, the amount of keto tautomer is expected to be even lower than in acetylacetone [6], [215]. In pH_2 the amount of keto tautomer for acetylacetone was determined to be 4.5% [9]. So, it is not surprising to obtain a similar result in cryogenic matrices.

VI.2.1. Raman and FT-IR spectrum in argon matrix

Raman and infrared spectra in argon matrix were obtained at 11 K (see Figure VI.4). The comparison with their theoretical counterparts confirms that our calculations are not able to correctly reproduce the experimental spectra. Nevertheless, it should be remarked that in the case of Raman a better agreement is

⁵⁷ The basis set was decreased (less diffusion functions were added) and the functional was changed in order to decrease the computational effort. The attempts made for anharmonic calculations with M06-2X/6-311++G(3df, 3pd) were too long and did not converged.

3-CHLOROACETYLACETONE

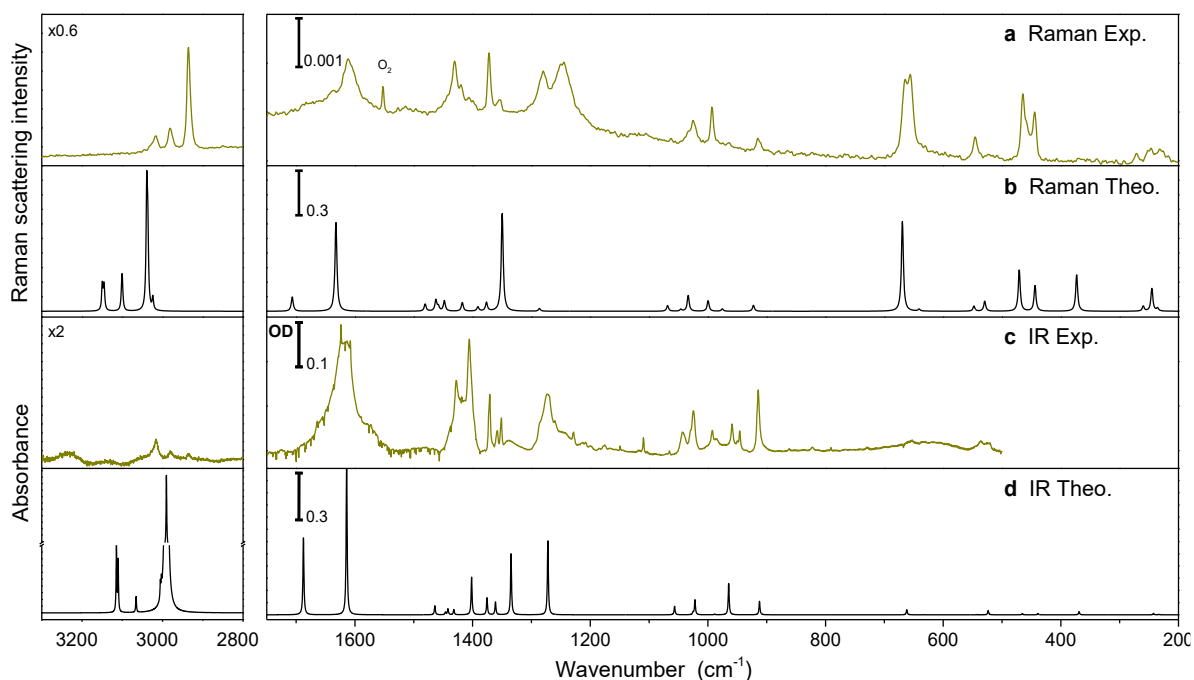


Figure VI.4: Vibrational spectra of chloroacetylaceton in argon matrix at 11K (a) Experimental and (b) theoretical Raman spectra. (c) Experimental and (d) theoretical infrared spectra. Lower frequencies are not shown in the experimental IR spectrum because of detector cutoff. Theoretical spectra are calculated in the harmonic approximation and frequencies are scaled by 0.977. There is a break in the intensity axis of the left panel of (d). Raman intensity is given in arbitrary units.

obtained for frequencies below 1100 cm^{-1} . Also, the access to lower frequencies ($<500\text{ cm}^{-1}$) in Raman spectra allows to have more experimental information to compare with the theoretical spectrum. In the FT-IR spectrum in argon matrix the out of plane OH mode (around 959 cm^{-1}) is observed as a group of three bands. Only one band stays after annealing of the sample at 30 K, which demonstrates the presence of site effects in argon matrix.

We can say in advance that the theoretical spectrum of the CCC conformer in this molecule presents the biggest disagreement with the corresponding experimental spectrum. As said before, chloroacetylaceton has the strongest hydrogen bond in the series of analogs analyzed in this thesis (see section I.2.1.2). A strong intramolecular hydrogen bond in this molecule should reinforce the hydrogen transfer and the π (double) bond delocalization in the internal ring, increasing the coupling between internal modes.

It is interesting to note that like in acetylaceton the band at 375 cm^{-1} (with non-negligible intensity) predicted by theoretical Raman calculation is not observed in the experiment (see Figure V.7). The corresponding modes in both molecules are almost identical, and are one of the two low frequency modes related to hydrogen transfer. The other mode, with opposite phase, appears at lower frequencies and with

a low intensity. In these modes the molecule vibrates in such a way that the two oxygen atoms approach each other, favoring the hydrogen transfer.

VI.3. UV laser irradiation

VI.3.1. Electronic absorption spectra

The electronic spectra of chloroacetylacetone in neon matrix were obtained for the deposited sample and after UV irradiation at 312 nm. The spectra are shown in Figure VI.5.

The UV absorption spectrum of the deposited sample shows that the inclusion of the chlorine atom in the α position of acetylacetone causes a clear bathochromic shift (~ 20 nm) on the $\pi \rightarrow \pi^*$ absorption band of the CCC conformer. In fact, it represents the largest shift observed for all the halogenated derivatives of acetylacetone studied in this work. The position of the most intense band of the isomers produced after the UV laser irradiation (254 nm) is also shifted to higher wavelengths compared to acetylacetone (240 nm). A second, less intense band is also observed near 231 nm, after UV irradiation. In analogy with acetylacetone, this band should belong to a second specie formed after irradiation. So, at least two open enol conformers are expected to be found in the sample.

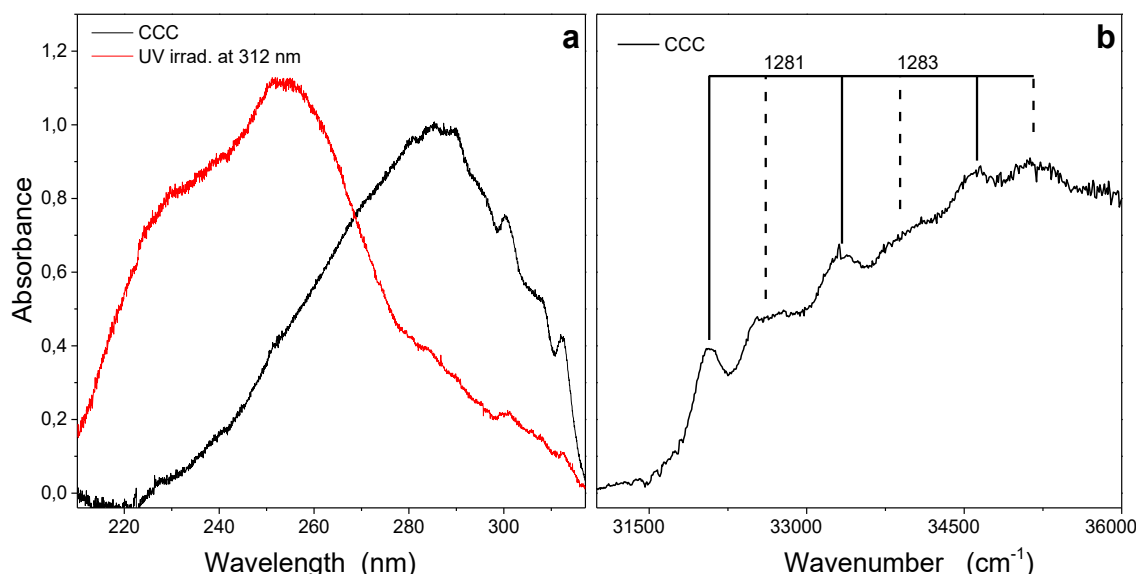


Figure VI.5: Electronic absorption spectra of chloroacetylacetone in neon matrix. a) Left panel: deposited sample (black) and after irradiation at 312 nm (red). b) Right panel: Zoom of the deposited sample spectrum in wavenumber (cm⁻¹). Solid and dashed lines indicates two possible vibrational progressions. The numbers indicate the values of the frequency shift in the progression marked by the solid line.

3-CHLOROACETYLACETONE

Table VI.2: IR and Raman assignment of the CCC conformer of chloroacetylacetone. Experimental IR frequencies (cm^{-1}) of the chelated enol form of AcAcCl in neon, *para*-hydrogen and argon matrices, along with Raman assignment in argon. Calculated harmonic frequencies (cm^{-1}) at M06-2X/6-311++G(3df,3pd) level are included for comparison. A scaling factor of 0.977 is used. Theoretical infrared intensities (km/mol) and Raman scattering activities ($\text{\AA}^3/\text{a.m.u.}$) are obtained in the harmonic approximation. Lines in grey correspond to a tentative assignment.

Experimental				Theoretical		
IR		Raman		Harmonic*sf	Int.	
Ne	pH ₂	Ar			IR	Raman
3033.0				3114.6	7	58
3025.0	3017.0	3016.0	3017.0	3110.2	5	56
2975.0	2987.0	2981.0	2981.0	3066.7	0.3	41
				3065.6	1	47
				3005.5	2	234
	2933.0	2936.0	2936.0	3003.0	1	145
2862.0	2894.0			2990.4	372	26
1649.0	1646.0		1637.0	1687.6	207	10
1617.0	1616.0	1616.0	1612.0	1614.2	419	57
1464.0	1459.0			1464.2	24	4
				1446.2	7	6
1445.0	1443.0			1441.9	16	2
1432.0	1429.0	1428.0	1431.0	1431.9	14	6
1411.0	1412.0					
1400.0	1397.0	1406.0		1401.7	102	4
1376.0	1374.0	1371.0	1372.0	1375.5	46	2
1363.0	1362.0	1358.0				
1359.0	1357.0	1351.0	1354.0	1322.9	34	4
1315.0	1315.0	1274.0	1280.0	1334.7	165	47
1283.0	1283.0					
1278.0	1281.0			1272.1	200	1
1037.0	1038.0	1042.0		1056.7	23	2
				1034.3	0.001	1
1031.0	1030.0	1024.0	1025.0	1025.3	6	0.02
				1022.0	40	5
993.0	992.0	993.0	993.0	988.5	2	3
970.0	972.0	959.0		964.7	85	1
914.0	913.0	914.0	914.0	912.3	36	2
		654.0	665.0	661.9	14	17
			656.0			
		631.0	631.0	633.9	0.4	0.3
		536.0	546.0	541.7	1	1
		523.0		523.5	12	1

Experimental			Theoretical		
IR		Raman	Harmonic*sf	Int.	
Ne	pH ₂	Ar		IR	Raman
		465.0	465.5	3	5
		444.0	439.0	4	3
			369.0	9	3
		271.0	257.0	0.0001	0.3
		247.0	242.5	4	1
		230.0	233.0	1	0.2
			178.5	0.02	0.2
			163.7	0.1	0.1
			113.9	1	0.3
			88.1	3	0.05

3-CHLOROACETYLACETONE

Table VI.3: Position (nm) of the $\pi \rightarrow \pi^*$ ($S_2 \leftarrow S_0$) electronic transition of chloroacetylacetone in neon matrix, for the CCC conformer and after 312 nm UV laser irradiation. Values corresponding to acetylacetone are also given for a direct comparison. Theoretical values obtained with TD-DFT at B3LYP/6-311G++(3df,3pd) are shown in parenthesis. The energies (eV) of the HOMO/LUMO orbitals are also included.

	AcAcCl	AcAcH8
CCC	285 (271)	265 (244)
HOMO/LUMO (eV)	-6.7036/-1.8395	-6.8759/-1.5183
After 312 nm irradiation	254 231	~240

TD-DFT calculations were performed for acetylacetone and the analogs analyzed in this thesis. The results are shown in parenthesis in Table VI.3. The TD-DFT calculations described well the marked bathochromic effect observed for the $\pi \rightarrow \pi^*$ absorption band in chloroacetylacetone. The effect of the substitution of the chlorine atom (auxochrome) in the α position can be analyzed from the energies of the HOMO/LUMO orbitals involved in the transition. The values suggest that the chlorine atom has a slight repulsive effect on the electrons of the HOMO orbital, increasing its energy, while it stabilizes the LUMO.

On the other hand, it can be noticed in the experimental absorption band of the CCC conformer the presence of a structure in the low frequency part (see right panel Figure VI.5). One can distinguish at least two vibronic progressions in this structure, one with broader bands than the other. The origin of the first one, with the narrowest bands, could correspond to the origin of the electronic transition (0_0^0 band) around 32066 cm^{-1} . The shifts between the bands in each progression are very similar, and can be assigned to the excitation of a vibrational mode around 1280 cm^{-1} in the excited state. The second progression seems to be related to a combination of the same mode in the first progression and a mode near 540 cm^{-1} (shift from the origin).

VI.3.2. Electronic excitation

The UV laser irradiation experiments to obtain the open enol conformers start at 312-290 nm (different initial irradiation wavelengths were used in different experiments). These initial irradiations induce the formation of two groups of bands in the IR spectrum and the decrease of those from CCC conformer: the two groups are called first and second group and differ by their production kinetics, the first one growing the fastest. Then, under irradiation at 280-270 nm, the amount of the second group of bands increases at the expense of the first group. When irradiating the sample at 260 nm in the following step, this behavior was inverted, *i.e.* the first group grows again while the second decreases. A small increase of the amount of CO molecule is observed when irradiating at wavelengths lower than 270 nm, a clear sign of photofragmentation.

The analysis of these results shows that there is only one conformer in each group of open enol conformers. Both conformers were identified after comparison with the theoretical calculations.

VI.3.2.1. CTC conformer

In contrast to CCC conformer, the match between the experimental and theoretical spectra of the open enol conformers is good. CTC was identified as the conformer belonging to the first group of bands (see Figure VI.6). This conformer is the lowest in energy after CCC.

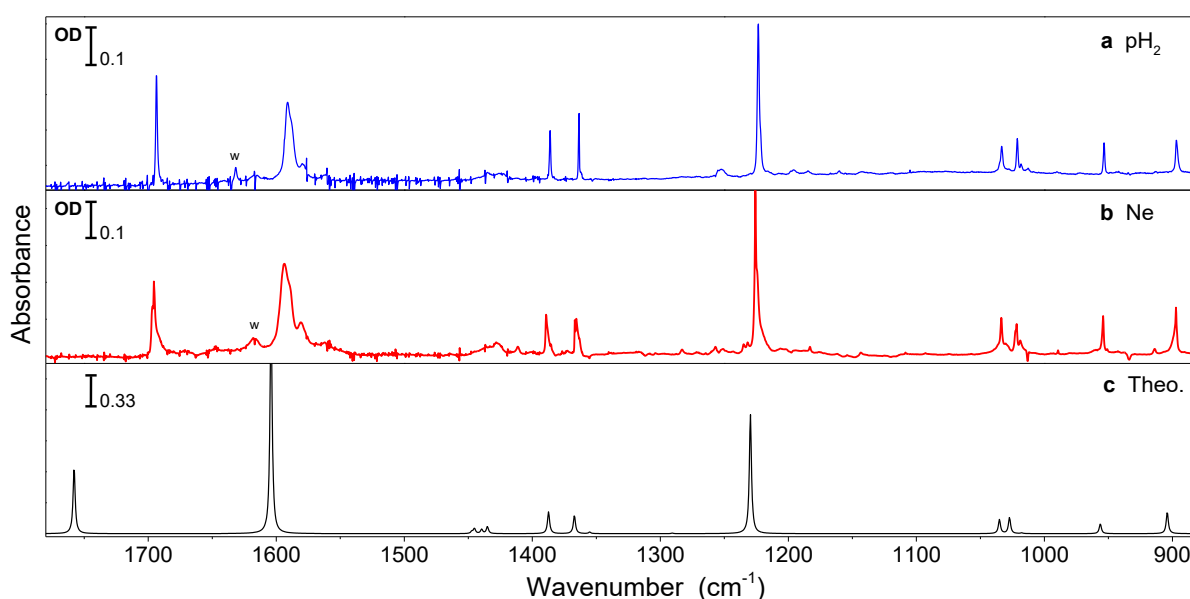


Figure VI.6: Infrared experimental spectra of the CTC conformer in (a) neon and (b) *para*-hydrogen matrices. (c) Harmonic scaled theoretical spectra (0.977) with M06-2X/6-311++G(3df,3pd).

Band assignment is given in . An important result that supports also the assignment is that the OH stretching mode (3495.8 cm^{-1} in *para*-hydrogen) is clearly redshifted compared to the same conformer in acetylacetone (3622 cm^{-1}). This is an important signature of the interaction between the chlorine and the hydrogen hydroxyl atom.

VI.3.3. TCT conformer

The second group of bands formed upon irradiation was assigned to TCT conformer. The experimental spectra in neon and *para*-hydrogen matrices as well as the theoretical harmonic spectrum are shown in Figure VI.7. The theoretical spectra of TCC and TTC is also included for comparison.

The match between experimental and theoretical spectra is good, but, more bands than predicted by the theoretical calculation of the TCT conformer are observed in the experimental spectra. They are not related

3-CHLOROACETYLACETONE

Table VI.4: Assignment of the CTC and TCT conformers of chloroacetylacetone (AcAcCl). Experimental frequencies (cm^{-1}) in neon and *para*-hydrogen matrices, compared to calculated harmonic frequencies at M06-2X/6-311++G(3df,3pd). Intensities (km/mol) obtained in the harmonic approximation. Scaling factor (sf): 0.977.

Frequencies				
Experimental		Theoretical Harmonic*sf		Int.
Ne	pH ₂	CTC	TCT	
3647.3				
3628.0	3635.6		3806.1	125
3506.0	3496.1	3698.7		76
		3113.2		5
3024.0	3018.0	3108.3		6
		3082.9		0.3
2987.0	2976.0	3065.6		2
		3016.1		3
2943.0	2941.0	3001.8		0.2
			3135.0	0.4
3024.0	3015.2		3111.9	6
2986.0	2990.6		3080.9	3
2956.5	2950.6		3036.4	4
	2939.9		3010.7	1
2931.7	2922.0		2982.5	14
1697.4	1693.9		1771.9	184
1697.0				
1695.7	1693.7	1757.9		155
1661.9	1658.7			
1644.9	1643.1		1688.3	243
1594.6	1591			
1590.6	1588.5	1604.0		534
			1461.3	7
1439.4	1436.8		1448.6	10
		1447.3		5
1433.0	1434.0	1445.2		12
		1439.6		10
			1444.5	3
1427.8	1425.2		1436.8	16
1426.7	1424.5	1435.1		16
1387.1	1384.1		1389.2	57
1388.5	1386.3	1387.3		51
1366.3	1364.7		1367.6	32

Frequencies				Int.
Experimental		Theoretical Harmonic*sf		
Ne	pH ₂	CTC	TCT	
1365.6	1363.6	1367.1		43
		1355.2		4
1313.3	1310.8		1325.9	96
		1290.6		1
1255.6	1256.8		1258.8	64
1225.8	1223.7	1229.6		280
1224.4				
1197.6	1197.8		1202.2	131
			1038.4	0.02
		1035.2		29
1033.9	1033.4	1034.8		4
1034.7	1033.4		1030.7	58
1022.7	1021.2	1027.3		37
	1023.9		1025.5	5
1018.8	1018.3	1017.8		2
1012.9	1012.5		1012.8	80
954.5	953.4	956.3		23
933.7	933.7		942.8	54
909	908.2		915.6	28
898.0	896.9	904.0		51

3-CHLOROACETYLACETONE

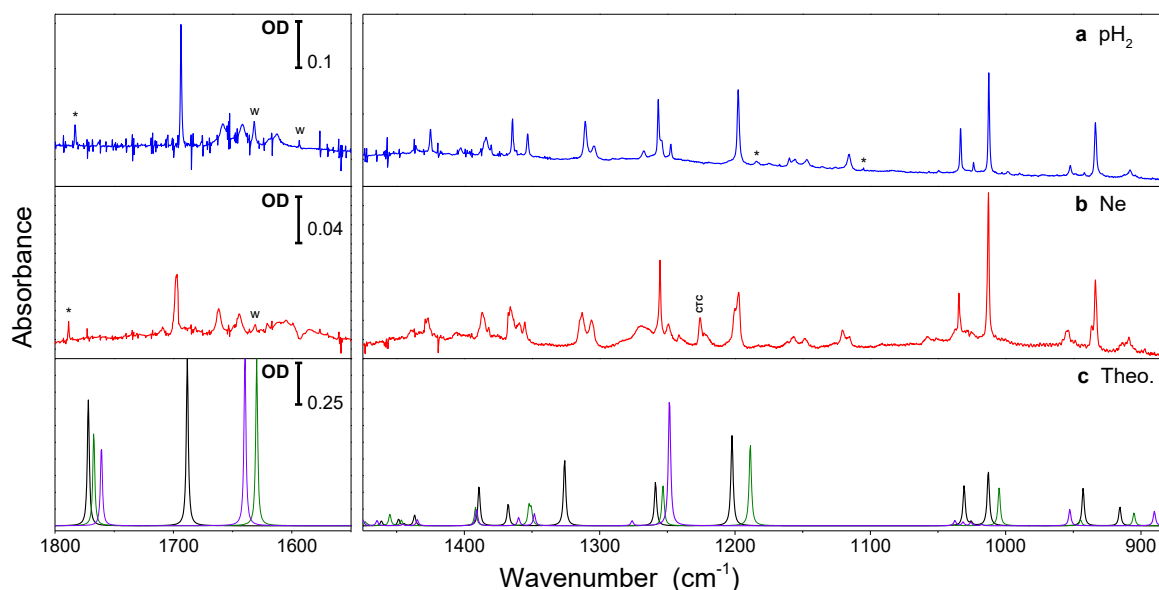


Figure VI.7: Infrared experimental spectra of the TCT conformer in (a) neon and (b) *para*-hydrogen matrices. (c) Harmonic scaled theoretical spectra (0.977) with M06-2X/6-311++G(3df,3pd) (black). In (c) the theoretical spectra of TCC (light green) and TTC (light violet) conformers are also included. * impurities in *para*-hydrogen. The band in neon marked with CTC label correspond to the most intense band of this conformer, and is observed due to a bad compensation in the subtraction.

with the impurities observed in the deposition (only those marked with *). These bands are observed in both neon and *para*-hydrogen and they have a similar evolution as the TCT assigned bands. The theoretical spectra of the other open enol conformers were compared with the experiment. In Figure VI.7 the theoretical spectra of TTC and TCC are included as example. The best match is obtained for TTC, but is not as good as for TCT. Nevertheless, it cannot be discarded as the source of these bands. Additional experiments are needed to confirm this hypothesis. Some small fragmentation is observed in *para*-hydrogen matrix (increase of CO bands) but not in neon, eliminating the possibility of bands from fragments.

Finally, the presence of the TCT conformer as stable product after UV irradiation suggest that the energy of this conformer is lower than TCC, as predicted from theoretical calculations (see Figure VI.1).

VI.4. Deuterated chloroacetylacetone in *p*H₂

VI.4.1. Deposited sample

Preliminary studies in *para*-hydrogen were performed on the deuterated analog of chloroacetylacetone. Like in acetylacetone, the isotopologue was obtained by deuteration synthesis (described in section IV.1.2.). The spectrum of the deposited sample is shown in Figure VI.8. Water was not completely eliminated in the final

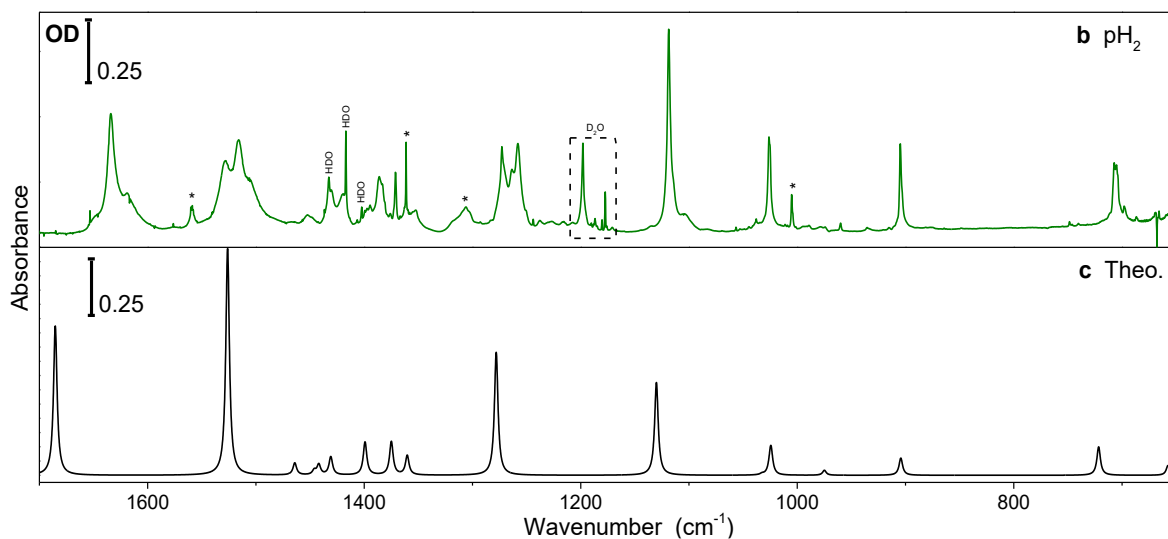


Figure VI.8: (a) Experimental infrared spectrum of deposited sample of deuterated chloroacetylacetone in *para*-hydrogen matrix. (b) Theoretical harmonic calculation of the CCC-Cl(D) conformer at M06-2X/6-311++G(3df,3pd). A scaling factor of 0.977 is used to correct the theoretical frequencies. Double and monodeuterated water bands are assigned in the experimental spectra. * Unassigned bands appearing after deuteration

step of the synthesis and several bands can be observed (and are indicated) in the spectrum. Despite the presence of water in the sample, the assignment of the bands belonging to the CCC-Cl(D) conformer can be done when comparing with its theoretical spectrum (see Figure VI.8). The match between both spectra (frequencies and relative intensities) is better than for hydrogenated chloroacetylacetone. This could be due to a decrease of the anharmonic character of the OH modes when deuterium is present. In addition, there is also a decrease in the strength of the internal hydrogen bond and in the coupling between the normal modes.

Like in acetylacetone and its OD deuterated isotopologues, the overall bandwidth seems to decrease when the hydroxyl hydrogen is exchange with deuterium in chloroacetylacetone. Nevertheless, more and better (*i.e.* less water) samples need to be analyzed to confirm this assertion.

VI.4.2. Open enol conformers

The deposited sample was irradiated with the OPO laser from 290 to 260 nm in different steps. From the beginning of the irradiation at 290 nm four different bands start to growth in the OD stretching region (2700-2550 cm^{-1}), see Figure VI.9 (a) and (b) for comparison. One of these four bands, is clearly redshifted from the others (near 2585 cm^{-1}), suggesting a conformation in which the deuterium is interacting with the chlorine atom, *i.e.* XTC.

3-CHLOROACETYLACETONE

Table VI.5: CCC-Cl(D) conformer assignment. Experimental frequencies (cm^{-1}) of the chelated enol form of AcAcCl(D) in *para*-hydrogen matrix, compared to calculated harmonic frequencies at M06-2X/6-311++G(3df,3pd). Intensities (km/mol) obtained in the harmonic approximation. Scaling factor (sf): 0.977.

Exp.	Theoretical	
	Harmonic*sf	Int.
3020.6	3114.5	5
3016.8	3110.2	4
2975.3	3066.7	0.3
2972.6	3065.6	1
2944.7	3005.5	0.5
2937.2	3002.9	0.001
2030.0	2190.9	265
1634.1	1685.3	235
1619.1		
1528.8		
1516.6	1526.2	358
1506.8		
1452.7	1464.1	19
	1446.2	7
1430.6	1441.9	16
	1430.8	29
1420.0	1399.2	52
1386.0	1374.9	53
1371.3	1360.2	31
1352.5		
1272.7		
1264.2	1278.1*	194
1258.6		
1118.8	1130.1	146
	1025.3	6
1026.0	1024.3	42
	1001.1	0.1
960.3	975.0	8
904.8	904.4	27
707.2	721.6	45
705.4		
654.6	657.6	15

* The three bands are included because the experimental data do not allow to know if one of these bands belongs to a complex or another species.

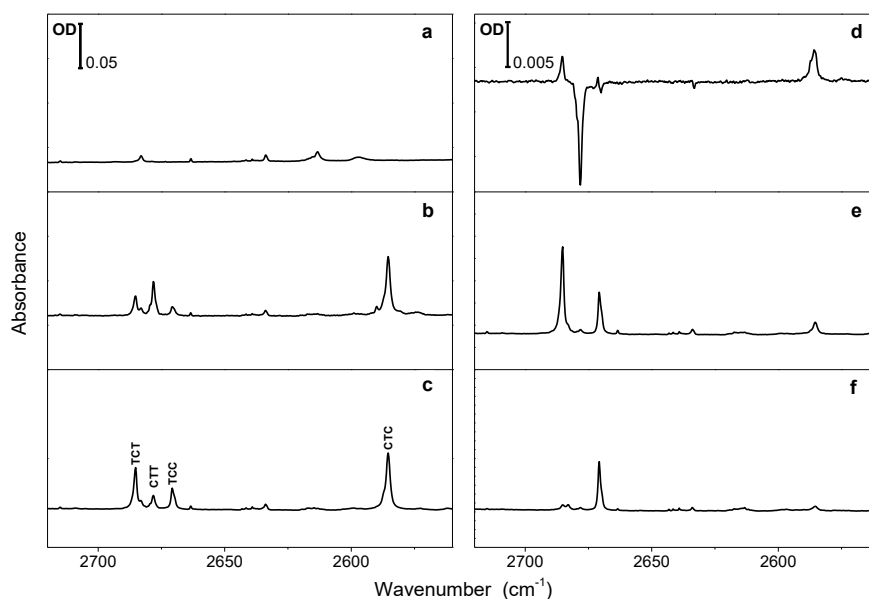


Figure VI.9: Experimental infrared spectra of deuterated chloroacetylacetone in *para*-hydrogen matrix: (a) deposited sample; (b)-(f) are in sequence, (b) irradiation at 290 nm for 30 min, (c) 280 nm for 30 min, (d) evolution of the spectrum 125 min after irradiation, (e) UV irradiation at 270 nm, (f) UV irradiation at 260 nm for 30 min. Same OD for all spectra except (d).

Similar to acetylacetone (D2), a temporal evolution is observed after the end of the UV irradiation at 290 nm in some of the bands (see Figure VI.9 b, c, and d). The change suggests an interconversion process between conformers with different deuterium conformation.

A subsequent irradiation at 270 nm increase the amount of two of the conformers at the expense of the other two. Finally, almost one species is present when 260 nm irradiation is performed. No temporal evolution is observed in the sample 90 min after finishing irradiation.

The different behavior of each component over UV irradiation and the temporal evolution allows to separate the four species. They are discussed in the next section.

VI.4.2.1. First group (CTC(D) and CTT(D))

In the first group we consider the conformers formed in higher amount with the UV irradiation at 290 nm. The temporal evolution after irradiation is more evident in this pair. The comparison of the experimental spectra with the theoretical harmonic calculations (Figure VI.10) allow to assign these conformers to CTC(D) and CTT(D). The experimental spectra presented here is the result of the subtraction of different experimental spectra, to eliminate the rest of CCC-Cl(D) and the other open enol conformers formed. In the case of CTC(D) the match with the theoretical spectrum is good. In addition, the redshifted OD band is observed in the experimental spectra of this conformer, confirming its assignment. For CTT(D) the

3-CHLOROACETYLACETONE

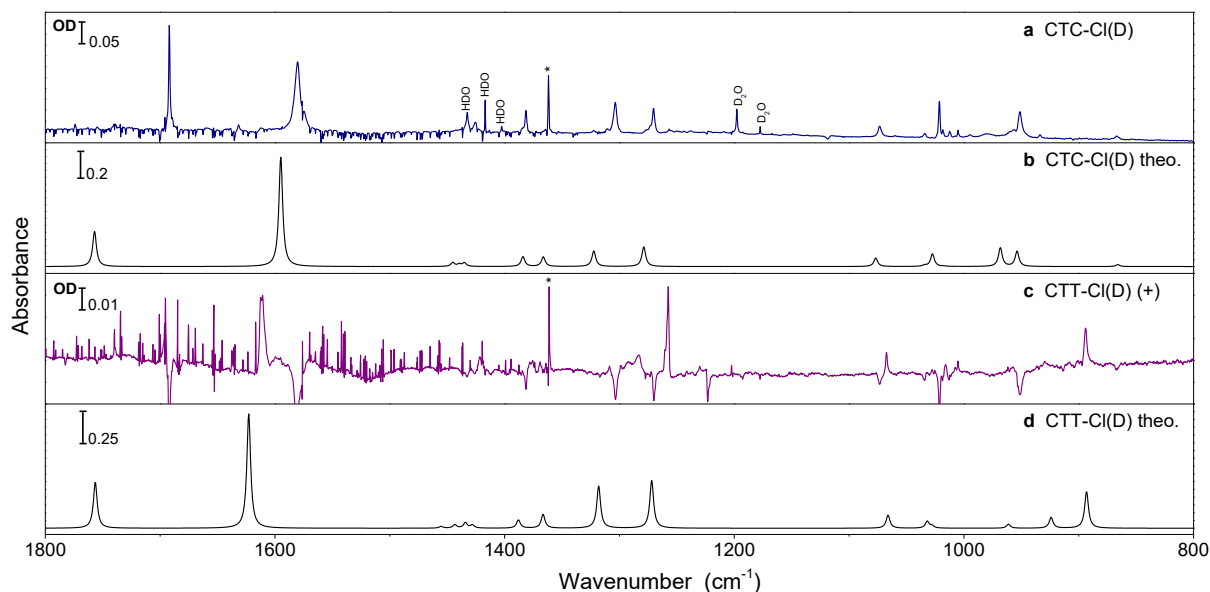


Figure VI.10: First group of open enol conformers of deuterated chloroacetylacetone in *para*-hydrogen matrix. (a) Experimental and (b) theoretical harmonic spectra of CTC-Cl(D) conformer. (c) Experimental (only positive bands, the negative bands belong to CTC-Cl(D)) and (d) theoretical harmonic spectra of CTT-Cl(D) conformer at M06-2X/6-311++G(3df,3pd). A scaling factor of 0.977 is used to correct the theoretical frequencies. Double and monodeuterated water (trapped in the matrix) bands are assigned in the experimental spectra. * Unassigned band. Atmospheric water compensation is observed in (c) due to bad compensation.

comparison is more difficult due to a lower amount of this conformer, but there is no doubt about its presence.

VI.4.2.2. Second group (TCT-Cl(D))

The two other species observed in the OD stretching region are included in the second group of conformers. TCT-Cl(D) conformer was identified as the first of them when comparing with the set of theoretical spectra. The theoretical spectra of TCT-Cl(D), TCC-Cl(D) and TTC-Cl(D) are compared in Figure VI.11.

On the other hand, the assignment of the second conformer is not clear when comparing with the theoretical spectra. In Figure VI.9 panel (d) there is a small decrease in intensity of the band placed at 2670 cm^{-1} , which correspond to the second species. This result would suggest that TCC-Cl(D), the pair of TCT-Cl(D), should be the formed conformer, as indicated in panel c. Nevertheless, the evolution of the other bands in the spectrum does not show a clear behavior. Although further experiments need to be conducted to do a rigorous assignment, we tentatively assign this conformer to TCC-Cl(D).

The results of UV irradiation obtained in the isotopologues of chloroacetylacetone are in agreement with those already discussed in acetylacetone. The CTZ and TCZ pairs of conformers are both produced after UV irradiation, and a driven tunneling effect conducts the system to the most stable conformer of each pair.

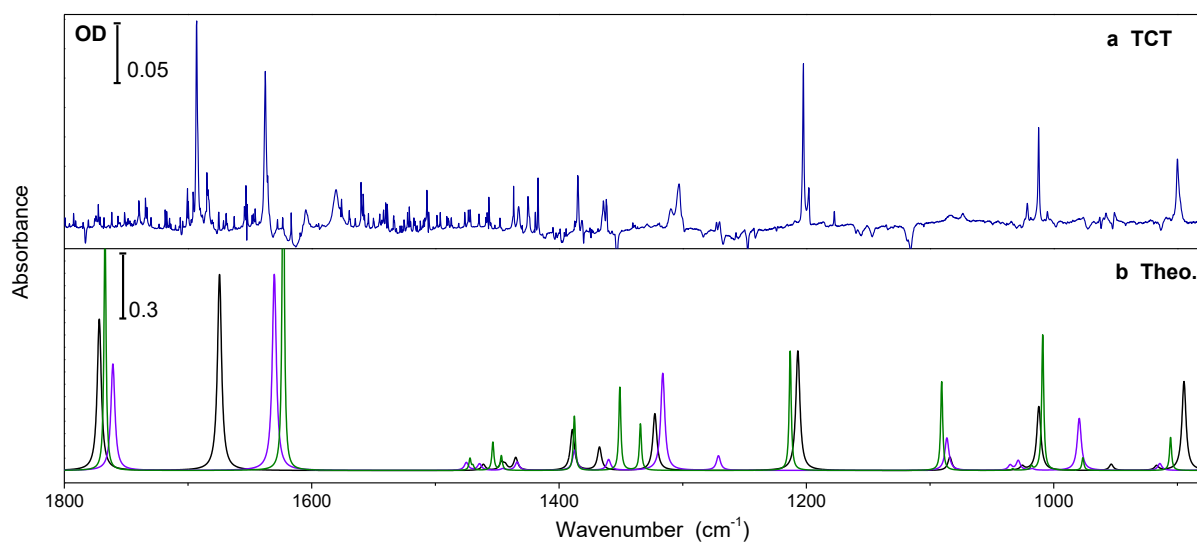


Figure VI.11: TCT-Cl(D) conformer of deuterated chloroacetylacetone in *para*-hydrogen matrix. (a) Experimental and (b) theoretical harmonic spectra (black) at M06-2X/6-311++G(3df,3pd). Theoretical spectra of TTC (light violet) and TCC (light green) conformers are also included for comparison. A scaling factor of 0.977 is used to correct the theoretical frequencies. Atmospheric water is observed in (b) due to bad compensation.

3-CHLOROACETYLACETONE

Table VI.6: CTC-Cl(D) and CTT-Cl(D) conformer assignment. Experimental frequencies (cm^{-1}) in *para*-hydrogen matrix, compared to calculated harmonic frequencies at M06-2X/6-311++G(3df,3pd). Intensities (km/mol) obtained in the harmonic approximation. Scaling factor (sf): 0.977.

Frequency			
Experimental	Theoretical Harmonic*sf		Int.
pH_2	CTC	CTT	
3018.0	3113.2		5
		3113.2	6
	3108.3		6
		3084.8	0.1
2989.0	3082.9		0.3
		3077.7	8
		3067.5	2
2976.0	3065.6		2
2940.0	3016.1		3
		3003.6	0.1
2927.0	3001.8		0.3
2916.2		2996.5	22
2678.2		2773.7	78
2585.5	2690.6		44
1692.1	1757.1		155
1695.5		1756.5	148
1611.7		1622.8	368
1580.5	1594.9		485
		1455.4	6
	1445.2		12
1432.7	1445.0		5
		1443.4	11
	1439.6		10
1425.8	1435.1		16
		1434.2	18
		1428.1	10
		1388.0	26
1381.6	1384.0		43
1369.6		1366.5	44
1363.8	1366.3		43
1304.0	1322.4		68
1283.6		1318.1	136
1270.4	1278.8		87
1257.8		1271.9	154
1073.5	1076.8		38

Deuterated chloroacetylacetone in pH2

Frequency			
Experimental	Theoretical Harmonic*sf		Int.
pH ₂	CTC	CTT	
1067.4		1066.1	42
1033.6	1034.4		5
1016.2		1032.0	22
		1027.8	7
1021.4	1027.4		56
1018.4	1017.7		1
		1014.0	0.1
956.4	968.3		83
		961.3	13
951.5	953.8		67
930.0		924.1	35
894.5		893.2	118
867.4	866.0		8

3-CHLOROACETYLACETONE

Table VI.7: TCT-Cl(D) conformer assignment. Experimental frequencies (cm^{-1}) in *para*-hydrogen matrix, compared to calculated harmonic frequencies at M06-2X/6-311++G(3df,3pd). Intensities (km/mol) obtained in the harmonic approximation. Scaling factor (sf): 0.977.

Frequencies		
Experimental	Theoretical	Int.
ν_{H_2}	Harmonic*sf	
	3135.1	0.4
3016.1	3111.9	6
2990.0	3080.6	3
2950.4	3036.3	4
2939.9	3010.5	1
	2982.5	15
2685.4	2771.2	78
1693.4	1771.8	191
1637.7	1674.5	248
	1461.2	8
1436.9	1446.5	10
1432.8	1443.6	6
1425.2	1435.0	16
1384.8	1389.2	52
1364.5	1367.3	29
1310.5	1322.5	72
1202.5	1206.9	151
1083.8	1084.0	17
	1038.4	0.02
1023.8	1025.5	5
1012.3	1012.1	81
957.9	953.5	8
908.4	916.9	6
901.0	894.7	112

Chapter VII Hexafluoroacetylacetone

In this section, we focus our attention in another kind of halogenated analog: hexafluoroacetylacetone. This molecule allows to analyze the effect of heavier methyl groups in the dynamics of the system, and add another possible interaction through the presence of the fluorine atoms: F...H-X interaction. At the same time the presence of such very electronegative atoms introduces strong inductive effects in the molecule, changing the characteristics of the hydrogen bond.

VII.1. Theoretical results

The energy order for the conformers of hexafluoroacetylacetone at M06-2X/6-311++G(3df,3pd) level of theory are shown in Figure VII.1. The values shown are corrected with the Zero-Point Energy of each conformer.

If this energy diagram is compared to the one for acetylacetone (see Figure V.1) we observe that the overall energy order for the conformers has changed. The biggest change is the decrease in the relative energy of the CCT conformer, which is now the third more stable enol conformer. Another change is the swap in the internal order of the CTC-CTT and TTC-TTT pairs. In the last case, the planar symmetry of the carbonated skeleton is completely broken due to the high repulsion between perfluoromethyl groups. B3LYP

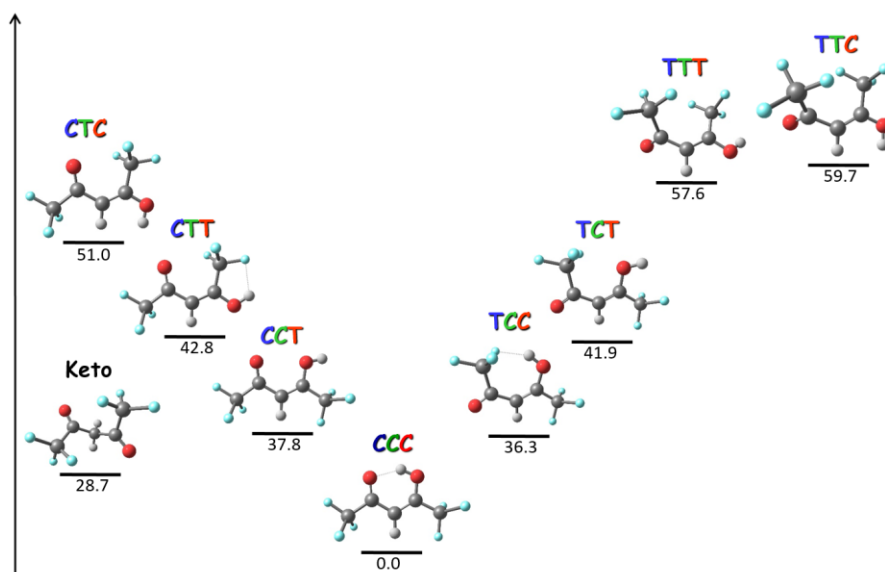


Figure VII.1: ZPE corrected theoretical energies for hexafluoroacetylacetone conformers calculated at M06-2X/6-311++G(3df,3pd) level of theory.

HEXAFLUOROACETYLACETONE

calculations were also performed with the same basis set. Very similar results were obtained, just inversion in the energy order of CCT and TCC conformers, and CTT and TCT conformers were observed. In these pairs of conformers, the energy difference is less than $1.5 \text{ kJ}\cdot\text{mol}^{-1}$, which is less than the absolute error for these methods. So, the important conclusion is that in both pairs the conformers have very similar energies.

Analysis of the electronic density (NCI calculation) was performed in the eight enol conformers to take into account the influence of non-covalent interactions in each of the XYZ-XYT pairs. The result shows that CTT and TCC conformers are most stable in pairs CTZ and TCZ because of the presence of an attractive non-covalent interaction in play between CF_3 and H-O groups (see Figure VII.3). In the case of CTC and CTT the effect is more evident if we compared the position of the perfluoromethyl group (OH side) with the methyl group of the corresponding conformers in AcAcH8. The perfluoromethyl group rotates around the bond to avoid the contact with the carbonyl oxygen, and in the case of CTT to be near to the hydrogen from the hydroxyl group.

The comparison was made only between the conformers of each XYZ-XYT pair in order not to disturb a lot the geometry of the molecule and be able to compare only the contributions from the non-covalent interactions.

Finally, it is worth to mention that the high stabilization of the CCT conformer (compared to the one in AcAcH8) seems not to be due to non-covalent interactions. A first guess was that it is stabilized by this kind of interaction because of the deviation from the carbonated skeleton plane of the perfluoromethyl (8°) and hydroxyl (6°) groups, that we also found in TCT (see Figure VII.2). But, it seems that in these cases the contribution is very small, probably due to a larger $\text{F}\cdots\text{H}$ distance

We should take into account that other kinds of interactions can play an important role in the stability of the molecule, such as electrostatic interactions (decrease in the electrostatic repulsion of the non-paired electron clouds of the oxygen atoms), which are not evaluated here.

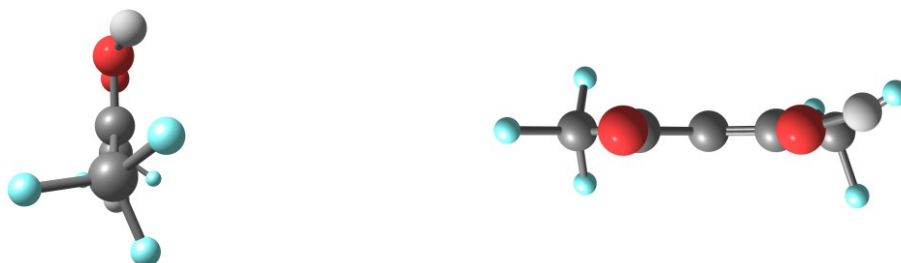
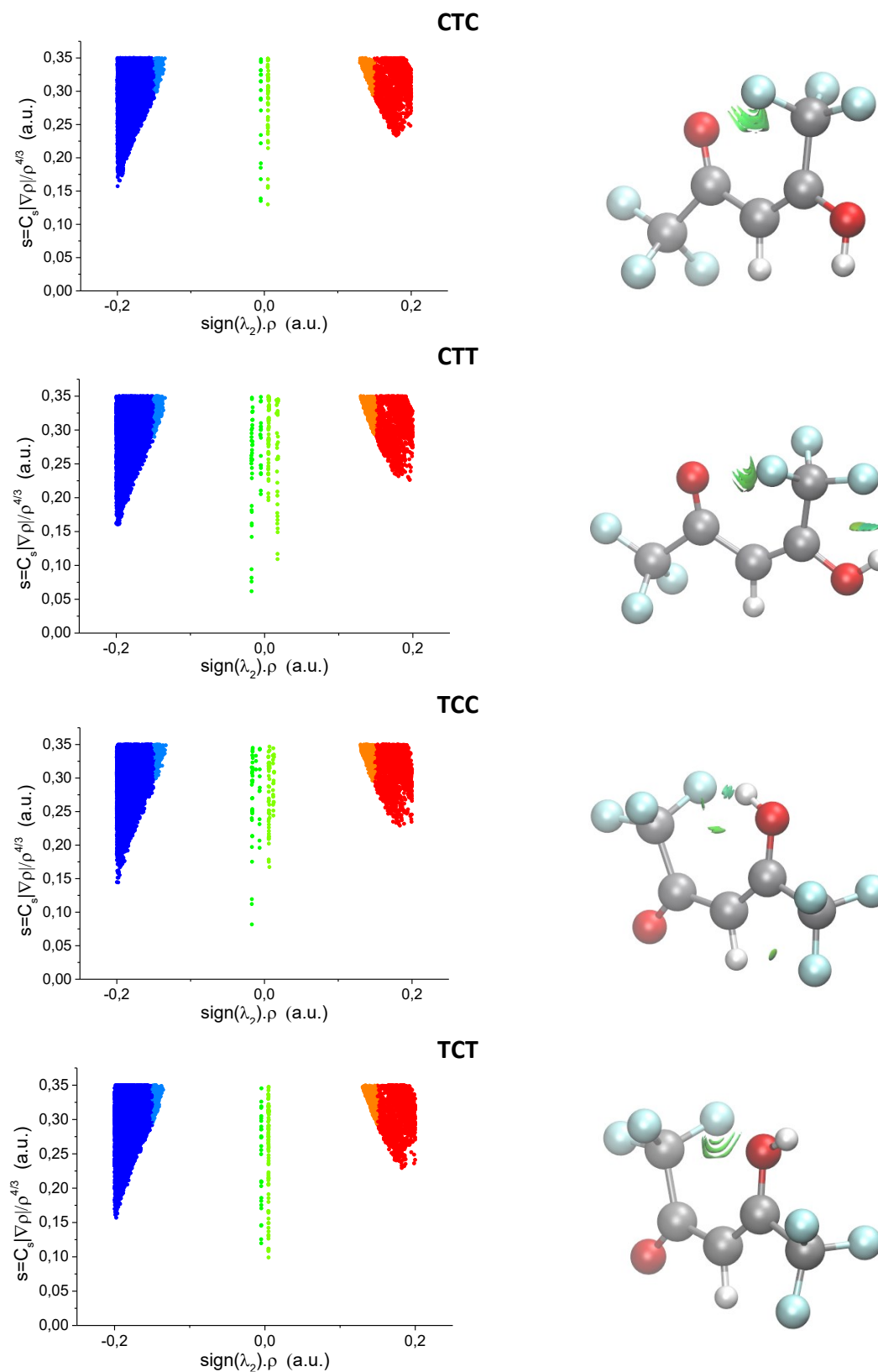


Figure VII.2: Distortion of the hydroxyl hydrogen and methyl group from the carbonated skeleton plane in the CCT conformer of hexafluoroacetylacetone. CCOH and OCCF dihedral angles have been multiplied by three for a better appreciation.

Figure VII.3: NCI calculation for the CTC-CTT and TCC-TCT pairs. Left: Graph of reduced density gradient (s) versus density multiplied by the sign of λ_2 (see section III.4). Right: Isosurface of s at 0.35; light blue corresponds to non-covalent interactions and green color corresponds to steric repulsion.



Before concluding this section, it should be remarked that in Figure VII.1 the geometry of the most stable conformer CCC correspond to the C_s symmetry, like in the case of acetylacetone and other β -diketones. Several authors have suggest that the C_{2v} symmetry only correspond to a transition state [70], [200], so, it was not computed in this work.

VII.2. Vibrational spectroscopy of as-deposited samples

VII.2.1. FT-IR spectrum in Ne and pH_2 matrices

Deposition conditions for hexafluoroacetylacetone were mentioned in section IV.2.1. . The obtained spectra in nitrogen (a), neon (b) and (c) *para*-hydrogen matrices are shown in Figure VII.4 for the 1800-650 cm^{-1} region. The calculated frequency spectrum in the harmonic approximation for the CCC conformer is also shown in panel (d).

From the comparison of the experimental and theoretical spectra we can be sure of the presence of the CCC conformer with a C_s symmetry. It should be pointed out that the match is very good when the M06-2X functional and 0.970 as value for scaling factor is used. The B3LYP functional was also used in calculations but the agreement was not as good as with the M06-2X functional, mainly in the CF₃ stretching region (see Figure VII.5). The assignment of the bands is shown in Table VII.1. The C=O + C=C and CF₃ stretching modes

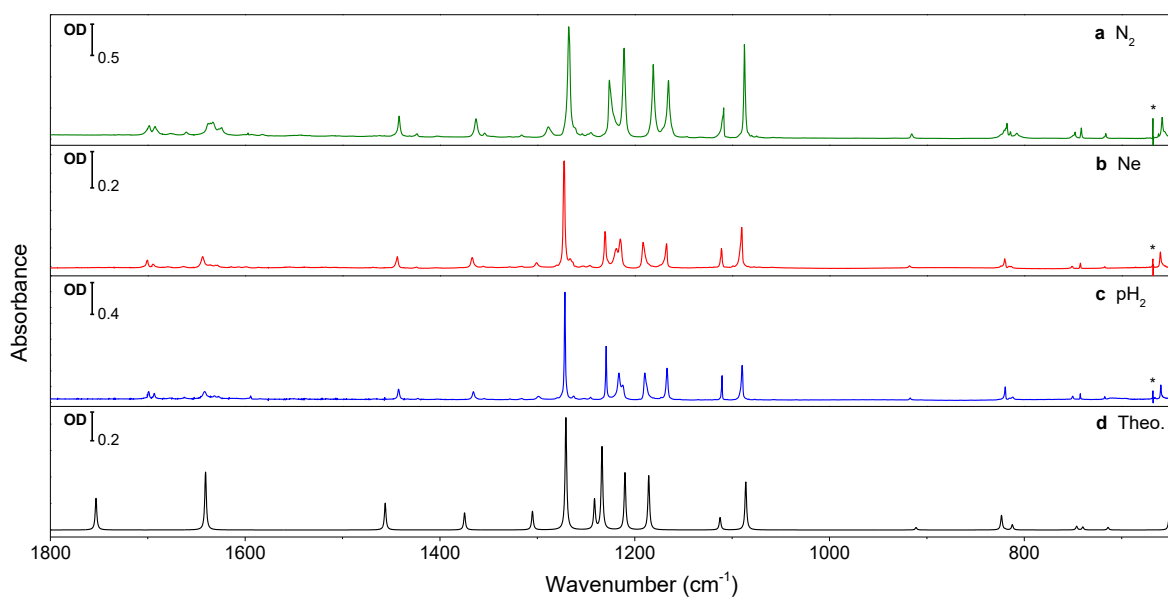


Figure VII.4: FT-IR of deposited hexafluoroacetylacetone in (a) nitrogen, (b) neon and (c) *para*-hydrogen matrices. (d) theoretical frequency calculation (M06-2X) of CCC conformer in harmonic approximation with 0.970 scaling factor. * artifacts

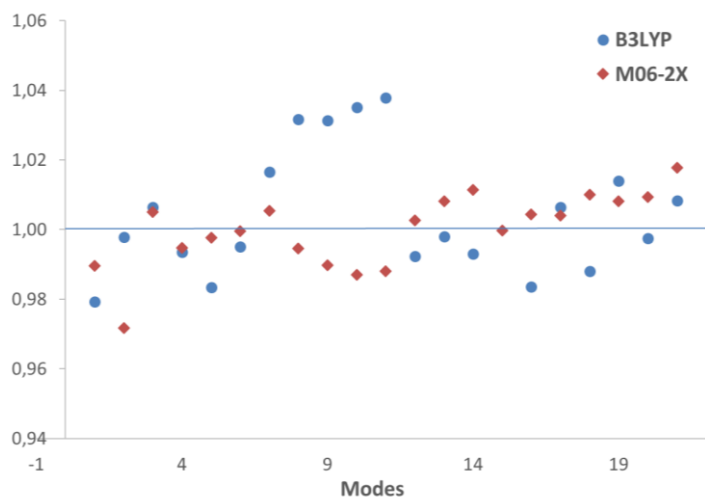


Figure VII.5: Comparison of the performance of B3LYP and M06-2X functionals versus experiment. The abscissa corresponds to the assigned modes, and goes from high (left) to low (right) frequencies. The ordinates correspond to the deviation of the $v_{\text{Theo}}/v_{\text{Exp}}$ ratio from 1 (corrected with the average value of each set). Theoretical harmonic frequencies were not scaled.

are less well described by the theory. Besides CCC no other enol conformer was found in the deposited sample. On the other hand, bands from keto tautomer were not found.

It is interesting to notice the presence of structure in some bands and specially in the C=O+C=C stretching region. The symmetric mode at lower frequencies ($\sim 1640 \text{ cm}^{-1}$) presents multiple bands in nitrogen and some additional small bands in neon and *para*-hydrogen. On the other hand, a clear doublet is observed for the antisymmetric C=O + C=C stretching band near 1695 cm^{-1} (see Figure VII.6). This doublet seems not to be due to site effects because it is present even in the soft *para*-hydrogen matrix. Moreover, the shift is the same in all the three matrices and equal to 6 cm^{-1} . The question that arises is: Is it a tunneling splitting?

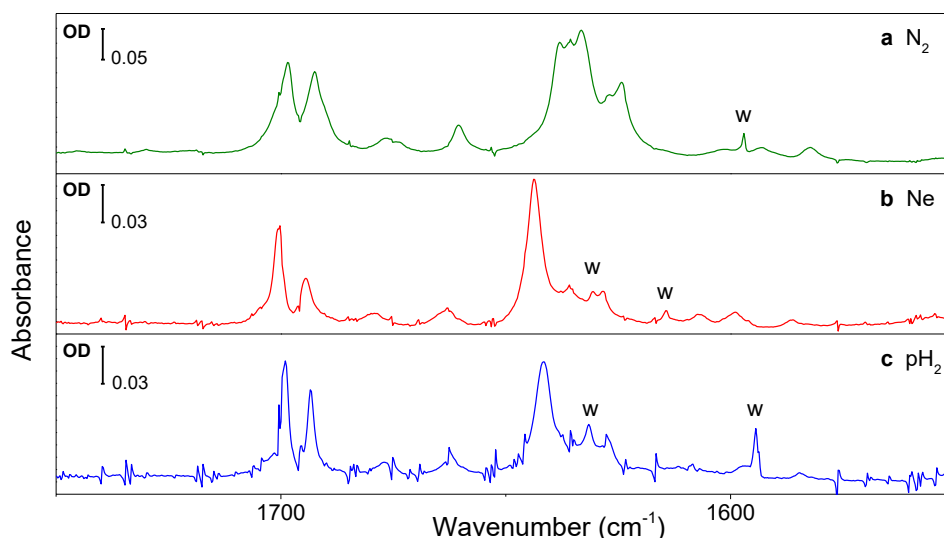


Figure VII.6: Expansion of Figure VII.4 in the $1750\text{-}1550 \text{ cm}^{-1}$ region in (a) nitrogen, (b) neon and (c) *para*-hydrogen matrices. A doublet appears in all the matrices near 1690 cm^{-1}

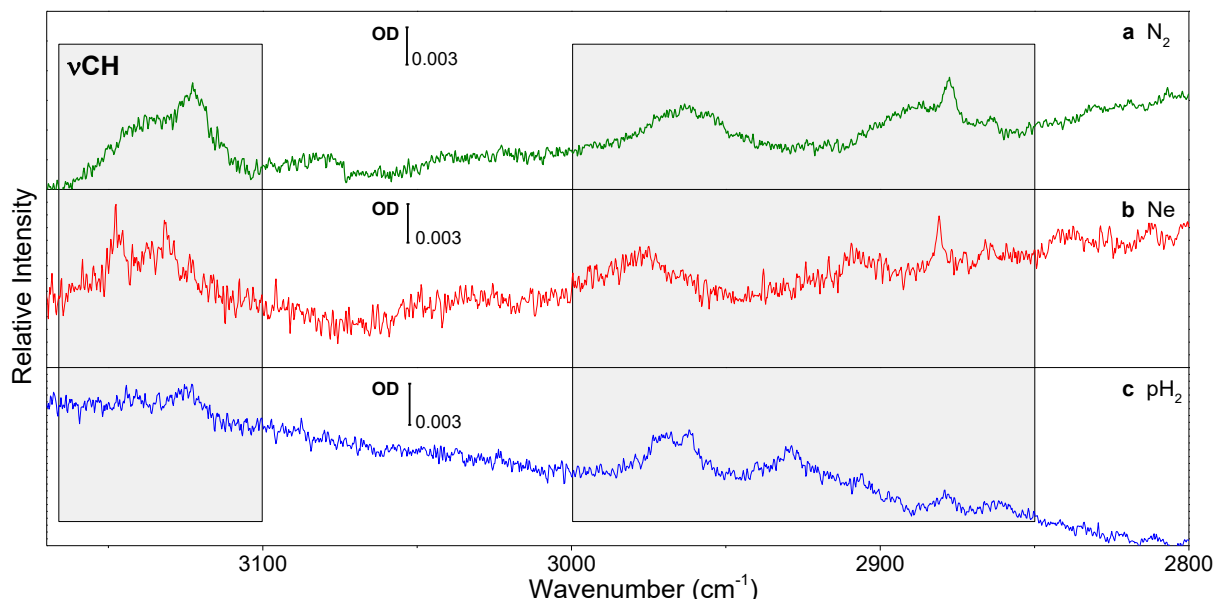


Figure VII.7: Experimental spectra in (a) nitrogen, (b) neon and (c) *para*-hydrogen matrices of the 3170-2965 cm^{-1} spectral region. Left panel: CH stretching band. Right panel: group of bands related to the CCC conformer and tentatively assigned to OH stretching mode.

Unfortunately, this question cannot be answered with certainty using only these results. To address this question, the study of the deuterated isotopologues should be done.

In the case of the high frequency modes, the only C-H stretching mode is found near 3120 cm^{-1} (see Figure VII.7). On the other hand, in previous works the OH stretching mode has been assigned in the gas phase to a group of bands near 3000-2965 cm^{-1} [55], [200]. In our matrix experiments at least three bands were found near to this region (see Figure VII.7).

The intensity of the groups of bands decrease after UV laser irradiation. Nevertheless, no clear assignment can be done from this fact other than it belongs to CCC. These bands could have another origin such as overtones or combination bands.

VII.2.2. Raman spectrum in argon matrix

The Raman and infrared spectra of the deposited sample in argon matrix (see Figure VII.8) supports the results obtained in the other matrices with FT-IR. The theoretical Raman and IR spectra for the CCC conformer match very well with the experimental ones, after applying the frequency scaling factor for both and the intensity corrections for Raman. We also observed in these spectra the presence of the doublet near 1690 cm^{-1} , with the same splitting value.

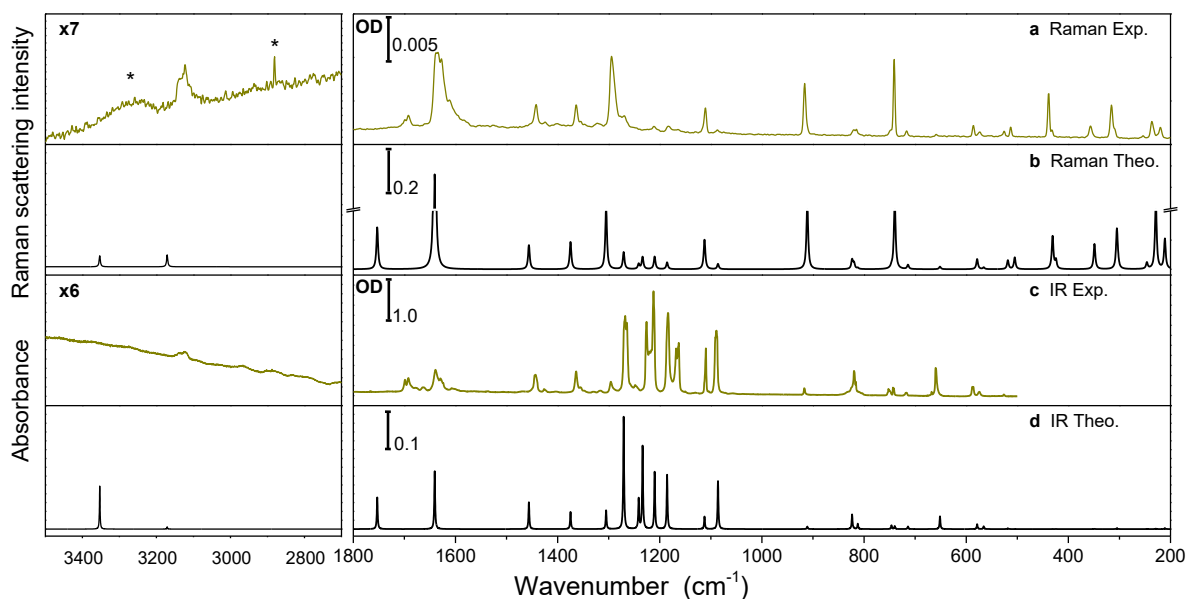


Figure VII.8: Experimental Raman (a) and infrared (b) spectra of hexafluoroacetylacetone in argon matrix at 11 K. Raman (c) and infrared (d) theoretical harmonic frequency calculations of CCC conformer (scaling factor: 0.970). There is a break in the intensity axis of the right panel of (b). Raman intensity is given in arbitrary units. * background

To conclude this part, we want to note the narrow bandwidth of the bands of almost all the modes of this molecule (around 1.7 cm^{-1} in overall), in comparison with other analogs systems (*e.g.* acetylacetone and chloroacetylacetone). Bands are quite narrow in all the matrices, and in both FT-IR and Raman spectra.

VII.3. UV laser irradiation

VII.3.1. Electronic absorption spectra

As in the previous systems, before performing the UV laser irradiation the electronic absorption spectrum of the CCC conformer in neon matrix was obtained. The spectrum is shown in Figure VII.9.

Two main absorption bands with some vibronic structure can be identified in the spectra. The first band near 270 nm corresponds to the CCC conformer we just demonstrated is the only present in the deposited sample. After irradiation at 290 nm, a new absorption band with maximum near 255 nm appears. This indicates the production of new species in the matrix. The electronic absorption spectrum of this molecule was previously obtained in gas phase by Nakanishi [71] and in argon matrix by Nagashima *et al.* [72]. In the first case only CCC conformer was accessible while in the second one broadband irradiation allowed them to investigate also non CCC conformers. The three results are resumed in Table VII.2.

Table VII.1: Vibrational assignment of the CCC conformer of hexafluoroacetylacetone. Infrared experimental frequencies (cm^{-1}) of the chelated enol form of AcAcF6 in nitrogen, neon and *para*-hydrogen matrices, and Raman experimental frequencies in argon matrix are compared to experimental values obtained by Nagashima *et al.* [72] in argon matrix. Calculated harmonic frequencies [M06-2X/6-311++G(3df,3pd)] (cm^{-1}) are also included for comparison. IR (km/mol) intensities and Raman scattering activities ($\text{\AA}/\text{u.m.a.}$) obtained in the harmonic approximation. Scaling factor (sf): 0.970

Assignment	Experimental						Theoretical		
	N ₂	Ne	pH ₂	Ar			Harmonic*sf	Int.	
				IR (this work)	Nagashima (IR)	Raman (this work)		IR	Raman
vOH							3353.2	206	43
vCH	3142.4	3148.7		3138.7			3171.0	11	40
	3123.4	3130.6	3126	3122.3		3125.9			
vCO + vC=C (as)	1698.7	1700.6	1699.0	1698.8		1699	1753.2	151	16
	1692.6	1694.3	1693.4	1692.0	1699.0	1692			
vCO + vC=C (s) + δ OH	1637.9			1639.3		1639	1640.7	276	93
	1632.7	1643.7	1641.5	1629.4	1640.0	1634			
	1624.3			1623.8		1627			
						1612			
vC-OH + δ CH	1441.9	1444.0	1442.5	1443.5	1445.0	1442	1456.2	128	7
δ OH + vcarbon chain (as)	1363.0	1366.9	1365.7	1363.7	1364.0	1363	1374.7	82	7
δ OH + vcarbon chain (s)	1288.8	1300.8	1298.8	1295.5	1296.0	1295	1305.0	89	15
δ OH + vCF ₃ (CO side) + C-CF ₃ (OH)	1267.6	1272.6	1271.7	1267.8	1269.0	1269	1270.7	536	4
				1264.4					
vCF ₃ (CO side)	1225.5	1230.5	1229.3	1226.1	1227.0		1241.3	143	1
				1220.3					
vCF ₃ (OH side)	1211.0	1219.7	1216.3	1216.6	1213.0	1211	1233.6	396	3
		1214.6	1212.3	1212.3					
vCF ₃ (OH side)	1181.0	1191.1	1189.7	1183.5	1185.0	1183	1210.0	272	3
vCF ₃ (CO side)	1165.4	1167.8	1166.8	1168.0	1168.0	1164	1185.6	259	1
				1162.6					

δ CH	1109.5	1111.1	1110.4	1109.9	1110.0	1110	1112.4	60	6
ν C-C	1087.2	1090.6	1089.7	1089.1	1092.0	1087	1086.0	230	1
Δ	915.5	917.9	917.2	917.4	918.0	916	911.2	12	10
Γ						823	823.4	70	1
δ_s CF ₃ (umbrella both sides) (as)	818.6	820.2	819.5	819.7	820.0	820	819.7	3	1
γ OH + γ CH	807.7	813.6	811.9			815	812.3	25	0.1
Γ	748.4	751.1	750.3	752.1	752.0	749	746.3	18	0.2
δ_s CF ₃ (umbrella both sides) (s)	741.4	742.4	742.5	742.7	744.0	741	739.9	14	8
Γ	716.6	717.5	717.4	717.4	719.0	716	714.0	12	0.4
δ_s CF ₃ (OH side)	658.5	660.1	659.8	659.8	660.0	659	651.4	61	0.2
δ_{as} CF ₃ (OH side)						585.7	578.6	23	1
δ_{as} CF ₃ (CO side)						573.3	565.8	13	0.1
δ_{as} CF ₃ (OH side) + δ_{as} CF ₃ (OH side)						525.5	518.5	3	1
δ_{as} CF ₃ (OH side) + δ_{as} CF ₃ (OH side)						512.7	505.0	0.3	1
δ_{as} CF ₃ (CO side)						438.2	430.9	0.2	2
δ_{as} CF ₃ (OH side)						432.1	424.3	1	0.5
δ F-C-CO						355.6	348.9	1	1
Δ						315.3	305.0	4	2
ρ CF ₃ (OH side)						309.4	302.9	0.02	0.1
ρ CF ₃ (CO side)						253.2	246.3	1	0.2
Δ						236.5	228.8	2	2
π CF ₃						219.7	211.1	4	1

^a main characteristic motions; ν , stretching; δ , in plane bending; γ , out of plane bending; ρ , in plane rocking; π , out of plane rocking; Δ , in plane ring deformation; Γ , out of plane ring deformation; s, symmetric; a, asymmetric

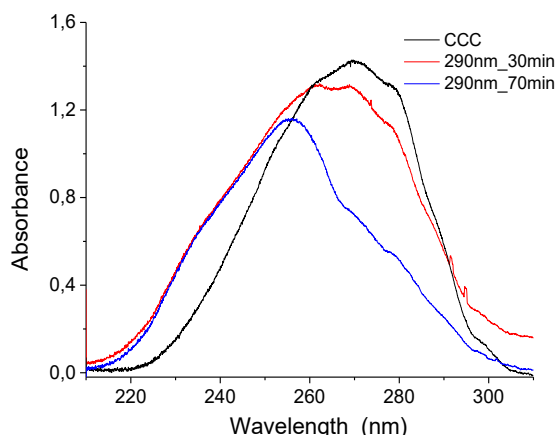


Figure VII.9: Electronic absorption spectra of hexafluoroacetylacetonone in neon matrix. (black) deposited sample, (red) 30 min of irradiation at 290 nm (blue) 70 min of irradiation at 290 nm.

Taking advantages of the knowledge of the absorption spectra we started the UV laser irradiation at 290 nm for more than 40 minutes. Next, the wavelength was gradually changed (by steps) to lower values. From the beginning of the irradiation CCC bands intensity decreased while a new group of bands was growing. Taking into account the different kinetics of the growing bands we were able to isolated two groups: one growing faster than the other when irradiating at 290 nm, and the second increasing very fast under irradiation at 265 nm. Comparison with theoretical frequency calculations of all the conformers allowed to assign these two groups to CTT and TCC conformers (Table VII.3). They are the two lowest energy open enol conformers (see Figure VII.1). In the next section, we describe the assignment and the features of the obtained infrared spectra after manipulation (subtraction of spectra to clean the other conformers).

Table VII.2: Position of the maximum of absorption for the $\pi \rightarrow \pi^*$ transition in the CCC conformer and after irradiation. Results in gas phase [71] and argon matrix [72] are compared to the one obtained in neon matrix in the present work.

Transition	Gas phase	Ar matrix		Present work Ne matrix	
	CCC	CCC	After irradiat.	CCC	After irradiat.
$\pi \rightarrow \pi^*$	267	272	249	270	253

VII.3.2. CTT conformer

In Figure VII.10 the experimental spectra of CTT in *para*-hydrogen and neon matrices along with the theoretical frequency calculation for this conformer is shown. As for the CCC conformer the agreement between experimental and theoretical spectra is good in overall. Once more the C=O+C=C and CF₃ stretching regions are not completely well described, but this incertitude is small enough to leave no doubt about the

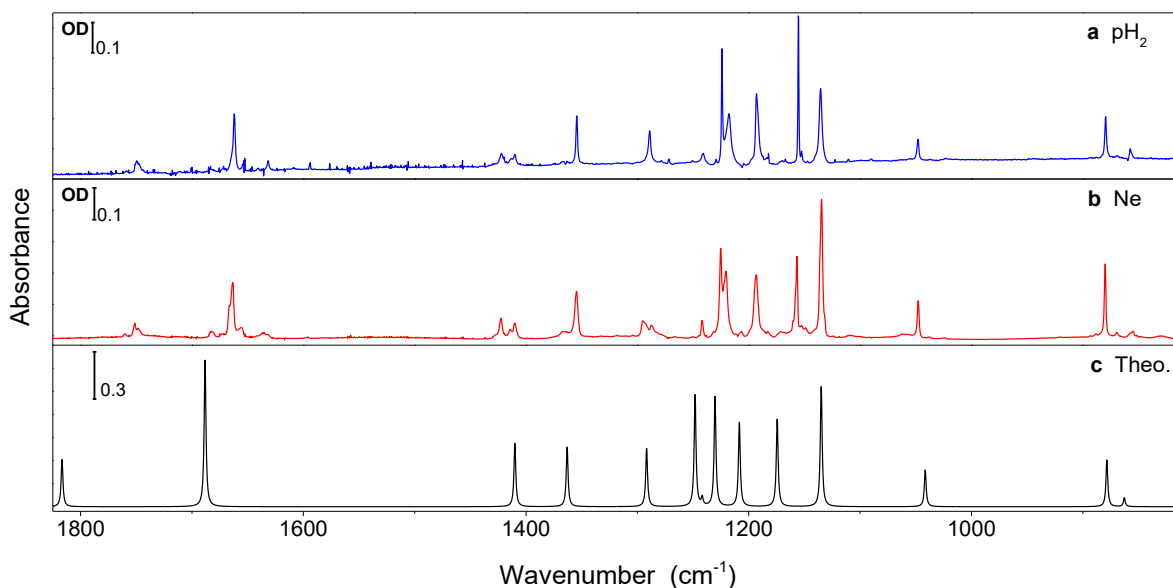


Figure VII.10: Experimental spectra of CTT conformer in (a) neon and (b) *para*-hydrogen matrices. . The spectra are the result of subtractions of different spectra along irradiation in order to remove CCC and TCC bands. Panel (c) shows theoretical frequency calculation (M06-2X) of CTT conformer in harmonic approximation with 0.970 scaling factor.

assignment. CTT conformer was previously found to be produced in argon matrix by a broadband mercury lamp⁵⁸ [72], which supports our result.

Despite the difficulties in the assignment of the CF₃ stretching zone (similar theoretical intensities) we were able to propose a correspondence between the theoretical and experimental modes present therein. We can note there are two bands at 1155.4 and 1224.0 cm⁻¹ in *para*-hydrogen which are narrower than the rest. According to their position and the theoretical calculation these bands should correspond to pure (or non-coupled) CF₃ stretching modes in both C=O and C-OH side of the molecule. This assignment is done based in the position of the first CF₃ theoretical band (1174.4 cm⁻¹) which suggests that the narrowest bands belong to these localized modes.

We can also note in the experimental spectra near 1400 cm⁻¹ the presence of a small multiplet (three bands, see Table VII.3). The theoretical calculation predicts only one band in this region, formed by the combination of OH and CH bending in plane mode. The shift between the two more intense bands is nearly the same in both matrices, *ca.* 12 cm⁻¹. No other band seems to be present as a multiplet. A possible assignment is a combination band between a CF₃ stretching fundamental and an overtone of the bending in plane mode of the same group (see Table VII.3). On the other hand, the bands near 1290 cm⁻¹ in neon are more likely to be due to a site effect when we compare them to the one in *para*-hydrogen.

⁵⁸ In a second article [19] a Xe lamp from a spectrofluorophotometer was used to reduce the irradiation bandwidth (around 10 nm), obtaining similar results.

HEXAFLUOROACETYLACETONE

Table VII.3: Vibrational assignment of the CTC and TCC conformers of hexafluoroacetylacetonone. Infrared experimental frequencies (cm^{-1}) in neon and *para*-hydrogen matrices. Calculated harmonic frequencies [M06-2X/6-311++G(3df,3pd)] (cm^{-1}) are also included for comparison. IR (km/mol) intensities were obtained in the harmonic approximation. Scaling factor (sf): 0.970.

Assignment	Frequencies				Int.
	Experimental		Theoretical Harmonic*sf		
	Ne	pH ₂	CTT	TCC	
vOH	3631.5	3623.7		3749.7	199
vOH	3612.8	3596.7	3732.5		261
vCH	3234.4			3146.8	11
vCH	3051.6	3048.8	3126.1		5
vCO + vC=C (as)	1751.7	1749.6	1816.7		124
vCO	1722.1	1719.3		1794.9	239
		1714.4			
vCO + vC=C (s) + δ OH	1663.6	1662.1	1688.3		387
	1655.5	1653.8			
vC=C	1659.5	1658.0		1683.3	293
vC-OH	1445.0	1443.5		1448.0	134
	1437.9	1435.9			
	1422.6	1421.8			
δ OH + δ CH	1414.5	1413.6	1410.0		167
	1409.8	1410.0			
vC-OH + vC-CH ₃	1354.8	1354.5	1363.1		157
vC-CH ₃ + δ CH	1365.4	1364.6		1361.0	56
vC-CH ₃ + δ OH + δ CH	1306.0	1304.4		1300.5	59
	1294.8				
vCF ₃ (CO side) + δ OH + δ CH	1286.9	1289.1	1291.7		153
vCF ₃ (both sides) + δ OH	1274.7	1272.3		1275.8	103
vCF ₃ (OH side)	1225.3	1224.0	1248.2		294
	1235.4				
vCF ₃ (both sides) + δ OH	1225.8	1227.0		1242.2	188
	1219.9				
vCF ₃ (both sides) + δ OH + δ CH	1241.8	1241.0	1241.8		21
vCF ₃ (CO side) + δ OH + δ CH	1220.5	1217.8	1230.3		290
vCF ₃ (OH side) + δ OH	1209.5	1206.8		1215.1	556
vCF ₃ (OH side) + δ CH	1193.5	1192.6	1208.4		221
vCF ₃ (OH side)	1184.0	1182.0		1204.4	283
vCF ₃ (CO side)	1157.1	1155.4	1174.4		231
vCF ₃ (CO side) + δ OH + δ CH	1156.4	1153.1		1161.5	287
vCF ₃ (OH side) + δ OH + δ CH	1134.9	1135.4	1134.9		317
vCF ₃ (CO side) + δ OH + δ CH	1119.1	1128.9		1133.1	239

Assignment	Frequencies				Int.
	Experimental		Theoretical Harmonic*sf		
	Ne	pH ₂	CTT	TCC	
vC-C	1047.8	1048.1	1041.5		97
vC-OH	1032.6	1030.3		1039.7	66
vCF₃ (CO side)	880.0	879.5	878.4		123
vC-CF₃	858.4	859.3		868.3	17
γCH				866.5	44
γCH	855.5	856.9	862.7		23
δsCF₃(OH side)	785.0	784.4	784.4		7
δsCF₃(CO side)	769.1			769.4	7
γCH + γC=O	747.6	747.0	749.7		5
δsCF₃(CO side)	731.7				
	730.2	731.6	728.8		65
δsCF₃(OH side)	730.0	730.3		726.5	13

^a main characteristic motions; **v**, stretching; **δ**, in plane bending; **γ**, out of plane bending; **ρ**, in plane rocking; **π**, out of plane rocking; **Δ**, in plane ring deformation; **s**, symmetric; **a**, asymmetric

VII.3.3. TCC conformer

As we mentioned before another open enol conformer is produced and stabilized in the matrix after lower wavelength irradiation (265 nm). In Figure VII.11 we can observe the assignment of the TCC conformer which grows faster than CTT when the 265 nm wavelength is used. The experimental spectra in neon and *para*-hydrogen matrices are shown. The frequency calculation in the harmonic approximation is also included for comparison.

The assignment of this conformer is a more challenging task than in the other cases. This is mainly due to the small infrared activity (intensity) of the modes out of C=O+C=C and CF₃ stretching, which as we already mentioned have the highest disagreement with theoretical results. Nevertheless, a careful comparison of all the open enol conformers allows us to suggest TCC as the conformer produced at shorter wavelength. We should remark this conformer was not found by Nagashima *et al.* in their studies in argon matrix [19]. In fact, only CTT was produced after the UV irradiation in argon matrix.

An interesting point is that the production of this second conformer is only enhanced in a very narrow range of wavelengths around 265 nm. Below 260 nm the system starts to go back to CCC, as it was also noted by Nagashima *et al.* in argon matrix [19]. At 268 nm CTT is mainly produced.

If the energy order given in Figure VII.1 is examined we may have a clue about why these two conformers are the ones stabilized in neon and *para*-hydrogen matrices. We remark the word “stabilized” because in

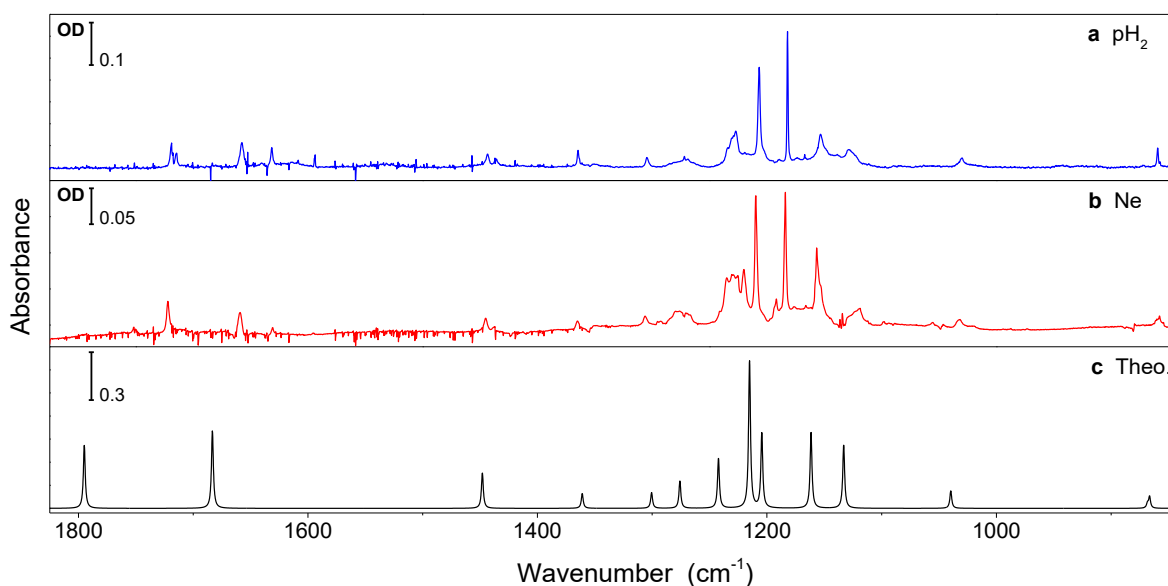


Figure VII.12: Experimental spectra of TCC conformer in (a) neon and (b) *para*-hydrogen matrices. . The spectra are the result of subtractions of different spectra along irradiation in order to remove CCC and CTT bands. Panel (c) shows theoretical frequency calculation (M06-2X) of TCC conformer in harmonic approximation with 0.970 scaling factor.

principle other conformers could be produced after irradiation. Our hypotheses are the next: first, TTT and TTC conformers are not produced because of their high energy and repulsive geometry. Second, if the UV irradiation produce one of the conformers of the pairs CTC-CTT or TCT-TCC, the system will always end in the most stable conformer of the pair. This guess is based in the results obtained for normal and deuterated acetylacetone, where we saw that the tunneling effect takes part in the dynamics of interconversion process (which is very fast for the non-deuterated molecule). These two hypotheses can explain the stabilization of CTT and TCC conformers. On the other hand, CCT which is the most stable open enol conformer, if produced should be converted very fast to CCC also by a tunneling driven process.

The final assignment for the open enol conformers is shown in Table VII.3.

HEXAFLUOROACETYLACETONE

Chapter VIII Trifluoroacetylacetone

Up to this point, only symmetric analogs (regarding the structure of the methyl groups) of acetylacetone have been studied. In this chapter the asymmetric analog, trifluoroacetylacetone is analyzed.

VIII.1. Theoretical results

Due to the asymmetric nature of this molecule the number of possible conformers is twice the number for the previous analyzed analogs. One set corresponds to the presence of the CF_3 group in the carbonyl ($\text{C}=\text{O}$) side and the other with the CF_3 in the hydroxyl (OH) side. The theoretical energy order (at M06-2X/6-311++G(3df,3pd) level of theory) relative to the most stable enol conformer is shown in Figure VIII.1.

The first thing to remark is that the energetic order of the $\text{AcAcF}_3(\text{CO})$ is the same of AcAcF_6 , while the one for $\text{AcAcF}_3(\text{OH})$ is the same of AcAcH_8 . The relative energy order obtained is very similar to the one obtained by Minoura *et al.* [20] using B3LYP/6-31G* level of theory. The only difference is the stabilization of the

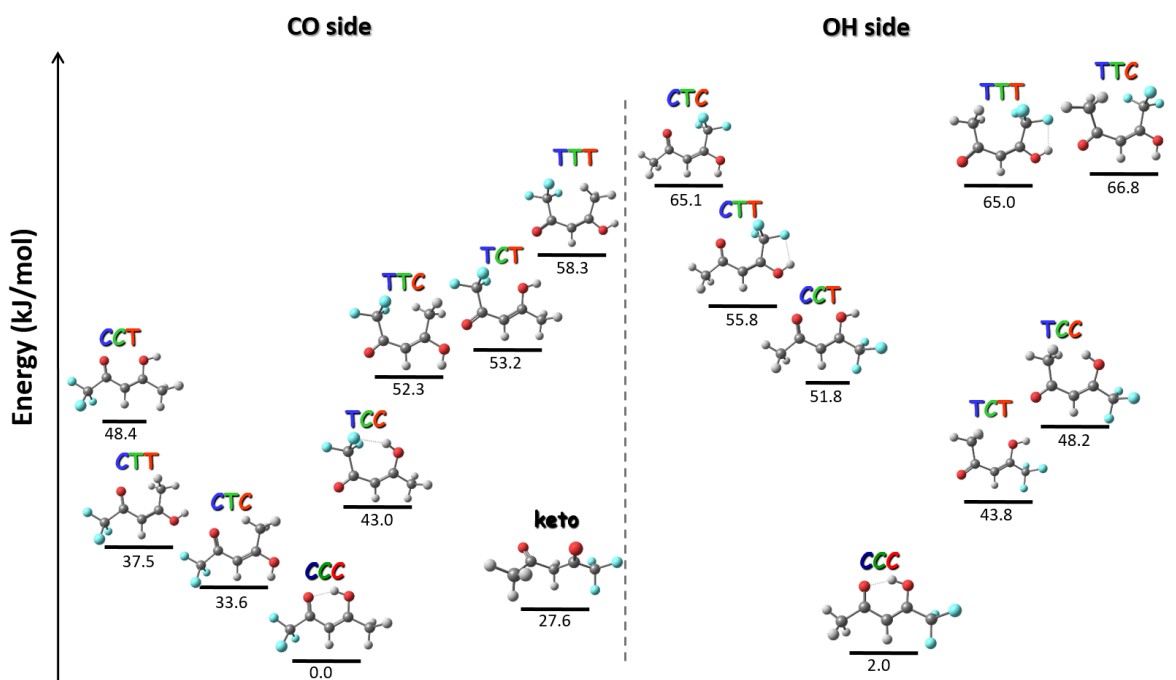


Figure VIII.1: Schemes and theoretical relative energies (kJ/mol) of open enol conformers of the CO and OH isomers (depending on the CF_3 position) and keto tautomer compared to the CCC(CO) conformer, in AcAcF_3 at M06-2X/6-311++G(3df,3pd) level of theory. Zero Point Energy is included in each reported value.

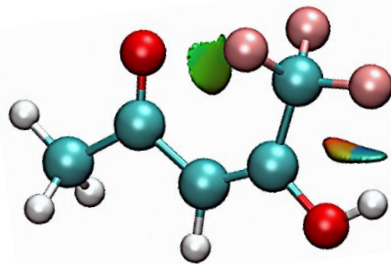


Figure VIII.2: NCI calculation for the CTT(OH) conformer of trifluoroacetylacetone. Isosurface of s at 0.35; light blue corresponds to non-covalent interactions and green color corresponds to steric repulsion.

CTT(OH) conformer, probably due to a better description of the non-covalent interaction between the fluorine (CF₃) and hydrogen (OH) atoms (see Figure VIII.2).

It should be noted that the CCC(OH) conformer is only 2.0 kJ.mol⁻¹ higher in energy than the CCC(CO) conformer. In previous reports values between 3.4–5.7 kJ.mol⁻¹ have been found using B3LYP/6-31G* and higher basis sets [20], [69], [78], [216]. The proton transfer barrier has also been estimated in a previous study, the value obtained was 11 kJ/mol at B3LYP/6-31G** level of theory [78]. The low energetic separation between both conformers and the relatively low barrier imply that at low temperatures the CCC(OH) conformer will convert to CCC(CO) by tunneling effect, and only this conformer should be observed.

VIII.2. Vibrational spectroscopy of as-deposited samples

VIII.2.1. FT-IR spectrum in Ne and *p*H₂ matrices

The experimental spectra of the deposited sample in *para*-hydrogen and neon are shown in Figure VIII.3. The overall spectra are similar to the one obtained by Minoura *et al.* in argon matrix [20]. Nevertheless, some differences between neon and *para*-hydrogen in the 1250-1150 cm⁻¹ region are clearly observed. The spectra in both matrices differ in the amount and bandwidth of bands in this region. In Figure VIII.3 the theoretical harmonic (scaled) spectra of CCC(OH) and CCC(CO) are shown. The comparison with experimental spectra gives an overall better match for the CCC(CO) conformer. This result is also in agreement with the expected theoretical energy order and the results in argon matrix.

Nevertheless, some bands cannot be explained from the theoretical spectrum (region between 1300-1150 cm⁻¹). There are more bands than the number of fundamental transitions predicted by theory. Moreover, they were easily observed in argon matrix also, but no discussion about their origin was made by Minoura

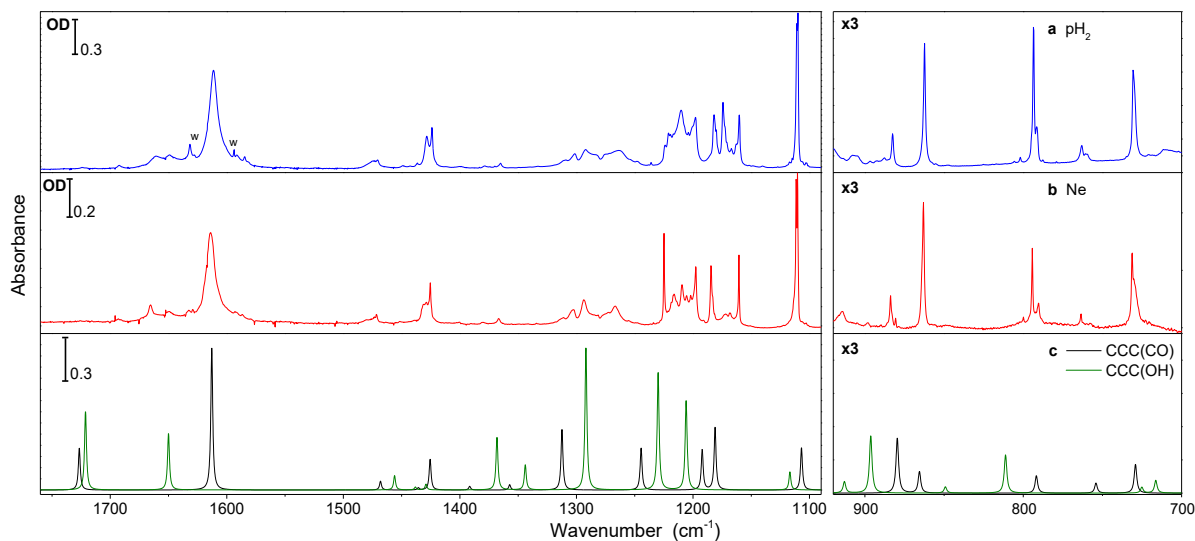


Figure VIII.3: FT-IR of deposited trifluoroacetylacetone in (a) *para*-hydrogen, and (b) neon matrices and (c). theoretical frequency calculation (M06-2X) of the two CCC conformers in harmonic approximation with 0.973 scaling factor.

et al. [20]. The first group of bands around 1280 cm^{-1} is composed of at least three broad bands placed in the region of the theoretically predicted OH in plane bending mode. The second group (around 1200 cm^{-1}) is composed by several bands, and calculations show that they correspond to the CF_3 stretching modes. The number, relative intensity and bandwidth of the bands in this region depend on the matrix (argon, neon and *para*-hydrogen).

VIII.2.2. Raman spectrum

The Raman spectrum in argon matrix was also obtained (Figure VIII.4). The theoretical spectra of the two CCC conformers is also included. The match with theoretical spectrum of CCC(CO) is quite good in overall, supporting the previous assignment. In this case the second group of bands previously mentioned is not observed because of the low Raman intensity of the high polar CF_3 stretching modes. Only one band at 1199 cm^{-1} corresponding to a $C_{sp_2} - H$ in plane bending is observed. On the other hand, the first group of bands (near 1280 cm^{-1}) is easily identified because of its high intensity.

TRIFLUOROACETYLACETONE

Table VIII.1: Vibrational assignment of the CCC(CO) conformer of trifluoroacetylacetone. Infrared experimental frequencies (cm^{-1}) of the chelated enol form of AcAcF3 in neon, *para*-hydrogen and argon matrices; and Raman experimental frequencies in argon matrix. Calculated harmonic frequencies [M06-2X/6-311++G(3df,3pd)] (cm^{-1}) are also included for comparison. IR intensities (km/mol) and Raman scattering activities ($\text{\AA}/\text{u.m.a.}$) obtained in the harmonic approximation. A scaling factor of 0.973 is used to correct the harmonic theoretical frequencies.

Frequency				Theoretical		
Ne	pH_2	Ar		Harmonic*sf	Int.	
		Infrared	Raman		IR	Raman
				3262.9	234	39
				3168.9	2	47
3021	3016.4	3020	3020	3097.4	4	42
2980	2977.1	2980.0	2980.0	3053.5	1	80
2930	2932	2935	2935	2991.1	1	247
1666	1660.5	1660.5				
1650	1648	1648	1656	1726.6	176	20
1614.6	1611.6	1608.7	1607.6	1612.9	599	66
1471.8	1470.6	1474		1468.1	37	4
	1436.6	1435.4	1436.2	1435.6	9	4
1431.3						
1429.1	1428.7	1425	1425	1425.6	129	10
1426.1	1423.9	1423				
				1391.6	16	1
1367.0	1365.1	1363.7		1357.3	23	19
1312	1310	1310	1312			
1303	1301.6	1301	1302			
1293.6	1292.2	1290	1290			
1286	1283	1282	1283			
1273	1275	1274	1274	1248.4	255	26
1266.9	1263	1263	1263			
1255.5	1254	1250				
	1248					
1225	1224.3			1244.5	177	1
1218.7	1221.1					
1216.7	1219.4	1218				
1213.6	1216.9	1213.2				
1209.5	1210.2	1208.3	1208			
1205.7	1207.3	1207.5		1192.1	170	10
1202	1203.9	1199.5	1199.5			
1197.6	1200.7	1197.5				
	1197.8					

Vibrational spectroscopy of as-deposited samples

Frequency			Theoretical			
Ne	pH ₂	Ar		Harmonic*sf	Int.	
		Infrared	Raman		IR	Raman
1184	1181.9	1178				
1183.1	1180	1175				
1172	1174.3	1167				
1168	1172.7	1155				
1160.7	1170.9			1181.0	264	1
	1167.1					
	1163.0					
	1160.4					
1111.5	1111	1110				
1110.3	1110	1109	1111	1106.9	178	1
1039.5						
1038.3	1037.5	1035.9	1037.2	1035.0	3	1
1012.4		1009				
1011	1010.3	1008	1010.0	1005.2	7	1
944.6	944.7	945.7				
942.6	942.2	941.7	944.8	941.3	5	10
883.9	882.5			879.6	78	0.3
863	862.4	861.7	862.8	865.6	30	1
794.3	793.6					
790.5	791.4	790.9		791.7	25	0.3
763.6	763.2	761.6		754.1	14	0.2
731.3	730.6		729.7			
730.1	730	729.7	720.9	729.1	41	6
			592	581.6	0.5	2
				574.5	8	0.3
			524.6	513.9	19	6
			517.9	510.2	4	0.3
			439.0	431.8	1	1
			394.0	384.2	4	0.3
			312.4			
			315.4	315.9	1	2
			309.6			
				265.5	1	0.1
			263.0	245.1	7	2
			186.0	172.9	0.4	0.4

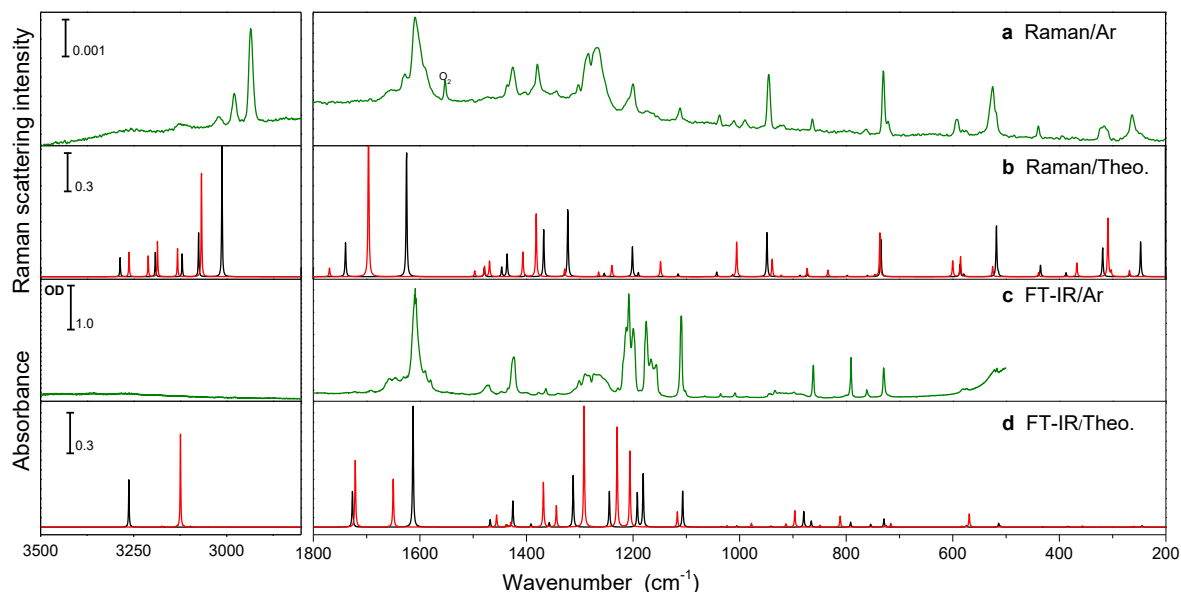


Figure VIII.5: Experimental and theoretical (M06-2X/6-311++g(3df,3pd)) Raman and FT-IR spectra of trifluoroacetylaceton (AcAcF₃) in argon matrix. Raman: (a) experimental and (b) theoretical; Infrared: (c) experimental and (d) theoretical. A scaling factor of 0.973 is used on the harmonic theoretical spectra. (black) CCC(O) conformer and (red) CCC(OH) conformer theoretical spectra. Raman intensity is given in arbitrary units.

VIII.3. UV laser irradiation

VIII.3.1. Electronic absorption spectrum

The electronic absorption spectrum of trifluoroacetylaceton in neon matrix is shown in Figure VIII.6 for the deposited sample and after two different irradiation sequences from two different samples: 285 + 270 nm and 260 + 245 nm. No bibliographic reference was found about the UV spectrum of this molecule.

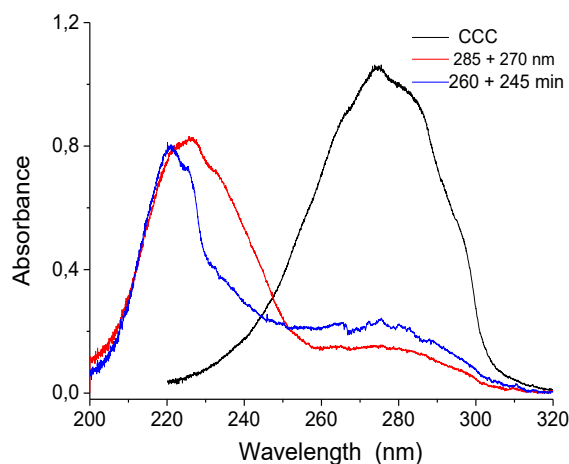


Figure VIII.6: Electronic absorption spectra of trifluoroacetylaceton: (black) deposited sample, corresponding to CCC(O) conformer (red) after 285 + 270 nm irradiation sequence (blue) after 260 + 245 nm irradiation sequence.

Similarly to the other analogs of acetylacetone, the electronic absorption spectrum of the deposited sample shows a broad band around 277 nm corresponding to the $\pi \rightarrow \pi^*$ transition. The band shows some broad structure, but not as clear as in chloroacetylacetone. We can also remark that this transition is redshifted compared to AcAch8 and AcAcF6. On the other hand, two other bands strongly blueshifted can be distinguished after the irradiation sequences: 221 and 226 nm. By similarity with the other β -diketones, these bands must belong to open conformers, and two groups of conformers are expected to be formed after UV laser irradiation.

VIII.3.2. Open enol conformers

The UV laser irradiation in neon and *para*-hydrogen was carried out like in the previous systems. Irradiation starts at a high wavelength (290 nm) placed to the red side of the electronic absorption band, and it was subsequently changed to lower values (until 230 nm). The formation of three open enol conformers was observed (CTC(CO), CTT(OH) and TCT(OH)), similarly to the result obtained by Minoura in argon matrix [20]. The increase of each conformer greatly depends on the irradiation wavelength sequence used.

VIII.3.2.1. CTC(CO)

Mainly one conformer is formed when UV irradiation starts (290-285 nm): CTC(CO). The identification of this conformer was done by comparison with the theoretical spectra of the different conformers (see Figure VIII.7). The match with the theoretical spectrum is rather good. CTC(CO) conformer is the most stable open enol conformer of both possible sets of conformers.

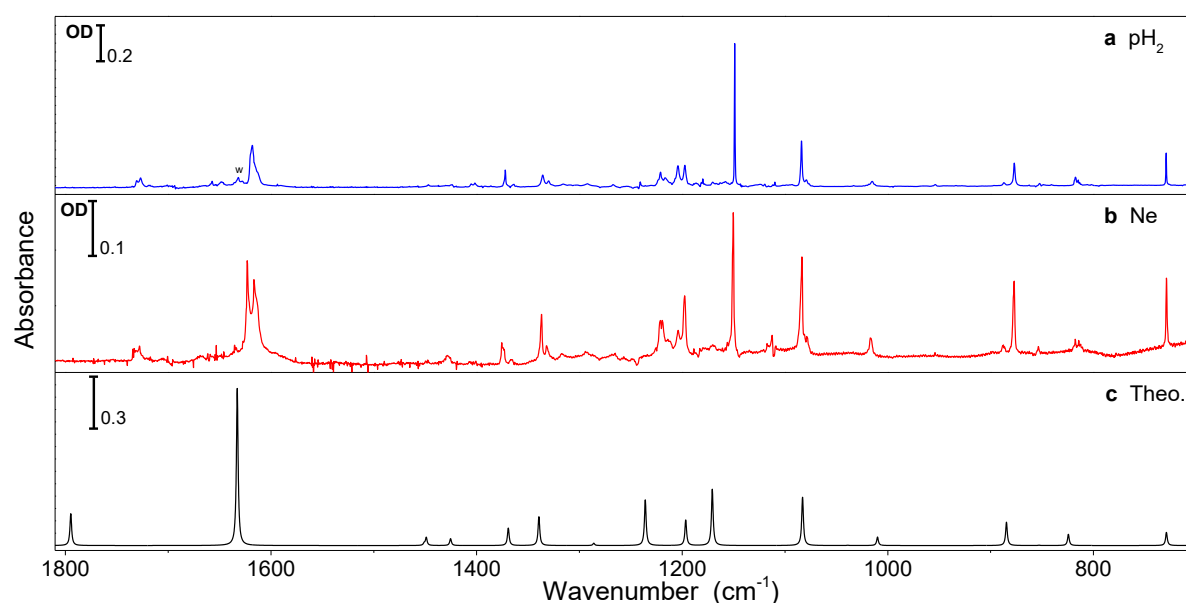


Figure VIII.7: Experimental spectra of the CTC(CO) conformer of trifluoroacetylacetone in (a) *para*-hydrogen and (b) neon matrices. (c) theoretical harmonic spectrum, a scaling factor of 0.973 is used.

TRIFLUOROACETYLACETONE

Table VIII.2: Vibrational assignment of the CTC(CO) conformer of trifluoroacetylaceton. Infrared experimental frequencies (cm^{-1}) of the chelated enol form of AcAcF₃ in neon and *para*-hydrogen. Calculated harmonic frequencies [M06-2X/6-311++G(3df,3pd)] (cm^{-1}) are also included for comparison. IR intensities (km/mol) are obtained in the harmonic approximation. A scaling factor of 0.973 is used to correct the harmonic theoretical frequencies.

Frequency		Theoretical	
Ne	pH ₂	Harmonic*sf(0.973)	Int.
3614.8	3597.6	3751.4	76
3022.0		3134.8	6
2967.0		3102.8	5
2932.0		3046.6	1
		2990.5	4
1732.2	1730.9		
1728.3	1727.4	1794.7	148
1623.2			
1616.3	1618.5	1632.8	732
1448.4	1447.3	1451.0	10
		1449.0	37
1428.4	1424.5	1425.3	32
1374.6	1372.4	1369.2	81
1337.3	1335.9		
1331.9	1330.2	1339.4	134
1293.0	1292.3	1286.0	11
1221.5			
1219.3	1221.3	1235.9	213
1204.2	1204.3		
1197.8	1197.7	1196.6	119
1150.5	1149.0	1170.7	262
1083.8	1084.0	1082.9	225
		1039.0	1
1016.6	1015.3	1010.0	40
877.4	877.2	884.6	109
853.7	852.6	852.9	1
817.9	817.7		
814.1	815.0	824.4	53
		754.7	0.0
729.1	729.4	729.0	61

VIII.3.2.3. CTT(OH) and TCT(OH)

The second group of conformers is produced from the beginning of the irradiation at 285 nm, but in a lower amount. This group is mainly formed when CTC(CO) conformer is irradiated at 270 nm or the CCC conformer is directly irradiated with 260 nm wavelength from the beginning. Two conformers were identified in this group. Different ratios between the two conformers are obtained depending on the irradiation sequence used.

The conformers were identified by comparison with theoretical calculations. The spectra in neon and *para*-hydrogen matrices are shown in Figure VIII.8 and Figure VIII.9. The conformers are: CTT(OH) and TCT(OH). In both cases, the match with theoretical calculation is quite good. The biggest disagreement is observed in the 1300-1100 cm^{-1} region like in AcAcF6. Both conformers are the most stable species of their XYC-XYT pair (see Figure VIII.1).

No other conformer was produced. We observed the same set of conformers obtained by Minoura *et al.* [20] in argon matrix. The only difference is that they observed, during the irradiation process, the formation of a transient conformer: CTT(CO). We did not perform such kind of measurement because of experimental constraints. Our results and those from Minoura suggests that the matrix has no influence in the conformer production.

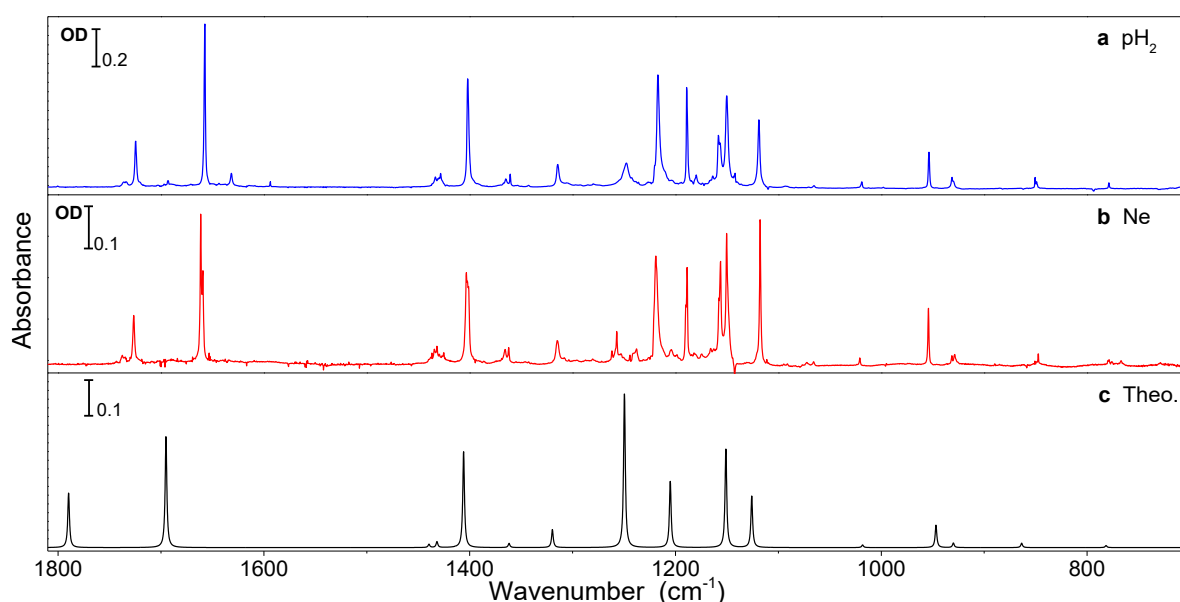


Figure VIII.8: Experimental spectra of the CTT(CO) conformer of trifluoroacetylacetone in (a) *para*-hydrogen and (b) neon matrices. (c) theoretical harmonic spectrum, a scaling factor of 0.973 is used.

TRIFLUOROACETYLACETONE

Table VIII.3: Vibrational assignment of the CTT(OH) and TCT(OH) conformers of trifluoroacetylacetone. Infrared experimental frequencies (cm⁻¹) of the chelated enol form of AcAcF₃ in neon and para-hydrogen. Calculated harmonic frequencies [M06-2X/6-311++G(3df,3pd)] (cm⁻¹) are also included for comparison. IR intensities (km/mol) are obtained in the harmonic approximation. A scaling factor of 0.973 is used to correct the harmonic theoretical frequencies. Scaling Factor (sf): 0.973.

Frequencies				
Experimental		Theoretical Harmonic*sf		Int.
Ne	pH ₂	CTT(OH)	TCT(OH)	
3626.1	3613.5	3758.1		233
3631.8	3612.8		3756.8	177
3026.1	3014.8		3155.0	5
2983.2	2980.8		3099.6	6
2931.8	2929.7		3057.3	2
	2902.3		2991.8	0.1
		3121.0		2
3031.5	3030.9	3098.9		5
	3022.6			
2970.9	2966.1	3042.8		3
	2923.6	2980.6		1
1726.6	1714.7	1789.8		151
1709.9	1709.5		1768.9	251
	1705.5			
1697.2	1693.3		1737.2	99
1661.4	1657.5	1695.1		308
1659.4				
1435.8	1434.9		1440.2	10
1434.5	1433.5	1439.6		9
1431.9				
1429.5	1428.3	1431.8		16
1425.3				
1424	1422.2		1431.0	64
1403.3				
1402.4	1402	1405.9		265
1401.2				
1394.3	1394.3		1405.2	96
1369	1367.4		1364.0	46
1365.7	1365.1	1361.7		12
1362.3	1360.7			
1314.8	1314.6	1319.6		50
1306.1	1306.4		1303.2	42

Frequencies				
Experimental		Theoretical Harmonic*sf		Int.
Ne	pH ₂	CTT(OH)	TCT(OH)	
1249.4	1248.3		1256.4	218
1219.1	1217.2	1249.7		268
1239.4	1248	1249.5		160
1243.8	1242.6		1242.7	183
1221.2	1220.5		1237.6	444
1190.1	1189	1205.1		184
1188.8				
1146				
1143.5	1142.3		1164.7	281
1156.5	1157.4			
1150.5	1150.3	1151.0		273
1117.7	1119.0	1125.9		142
1076.8	1077.8		1084.6	12
1027.4	1026.4		1024.9	7
1021	1019.1	1018.2		7
995.4	995.0		989.8	32
954.4	953.8	946.9		62
931.5	931.5	930.0		13
928.8	930.0			
958.1	856.3		868.9	31
956.2				
847.6	850.6	863.6		12
	849.1			
850	851.1		856.5	25
809.9	810.9		809.1	7
779.5	778.9		781.6	6
712.7	713.4		709.5	18
			699.5	3
	676.5	685.1		2
	653.9	650.7		14

TRIFLUOROACETYLACETONE

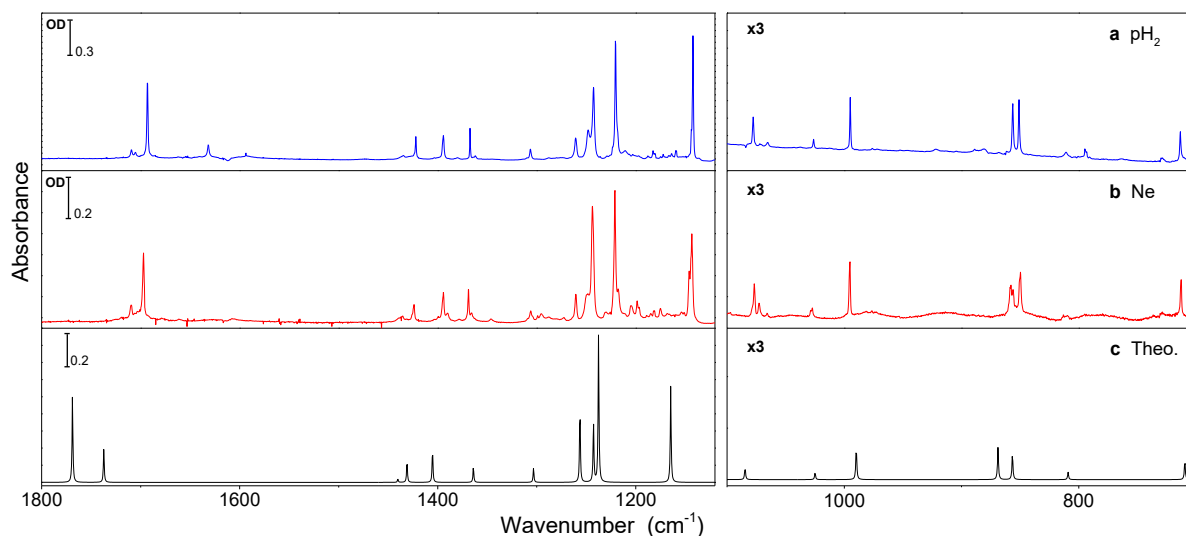


Figure VIII.10: Experimental spectra of the TCT(CO) conformer of trifluoroacetylaceton in (a) *para*-hydrogen and (b) neon matrices. (c) theoretical harmonic spectrum, a scaling factor of 0.973 is used.

These are the first results we have obtained in the trifluoroacetylaceton analog. The analysis of other results is still in progress, especially the presence of multiple bands in the CF_3 region and the presence of additional bands that could be related to the CCC(OH) conformer. An interesting result is that multiple stable conformers are produced, and in some of them (CTT(OH) and TCT(OH)) a proton transfer occurs in the excited state to change the hydrogen between the two asymmetrical oxygen of the molecule. The mechanism of production of these conformers was already detailed by Minoura *et al.* from their results in argon matrix [20], which are the same to the one obtained by us in neon and *para*-hydrogen. The main ideas behind this mechanism are discussed in section XI.3.

Chapter IX 2-Chloromalonaldehyde

In this section the dynamics and photodynamics of 2-chloromalonaldehyde in neon and *para*-hydrogen matrices are analyzed. The objective is to compare the behavior of this molecule with malonaldehyde, the smallest β -dicarbonyl. The reduced dimensionality of this system compared to acetylacetone makes easier the interpretations of the results. First, the results from theoretical calculations are discussed. Then, the deposited and irradiated samples are analyzed.

IX.1. Theoretical results

The energy order for the conformers of 2-chloromalonaldehyde after geometry optimization at M06-2X level of theory is shown in Figure IX.1. The values in the figure are corrected with the Zero-Point Energy of each conformer. The geometry shown for the CCC conformer correspond to the C_s symmetry. Because it is the first time this molecule is studied we also performed geometry optimization for the C_{2v} symmetry. The results show this geometry corresponds to a first order transition state and not to a minimum in the potential energy surface. Besides, this result is similar to those obtained for all the other β -dicarbonyl systems,

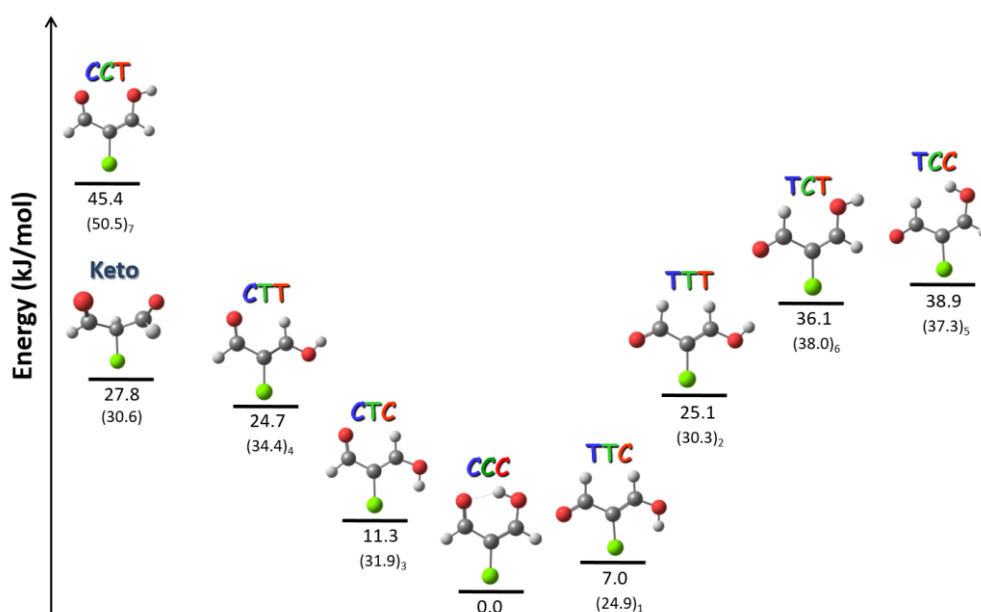


Figure IX.1: Zero-Point Energy corrected theoretical energies (kJ.mol⁻¹) for 2-chloromalonaldehyde conformers calculated at M06-2X level of theory. The values in parenthesis belong to the same conformers in malonaldehyde. The index illustrates the relative order in malonaldehyde.

2-CHLOROMALONALDEHYDE

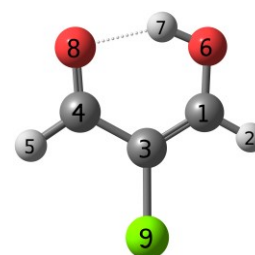
including malonaldehyde, the parent molecule [217]. We performed our own calculation of malonaldehyde using the same theoretical level as in chloromalonaldehyde, in order to be able to compare the energies.

The difference between the energy corresponding to the C_{2v} and C_s symmetries ($\Delta E^H = C_{2v} - C_s$) gives an idea of the hydrogen transfer barrier high. If all modes are taken into account for ZPE contribution, the value of ΔE^H obtained for 2-chloromalonaldehyde (15.9 kJ.mol⁻¹) is a little bit higher than the one for malonaldehyde (13.2 kJ.mol⁻¹)⁵⁹. If the lower frequency mode is not taken into account in both symmetries (removing the contribution of the imaginary frequency) the values are closer: 12.8 and 12.2 kJ.mol⁻¹ for 2-chloromalonaldehyde and malonaldehyde respectively. These results suggest that the barrier for proton transfer is not greatly affected when the chloro atom is included.

The energy diagram can be compared with the one for malonaldehyde. The ZPE corrected energies for malonaldehyde at the same level of theory are shown in parenthesis (see Figure IX.1), with an index indicating their order. There are two main consequences related with the changes of the α hydrogen by a chloro atom. First, the energy order changes. An example is that the TCT-TCC conformers exchange their relative position compared to malonaldehyde. Second, there is a general decreasing on the energy of the conformers relative to the most stable CCC conformer. This change is more important for CTC (12.7 kJ.mol⁻¹) and TTC (6.5 kJ.mol⁻¹) conformers, which are very close in energy to CCC. Like in chloroacetylacetone, the stabilization of the CTC and TTC conformers is due to a non-covalent interaction between the chloro atom

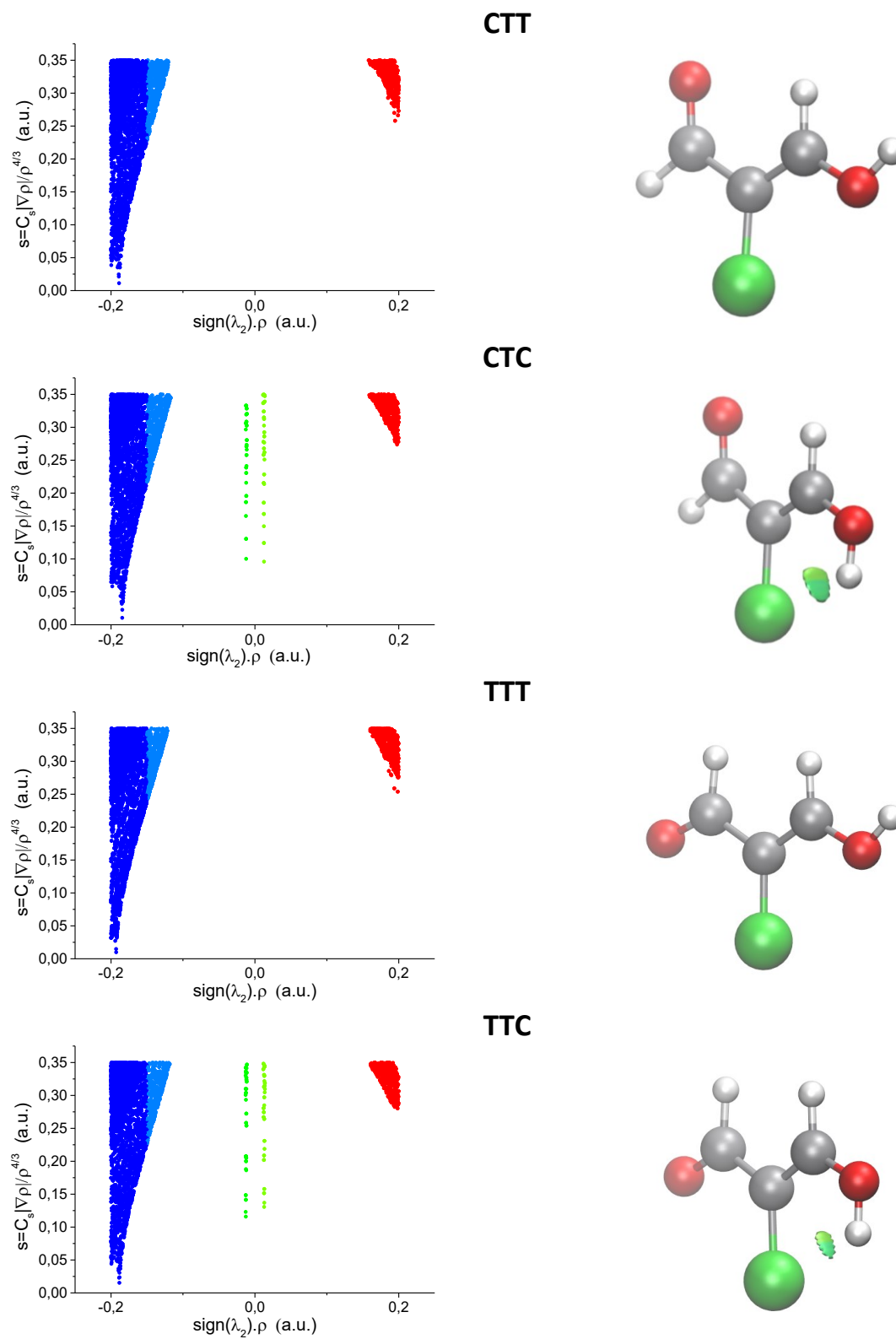
Table IX.1: Optimized geometric parameters at M06-2X/6-311++G(3df,3pd) of the CCC conformer (in the C_s symmetry) of 2-chloromalonaldehyde. R: distance (in Ångström), A: angle (in degrees) and D: dihedral angle (in degrees)

R (Å)		A (°)		D (°)	
C-H (1-2)	1.083	2-1-3	121.6	2-1-3-9	0.0
C=C (1-3)	1.352	2-1-6	114.4	5-4-3-9	0.0
C-O (1-6)	1.314	3-1-6	124.0	9-3-4-8	180
C-C (3-4)	1.448	1-3-4	120.7	9-3-1-6	180
C-Cl (3-9)	1.727	1-3-9	120.8	3-1-6-7	0.0
C-H (4-5)	1.099	1-6-7	107.7	4-8-7-6	0.0
C=O (4-8)	1.220	4-3-9	118.5		
O-H (6-7)	0.985	3-4-5	116.7		
H...O (7-8)	1.732	3-4-8	122.5		
		5-4-8	120.8		
		4-8-7	101.0		
		6-7-8	144.0		



⁵⁹ The value obtained for malonaldehyde is near the lower limit of the range of values (13-19 kJ.mol⁻¹) previously obtained through theoretical calculations by other groups [50]. Experimental value indirectly estimated from the tunneling splitting (21.6 cm⁻¹) is 27,6 kJ.mol⁻¹.

Figure IX.2: NCI calculation for the CTT-CTC and TTT-TTC pairs. Left: Graph of reduced density gradient (s) versus density multiplied by the sign of λ_2 (see section III.4.). Right: Isosurface of s at 0.35; light blue corresponds to non-covalent interactions and green color corresponds to steric repulsion.



2-CHLOROMALONALDEHYDE

and the hydrogen from the hydroxyl group. This was confirmed through the analysis of the reduce density gradient (s) in the NCI calculation. The results are shown in Figure IX.2.

In the graph at the left panel, the presence of a non-covalent interaction is identified in CTC and TTC by the green dots at low density values near zero (already explained in AcAcCl). In the right panel, it can be observed that the non-covalent interaction is located in the Cl \cdots H-O moiety. The distance between the chloro atom and the hydrogen is 2.480 Å in TTC and 2.488 Å in CTC far from 1.732 Å of the O \cdots H distance in IHB bond of the CCC conformer.

From the structural point of view, the insertion of the bulky chloro in the α position does not modify the structure of the carbonated skeleton, which maintain its planarity (see CCC structure, Table IX.1).

IX.2. Vibrational spectroscopy of as-deposited samples

IX.2.1. FT-IR spectrum in Ne and pH_2 matrices

Deposition conditions for 2-chloromalonaldehyde are explained in section IV.2.1. . The obtained spectra in *para*-hydrogen (a) and neon (b) matrices are shown in Figure IX.3 for the 700-1800 cm^{-1} region. The calculated frequency spectrum for the CCC conformer is also shown in panel (c).

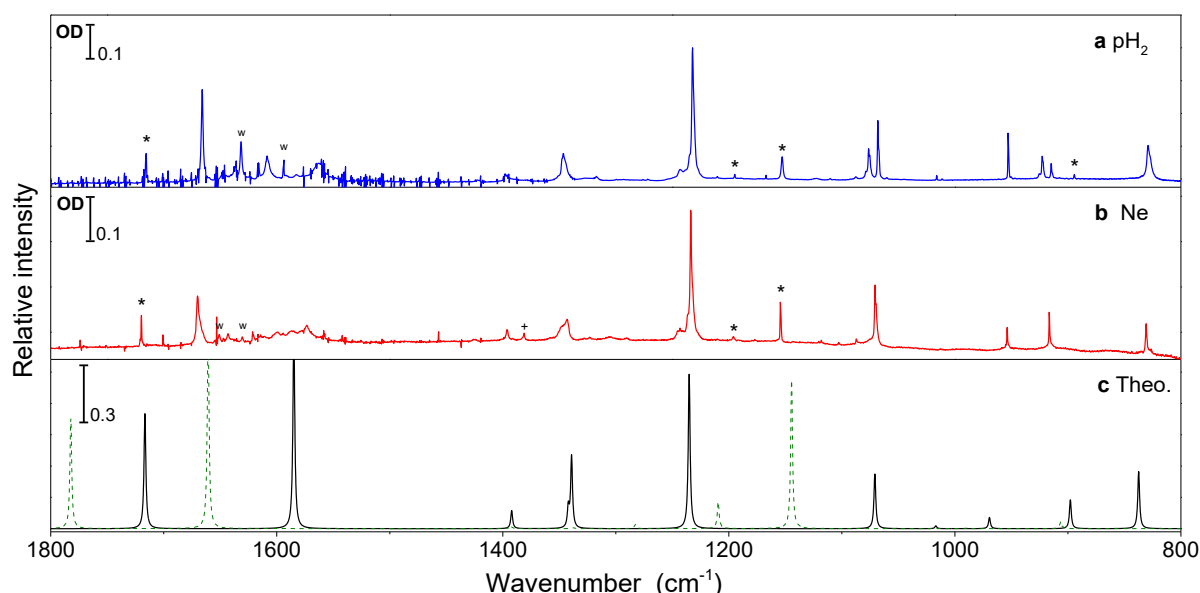


Figure IX.3: FT-IR of deposited 2-chloromalonaldehyde in (a) *para*-hydrogen and (b) neon matrices. (c) theoretical frequency calculation (M06-2X/6-311++G(3df,3pd)) of CCC (black line) and TTC (green dashed) conformers in harmonic approximation with 0.968 scaling factor. * denotes bands belonging to another conformer (TTC). w denotes water bands. + unidentified band

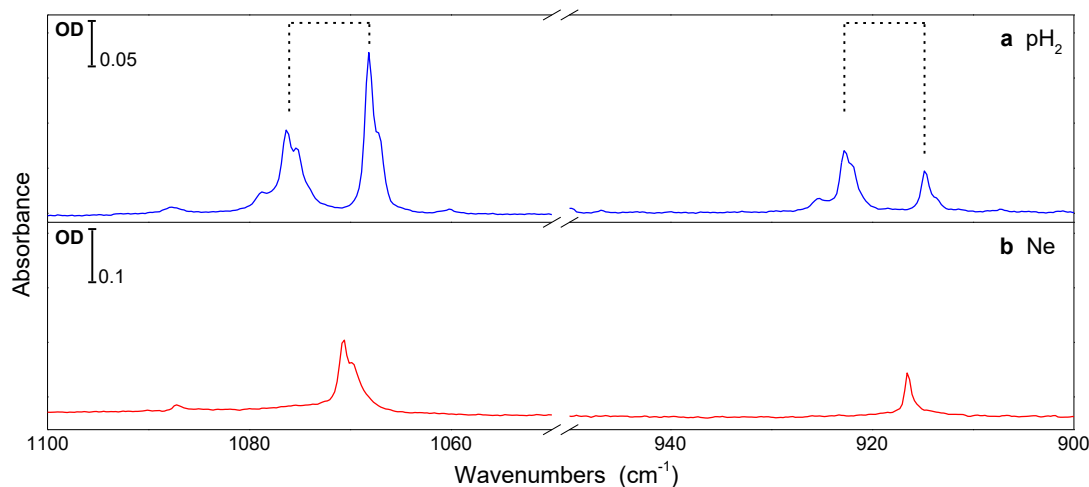


Figure IX.4: Zoom of the 1100-900 cm^{-1} spectral region showing the splitting (8 cm^{-1}) in *para*-hydrogen matrix of two modes at 1070.6 and 916.5 cm^{-1} in neon matrix. A break is present between the 1050-950 cm^{-1} region for a better comparison. An additional small doublet is present in this region

Some interesting results are obtained from these spectra. First, the match of the theoretical spectrum with the experimental spectra is quite good. This indicates that the CCC conformer predominates in the matrix, as expected from the energy calculations. We also made frequency calculations in the harmonic approximation with B3LYP functional and MP2, but the match was less good. Anharmonic frequency calculation was also computed, and no improvement is obtained comparing to the harmonic scaled one. The nice agreement between harmonic theoretical frequencies and experimental spectra permits to make the assignment of the CCC conformer with high confidence. The results are shown in Table IX.2.

Second, it can be observed from the comparison of experimental and theoretical spectra that CCC is not the only conformer present in the deposited sample. There are several small (and medium intensity) bands, some of them marked with an asterisk (*), that belong to a different species. The analysis of the UV irradiation experiments and the theoretical spectra, discussed in the next section, allow us to confirm that they correspond to a low energy open enol conformer (TTC). Among all the molecules studied in this thesis this is the only one for which an enol conformer different from CCC is observed in the deposited sample.

Third, in the 1100-900 cm^{-1} region we can observe that in *para*-hydrogen matrix there are two doublets that are not present in neon (Figure IX.4). Moreover, the splitting of these two doublets is the same ($\sim 8 \text{ cm}^{-1}$) and it was observed with different samples. If we take a closer look to each doublet we can find a small structure, explained later. The assignment made for the molecule in Table IX.2 shows that the two modes (at 1070.6 and 916.5 cm^{-1} in neon matrix) correspond to a collective motion of the atoms in the internal ring (see also Figure IX.5). There is another small doublet in *para*-hydrogen around 1013 cm^{-1} with a shift between bands of 4.8 cm^{-1} . The corresponding mode is an out of phase bending of the aldehydic hydrogens. In any of these modes the oxygen atoms get closer to each other more than 0.04 Å.

2-CHLOROMALONALDEHYDE



Figure IX.5: Normal modes corresponding to the 1070.6 (left) and 916.5 cm⁻¹ (right) bands in neon matrix, and doublets in *para*-hydrogen.

In previous studies made in supersonic jets for malonaldehyde, Suhm *et al.* [218]–[220] found the presence of tunneling splitting for some modes (OH and CH's in plane bending). However, no splitting was found in xenon, argon, neon and nitrogen matrices [51], [205], [221]. These studies suggest that there is a reduction of the total symmetry in the molecule/matrix system, and a breakup of the symmetric double well potential when the molecule is in asymmetric sites. Unfortunately, no studies have been published on this molecule in the “soft” *para*-hydrogen matrix, that should have a lower impact in this symmetry breakup effect.

It is unlikely that the observed splitting in *para*-hydrogen is due to site effects, because they are almost not present in this matrix. In addition, anharmonic frequency calculations were performed and no Fermi resonance transition involving these two modes occur, excluding this possibility. On the other hand, the line shape and values of the splitting and the intensity ratio were always the same in different samples, with different amounts of water impurities, and sample concentration (which was always low). No temporal evolution during 2 h, which could indicate *ortho-para* conversion of hydrogen molecules, was observed in the sample. No change in these bands was also observed during and after annealing of the samples at 4.2 K. A possible explanation will be the presence of a tunneling splitting. Nevertheless, other experiments need to be conducted to support this hypothesis. First, the study in the gas phase, in supersonic jet and other matrices like argon (higher temperature range available) of the halogenated molecule. Second, the study of the deuterated analogs of 2-chloromalonaldehyde. Third, the study of malonaldehyde in *para*-hydrogen matrix (preservation of symmetry). About the last suggestion, we already have done preliminary studies of malonaldehyde in *para*-hydrogen, but not conclusive results have been obtained until now.

IX.2.2. Raman spectrum in argon matrix

Like in the other systems, Raman spectrum was recorded as a complementary experiment to FT-IR. The spectrum was much harder to obtain for this molecule because of its low vapor pressure, even at 80°C. The obtained spectrum is shown in Figure IX.6 along with the theoretical Raman spectra of the CCC and TTC conformers for comparison.

Vibrational spectroscopy of as-deposited samples

Table IX.2: Experimental frequencies (cm^{-1}) obtained from the infrared spectra of the chelated enol form of chloromalonaldehyde in neon and *para*-hydrogen matrices, and Raman spectrum in argon matrix. Theoretical harmonic frequencies (cm^{-1}), IR intensities (km/mol) and Raman scattering activities ($\text{\AA}/\text{a.m.u}$) calculated at M06-2X/6-311++G(3df,3pd) level of theory are also given for comparison. A scaling factor of 0.968 is used to correct the harmonic theoretical frequencies.

Assignment	Experimental			Theoretical Harmonic*sf	Theo. Int.	
	IR		Raman		IR	Ram.
	Ne	pH ₂	Ar			
νOH				3280.8	208	24
$\nu\text{CH(OH)}$				3112.0	8	82
$\nu\text{CH(CO)}$	2875.1	2876.7		2945.5	40	96
$\nu\text{CO}+\nu\text{C=C (as)}$	1670.2	1665.8	D	1716,6	175	13
	1600	1608.8				
$\nu\text{CO}+\nu\text{C=C (s)} + \delta\text{OH}$	1586.7	1582.3	D	1584.9	303	62
	1573.5	1563				
$\delta\text{CH(CO)}+\delta\text{CH(OH) (s)}$	1396.2	1387.0	1391	1392.1	28	1
$\delta\text{CH(CO)}+\delta\text{CH(OH) (as)}$	1347.7	1346.4	1344	1342.1	31	9
$\delta\text{OH} + \delta\text{CH(OH) (as)}$	1343			1339.2	110	24
$\delta\text{OH} + \delta\text{CH(OH) (s)}$	1233.6	1232.3		1235.1	236	0.1
		1076.4				
$\nu\text{C-C}$	1070.6	1068.1	1068	1070.8	83	6
		1016.1				
$\gamma\text{CH(CO)}+\gamma\text{CH(OH) (as)}$		1011.3		1016.9	4	0.4
$\gamma\text{CH(CO)}+\gamma\text{CH(OH) (s)} + \gamma\text{OH}$	953.7	952.8		969.4	17	1
		922.5				
Δ	916.5	914.7	914	897.8	44	12
γOH	830.8	829.3		837.4	87	1
Δ			505	500.6	16	4
			474			
$\nu\text{C-Cl}$			468	470.7	6	7
γCH				368.8	2	1
γCH				281.9	2	1
			278	277.9	4	3
$\delta\text{C-Cl}$						
$\delta\text{C-C=C}$			232	232.9	7	0.4
γCH			225	212.3	6	1

^a main characteristic motions; ν , stretching; δ , in plane bending; γ , out of plane bending; ρ , in plane rocking; π , out of plane rocking; Δ , in plane ring deformation; s , symmetric; a , asymmetric

^b sf: scaling factor (0.968)

D: several bands are observed in this region and the assignment is not clear

2-CHLOROMALONALDEHYDE

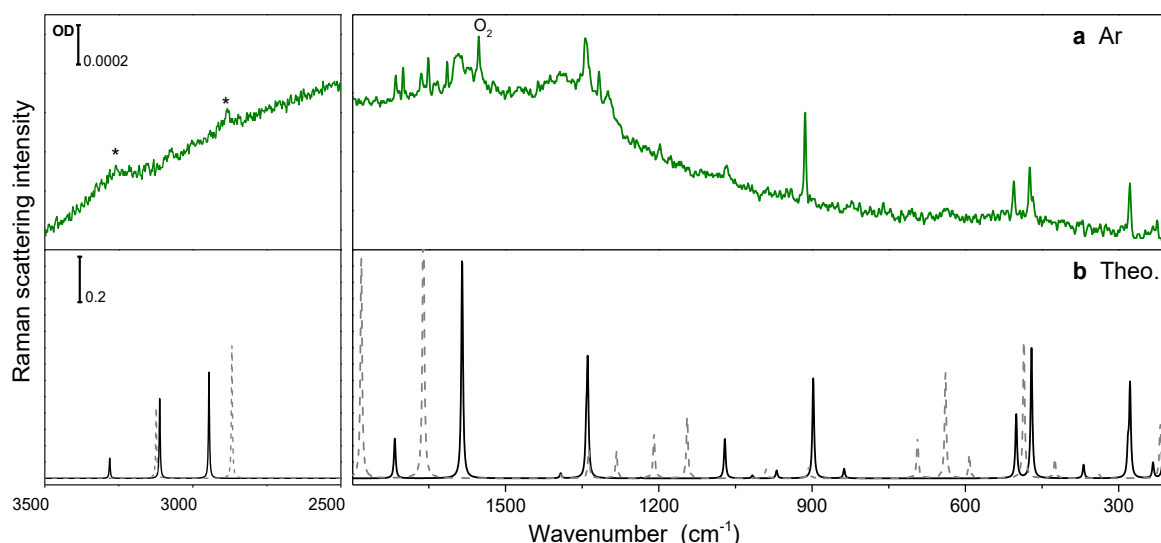


Figure IX.6: Raman spectra of 2-chloromalonaldehyde. (a) experimental spectrum in argon matrix at 11 K (b) theoretical harmonic frequency calculations of CCC conformer (black lines) and TTC conformer (grey dashed lines). * background. Raman intensity is given in arbitrary units.

The Raman spectrum leaves no doubts about the presence of the CCC conformer. The match is good for most of the theoretical normal modes. However, there are some extra bands that cannot be assigned to CCC monomers. The theoretical spectrum of TTC is also shown in Figure IX.6 (grey dots). The presence of the TTC conformers is less evident in this spectrum than in FT-IR, even when there are some bands which seems to correspond with the theoretical spectrum (1197.5 and 637 cm⁻¹). The amount of TTC conformers is small in the samples and because the low sensitivity of Raman they should be more difficult to observe. Another possibility is the presence of dimers in the sample due to the higher concentration compared to samples in FT-IR experiments.

Before concluding this part, it is worthwhile to analyze the small structure observed in the doublets. A closer look to Raman spectra reveals that there is another band with a structure. This band appears in the Raman spectrum at low frequencies, around 471 cm⁻¹ and has a 6 cm⁻¹ difference between in each component. Taking into account that the chloro atom has two stable isotopes, Cl³⁵ and Cl³⁷, with 75.78% and 24.22% natural abundance, theoretical calculations were performed for both. The frequency difference for each mode is shown in Figure IX.7 The difference is higher in modes in which chloro atom has a bigger participation. The three experimental bands in which the structure is observed belong to modes number 10, 13 and 16 with a non-zero difference in frequency (bands marked with * and + in Figure IX.7). The experimental difference is well reproduced for mode 10 and 16 (1074.1 and 472.1 cm⁻¹ respectively), but the theoretical value for mode 13 (at 900.6) is two times smaller than the experimentally observed (theo. 0.3 cm⁻¹ and exp. ~0.6 cm⁻¹). The ratio between each component in mode 10 and 13 are closer to 0.33, the theoretical expected value.

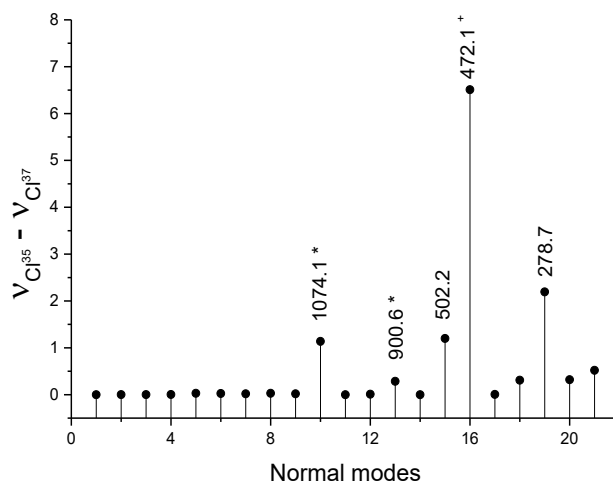


Figure IX.7: Frequency difference for Cl^{35} and Cl^{37} isotopologues of 2-chloromalonaldehyde. Modes marked with * correspond to the doublets observed in Figure IX.4, a small internal doublet structure is observed in each of them. The mode marked with ⁺ correspond to the maximum shift, which is observed in the experimental Raman spectrum. The frequency values shown correspond to theoretical harmonic calculation for the Cl^{35} isotopologue.

IX.3. UV laser irradiation: Isomerization

IX.3.1. UV absorption spectra in solid neon

Similarly to the previous systems, the electronic absorption spectrum of the molecule was first obtained before performing the UV laser irradiation. The obtained spectrum is shown in Figure IX.8.

In contrast to β -diketones two main bands are observed in the UV spectrum of the deposited sample. There is a clear absorption band near the 285 nm, associated to the $\pi \rightarrow \pi^*$ transition in the CCC conformer. The same transition for malonaldehyde is placed at 269 nm, which implies a bathochromic shift after the

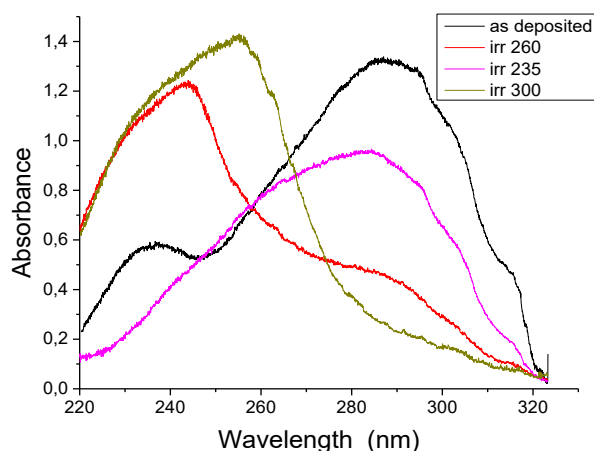


Figure IX.8: Electronic absorption spectrum of chloromalonaldehyde in neon matrix. The different colored spectra correspond to successive irradiations in the next order: (black) deposited sample, (blue) after irradiation at 260 nm, (rose) after irradiation at 235 nm, (dark yellow) after 300 nm irradiation.

2-CHLOROMALONALDEHYDE

inclusion of the chloro atom in alpha position, as observed for chloroacetylacetone and acetylacetone. Irradiation of the deposited sample at 300 nm and 260 nm show a depletion of the CCC band and the increase of two different bands placed at 235 nm and 254 nm. The position of these bands corresponds well to the region of the $\pi \rightarrow \pi^*$ transition band of the non-chelated forms previously observed in argon, xenon and nitrogen by Trivella *et al.* in malonaldehyde [222]. The band initially observed at lower wavelength in the deposited sample agrees with the blueshifted one produced after irradiation. In fact, this band is produced even with the UV lamp broadband source, during the acquisition of the CCC conformer (deposited sample) spectrum. From the spectra we can notice that after the 260 + 235 nm irradiation sequence we produce only the CCC conformer. The UV spectra suggest that it is possible to separate three different group (one of them CCC) with the correct irradiation sequence.

IX.3.2. Isomerization

The UV laser irradiation to produce the open enol conformers was started at 290 nm for more than 40 minutes. Next, the wavelength was subsequently changed to lower energies until 230 nm. During the irradiation at 290 nm CCC bands intensity decrease while a new group of bands growth, including those marked with * in Figure IX.3. Taking into account the different kinetics of the growing bands and a different response to low wavelength irradiation we were able to isolated two groups. Comparison with theoretical frequency calculations allowed to assign these two groups to TTC and CTC conformers. Both conformers are the two lowest energy open enol conformers (see Figure IX.1).

IX.3.2.1. TTC conformer

In Figure IX.9 the experimental spectra of TTC in *para*-hydrogen and neon matrices is shown. The frequency calculation in the harmonic approximation is also shown for comparison. The match between the theoretical and experimental spectra is good. The theoretical spectra of the other conformers do not resemble the experimental spectra, leaving no doubts about the assignment.

In both, neon and *para*-hydrogen there is an additional band (around 1118 cm^{-1} in neon), which does not correspond with any fundamental transition. Anharmonic frequency calculations were also performed searching for the possible presence of harmonic and combinations bands in this region. Three combination bands at less than 35 cm^{-1} can be present ($1142 [218+906]$, $1150 [133+990]$, $1098 [133+906] \text{ cm}^{-1}$). The assignment is shown in Table IX.3.

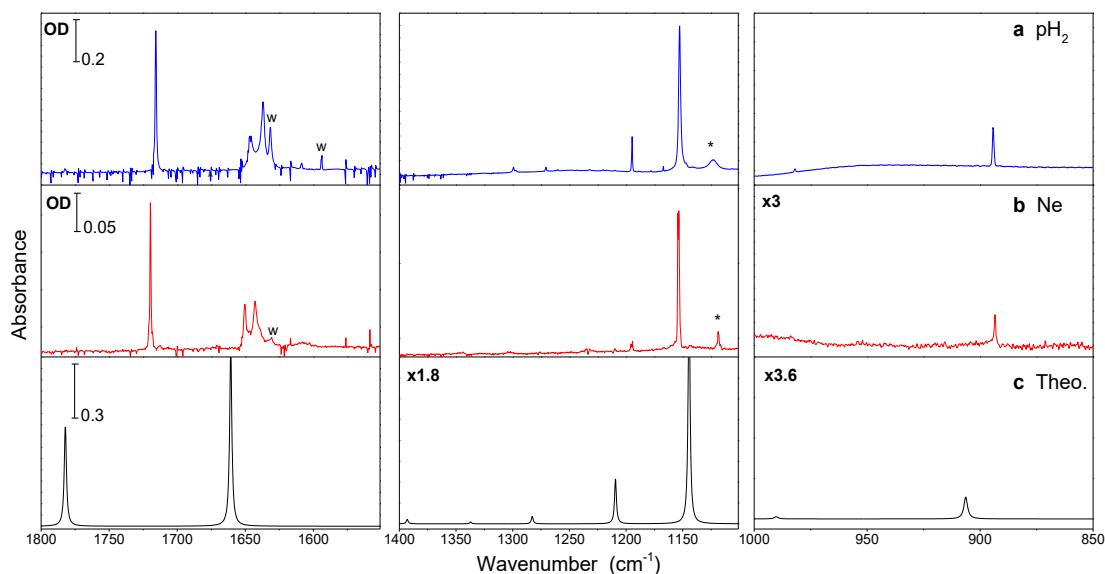


Figure IX.9: Experimental TTC spectra in (a) *para*-hydrogen and (b) neon matrices. The spectra are the result of subtractions of different spectra along irradiation in order to remove CCC and CTC bands. Panel (c) shows theoretical frequency calculation (M06-2X) of TTC conformer in harmonic approximation with 0.968 scaling factor. * unassigned bands. ^w water band

IX.3.2.2. CTC and TCT conformers

Figure IX.10 shows the experimental spectra of CTC in *para*-hydrogen and neon matrices along with the theoretical frequency calculation for this conformer. As expected, the difference in bands position between both matrices is small. In neon matrix, site effects can be clearly observed (bands at 1093.2 and 1217.9 cm^{-1}). The match with theoretical calculation is quite good. The assignment can be observed in Table IX.3. In addition, there are few other bands (marked with asterisk in *para*-hydrogen spectrum) which can be unambiguously assigned to the TCT conformer (values in $p\text{H}_2$: 3656.6; 1702.9; 1652.5; 1262.8; 887.5 cm^{-1}). The theoretical spectrum of this conformer is also included in Figure IX.10 for comparison.

There are two interesting results from the UV irradiation in neon matrix at 8 K. First, the UV induced conversion process from CCC conformer to CTC (and TTC) and TTC conformers can be totally reversed by changing the irradiation wavelength to lower values (≤ 240 nm). The corresponding UV spectrum is shown in Figure IX.8 with a pink color, and corresponds obviously to the CCC conformer alone. This result is an indication that CCC and the formed open enol conformers have well separated electronic absorption bands. Second, this process can be selective, it means that the open enol conformers can be converted back to CCC. Whether one conformer or the other is converted back depends of the irradiation wavelength. This effect is mainly observed in TTC and CTC conformers; the behavior of TCT is not yet clear. In practice, the 290 nm UV irradiation converts CCC in CTC and TTC. If UV laser is set now at 250 nm CTC conformer transform back to CCC while the amount of TTC almost does not change. But, if we irradiate at 240 nm the behavior of the

2-CHLOROMALONALDEHYDE

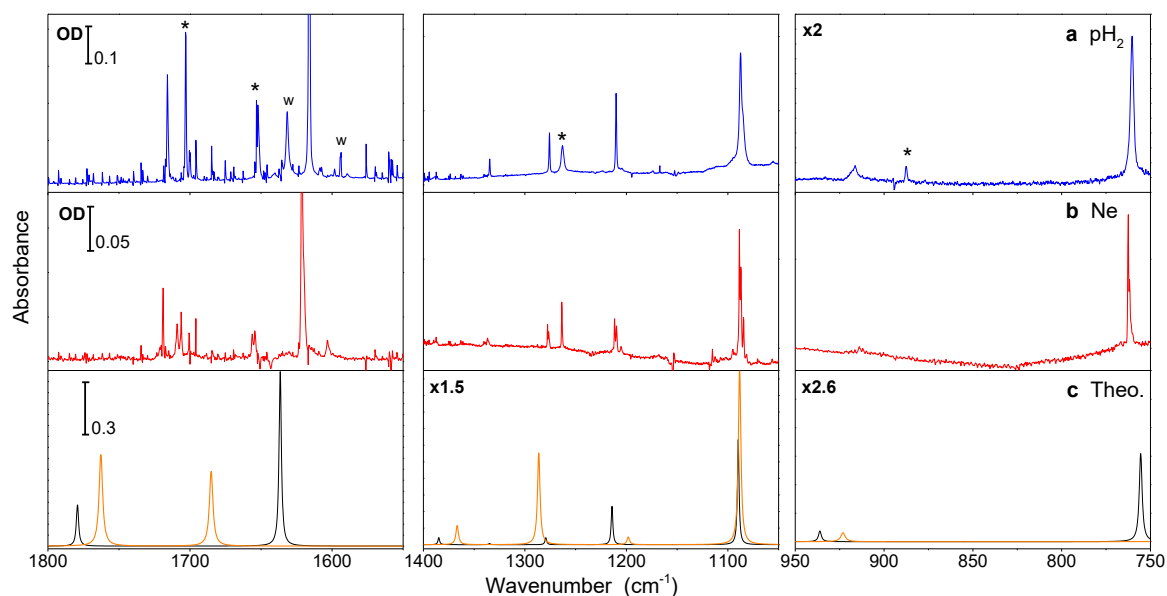


Figure IX.10: Experimental CTC spectra in (a) *para*-hydrogen and (b) neon matrices. The spectra are the result of subtractions of different spectra along irradiation in order to remove CCC and TTC bands. Panel (c) shows theoretical frequency calculation (M06-2X) of CTC conformer (black) and TCT conformer (orange) in harmonic approximation with 0.968 scaling factor. ^w water bands

open enols conformers is exchanged. A graphical scheme of all process is represented in Figure IX.11 We remark that the process is entirely reversible in neon at 8K and no fragmentation was observed. However, the experiment was also done at 3K in neon matrix (with different irradiation sequence), and even when the same conformers were produced, fragmentation was observed when lower UV wavelengths were used (≤ 240 nm). The experiments done in *para*-hydrogen show a similar behavior to those in neon at 3K.

Another important result is that the assignment done permits to identify TTC as the conformer found in the deposition along with CCC. In fact, a closer inspection of the spectra shows that there is also a smaller

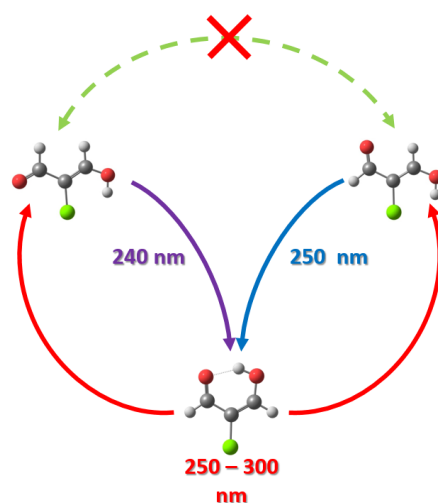


Figure IX.11: Irradiation scheme of 2-chloromalonaldehyde in neon matrix at 8K. Irradiation at 250-300 nm over CCC conformer produce CTC and TTC conformers. Open enol conformers can be selectively converted back to CCC by adjusting the wavelength. During this process no conversion between open enol conformers occurs.

amount of CTC in the deposited sample. Even if both conformers are closer to CCC, the energy that separate them is higher than thermal energy at 298 K (2.5 kJ/mol). In both cases the molecule needs to rotate around the double bond to form the open enol conformers from CCC. This eliminates the possibility of photoisomerization induced by the global IR source. Another possibility is they are already in equilibrium in the solid phase. Unfortunately, there are no information published about this molecule in the solid phase.

IX.3.3. Comparison with malonaldehyde

The results already presented for 2-chloromalonaldehyde can be compared to those obtained for malonaldehyde by Trivella *et al.* [50], [222]. First, it should be taken into account that their studies were carried out in argon, xenon, nitrogen and neon matrices. But, the results in the last matrix are not as clear as for the other matrices, because bands are broad. This is the first difference with 2-chloromalonaldehyde, the bandwidth, which is quite narrow for most of the bands in neon matrix.

Photoisomerization studies for malonaldehyde show that almost all the open enol conformers can be produced by UV irradiation, being the exception the high energy CCT conformer. As we have shown, in the case of 2-chloromalonaldehyde, only the lowest energy open enol conformers of each group (CTC, TTC and TCT) are obtained. The same result is also observed in the analogs of the β -diketone family studied in this work. It is intuitive to believe that in the studies performed with malonaldehyde there could be a matrix effect in play stabilizing the higher energy conformers and increasing the O-H barrier high, and this effect should be higher for heavier hosts like xenon, argon and nitrogen. But, all these conformers were also observed in neon and no spontaneous interconversion process was observed between any XYC-XYT pairs. In this case, it will be advisable to do photoisomerization studies of chloromalonaldehyde at least in argon matrix.

2-CHLOROMALONALDEHYDE

Table IX.3: Experimental frequencies (cm^{-1}) of the CTC and TTC conformers of chloromalonaldehyde in neon and *para*-hydrogen matrices. Theoretical harmonic frequencies (cm^{-1}) and IR intensities (km/mol) calculated at M06-2X/6-311++G(3df,3pd) level of theory are also given for comparison. sf: scaling factor (0.968)

Assignment	Experimental		Theoretical Harmonic*sf		Theoretical Int.
	Ne	pH ₂	CTC	TTC	
vOH	3534.7	3524.1	3674.8		83
vOH	3512.9	3525.1		3663.3	84
vCH(OH)	3079.2	3085.4	3136.4		5
vCH(OH)		3085.4		3124.0	2
vCH(CO)	2858.5	2862.4	2897.9		54
	2839.9	2844.4			
vCH(CO)	2840.2	2862.4		2868.0	57
		2844.4			
vCO+vC=C (as)	1719.7	1715.6		1782.2	248
vCO+vC=C (as)	1719	1715.9	1779.2		135
		1702.9			
vCO+vC=C (s) + δ OH	1650.5	1646.2		1660.7	448
	1642.7	1637			
vCO+vC=C (s) + δ OH	1621.3	1616.1	1636.5		569
δ CH(CO)				1393.1	6
δ CH(CO)			1384.8		15
δ OH				1337.2	3
δ OH + δ CH(OH)	1336.5	1334.2	1334.9		3
δ CH(OH) + δ OH				1282.8	10
δ CH(OH)	1277.9	1275.7	1279.4		15
	1276.6				
δ OH + δ CH(OH)	1211.5	1210.2	1214.1		83
	1209.7				
vC-C + vC-O (as)	1195.7	1194.3		1209.4	61
	1194.1				
vC-C + vC-O (s)	1154.3	1152.8		1144.4	335
	1153.5				
vC-C + δ OH	1088.6	1087.7	1089.8		227
	1087.1				
γ CH(CO)			1003.4		1
γ CH(OH)	913.9	916.3	936.1		13
γ CH(CO)+ γ CH(OH) (as)		981.9		990.3	2
γ CH(CO)+ γ CH(OH) (s)	893.5	894.2		906.4	15
Δ	762.5	760.4	755.5		111
	761.7				

^a main characteristic motions; v, stretching; δ , in plane bending; γ , out of plane bending; ρ , in plane rocking; π , out of plane rocking; Δ , in plane ring deformation; s, symmetric; a, asymmetric

Chapter X Propyne-H₂O complex

Up to this point, we have studied systems with intramolecular hydrogen bonds, which are isolated in weak interacting environments such as cryogenic matrices. In order to extend the scope of our study we decided then to change the type of hydrogen bond under study. In this way, we chose the complex propyne-H₂O to explore the nature of the inter-molecular hydrogen bond that could be formed. We carried out this research in helium nanodroplets, which is a very weak interactive environment, ideal for the study of complexes. We should point out that the axis of frequencies (wavenumbers) is inverted in this chapter, in order to be able to compare with data from the literature.

X.1. Propyne monomer

The first step to address the propyne-H₂O complex starts with the study of the propyne molecule, its monomer and multimers. Propyne is a prolate symmetric top molecule ($I_a < I_b = I_c$). In the frame of the non-rigid rotator the rotational energy is given by:

$$F_v(J, K) = B_v J(J + 1) - D_J [J(J + 1)]^2 + (A_v - B_v)K^2 - D_K K^4 - D_{JK} J(J + 1)K^2 \quad (\text{X.1})$$

Where A_v and B_v are the rotational constants according to a and b axis; D_J , D_K and D_{JK} are the centrifugal distortion constants. J and K are the quantum numbers which have the values $K = 0, 1, 2, 3, \dots, J$ and fulfill $J \geq K$. In a $J + 1 \rightarrow J$ transition without change in K we will have:

$$\sigma(J + 1, K \rightarrow J, K) = 2B_v(J + 1) - 4D_J(J + 1)^3 - 2D_{JK}(J + 1)K^2 \quad (\text{X.2})$$

In the case of ro-vibrational transitions the term of the vibrational transition must be added. Moreover, it should be taken into account that the rotational and centrifugal distortion constants are not usually the same in each vibrational level. In this case the simplified expression in Equation (X.2) is no longer valid and a more complex expression needs to be used.

The monomer of propyne has been already studied in helium nanodroplets by Nauta and Miller [25] and Callegari *et al.* [199]. The work done by the latter was mainly focused on the first harmonic of the C-H acetylenic stretching (mode ν_1). On the other hand, Nauta and Miller extensively studied the fundamental transition of the same mode (ν_1). In our setup we only have access to the spectral region of this mode (in the free molecule, and in the complexes), which we will use for the study of our system. In Figure X.1 the

PROPYNE-H₂O complex

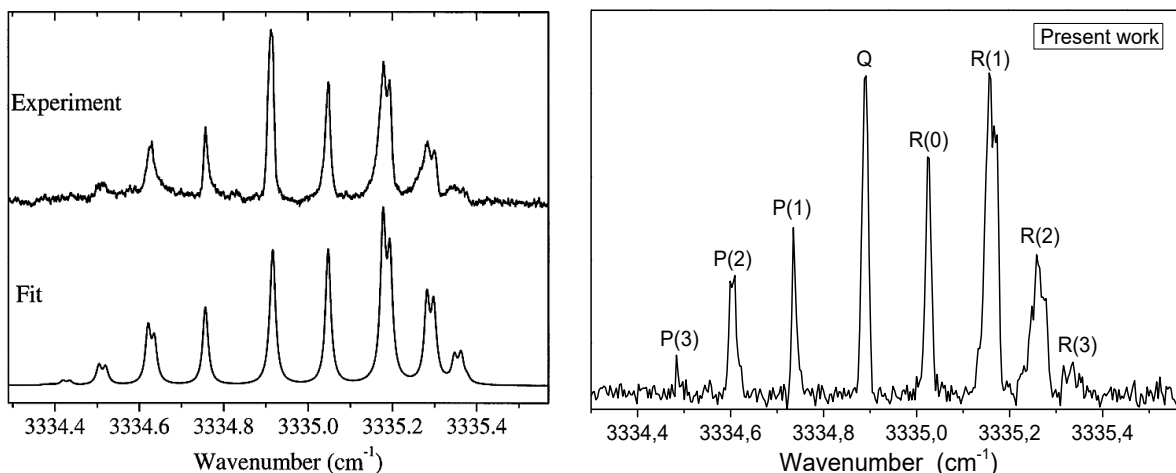


Figure X.1: CH acetylenic stretching region (ν_1) of propyne spectra in helium nanodroplets. Left: experimental (up) and theoretical simulation (bottom) spectra obtained by Nauta and Miller [25] (© Springer-Verlag Berlin Heidelberg 2001) Right: experimental spectrum obtained in this work with 0.003 cm^{-1} resolution.

results obtained by Nauta and Miller (left panel) are compared with the one obtained in the present work (right panel).

By comparing the spectra in Figure X.1 we can conclude first that we have succeeded in reproducing Nauta and Miller's results. This is an indication that our setup works well and we have a good starting point to continue with the study of the complex. The position of the bands are summarized in Table X.1.

At the working temperature (0.4 K) and by taking into account that $B_v'' \approx 0.074 \text{ cm}^{-1}$ (in helium droplets) the first four rotational levels of the ground state are mainly populated ($J = 0, 1, 2, 3$). In addition, only low K levels are populated. In the spectrum we can observe that the amount of P and R bands is in agreement with the four J populated levels. Lines belonging to $K = 0$ and $K = 1$ are clearly observed in the $R(1)$ and $R(2)$ bands. It does not mean that other bands do not present transitions from different K levels. But, as suggested by Nauta and Miller the asymmetric bandshape of some of the components could be also an indicative of line broadening associated with the liquid helium environment.

In addition to the experiments in helium droplets, we obtained the infrared spectrum of the molecule in *para*-hydrogen matrix for the first time. The spectrum in the CH acetylenic stretching region ν_1 is shown along with the spectrum in helium droplets in Figure X.2.

Table X.1: Comparison of the frequency of the Q band for the ν_1 fundamental in gas phase [235], helium droplets [25] and *para*-hydrogen matrix.

Constant	Gas phase	He Drop.	Present Work	
		Nauta & Miller	He Drop.	pH ₂
$\nu_0 \text{ (cm}^{-1}\text{)}$	3335.0594	3334.90	3334.89	3328.29

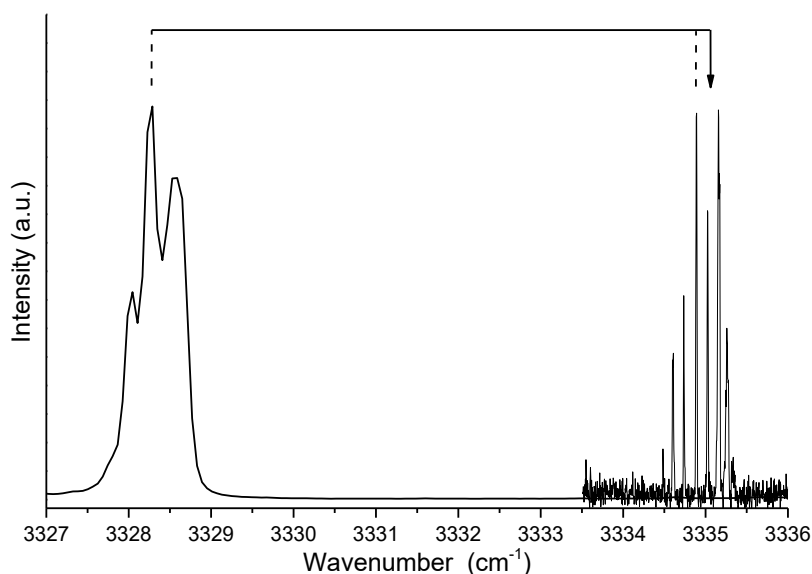


Figure X.2: Propyne FT-IR spectrum in *para*-hydrogen matrix with 0.125 cm^{-1} resolution (left) and in helium droplets with 0.003 cm^{-1} (right). The arrow indicates the position in the gas phase.

We can observe that in *para*-hydrogen the band preserve some rotational structure but is not completely resolved because of the spectrometer resolution. Nevertheless, it is clear that there is a red shift of around 6.80 cm^{-1} in the position compared to the gas phase. This shift is associated to a bigger perturbation on the ν_1 mode by the *para*-hydrogen matrix.

Other bands in the spectrum also show what it seems to be a rotational structure (see Figure X.3), but higher resolution and concentration studies are needed to confirm it. The entire assignment of the molecule in *para*-hydrogen matrix is shown in Table X.2. Theoretical calculations at MP2/aug-ccVTZ level of theory is also

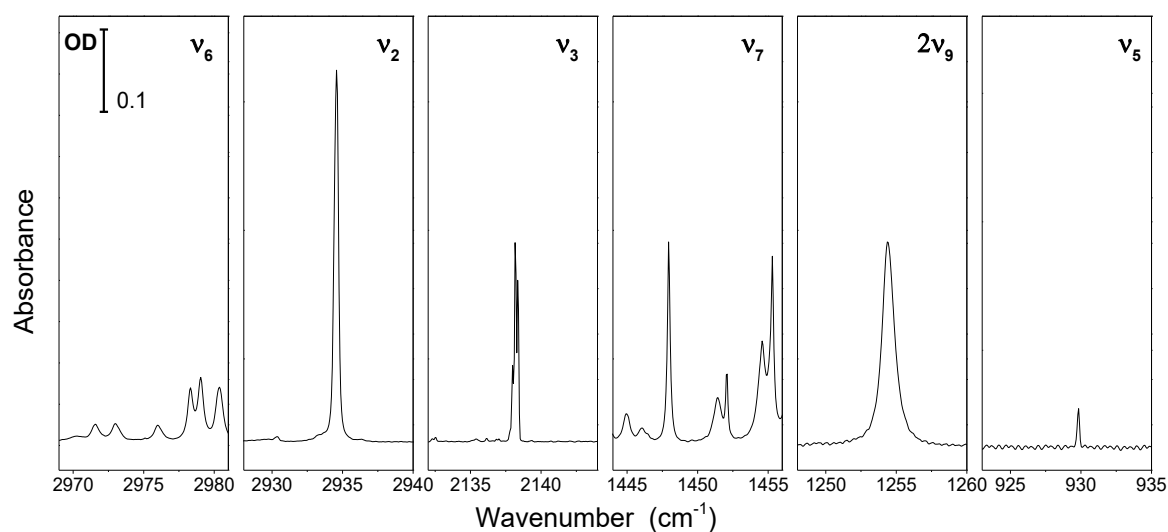


Figure X.3: FT-IR of propyne in *para*-hydrogen matrix. The spectral window of each mode assigned in Table X.2 is shown.

PROPYNE-H₂O complex

Table X.2: Vibrational assignment of propyne in para-hydrogen and krypton matrices. The values in argon matrix [127] and in the gas phase [223] are also included for comparison. Theoretical harmonic frequency calculation at MP2/aug-ccVTZ level is also included for comparison. No scaling factor are applied to the theoretical frequency values.

Mode (symmetry)	Experimental			Gas phase	Theoretical		Assignment
	pH ₂	Kr*	Ar		Harm.	Int.	
ν_1 (a_1)	3328.6						ν CH (acetylenic)
	3328.3	3315	3324	3334	3487.5	57	
	3328						
ν_2 (a_1)	2934.7	2926.7	2938	2918	3078.8	13	ν CH ₃
	2934.5						
ν_3 (a_1)	2138.4	2133.2		2142	2141.6	4	ν C \equiv C
	2138.2						
	2138						
ν_4 (a_1)				1382	1421.4	0.09	δ CH ₃
ν_5 (a_1)	929.8			931	948.7	0.6	ν C-C
ν_6 (e)	2980.4	2867.5	2980	3008	3164.0	4	ν CH ₃
	2979						
	2978.4						
	2976						
	2973						
ν_7 (e)	2971.6	1442	1446	1452	1503.1	8	δ CH ₃
	1455.3						
	1454.6						
	1451.5						
	1446						
	1444.9						
ν_8 (e)	1035.1			1053	1064.2	0.1	ρ CH ₃ (rocking)
	1034.7						
ν_9 (e)			630	633.1	638.9	45	τ CH
ν_{10} (e)			332		320.9	7	δ C \equiv C-C
			335				
			336.5				
$2\nu_9$	1255		1247	1254			
	1254.3						

*Bands below 1350 cm⁻¹ are not assigned because a sapphire window was used in these experiments (absorption of the internal window)

included for comparison. In this case DFT is not shown because the study of the complex with water (see section X.3.) did not yield reliable results (at least for the moment). Moreover, MP2 allows to have a good description of the interaction energy in the complex, that we will analyze later.

The FT-IR spectrum of the molecule was also obtained in krypton matrix. The assignment is included in Table X.2. All modes are redshifted in krypton compared to *para*-hydrogen and the gas phase. No structure is observed in this matrix, which indicates that the rotation of the molecule is completely hindered. Other bands with small intensity are observed in both matrices, probably related to overtones, combination and dimer bands. They are not discussed here because they have not been analyzed yet.

X.2. Propyne dimers

The obtained spectrum in helium droplets shows the presence of broader bands at lower frequencies (see Figure X.4). When propyne concentration is increased (through the change of propyne pressure in the chamber) the intensity of these bands increase, indicating the presence of multimers. Some of the new bands seem to have a rotational structure. The shape also changes by increasing the pressure.

The question arising now, is to know the stoichiometry of the multimers leading to the absorption of a particular band observed in the spectrum. CICR experiments (Cluster Isolated Chemical Reaction Spectroscopy) [224] have been used to answer this question. It is based on the fact that the pick-up of propyne in the helium clusters is a random process without memory. This process follows then a Poisson law. CICR experiments consists in following and recording the intensity of the bands of interest as a function of the pressure of the guest molecule (propyne). The evolution of these intensities should follow a Poisson's law or a linear combination of Poisson distributions. The knowledge of the Poisson law describing the

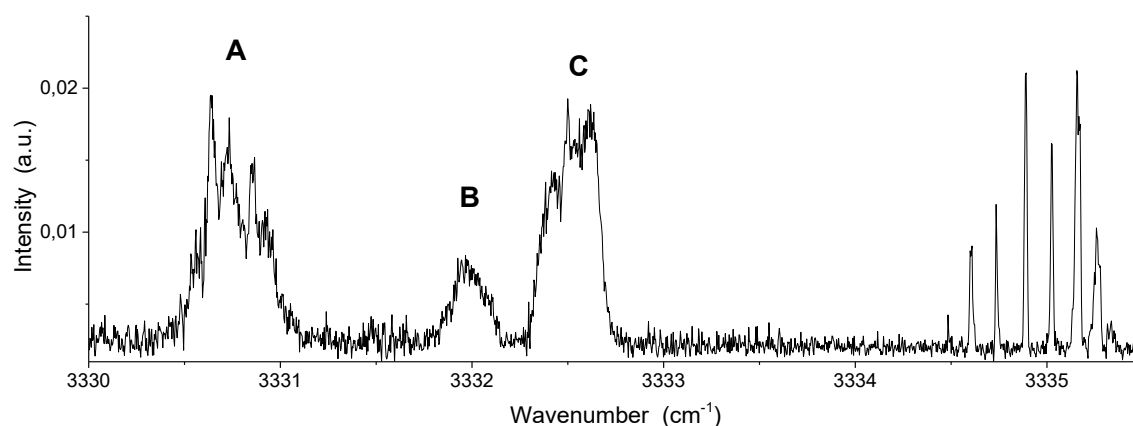


Figure X.4: Infrared spectrum of propyne in helium droplets. The ro-vibrational structure of the monomer is observed at higher frequencies, and bands (A, B and C) corresponding to multimers are placed at lower frequencies.

PROPYLENE-H₂O complex

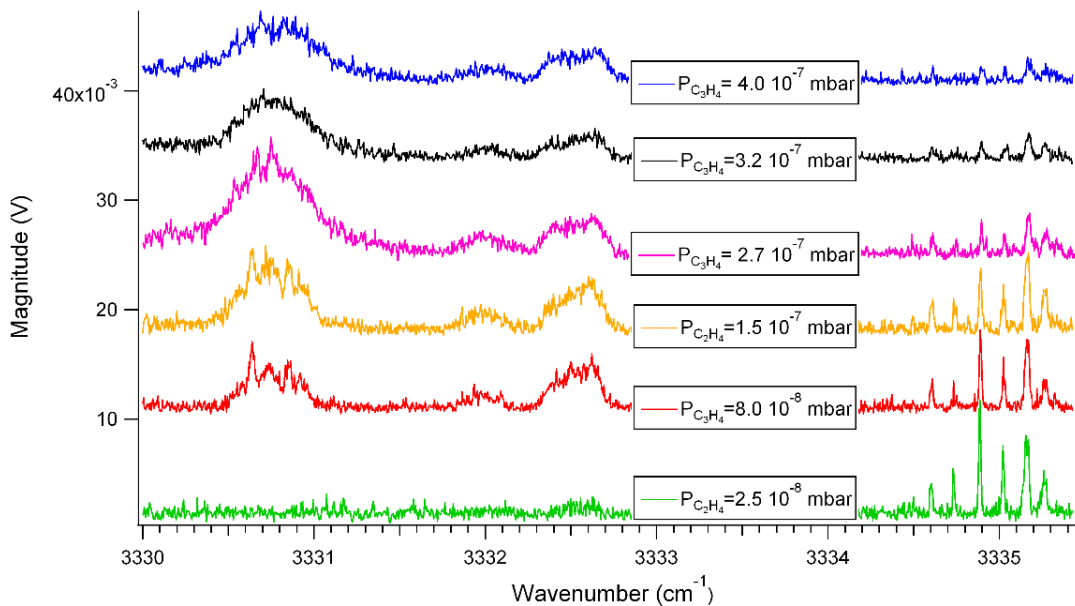


Figure X.6: Evolution of the infrared spectra of propyne in helium droplets as a function of propyne pressure.

evolution of a particular band allows the determination of the exact number of molecules at the origin of the absorption.

In the experiment, propyne pressure was increased and the spectra were obtained at fixed values of this variable (see Figure X.6). Then, each band was directly integrated and its intensity was plotted as a function of propyne pressure.

Monomer bands were also analyzed as a function of the propyne pressure. In this case, we know *a priori* that the experimental data must follow a first order Poisson distribution law (P_1). That is to say, the intensity of the bands of the monomer should come from clusters carrying one and only one propyne molecule. The evolution of one of the lines of the monomer (*e.g.* $R(1)$) shown in Figure X.5) is related to $P_1(C_3H_4)$, which

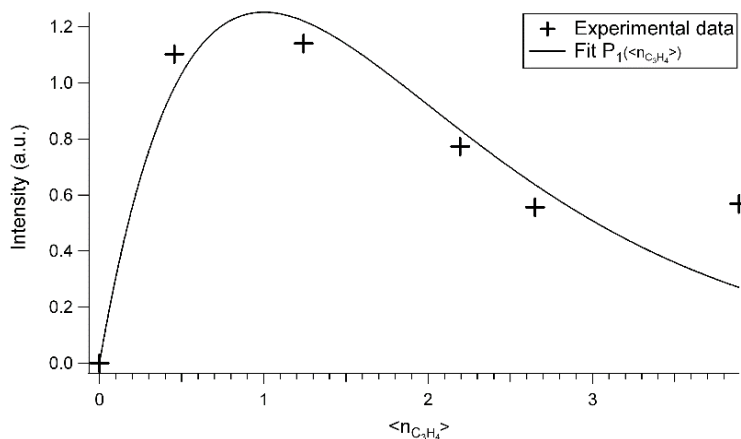


Figure X.5: Monomer intensity evolution. All the bands from the ro-vibrational structure were included in the integration. This evolution is used as reference for the Pressure \rightarrow $\langle n_{\text{molecule}} \rangle$ calibration

allows to change from $P_{C_3H_4}$ (propyne pressure) to $\langle n_{C_3H_4} \rangle$ (average number of propyne molecules per helium droplet). The factor obtained for the conversion in monomer bands is then used for the other bands. The evolution of the multimers bands was also analyzed. The case of the band at 3331.9 cm^{-1} (B) is shown in Figure X.7 as example. The fitting in this case is less good than for the monomer. Nevertheless, we can conclude that the bands at 3332.5 cm^{-1} (C) and 3331.9 cm^{-1} (B) have similar evolutions and the best fit is obtained with a P_2 law. These bands should correspond to absorption of photon by clusters which carry two molecules of propyne: the dimers. On the other hand, the band at 3330.7 (A) cannot be fitted to a second order Poisson law and it seems to be composed by different kinds of multimers. It is not surprising if one looks at the evolution of the propyne spectra as a function of the pressure of propyne (see Figure X.6). Indeed, the redder band appears structured at low pressure of propyne. These structures disappear at higher pressure of propyne. Moreover, the global shape of the band also changes as this bands become larger and larger when increasing the pressure of propyne.

These results suggest that there are at least two different dimer configurations. Two possibilities obtained from preliminary DFT theoretical calculations are the antiparallel and the T-shape configuration, but other possibilities cannot be excluded. Quantum theoretical calculations should be helpful in the configurational search and the assignment of the spectrum, and are part of the recommendations for the continuity of this work.

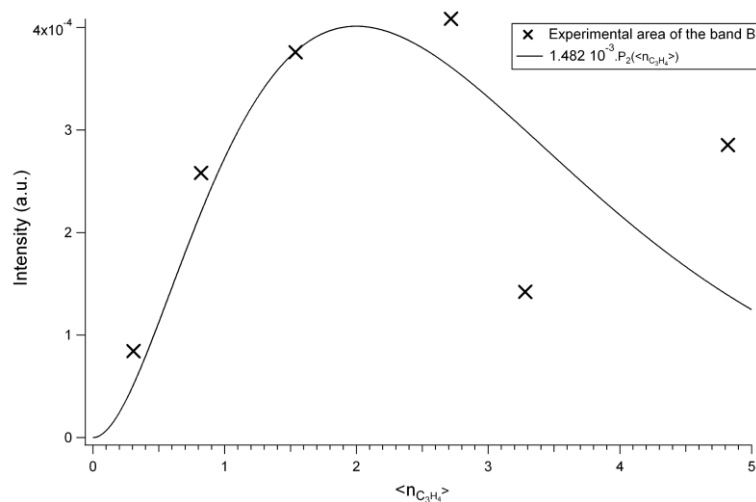


Figure X.7: B (3331.9) band intensity evolution. The coefficient used for Pressure $\rightarrow \langle n_{\text{molecule}} \rangle$ axis calibration is the same used for the R(1) band of the monomer

X.3. Propyne-H₂O complex

Once the characterization of the infrared spectrum of the molecule has been done we proceed to form the complex with water. The small alkyne-water complex is a very interesting system to test the balance between two different kinds of inter-molecular hydrogen bond. This could be better explained if we start with the acetylene-water complex and its isotopologues as example. This system has already been studied in argon matrix [225], gas phase [90], pulsed supersonic jet [226], and theoretical quantum calculations [227].

In principle we can have two possible main structures for the acetylene-water complex. In the first, one or two hydrogens from the water molecule are pointing to the triple bond electronic cloud of acetylene. In the second, the oxygen atom is interacting with the acetylenic hydrogen. The two possible structures are depicted in Figure X.8. As we can observe, in the first structure (**S1**) water acts as hydrogen donor while in the second one (**S2**) acts as hydrogen receptor.

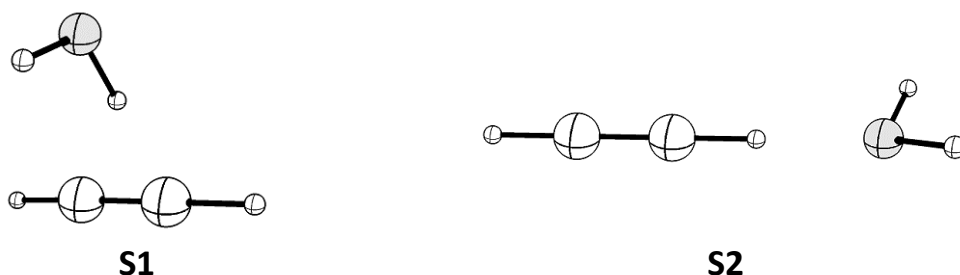


Figure X.8: Schematic representation of the two main stable configurations of the acetylene-water complex. S1: hydrogen donor water complex, S2: hydrogen acceptor water complex

All the studies done on this system (experimental and theoretical) agree that the second structure is the most stable and the only one observed. Experimentally, this was demonstrated by Engdahl and Nelander [225] by observing a big red shift of the CH acetylenic stretching mode ($\sim 49\text{-}62\text{ cm}^{-1}$). In principle, we expect to have a similar competition in propyne-water complex between the two structures already mentioned. No experimental study about the propyne-water complex was found in the bibliographic research done. Only one theoretical paper dedicated to this system was found [228]. In this paper Lopes *et al.* made DFT and MP2 calculations finding a new stabilizing interaction in the **S1** structure. In addition to the hydrogen (H₂O)-triple bond (C₃H₄) interaction an attractive interaction between the oxygen atom of water and one of the hydrogen from the methyl groups was suggested to take place. This implies the formation of a 5 members ring stable structure, depicted in Figure X.9.

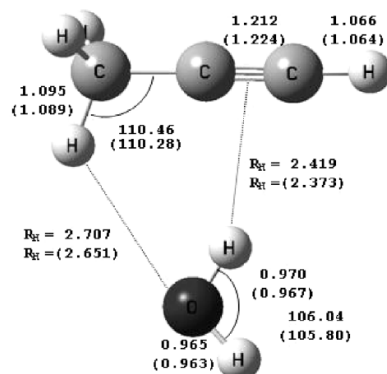


Figure X.9: Stable configuration of the propyne-water complex obtained by Lopes *et al* (Reprinted from reference [228]. Copyright (2006), with permission from Elsevier).

But, it is interesting to note that no reference to the **S2** structure is made in their paper. So, we decided to performed quantum theoretical calculations in order to verify the structure proposed by Lopes *et al.* and to check the stability of the **S2** structure.

X.3.1. Theoretical simulations

Theoretical simulations were performed for the **S1** and **S2** configurations of propyne-water complex at MP2/aug-ccVTZ level of theory. The results of the optimized geometries indicate that we should preferably find the **S1** configuration in the experimental spectrum because of its lower energy (Table X.3). If we take into account the frequency calculations, the CH acetylenic stretching mode in the **S1** configuration should be weakly affected by the complex, having a small shift to the red (~ 8 cm⁻¹). On the other hand, in the **S2** configuration this mode is strongly affected by the interaction with the oxygen from water, presenting a big shift to the red (~ 53 cm⁻¹). Frequency calculations suggest that it should be easy from the experimental point of view, to distinguish both configurations, because the large separation of the C-H acetylenic mode in each one.

Table X.3: Theoretical electronic energy + ZPE (Hartree/particle), and harmonic frequency (cm⁻¹) and intensity Intensities (km/mol) obtained in the harmonic approximation values for the C-H acetylenic mode in the S1 and S2 configurations of propyne-water complex. MP2/aug-ccVTZ level of theory was used (no scaling factor is applied). Intensities (km/mol)

	Electronic energy + ZPE (Hartree/particle)	Frequency	Intensity
S1	-192.654587	3480.0	62
S2	-192.652583	3434.7	229
ΔS2-S1	0.002004 (5.3 kJ/mol)		

X.3.2. Experimental results

The experimental conditions for the formation of the propyne-water complex in helium droplets were explained in section IV.6. . Different regions of the spectrum were scanned looking for new bands that could correspond to the complex. Indeed, a new band was found near 3329.80 cm⁻¹. In Figure X.10 bottom panel, a new band can be observed. Pure propyne spectrum is also shown (upper panel) for comparison.

This band is only observed when both molecules (water and propyne) are introduced in the system. Its position is around 5 cm⁻¹ downshifted regarding monomer band, which is consistent with the theoretical values obtained for the **S1** configuration. Like in the other cases, the new band seems to have a rotational structure. Unfortunately, at the time this manuscript was written no scan near the 3280 cm⁻¹ value was done. So, the presence of the **S2** configuration cannot be excluded.

The presence of the **S1** configuration would imply that the addition of the methyl group to the acetylene structure definitely changes the balance of interactions on the original molecule. The new interaction (O_{water}⋯H_{CH3}) completely modify the proton donor/acceptor configuration stability of the water molecule.

Nevertheless, even if the value of the shift agrees with the predicted theoretical value for the **S1** configuration, we cannot be completely sure of this assignment. The “kinetics” of this new band have not been done yet. So, we cannot discard that this band is due to a complex of water with *n* propyne molecules. Further experiments need to be done to get insight in the process.

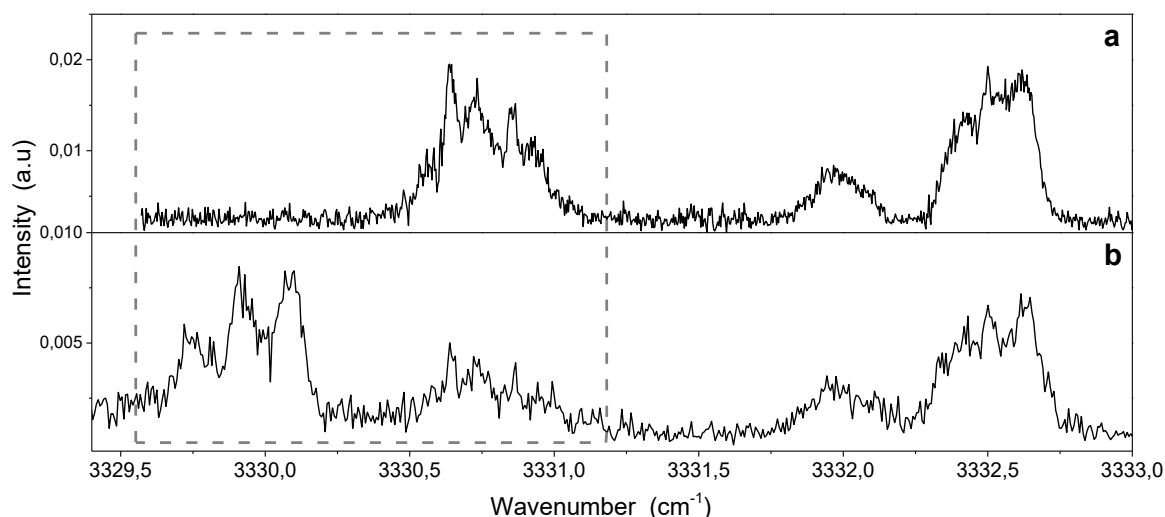


Figure X.10: (a) Propyne infrared spectrum in helium droplets in the 3333.0-3329.5 cm⁻¹ region, multimers bands are observed. (b) Propyne-water spectrum. The gray dashed square shows the presence of a new band when water molecules are added to the system.

Chapter XI Discussion

The discussion is focused on the three main processes explored in this thesis. First, the effect related to the internal hydrogen bond are summarized. Then, the effect on different spectroscopic variables in vibrational spectra is discussed. After, the possibility of nuclear spin conversion process is analyzed for each analog. Finally, a general mechanism intended to describe the photoisomerization process in the whole sets of β -dicarbonyl molecules is discussed.

XI.1. Hydrogen bond

The presence of a hydrogen bond implies notable changes in different structural, energetic and spectroscopic variables. So, some of these variables allow to evaluate the strength of the hydrogen bond and to compare the effect of different substituents in the original molecule. Previous studies in the β -diketone family have shown that the intramolecular hydrogen bond strength changes as $\text{AcAcF6} < \text{AcAcF3} < \text{AcAcH8} < \text{AcAcCl}$ [79], [229]. On the other hand, Trivella *et al.* have suggested that the IHB should be stronger in acetylacetone than in malonaldehyde [50]. In this section, structural and energetic variables obtained by theoretical calculations are first analyzed for each system.

XI.1.1. Geometric and energetic theoretical variables

We can get a good picture of the strength of the intramolecular hydrogen bond if we take a look to the geometric parameters obtained through theoretical calculations for each structure. These are shown in Table XI.1.

In intramolecular hydrogen bonded systems the coordinates involved in the hydrogen bond are the most affected. From Table XI.1 it is clear that the O-H \cdots O angle and O \cdots O distance significantly change when going from chloroacetylacetone to hexafluoroacetylacetone while the others geometric variables (related to the skeleton of the ring) only have small changes. The shorter O \cdots O distance and bigger O-H \cdots O angle⁶⁰ is an indication of a stronger hydrogen bond [5].

⁶⁰ The directional character of the hydrogen bond indicates that in most of the case the interaction is stronger when the interacting parts are in a linear configuration [5].

DISCUSSION

Table XI.1: Geometric parameters from the optimized geometries of the CCC conformer at M06-2X/6-311G++(3df, 3pd). All the distances between two atoms are given in Angströms (Å), and the angles in degrees (°).

Molecule	Distances					
	O····O	O-H	C=O	C-O	C=C	C-C
3-Chloroacetylacetone	2.500	1.001	1.233	1.314	1.366	1.449
Acetylacetone	2.528	0.998	1.233	1.318	1.361	1.445
Trifluoroacetylacetone (CO)	2.584	0.986	1.221	1.315	1.364	1.430
Hexafluoroacetylacetone	2.610	0.982	1.214	1.310	1.348	1.445
2-Chloromalonaldehyde	2.594	0.985	1.220	1.314	1.352	1.448
Malonaldehyde	2.570	0.990	1.23	1.312	1.355	1.440
Maximum deviation	0.11	0.019	0.019	0.008	0.018	0.019
Standard deviation	0.042	0.008	0.008	0.003	0.007	0.007

Molecule	Angles		
	O···H-O	O=C-C	C-C=C
3-Chloroacetylacetone	148.87	119.96	121.13
Acetylacetone	148.44	121.83	120.23
Trifluoroacetylacetone (CO)	145.54	125.74	119.52
Hexafluoroacetylacetone	142.02	124.96	118.32
2-Chloromalonaldehyde	144.03	122.52	120.67
Malonaldehyde	145.66	123.46	119.29
Maximum deviation	6.85	5.78	2.81
Standard deviation	2.6	1.93	0.93

As mentioned in section I.1.2. , the hydrogen bond in β -dicarbonyl molecules has a cooperative character, being classified as a Resonance-Assisted Hydrogen Bond (RAHB). In order to quantitatively compare the effect of delocalization in these kinds of systems the parameter λ (coupling parameter) is used [5] (see Equation (X.3)). Values approaching 0.5 indicates higher level of delocalization.

$$\lambda = \frac{(1 - \frac{Q}{0.320})}{2} \quad (\text{X.3})$$

Where $Q = q_1 + q_2 = d_{C-O} - d_{C=O} + d_{C-C} - d_{C=C}$ is known as the coordinate of π bond delocalization. The coupling parameter was computed for the set of molecules under study, through the geometric values given in Table XI.1. The results shown in Table XI.2 indicate that in the β -diketones delocalization, decreases from chloroacetylacetone to hexafluoroacetylacetone, with the exception of trifluoroacetylacetone. In fact, the highest value belongs to this molecule. This result implies that π delocalization is not the only variable which affects the IHB strength (*e.g.* inductive effects of fluorine in AcAcF₃ should provoke a decrease in the electron density of the carbonyl atom, decreasing the HB strength [78]). In the case of β -dialdehydes the higher π delocalization is found for malonaldehyde, showing a contrary trend when compared to

chloroacetylacetone and acetylacetone. This result suggests an important role of the methyl groups in the π delocalization system.

Table XI.2: Coupling parameter (λ) and related variables (q_1 , q_2 and Q , see text) for the set of β -dicarbonyl molecules under study.

Molecule	q_1	q_2	Q	λ
3-Chloroacetylacetone	0.081	0.083	0.164	0.243
Acetylacetone	0.085	0.084	0.168	0.237
Trifluoroacetylacetone (CO)	0.094	0.066	0.160	0.250
Hexafluoroacetylacetone	0.096	0.097	0.193	0.199
2-Chloromalonaldehyde	0.095	0.095	0.190	0.203
Malonaldehyde	0.086	0.085	0.172	0.232

Another simple way to quantify the strength of the intramolecular hydrogen bond in β -dicarbonyl systems is to compare the relative energy of the CCT conformer to CCC. This approach has been previously used by different authors in acetylacetone and malonaldehyde [230]–[232]. When applied to our set of β -diketones the trend previously obtained for geometric parameters versus IHB strength is reproduced (see Table XI.3).

Table XI.3: Relative energy ($\text{kJ}\cdot\text{mol}^{-1}$) of CCT conformer to CCC for the set of β -dicarbonyl molecules analyzed in this work. The values are calculated at M06-2X/3-611++G(3df,3pd).

	AcAcCl	AcAc	AcAcF3	AcAcF6	MA	MACl
$\Delta E(\text{CCT} - \text{CCC})$	78	63	48	38	51	45

Although this approach matches the expected trend, we must pay attention to its use. The method assumes that the difference in energy between both conformers is totally attributed to the hydrogen bond, which is not true, as originally noted by Buemi [69]. The relative energy can be affected by other factors, for example, steric factors or by specific interactions of the hydrogen atom from the hydroxyl group in the CCT conformer. The steric factor can be observed in chloroacetylacetone, where the methyl group (from the OH side) changes from *syn* to *anti* conformation when going from CCC to CCT (see Figure VI.1). This effect is only observed in this analog because of the symmetric configuration of the methyl groups in the CCC conformer. The second factor, specific interactions, can be observed in the case of the CCT conformer of hexafluoroacetylacetone, as explained in section VII.1. Nevertheless, even in hexafluoroacetylacetone the specific interaction seems to be small (as shown by NCI calculations). So, the contributions of these two factors should be small compared to the difference in stabilization energy shown in Table XI.3 for each analog.

DISCUSSION

It is interesting to note from these results the difference in IHB strength when comparing chloroacetylacetone versus acetylacetone, and its corresponding β -dialdehydes analogs: chloromalonaldehyde and malonaldehyde. Like for the coupling parameter (λ), the behavior is inversed. The chlorine atom in the alpha position has three different effects on the molecule: inductive (-I), mesomeric (+M) and steric. Our results agree with previous studies which suggest that the inclusion of an electron withdrawing group⁶¹ in the alpha position should lead to a weakening of the IHB as observed in the case of the β -dialdehydes [10]. However, the behavior is inversed in the case of the β -diketone pair. This has been explained by Tayyari *et al.* as a repulsive effect of the chloro atom which interacts through its lone electron pairs with the π cloud of carbons pushing the oxygen atoms toward each other, and increasing the IHB strength [62].

XI.1.2. Spectroscopic variables

XI.1.2.1. Frequency shift

Vibrational frequencies are one of the most affected variables when hydrogen bond takes place. There usually exists a correlation between the strength of the hydrogen bond and the position of the stretching and bending modes of the O-H involved in the bond. The general rule indicates that the strongest the hydrogen bond the biggest the shift is. Nevertheless, usually the shift is not in the same direction, for stretching modes there is a redshift and for bending ones a blueshift⁶². In the β -diketones systems under study the effect on the bending modes can be compared when going from chloroacetylacetone to hexafluoroacetylacetone (Table XI.4). The effect on chloroacetylacetone and acetylacetone is shown in Figure XI.1.

It can be observed that the in plane OH bending mode is very broad in acetylacetone but its center is at lower frequencies compared to chloroacetylacetone. The same behavior is clearly observed for the out of plane mode. The position of these modes remains almost unaltered from neon to *para*-hydrogen matrix. Unfortunately, the OH stretching modes cannot be compared because they are not observed in matrix for these two molecules.

⁶¹ Chlorine is a weak electron withdrawing group

⁶² The redshift in ν_{OH} can be explained by the lengthening of OH in a flatter potential when the HB is stronger. On the other hand the δ_{OH} and γ_{OH} blueshift can be explained by the motion of the hydrogen in a privileged direction (between the two oxygen) with steeper walls in the other directions.

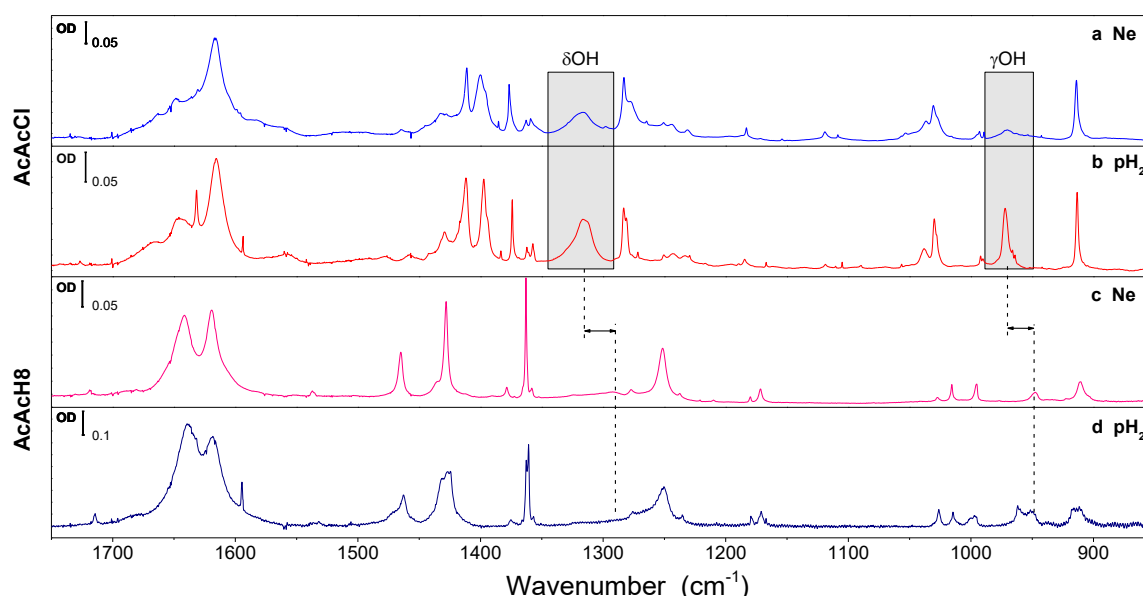


Figure XI.1: FT-IR spectra of the CCC conformer (deposited sample) of chloroacetylacetone in (a) neon and (b) *para*-hydrogen matrices; and acetylacetone in (c) neon and (d) *para*-hydrogen matrices.

In Table XI.4 the frequencies of the bending modes in neon matrix for the four molecules are included. Comparing the values, it is clear that the effect of the strength of the hydrogen bond is more evident for the OH out of plane bending mode than for the OH in plane bending mode. The OH in plane bending modes are usually coupled to many modes in the molecule (from the semi-ring character) which contributes to the spread in frequency. We should also pay attention to the fact that because they are usually very broad (*e.g.* acetylacetone and trifluoroacetylacetone) to define its center implies a bigger uncertainty. Nevertheless,

Table XI.4: Frequency position and bandwidth (in parenthesis) of the OH in plane (δ OH) and out of plane (γ OH) bending modes of β -diketones molecules under study, and ν OD, δ OD and γ OD for AcAcCl(D) and AcAc(D2) in neon matrix.

	AcAcCl	AcAc	AcAcF3	AcAcF6
δ OH	1317 (21.2)	1297 [†] (77.5)	1303.6/1294* (4.4/4.4)	1301 (2.8)
γ OH	972 (11.4)	948 (5.5)	883.9 (1.1)	814 (1.3)
δ OD	1118 (2.7)	1088 (2.3)	-	-
γ OD	706 (8)	708 (1.1)	-	-
ν OD	2030 [†]	2000 [†]	-	-

[†] The band is very broad

* The assignment is not completely clear. There are several bands in this region. The bands reported are the clearest bands, and the corresponding bandwidths are the smallest from the group of bands.

DISCUSSION

even if the trend is not clear for the in plane bending modes, the maximum shift observed (21 cm^{-1}) is seven times smaller than for the out of plane bending modes (158 cm^{-1}) the latter being well localized.

Interesting results are also obtained from the comparison of the position of the OD modes in the case of the deuterated samples of AcAcH8 and AcAcCl. First, no change is observed in the trend of the OD in plane bending mode compare to the non-deuterated sample, which confirms the complex coupling pattern of this mode. On the other hand, similar frequency values are obtained for the OD out of plane modes, which indicates a further weakening of the IHB of AcAcCl compared to AcAcH8 after deuteration. This hypothesis is also supported by the fact that the OD stretching mode in AcAc(D2) is redshifted in comparison to the AcAcCl(D) analog.

XI.1.2.2. Bandwidth

The bandwidth is one of the most affected variables by a change in the hydrogen bond strength. The stretching and bending vibrations of groups directly involved in the hydrogen bond are the most affected. Nevertheless, other modes coupled to the modes involved in the interaction, can also be altered. Bandwidth can be affected by the matrix environment due to possible strong vibration-phonon coupling. Nevertheless, the spectra of AcAcH8 in neon and in the gas phase [233] are rather similar in terms of mode dependent widths, indicating that broadening of specific bands is intrinsic to the molecule. In Figure XI.2, the spectra of the CCC conformer in neon matrix of chloroacetylacetone, acetylacetone and hexafluoroacetylacetone are

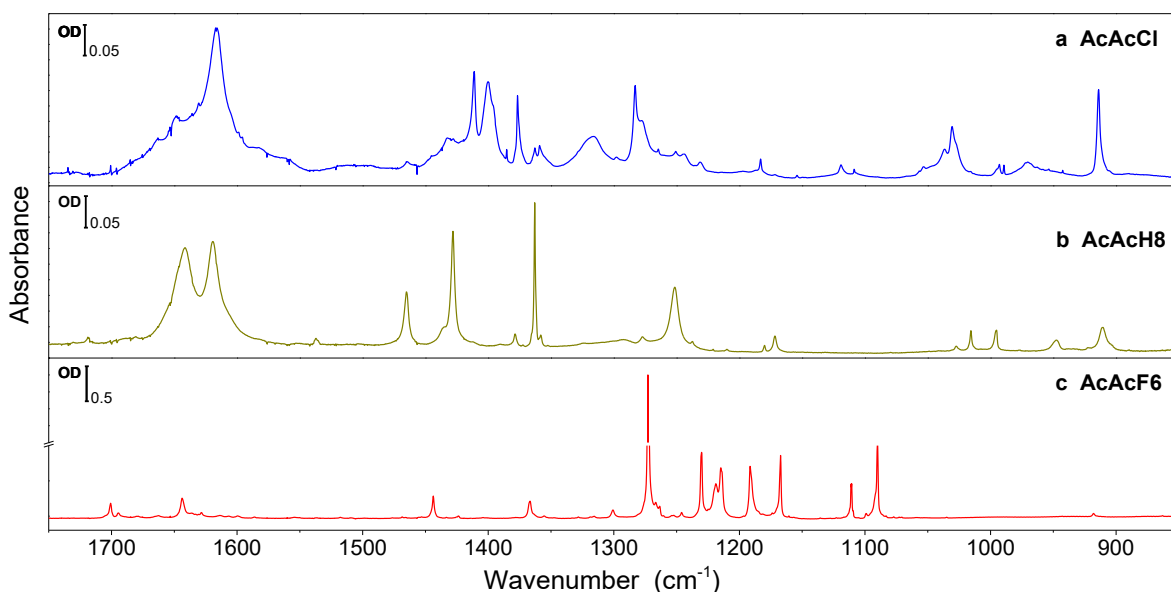


Figure XI.2: Comparison of the FT-IR spectra in neon matrix of (a) chloroacetylacetone, (b) acetylacetone and (c) hexafluoroacetylacetone. There is a break in (c), the optical density in this case is referred to the lower part.

shown for comparison. Neon matrix is chosen over *para*-hydrogen in order to be able to include acetylacetone, which has larger bands in *p*H₂ due to nuclear spin conversion (see section V.2.5.).

It can be observed that there is a decrease in the overall bandwidth when going from strong (chloroacetylacetone) to weaker (hexafluoroacetylacetone) intramolecular hydrogen bond. A comparison of the bandwidth distribution can be observed in form of histogram in Figure XI.3. This trend is not observed in all the modes (it should be taken into account that the set of normal modes is not same for each molecule), allowing to have an idea of which modes are not coupled with OH stretching and bending modes.

As previously mentioned for AcAc(D₂) in section V.2.2., a strong deuteration effect was observed in the bandwidths of the modes of the CCC conformer of acetylacetone. A reduction of the bandwidth of the bands corresponding to OH/OD modes occurs upon exchange of the hydroxyl hydrogen by deuterium, and it was explained by a decrease of the tunneling transfer of the hydrogen atom (which decrease the delocalization of the proton between the two oxygen). The results of the monodeuterated isotopologue of chloroacetylacetone allows to extract deeper conclusions: (1) the reduction of the bandwidth is observed in both neon and *para*-hydrogen matrices, (2) in the stretching and two bending modes of the hydroxyl group and (3) for different molecules: acetylacetone and chloroacetylacetone isotopologues. So, it is clear that the broadening effect comes from an internal process (tunneling effect) and it is general for IHB systems. On the other hand, in each case the narrowing in the bandwidth upon deuteration is also observed in many modes of the molecules, which allows to state that many modes are coupled to the OH/OD modes.

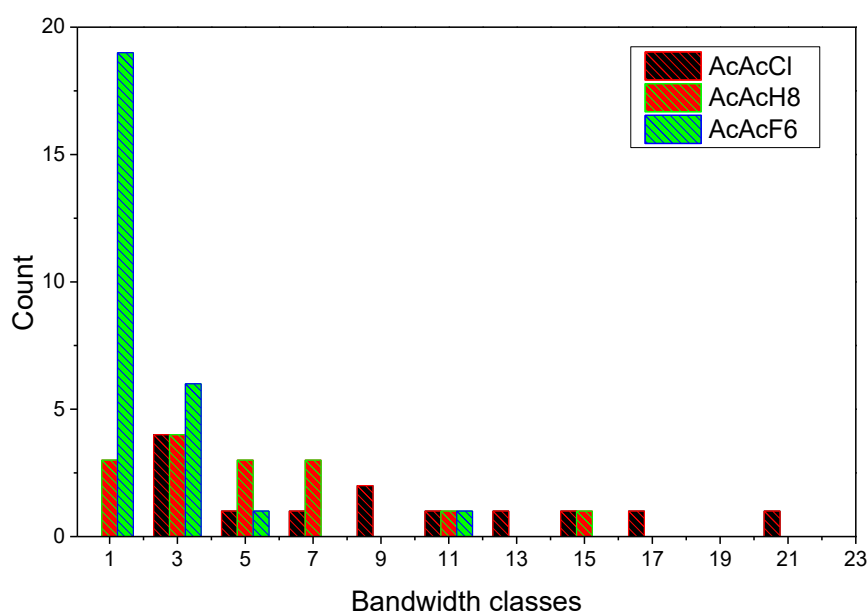


Figure XI.3: Histogram of bandwidth for acetylacetone (15 modes), chloroacetylacetone (13 modes) and hexafluoroacetylacetone (27 modes) in neon matrix. The δ OH mode (77 cm^{-1}) of acetylacetone is not shown in the histogram.

DISCUSSION

XI.1.3. Environment

The environment can perturb the vibrational dynamics of the guest molecule by two main mechanisms: first, through specific interactions between the guest molecule and atoms or molecules from the solvent (inducing frequency shifts), and second through the coupling of the vibrational levels with the solvent (phonons in crystallographic lattices). In our case because only noble gases and *para*-hydrogen are used as host, the first mechanism should be small.

Nevertheless, the change produced by the environment cannot always be easily explained. For example, we showed in section IX.2.1. the different behavior of the CCC conformer of chloromalonaldehyde in neon and *para*-hydrogen, where some doublets are observed in the latter. Also, in overall the bandwidth of the bands observed for the molecules under study are smaller in *para*-hydrogen than in neon, where some site effects were observed in some cases.

In this section two examples of the influence of the environment in different modes are presented.

XI.1.3.1. Chloroacetylacetone

The first example of a change induced by the environment can be observed in Figure XI.1, by comparing the shape of the bands of chloroacetylacetone in neon and *para*-hydrogen. There is an increase in the bandwidth and a decrease in intensity when going from *para*-hydrogen to neon for the OH in-plane (δ OH) and out-of-plane (γ OH) bending bands. In fact, the effect seems to be more dramatic for the out of plane mode.

Modes involving the OH group are large amplitude motion modes which have a very anharmonic character. Following the arguments of Paulson and Anderson [131], there are two effects to take into account to explain the interaction with these low-interacting matrices: polarizability⁶³ and the distance of the first solvation shell to the guest molecule. It can be observed from that polarizability is bigger in *p*H₂ which means that it should be a more perturbing matrix. But, *p*H₂ also has a higher zero-point motion resulting in a greater neighbor distance (*p*H₂ 3.78 Å, Ne 3.16 Å). The last effect should keep the first solvation shell of *p*H₂ molecules further away from the guest molecule compared to neon. This means that the highly OH anharmonic modes which also have a bigger amplitude should be more affected by the closest neon atoms than the rest of the modes. In our case the widths are affected, which can be mainly explained by a larger coupling with phonons in neon matrix because of the steric effects produced by a closer host shell.

⁶³ The lack of permanent multipoles provokes that the interaction with neon and *para*-hydrogen is made through induction forces which depend on the polarizability.

XI.1.3.2. Glycolaldehyde molecule

We decided to study the influence of the environment on the vibrational modes in another system with intra-molecular hydrogen bond (IHB) to compare $p\text{H}_2$ and helium droplets environments. We chose glycolaldehyde molecule, which is the smallest molecule with IHB.

The vibrational spectroscopy of this molecule has been extensively studied in gas phase, supersonic jet and matrix isolation [86]–[88]. No previous reports in helium droplet were found. In contrast with the β -dicarbonyl family the OH stretching mode can be easily observed in all media. The main cause is that the geometry of the O-H \cdots O moiety do not favor the H \cdots O interaction (geometric constraint). The angle of the O-H \cdots O moiety is around 116° (according to B3LYP/6-311++G(3df,3pd) calculation) and the distance O \cdots O is 2.69 Å. The final effect is a weaker IHB in glycolaldehyde compared to the set of molecules shown in Table XI.3.

In Figure XI.4, the effect of the environment on the frequency position and bandwidth for the OH stretching mode of glycolaldehyde is shown. In the figure, we compare the results previously obtained by our group in *para*-hydrogen matrix with new results using the helium droplets technique [88]. Gas phase value (3549.43 cm^{-1} , dashed line) is taken as a reference [86].

A quick glance at the spectra is enough to note the change in position and bandwidth that occurs when we go from *para*-hydrogen to helium droplets environment (the frequency position in neon is also marked). The values are indicated in the graph. The results (smaller bandwidth and shift from gas phase) agree with the

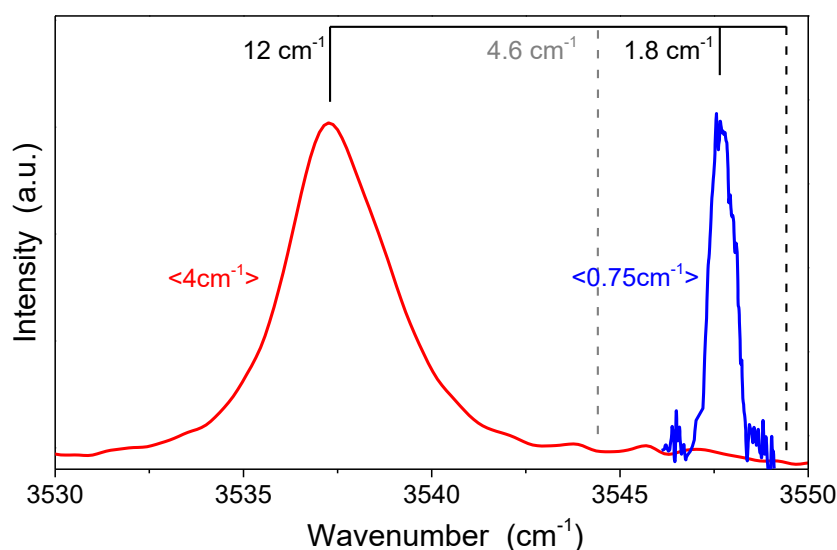


Figure XI.4: Infrared spectra of glycolaldehyde in the OH stretching mode region in helium droplets (blue) and *para*-hydrogen matrix (red). The black dashed line indicates the frequency of the band in the gas phase and the grey dashed line in neon matrix. The numbers indicate the shift compare to the gas phase, and the bandwidths (in colors and brackets).

DISCUSSION

less perturbative effect of the helium droplet environment. It should be noticed, that even in helium droplets no indication of rotational structure is observed (the rotational constants are very small: $A'' = 0.62 \text{ cm}^{-1}$, $B'' = 0.22 \text{ cm}^{-1}$, $C'' = 0.17 \text{ cm}^{-1}$ [234]). We remind that the resolution of our setup is 0.003 cm^{-1} . So, we can have the combination of a compressed ro-vibrational spectrum and a broadening due to the IHB.

XI.2. Nuclear Spin Conversion

The presence of a nuclear spin conversion process was observed in AcAcH8 and AcAcD2 in *para*-hydrogen matrix. The NSC process was also studied for the halogenated analogs of acetylacetone. In the case of chloroacetylacetone and hexafluoroacetylacetone no changes were observed in the spectra.

In the case of chloroacetylacetone, as remarked before, the methyl groups are in symmetrical positions. This implies that the hydrogen transfer is not coupled to the rotation of the methyl groups, because they are symmetrical. It should be noted that contrary to acetylacetone the rotational barrier of the methyl group in the CO side is notably higher than in the OH side⁶⁴, 518 and 125 cm^{-1} respectively (values determined at M06-2X/6-311++G(3df,3pd)). In correspondence, the torsional frequencies are also inversed, 167.6 (CO) and 116.6 cm^{-1} (OH). So, from these values we can expect a noticeable tunneling splitting in the less hindered rotor (OH side), and as a consequence to observe a NSC process. Nevertheless, no sign of evolution in the experimental spectra was found. One possibility is that the tunneling splitting is in fact very weak, which provokes that there will not be a noticeable disequilibrium in the population of the *A-E* states when the system is cooled down, and no transition occurs. This implies that no NSC process will be observed. Another possibility which cannot be excluded is that the kinetics is very slow and longer times of observations are needed. An important remark is that because there is no coupling between the hydrogen transfer and methyl rotation the splitting and the NSC process could be unobservable in the bands coupled to the hydrogen transfer (as observed in AcAcH8).

Fluorine atom has a spin of $1/2$ like hydrogen. In that case the arguments discussed for the CH_3 group are also applied for the CF_3 rotor. In the case of hexafluoroacetylacetone, the perfluoromethyl groups are more hindered than the methyl groups in acetylacetone. A previous work done by Evangelisti *et al.* using microwave spectroscopy [67] suggests that two factors are responsible of the rigidity of the perfluoromethyl groups. First, a higher rotational barrier compared to acetylacetone, and second (and more important) the heaviness of the CF_3 group (inertial effect). Their results suggest that the internal rotational splitting should

⁶⁴ Theoretical calculations performed by Lozada *et al.* [14] with a B3LYP/6-3111++G(3df,3pd) level gives the following values for the barriers: 32 cm^{-1} (CO side) and 411 cm^{-1} (OH side), and the torsional frequencies: 30 cm^{-1} and 119 cm^{-1} in AcAcH8.

be lower than $3 \times 10^{-7} \text{ cm}^{-1}$. Under these conditions there will not be a NSC because of lack of disequilibrium between the populations of the *A* and *E* states, as explained for chloroacetylacetone.

On the other hand, preliminary results show that there exists an evolution in the intensity of some bands in trifluoroacetylacetone. Microwave experiments and quantum calculations from Favero *et al.* [81] suggest that despite the heavier mass of the perfluoromethyl group, this one and the methyl group from trifluoroacetylacetone have similar reduced rotational barrier (s)⁶⁵, 40 and 31.7 cm^{-1} respectively⁶⁶. This conclusion is derived from the important fact that similar values of tunneling splitting were found for both rotors. Our theoretical calculations show that the torsional frequencies in each group are equal to 17 cm^{-1} (CF_3) and 134 cm^{-1} (CH_3). The splitting obtained by Favero *et al.* for the ground state seems to be very small ($< 1 \text{ cm}^{-1}$). So, we will be in the same case of the lack of disequilibrium, and no NSC is expected to be observed under such conditions. The evolution of the intensities observed in the spectrum could be due to conversion of the oH_2 impurities in the matrix, as explained for AcAcD2, whereas experiments were performed with a very low amount of oH_2 ($< 0.1\%$). In this case, more experiments need to be done in order to have a better comprehension of the empirical facts.

XI.3. Open enol conformers production

The UV laser irradiation experiments carried out for the set of molecules studied in this work can provide a general picture on how photoisomerization process take place in the analogs of acetylacetone. The arguments used in this discussion are based in some of the ideas given by Minoura *et al.* in their study about the photoisomerization of AcAcF3 in argon matrix [20] and in the theoretical study done by Chen *et al.* [42].

As mentioned in section I.1.1. , previous studies done on the photoisomerization process in acetylacetone have suggest that the mechanism starts with the Franck-Condon excitation ($\pi \rightarrow \pi^*$) to the $S_2(\pi\pi^*)$ state [232]. The deexcitation pathway involves a decay to the $S_1(n\pi^*)$ state through vibronic interaction, which then relaxes to the $T_1(\pi\pi^*)$ state by means of a $S_1/T_1/T_2$ three-surface intersection. This picture has also been supported by the experimental works of Xu *et al.* [53] and Poisson *et al.* [54]. Nevertheless, as experimentally demonstrated, in the gas phase the dissociation channel is favored [74]. The whole process is depicted in the left panel of Figure XI.5, taken from reference [42]. Only in matrix the formation and stabilization of the open enol conformers is clearly observed. The calculations done by Chen *et al.* also

⁶⁵ The reduced rotational barrier takes into account the mass of the rotating atoms.

⁶⁶ The heights of the torsional barriers derived by Favero *et al.* from these values are 30 (CF_3) and 360 (CH_3) cm^{-1} .

DISCUSSION

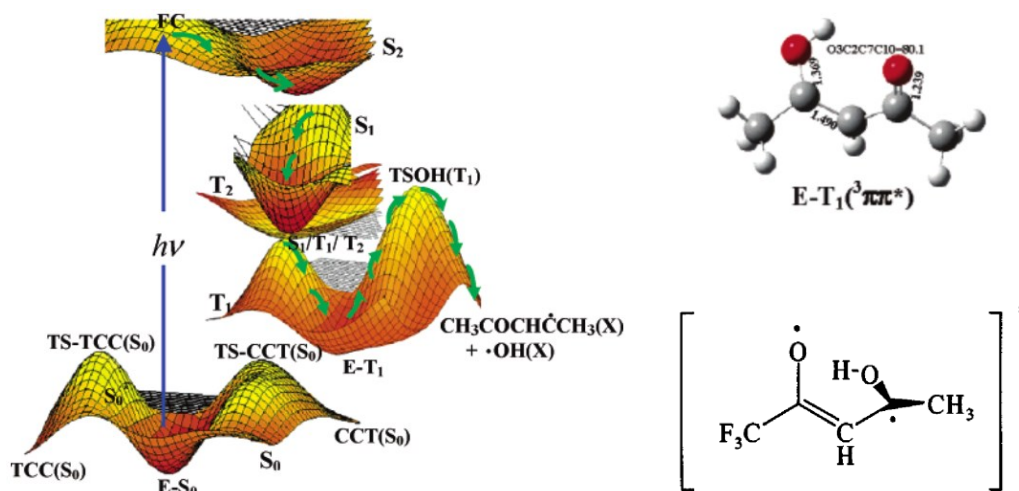


Figure XI.5: Left panel: Theoretical scheme of the vertical excitation and possible relaxation pathway of acetylacetone after UV irradiation ($\pi \rightarrow \pi^*$ transition). Taken from Chen *et al.*, ("Adapted with permission from reference [232]. Copyright 2014 American Chemical Society"). Right panel: (top) Geometry of the T_1 excited state of AcAcH₈ according to the previous reference; (bottom) schematic representation of the T_1 excited state of AcAcF₃ adapted with permission from reference [20]. Copyright 2006 American Chemical Society.

suggest that rotational isomerization can easily proceed in the $T_1(\pi\pi^*)$ state. In this state, there is a rupture of the planar configuration of the molecule (see Figure XI.5 right panel), which do not occur in the other states.

The experimental data (similar UV spectra) and theoretical calculations (oscillator strength in vertical transitions) obtained for the analogs of acetylacetone show that the excitation of the CCC conformer always proceed as a $\pi \rightarrow \pi^*$ transition (in the C=C bond) between $S_2 \leftarrow S_0$ electronic levels. This sets a common starting point for the subsequent mechanism of relaxation. In addition, we assume that a similar mechanism can take the systems from the $S_2(\pi\pi^*)$ excited state to the $T_1(\pi\pi^*)$ state where the isomerization takes place. Of course we cannot assure that the deexcitation pathway follows the same scheme as in acetylacetone. But, the fact that isomerization only proceeds in the $T_1(\pi\pi^*)$ and that similar results are always obtained (as we will see later) suggest that this assumption is actually believable.

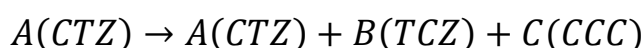
As we have seen in previous chapters, two main groups of open enol conformers are always formed after UV laser irradiation: CTZ (first group) and TCZ (second group) conformers. First group is mainly produced after irradiation of the CCC conformer at wavelength between 270-310 nm. Second group is also produced after irradiation of CCC but in a low quantity. This group is mainly observed when the first group is irradiated at lower wavelengths: 250-280 nm. A common characteristic to both groups is that the most stable conformer of each group is always observed. Indeed, the results obtained from the studies on the deuterated isotopologues of acetylacetone and chloroacetylacetone have shown that after irradiation both conformers from the XYC-XYT produced pair are observed. After, conversion in the ground state between

the less stable and more stable conformer occurs through tunneling effect of the hydroxyl hydrogen. The kinetics of this process is very fast for the non-deuterated molecules which explains why only the most stable species of the pair is observed at the end of the irradiation. The fast tunnel effect of the hydroxyl hydrogen also explains why the CCT conformer has never been produced, even in the case of hexafluoroacetylacetone where it is the most stable open enol conformer.

On the other hand, the fact that in our studies and those of Nagashima, for each analog, the same set of conformers is produced in argon, neon and *para*-hydrogen matrices suggests that the host do not play a specific role in the relaxation mechanism. It means, the matrix plays the role of a cold bath which takes part of the excess energy favoring the photoisomerization and avoiding photofragmentation. But, this could be not completely true. In the case of acetylacetone the TCT conformer was observed as a stable product in $n\text{H}_2$ and $n\text{D}_2$ matrices along with the “most” theoretically stable TCC conformer (and small amount of TTC) [15]. These results suggest that the TCT is stabilized by a specific interaction with the host molecules of $n\text{H}_2$ and $n\text{D}_2$, which reduce the tunneling probability to pass to TCC.

The experimental and theoretical results allow to explain the formation of the two groups. First, experiments show that it is more probable to produce CTZ conformers after excitation of CCC (whatever the irradiation wavelength in the UV absorption of CCC). In the $T_1(\pi\pi^*)$ state, the C=C bond has a single bond character. The weakening of this bond will favor the rotation around the original C=C bond allowing the formation of conformers of the type XTZ. We should remark that the probability of forming TTZ conformers is usually very low because two bonds need to be rotated, being CTZ the main products.

In the case of the second group, the experimental evidence indicates that the conformers are mainly formed by irradiation (250-280 nm) of the first group of conformers (CTZ). They are in fact formed as minor products directly from CCC as proved by kinetics studies on AcAcH8 [15]. Like in the case of CCC, the excitation of CTZ conformers proceeds via a $\pi \rightarrow \pi^*$ excitation ($S_2 \leftarrow S_0$) followed by relaxation in the T_1 state, weakening the C=C double bond. Then, the system can return to a X CZ configuration (producing at the end CCC) or to TCZ conformers. The production of TCZ conformers should be less probable because two bonds need to be rotated. Nevertheless, these conformers absorb at lower wavelengths compared to CTZ, being at the end a stable final product. This imposed a scheme like:



Under irradiation with wavelengths exciting CTZ, CCC is usually also excited and can react, whereas TCZ is not (or weakly) excited. Then, even if the production channel to TCZ has a small probability, once the

DISCUSSION

conformer is formed it does not return to the initial conformers (CTZ and CCC), which will then be depleted over time (or reach an equilibrium amount).

An interesting case is trifluoroacetylacetone. The asymmetry of the molecule provokes that after UV excitation, hydrogen transfer occurs in the excited state (see Figure XI.5, scheme of AcAcF₃ (T_1) geometry), as experimentally observed. The mechanism for this molecule was detailed by Minoura *et al.* in a nice work [20], but it used similar arguments to those explained here.

It is worth to mention that these arguments are also valid for chloromalonaldehyde. Only the most stable conformers are observed. In this case there is not steric repulsion between the methyl groups and the TTC conformer is observed as the most stable conformer, which demonstrates the importance of this interaction in the conformer production.

It is important to note that in all the systems after the UV excitation of the CCC conformer at wavelengths between 290-310 nm, almost no fragments were produced. If a recombination process takes place is very likely that we will observe some of the escaping fragments in *para*-hydrogen matrix, thanks to the softness of this matrix. The experimental evidence disfavors this mechanism. Nevertheless, at lower wavelength fragments start to growth (CO product is clearly observed), which suggests that some recombination could take place in the formation of the second group of conformers.

Conclusions

The dynamics and photodynamics of five β -dicarbonyl molecules in cryogenic matrices were studied by means of electronic and vibrational (FT-IR and Raman) spectroscopies as just deposited samples and upon selective UV and IR laser irradiation. Neon and *para*-hydrogen were mainly chosen as host matrices because of their small perturbative properties. In all the cases the chelated enol tautomer (CCC) was found as the predominant species after deposition of the samples. In fact, the amount of keto tautomer was very low in all the systems, being only clearly observed in double deuterated acetylacetone.

Experimental evidences of a Nuclear Spin Conversion process were found in the CCC conformer of double deuterated acetylacetone trapped in *para*-hydrogen matrix, assigned to NSC in the methyl group from the carbonyl side. The absence of this process in the other three β -diketones (halogenated compounds) is explained by a very small splitting in the vibrational ground state which does not produce a noticeable population disequilibrium with the thermal change during deposition.

The influences of the intramolecular hydrogen bond strength in spectroscopic variables were analyzed for the CCC conformer within the set of β -dicarbonyl molecules. There is a marked red shift in the out of plane OH mode when going from chloroacetylacetone to hexafluoroacetylacetone following the decreasing trend of hydrogen bond strength. The behavior is not clear in the case of the in plane OH bending mode. The experiments show a clear overall broadening of the infrared bands in chloroacetylacetone compared to hexafluoroacetylacetone which has the weakest hydrogen bond.

The photoisomerization process was studied in the β -dicarbonyl set of molecules. The experimental results allow to make general conclusions: (1) only a reduced set of open enol conformers is observed after UV laser irradiation in each molecule, (2) the conformers observed in non-deuterated isotopologues at the end of the irradiation are not always the most stable conformers after CCC, but (3) they are always the most stable conformers of their corresponding XYC-XYT pairs (hydroxyl hydrogen configuration).

The last result was explained by the observation of a tunneling process in the ground state of the deuterated isotopologues of acetylacetone and chloroacetylacetone. This confirms that several conformers can be initially produced and some of them disappear by an interconversion process driven by tunnel effect. In the case of double deuterated acetylacetone, the experimental kinetics shows a good agreement with

CONCLUSIONS

theoretical calculation using the WKB approximation. The same procedure is recommended to be done in the case of deuterated chloroacetylacetone, which it seems to have faster kinetics.

In addition to the previous conclusions we can add that (4) two groups of conformers with different photodynamic behavior are always observed in each system, (5) the first group is generally composed by CTZ conformers and the second one by TCZ, with ordering coming from the predominance in the first steps of photoisomerization of CCC.

The stabilization of some conformers in the halogenated molecules can be explained by the presence of Non Covalent Interactions, as shown by the NCI calculations. Nevertheless, other kinds of interactions *e.g.* electrostatic interactions, need to be taken into account to have a complete picture and to explain for example the high theoretical stabilization of the CCT conformer of hexafluoroacetylacetone.

Similar results in neon and *para*-hydrogen matrix were obtained for the photoisomerization products of hexafluoroacetylacetone and trifluoroacetylacetone compared to those previously reported in argon, indicating no specific participation of the matrix in the process. The infrared spectrum of the CCC conformer of trifluoroacetylacetone shows the presence of additional bands to those expected by the theoretical calculation. In addition, a complex pattern observed in the CF₃ stretching region has not yet been explained.

Microwave spectroscopy experiments are encouraged to experimentally confirm the geometry of the CCC conformer of chloroacetylacetone, especially methyl configuration and their rotational barrier. These results could definitely help in the understanding of the role of the methyl groups in the intramolecular hydrogen transfer process in these molecules.

More questions than answers appear after the study of chloromalonaldehyde. First, two open enol conformers (TTC and CTC) are observed along with the CCC conformer in the deposited sample. The first hypothesis is that they are already present in small amounts in the original crystalline solid. X-Rays diffraction experiments are proposed to test this hypothesis. Other experiments are already in progress to address this question. Second, a very clear splitting in two vibrational modes is observed in *para*-hydrogen matrix and not in neon matrix. Their origin is still unknown. We proposed to carry out experiments in another matrix like argon, and also in the gas phase, most probably in supersonic jets because of the low pressure of the molecule. In addition, the study of the deuterated isotopologue and of malonaldehyde in *para*-hydrogen matrix is also encouraged looking for possible tunneling splitting. Finally, the photodynamic of this system shows that it could be reversibly converted between three different main species by means of selective UV laser irradiation, and so could be a model for a molecular memory system.

In most of the cases the results obtained by the theoretical calculations have a good match with the experiments. We observed in double deuterated acetylacetone that anharmonic calculations did not show a big improvement compared to scaled harmonic calculations. In the case of halogenated analogs, the meta-GGA M06-2X functional give a better overall match with the experimental spectra than the hybrid B3LYP functional. A reasonable explanation is that M06-2X functional already includes terms to capture medium-range electron correlation, and it has been parametrized including non-covalent interacting molecules. For an improvement of the B3LYP performance the use of Grimme's dispersion terms like D3 are advisable to be tested. The specific mismatch of the theoretical and experimental spectra in the CCC conformer of chloroacetylacetone is still under analysis. Strong coupling effects due to a stronger hydrogen bond are considered as a possible explanation.

The study of intermolecular hydrogen bonded complexes in very small perturbative environments, like helium droplets, was also carried out. The propyne-water complex was analyzed in helium droplets. First, the ro-vibrational spectrum of propyne monomer was obtained and compared to literature. Then, the evolution of the signal intensity versus propyne pressure ("kinetics") allows to identified three bands corresponding to propyne multimers. The analysis of these bands allows to specifically assign two of them to dimers of propyne. Quantum chemical calculations need to be further developed to proposed the dimers structure. A new band was observed when water was introduced in the system, indicating the formation of a complex with propyne. The observed shift agrees with the obtained theoretical value for the **S1** configuration of the propyne-water complex, in which water acts as a proton donor. Nevertheless, further experiments need to be done to confirm the assignment and to discard complexes with propyne multimers. In addition, the study of the acetylene-water complex in helium droplets is recommended. Finally, the presence of ro-vibrational structure in the FT-IR spectrum of propyne trapped in *para*-hydrogen matrix indicates that the rotation of this molecule around the a axis is not hindered. Further experiments looking for the possible presence of Nuclear Spin Conversion are advisable.

CONCLUSIONS

References

- [1] G. R. Desiraju, P. S. Ho, L. Kloo, A. C. Legon, R. Marquardt, P. Metrangolo, P. Politzer, G. Resnati, and K. Rissanen, "Definition of the halogen bond (IUPAC Recommendations 2013)," *Pure Appl. Chem.*, vol. 85, no. 8, pp. 1711–1713, 2013.
- [2] G. C. Pimentel and A. McClellan, *The Hydrogen bond*. San Francisco and London: W. H. Freeman and Company, 1960.
- [3] E. Arunan, G. R. Desiraju, R. A. Klein, J. Sadlej, S. Scheiner, I. Alkorta, D. C. Clary, R. H. Crabtree, J. J. Dannenberg, P. Hobza, H. G. Kjaergaard, A. C. Legon, B. Mennucci, and D. J. Nesbitt, "Defining the hydrogen bond: An account (IUPAC Technical Report)*," *Pure Appl. Chem.*, no. July, pp. 1–18, 2011.
- [4] S. Bratoz and D. Hadzi, "Infrared spectra of molecules with hydrogen bonds," *J. Chem. Phys.*, vol. 27, no. 5, pp. 991–997, 1957.
- [5] G. Gilli and P. Gilli, *The nature of the hydrogen bond*. New York: Oxford University Press, 2009.
- [6] N. V Belova, H. Oberhammer, G. V Girichev, and S. A. Shlykov, "Tautomeric Properties and Gas-Phase Structure of 3-Chloro-2,4-pentanedione," *J. Phys.*, vol. 112, pp. 3209–3214, 2008.
- [7] M. M. Folkendt, B. E. Weiss-Lopez, J. P. Chauvel, and N. S. True, "Gas-Phase HNMR Studies of Keto-Enol Tautomerism of Acetylacetone, methyl Acetoacetate, and Ethyl Acetoacetate," *J. Phys. Chem. A*, vol. 89, no. 15, pp. 3347–3352, 1985.
- [8] R. Srinivasan, J. S. Feenstra, S. T. Park, S. Xu, and A. H. Zewail, "Direct determination of hydrogen-bonded structures in resonant and tautomeric reactions using ultrafast electron diffraction.," *J. Am. Chem. Soc.*, vol. 126, no. 8, pp. 2266–7, 2004.
- [9] R. R. Lozada-García, J. Ceponkus, W. Chin, M. Chevalier, and C. Crépin, "Acetylacetone in hydrogen solids: IR signatures of the enol and keto tautomers and UV induced tautomerization," *Chem. Phys. Lett.*, vol. 504, no. 4–6, pp. 142–147, 2011.
- [10] J. L. Burdett and M. T. Rogers, "Keto-Enol Tautomerism in β -Dicarbonyls Studied by Nuclear Magnetic Resonance Spectroscopy. I. Proton Chemical Shifts and Equilibrium Constants of Pure Compounds," *J. Am. Chem. Soc.*, vol. 86, no. 11, pp. 2105–2109, Jun. 1964.
- [11] S. J. Grabowski, "An estimation of strength of intramolecular hydrogen bonds - Ab initio and AIM studies," *J. Mol. Struct.*, vol. 562, no. 1–3, pp. 137–143, 2001.
- [12] N. Nagashima, S. Kudoh, M. Takayanagi, and M. Nakata, "UV-induced photoisomerization of acetylacetone and identification of less-stable isomers by low-temperature matrix-isolation infrared spectroscopy and density functional theory calculation," *J. Phys. Chem. A*, vol. 105, no. 48, pp. 10832–10838, 2001.
- [13] T. Ishida, F. Hirata, and S. Kato, "Thermodynamic analysis of the solvent effect on tautomerization of acetylacetone: An ab initio approach," *J. Chem. Phys.*, vol. 110, no. 8, p. 3938, 1999.
- [14] R. R. Lozada-García, J. Ceponkus, M. Chevalier, W. Chin, J.-M. Mestdagh, and C. Crépin, "Nuclear spin conversion to probe the methyl rotation effect on hydrogen-bond and vibrational dynamics," *Angew. Chemie - Int. Ed.*, vol. 51, no. 28, pp. 6947–6950, 2012.
- [15] R. R. Lozada-García, J. Ceponkus, M. Chevalier, W. Chin, J.-M. Mestdagh, and C. Crépin, "Photochemistry of acetylacetone isolated in parahydrogen matrices upon 266 nm irradiation," *Phys. Chem. Chem. Phys.*, vol. 14, no. 10, pp. 3450–9, 2012.
- [16] K. J. Muyskens, J. R. Alsum, T. A. Thielke, J. L. Boer, T. R. Heetderks, and M. A. Muyskens, "Photochemistry of UV-excited trifluoroacetylacetone and hexafluoroacetylacetone I: Infrared spectra of fluorinated methylfuranones formed by HF photoelimination," *J. Phys. Chem. A*, vol. 116, no. 50, pp. 12305–12313, 2012.

REFERENCES

- [17] G. C. Pimentel, F. M. G.-Tablas, J. Hartmann, and E. Whittle, "Photoelimination of HF by hexafluoroacetylacetone: A tandem laser study," *Int. J. Chem. Kinet.*, vol. 8, no. 6, pp. 877–882, Nov. 1976.
- [18] P. Roubin, T. Chiavassa, P. Verlaque, L. Pizzala, and H. Bodot, "FT-IR study of UV-induced isomerization of intramolecularly hydrogen-bonded carbonyl compounds isolated in xenon matrices," *Chem. Phys. Lett.*, vol. 175, no. 6, pp. 655–659, 1990.
- [19] N. Nagashima, S. Kudoh, and M. Nakata, "Infrared and UV-visible absorption spectra of hexafluoroacetylacetone in a low-temperature argon matrix. II. Detection of the $n\pi^*$ transition by monitoring IR spectral changes due to photoisomerization," *Chem. Phys. Lett.*, vol. 374, no. 1–2, pp. 67–73, 2003.
- [20] Y. Minoura, N. Nagashima, S. Kudoh, and M. Nakata, "Mechanism of UV-induced conformational changes among enol-type isomers of (trifluoroacetyl)acetone studied by low-temperature matrix-isolation infrared spectroscopy and density functional theory calculation," *J. Phys. Chem. A*, vol. 108, no. 12, pp. 2353–2362, 2004.
- [21] S. Coussan, C. Manca, Y. Ferro, and P. Roubin, "UV and IR photoisomerizations of an intramolecularly H-bonded molecule: acetylacetone trapped in nitrogen matrix," *Chem. Phys. Lett.*, vol. 370, pp. 118–125, 2003.
- [22] I. R. Dunkin, *Matrix-Isolation Techniques: A Practical Approach*. Oxford University Press, 1998.
- [23] T. Momose and T. Shida, "Matrix-Isolation Spectroscopy Using Solid Parahydrogen as the Matrix: Application to High-Resolution Spectroscopy, Photochemistry, and Cryochemistry," *Bulletin of the Chemical Society of Japan*, vol. 71, no. 1, pp. 1–15, 1998.
- [24] M. Okumura, M. C. Chan, and T. Oka, "High-resolution infrared spectroscopy of solid hydrogen: The tetrahexacontapole-Induced $\Delta J=6$ Transitions," *Phys. Rev. Lett.*, vol. 62, no. 1, pp. 32–35, 1989.
- [25] K. Nauta and R. E. Miller, "The Spectroscopy of Molecules and Unique Clusters in Superfluid Helium Droplets," in *Atomic and Molecular beams*, R. Campargue, Ed. Springer-Verlag Berlin Heidelberg GmbH, 2001, pp. 775–792.
- [26] L. Pauling, "The application of the quantum mechanics to the structure of the hydrogen molecule and the molecule-ion and the related problems," *Chem. Rev.*, vol. 5, no. 2, pp. 173–213, 1928.
- [27] P. Muller, "Glossary of terms used in physical organic chemistry," *Pure Appl. Chem.*, vol. 66, no. 5, pp. 1077–1184, 1994.
- [28] G. R. Desiraju, "A bond by any other name," *Angew. Chem. Int. Ed.*, vol. 50, no. 1, pp. 52–59, 2011.
- [29] D. Hadzi and H. W. Thompson, Eds., *Hydrogen bonding*. Pergamon Press.
- [30] G. Desiraju and S. Thomas, *The Weak Hydrogen Bond*. Oxford University Press, 2001.
- [31] C. S. Pérez and P. J. Ortiz, *Espectroscopía (Tomo I)*, 1st ed. La Habana: Ed. Félix Varela, 2011.
- [32] W. Urbaniak, K. Jurek, K. Witt, and G. Andrzej, "60 years of the Faculty of Chemical Technology and Engineering UT & LS in Bydgoszcz Properties and application of diketones and their derivatives," *Chemik*, no. 4, pp. 2–6, 2011.
- [33] M. José Mayoral, P. Cornago, R. M. Claramunt, and M. Cano, "Pyridyl and pyridiniumyl β -diketones as building blocks for palladium(ii) and allyl–palladium(ii) isomers. Multinuclear NMR structural elucidation and liquid crystal behaviour," *New J. Chem.*, vol. 35, no. 5, p. 1020, 2011.
- [34] G. G. Condorelli, S. Gennaro, and L. Fragala, "In-Situ Gas-Phase FTIR Monitoring of MOCVD Processes: LaF3 Films Using the Second Generation La(hfac)₃-diglyme Precursor," *Chem. Vap. Depos.*, vol. 6, no. 100 C, p. 185, 2000.
- [35] K. Hinsen and B. Roux, "Potential of mean force and reaction rates for proton transfer in acetylacetone," *J. Chem. Phys.*, vol. 106, no. 9, pp. 3567–3577, 1997.
- [36] I. Matanović, N. Došlić, and Z. Mihalić, "Exploring the potential energy surface for proton transfer in acetylacetone," *Chem. Phys.*, vol. 306, no. 1–3, pp. 201–207, 2004.

- [37] J. Mavri and J. Grdadolnik, "Proton transfer dynamics in acetylacetone: A mixed quantum-classical simulation of vibrational spectra," *J. Phys. Chem. A*, vol. 105, no. 10, pp. 2045–2051, 2001.
- [38] F. Dolati, S. F. Tayyari, M. Vakili, and Y. A. Wang, "Proton transfer in acetylacetone and its α -halo derivatives," *Phys. Chem. Chem. Phys.*, vol. 18, no. 1, pp. 344–350, 2016.
- [39] M. Temprado, M. V. Roux, P. Umnanant, H. Zhao, and J. S. Chickos, "The thermochemistry of 2,4-pentanedione revisited: Observance of a nonzero enthalpy of mixing between tautomers and its effects on enthalpies of formation," *J. Phys. Chem. B*, vol. 109, no. 25, pp. 12590–12595, 2005.
- [40] N. V. Belova, V. V. Sliznev, H. Oberhammer, and G. V. Girichev, "Tautomeric and conformational properties of beta-diketones," *J. Mol. Struct.*, vol. 978, no. 1–3, pp. 282–293, 2010.
- [41] N. Nagashima, S. Kudoh, M. Takayanagi, and M. Nakata, "UV-induced photoisomerization of acetylacetone and identification of less-stable isomers by low-temperature matrix-isolation infrared spectroscopy and density functional theory calculation," *J. Phys. Chem. A*, vol. 105, no. 48, pp. 10832–10838, 2001.
- [42] X. B. Chen, W. H. Fang, and D. L. Phillips, "Theoretical studies of the photochemical dynamics of acetylacetone: Isomerization, dissociation, and dehydration reactions," *J. Phys. Chem. A*, vol. 110, no. 13, pp. 4434–4441, 2006.
- [43] A. Trivella, T. N. Wassermann, J. M. Mestdagh, C. M. Tanner, F. Marinelli, P. Roubin, and S. Coussan, "New insights into the photodynamics of acetylacetone: isomerization and fragmentation in low-temperature matrices," *Phys. Chem. Chem. Phys.*, vol. 12, no. 29, p. 8151, 2010.
- [44] P. K. Verma, F. Koch, A. Steinbacher, P. Nuernberger, and T. Brixner, "Ultrafast UV-induced photoisomerization of intramolecularly H-bonded symmetric beta-diketones," *J. Am. Chem. Soc.*, vol. 136, no. 42, pp. 14981–14989, 2014.
- [45] I. R. J. and W. Ingemar, "Enthalpy of Vaporization of Organic Compounds at 25C. V. Acetylacetone," *Acta Chem. Scand.*, vol. 24, no. 2, pp. 589–592, 1970.
- [46] J. N. Spencer, E. S. Holmboe, M. R. Kirshenbaum, D. W. Firth, and P. B. Pinto, "Solvent effects on the tautomeric equilibrium of 2,4-pentanedione," *Can. J. Chem.*, vol. 60, pp. 1178–1182, 1982.
- [47] W. Caminati and J. U. Grabow, "The C_{2v} structure of enolic acetylacetone," *J. Am. Chem. Soc.*, vol. 128, no. 3, pp. 854–857, 2006.
- [48] S. A. Broadbent, L. A. Burns, C. Chatterjee, and P. H. Vaccaro, "Investigation of electronic structure and proton transfer in ground state acetylacetone," *Chem. Phys. Lett.*, vol. 434, no. 1–3, pp. 31–37, 2007.
- [49] I. Matanović and N. Došlić, "Infrared Spectroscopy of the intramolecular hydrogen bond in acetylacetone: A computational approach," *J. Phys. Chem. A*, vol. 109, no. 18, pp. 4185–4194, 2005.
- [50] A. Trivella, S. Coussan, T. Chiavassa, P. Theule, P. Roubin, and C. Manca, "Comparative study of structure and photo-induced reactivity of malonaldehyde and acetylacetone isolated in nitrogen matrices," *Low Temp. Phys.*, vol. 32, no. 11, pp. 1042–1049, 2006.
- [51] A. Trivella, P. Roubin, P. Theule, M. Rajzmann, S. Coussan, and C. Manca, "UV and IR photoisomerization of acetylacetone trapped in a nitrogen matrix," *J. Phys. Chem. A*, vol. 111, no. 16, pp. 3074–3081, 2007.
- [52] H. P. Upadhyaya, A. Kumar, and P. D. Naik, "Photodissociation dynamics of enolic-acetylacetone at 266, 248, and 193 nm: Mechanism and nascent state product distribution of OH," *J. Chem. Phys.*, vol. 118, pp. 2590–2598, 2003.
- [53] S. Xu, S. T. Park, J. S. Feenstra, R. Srinivasan, and A. H. Zewail, "Ultrafast electron diffraction: Structural dynamics of the elimination reaction of acetylacetone," *J. Phys. Chem. A*, vol. 108, no. 32, pp. 6650–6655, 2004.
- [54] L. Poisson, P. Roubin, S. Coussan, B. Soep, and J. M. Mestdagh, "Ultrafast dynamics of acetylacetone (2,4-pentanedione) in the S_2 state," *J. Am. Chem. Soc.*, vol. 130, no. 10, pp. 2974–2983, 2008.
- [55] H. Ogoshi and K. Nakamoto, "Normal-Coordinate Analyses of Hydrogen-Bonded Compounds. V. The Enol Forms of Acetylacetone and Hexafluoroacetylacetone," *J. Chem. Phys.*, vol. 45, no. 8, pp. 3113–3120, 1966.
- [56] S. F. Tayyari, T. Zeegers-Huyskens, and J. L. L. Wood, "Spectroscopic study of hydrogen bonding in the enol form

REFERENCES

- of β -diketones-I. Vibrational assignment and strength of the bond," *Spectrochim. Acta Part A Mol. Spectrosc.*, vol. 35A, no. 12, pp. 1265–1275, 1979.
- [57] S. F. Tayyari, T. Zeegers-Huyskens, J. L. L. Wood, T. Th. Zeegers-Huyskens, and J. L. L. Wood, "Spectroscopic study of hydrogen bonding in the enol form of β -diketones-II. Symmetry of the hydrogen bond," *Spectrochim. Acta Part A Mol. Spectrosc.*, vol. 35, no. 12, pp. 1289–1295, 1979.
- [58] S. F. Tayyari and F. Milani-nejad, "Vibrational assignment of acetylacetone," *Spectrochim. Acta Part a-Molecular Biomol. Spectrosc.*, vol. 56, no. 14, pp. 2679–2691, 2000.
- [59] M. R. Johnson, N. H. Jones, A. Geis, A. J. Horsewill, and H. P. Trommsdorff, "Structure and dynamics of the keto and enol forms of acetylacetone in the solid state," *J. Chem. Phys.*, vol. 116, no. 13, pp. 5694–5700, 2002.
- [60] W. M. Coleman III and B. M. Gordon, "Examinations of the Matrix Isolation Fourier Transform Infrared Spectra of Organic Compounds : Part IX," *Appl. Spectrosc.*, vol. 42, no. 4, pp. 666–670, 1988.
- [61] Z. Yoshida, H. Ogoshi, and T. Tokumitsu, "Intramolecular hydrogen bond in enol form of 3-substituted-2,4-pentanedione," *Tetrahedron*, vol. 26, no. 24, pp. 5691–5697, 1970.
- [62] S. F. Tayyari, M. Zahedi-Tabrizi, R. Afzali, S. Laleh, H. A. Mirshahi, and Y. A. Wang, "Structure and vibrational assignment of the enol form of 3-chloro-pentane-2,4-dione," *J. Mol. Struct.*, vol. 873, no. 1–3, pp. 79–88, 2008.
- [63] A. F. Jalbout, M. Ali Naseri, M. Fazli, H. Raissi, M. Rezaei, A. Nowroozi, and A. de Leon, "Molecular structure and vibrational assignment of α -chloro acetylacetone: A density functional theory study," *Int. J. Quantum Chem.*, vol. 109, no. 7, pp. 1481–1496, 2009.
- [64] G. Malandrino, R. Lo Nigro, C. Benelli, F. Castelli, and I. L. Fragala, "Volatile Cell Hexafluoroacetylacetonate Glyme Adducts as Promising Precursors for the MOCVD of CeO₂ Thin Films," *Chem. Vap. Depos.*, vol. 6, no. 5, p. 233, 2000.
- [65] A. L. Andreassen, D. Zebelman, and S. H. Bauer, "Hexafluoroacetylacetone and Hexafluoroacetic Anhydride," *J. Am. Chem. Soc.*, vol. 93, no. 5, pp. 1148–1152, 1971.
- [66] K. Iijima, Y. Tanaka, and S. Onuma, "Internal rotation of trifluoromethyl groups in hexafluoroacetylacetone," *J. Mol. Struct.*, vol. 268, no. 1–3, pp. 315–318, 1992.
- [67] L. Evangelisti, S. Tang, B. Velino, B. M. Giuliano, S. Melandri, and W. Caminati, "Hexafluoroacetylacetone: A 'rigid' molecule with an enolic Cs shape," *Chem. Phys. Lett.*, vol. 473, no. 4–6, pp. 247–250, May 2009.
- [68] P. Burk and I. a. Koppel, "An AM1 and PM3 study of hexafluoroacetylacetone," *J. Mol. Struct. THEOCHEM*, vol. 282, no. 3, pp. 277–282, 1993.
- [69] G. Buemi, "Ab initio DFT study of the hydrogen bridges in hexafluoro-acetylacetone, trifluoro-acetylacetone and some 3-substituted derivatives," *J. Mol. Struct. THEOCHEM*, vol. 499, pp. 21–34, 2000.
- [70] C. Chatterjee, C. D. Incarvito, L. A. Burns, and P. H. Vaccaro, "Electronic structure and proton transfer in ground-state hexafluoroacetylacetone," *J. Phys. Chem. A*, vol. 114, no. 24, pp. 6630–6640, 2010.
- [71] H. Nakanishi, H. Morita, and S. Nagakura, "Charge-transfer character in the intramolecular hydrogen bond: vacuum ultraviolet spectra of acetylacetone and its fluoro derivatives," *Bull. Chem. Soc. Jpn.*, vol. 51, no. 6, pp. 1723–1729, 1978.
- [72] N. Nagashima, S. Kudoh, and M. Nakata, "Infrared and UV-visible absorption spectra of hexafluoroacetylacetone in a low-temperature argon matrix. I. Structure of a non-chelated enol-type isomer," *Chem. Phys. Lett.*, vol. 374, no. 1–2, pp. 59–66, 2003.
- [73] J. E. Bassett and E. Whittle, "The photochemistry of hexafluoroacetylacetone in the vapour phase. Occurrence of a novel HF elimination reaction," *Int. J. Chem. Kinet.*, vol. 8, no. 6, pp. 859–876, 1976.
- [74] M.-C. Yoon, Y. S. Choi, and S. K. Kim, "Photodissociation dynamics of acetylacetone: The OH product state distribution," *J. Chem. Phys.*, vol. 110, no. 24, p. 11850, 1999.
- [75] B. Ómarsson, S. Engmann, and O. Ingólfsson, "Dissociative electron attachment to the complexation ligands

- hexafluoroacetylacetone, trifluoroacetylacetone and acetylacetone; a comparative experimental and theoretical study," *RSC Adv.*, vol. 4, no. 63, p. 33222, 2014.
- [76] B. Zarranz, A. Jaso, I. Aldana, and A. Monge, "Synthesis and anticancer activity evaluation of new 2-alkylcarbonyl and 2-benzoyl-3-trifluoromethyl-quinoxaline 1,4-di-N-oxide derivatives," *Bioorganic Med. Chem.*, vol. 12, no. 13, pp. 3711–3721, 2004.
- [77] M. S. Gordon and R. D. Koob, "An INDO Investigation of the Structure and Bonding of Acetylacetone and Trifluoroacetylacetone," *J. Am. Chem. Soc.*, vol. 433, no. 10, pp. 5863–5867, 1973.
- [78] H. Raissi, A. Nowroozi, M. Roozbeh, and F. Farzad, "Molecular structure and vibrational assignment of (trifluoroacetyl) acetone: A density functional study," *J. Mol. Struct.*, vol. 787, no. 1–3, pp. 148–162, 2006.
- [79] M. Zahedi-Tabrizi, F. Tayyari, Z. Moosavi-Tekyeh, A. Jalali, and S. F. Tayyari, "Structure and vibrational assignment of the enol form of 1,1,1-trifluoro-2,4-pentanedione," *Spectrochim. Acta - Part A Mol. Biomol. Spectrosc.*, vol. 65, no. 2, pp. 387–396, 2006.
- [80] V. V. Sliznev, S. B. Lapshina, and G. V. Girichev, "Ab initio structure investigation of the enol forms of β -diketones," *J. Struct. Chem.*, vol. 43, no. 1, pp. 47–55, 2002.
- [81] L. B. Favero, L. Evangelisti, B. Velino, and W. Caminati, "Morphing the Internal Dynamics of Acetylacetone by CH 3 \rightarrow CF 3 Substitutions. The Rotational Spectrum of Trifluoroacetylacetone," *J. Phys. Chem. A*, vol. 118, no. 24, pp. 4243–4248, Jun. 2014.
- [82] M. T. do N. Varella, Y. Arasaki, H. Ushiyama, V. McKoy, and K. Takatsuka, "Time-resolved photoelectron spectroscopy of proton transfer in the ground state of chloromalonaldehyde: Wave-packet dynamics on effective potential surfaces of reduced dimensionality," *J. Chem. Phys.*, vol. 124, no. 15, 2006.
- [83] M. T. do N. Varella, Y. Arasaki, H. Ushiyama, K. Takatsuka, K. Wang, and V. McKoy, "Real-time observation of intramolecular proton transfer in the electronic ground state of chloromalonaldehyde: an ab initio study of time-resolved photoelectron spectra," *J. Chem. Phys.*, vol. 126, no. 5, p. 54303, 2007.
- [84] Y. Arasaki, K. Yamazaki, M. T. do N. Varella, and K. Takatsuka, "Real-time observation of ground state proton transfer: A model study," *Chem. Phys.*, vol. 311, no. 3, pp. 255–268, 2005.
- [85] D. T. Halfen, A. J. Apponi, N. Woolf, R. Polt, and L. M. Ziurys, "A Systematic Study of Glycolaldehyde in Sagittarius B2(N) at 2 and 3 mm: Criteria for Detecting Large Interstellar Molecules," *Astrophys. J.*, vol. 639, no. 1, pp. 237–245, 2006.
- [86] T. J. Johnson, R. L. Sams, L. T. M. Profeta, S. K. Akagi, I. R. Burling, R. J. Yokelson, and S. D. Williams, "Quantitative IR spectrum and vibrational assignments for glycolaldehyde vapor: Glycolaldehyde measurements in biomass burning plumes," *J. Phys. Chem. A*, vol. 117, no. 20, pp. 4096–4107, 2013.
- [87] J. Altnöder, J. J. Lee, K. E. Otto, and M. A. Suhm, "Molecular Recognition in Glycolaldehyde, the Simplest Sugar: Two Isolated Hydrogen Bonds Win Over One Cooperative Pair," *ChemistryOpen*, vol. 1, no. 6, pp. 269–275, 2012.
- [88] J. Ceponkus, W. Chin, M. Chevalier, M. Broquier, A. Limongi, and C. Crépin, "Infrared study of glycolaldehyde isolated in parahydrogen matrix," *J. Chem. Phys.*, vol. 133, no. 9, pp. 1–7, 2010.
- [89] W. Chin, M. Chevalier, R. Thon, R. Pollet, J. Ceponkus, and C. Crépin, "Photochemistry of glycolaldehyde in cryogenic matrices," *J. Chem. Phys.*, vol. 140, no. 22, p. 224319, 2014.
- [90] E. Es-Sebbar, A. Jolly, Y. Benilan, and A. Farooq, "Quantitative mid-infrared spectra of allene and propyne from room to high temperatures," *J. Mol. Spectrosc.*, vol. 305, pp. 10–16, 2014.
- [91] D. Zhao and H. Linnartz, "The high-resolution infrared spectrum of the $\nu_3+\nu_8$ combination band of jet-cooled propyne," *Chem. Phys. Lett.*, vol. 595–596, pp. 256–259, 2014.
- [92] G. N. Lewis and D. Lipkin, "Reversible photochemical processes in rigid media: The dissociation of organic molecules into radicals and ions," *J. Am. Chem. Soc.*, vol. 64, no. 12, pp. 2801–2808, 1942.
- [93] T. Bally, "Matrix Isolation," in *Reactive Intermediate Chemistry*, R. A. Moss, M. S. Platz, and M. Jones, Eds. Wiley

REFERENCES

- Interscience, 2004, pp. 797–845.
- [94] E. Whittle, D. A. Dows, and G. C. Pimentel, "Matrix Isolation Method for the Experimental Study of Unstable Species," vol. 1943, pp. 22–24, 1954.
- [95] I. Norman and G. Porter, "Trapped Atoms and Radicals in a Glass 'Cage,'" *Nature*, vol. 174, pp. 508–509, 1954.
- [96] M. E. Jacox, "The spectroscopy of molecular reaction intermediates trapped in the solid rare gases," *Chem. Soc. Rev.*, vol. 31, pp. 108–115, 2002.
- [97] V. E. Bondybey, A. M. Smith, and J. Agreiter, "New Developments in Matrix Isolation Spectroscopy," *Chem. Rev.*, vol. 96, no. 6, pp. 2113–2134, Oct. 1996.
- [98] C. Araujo-Andrade, I. Reva, and R. Fausto, "Tetrazole acetic acid: tautomers, conformers, and isomerization," *J. Chem. Phys.*, vol. 140, no. 6, p. 64306, 2014.
- [99] H. Tanskanen, S. Johansson, A. Lignell, L. Khriachtchev, and M. Räsänen, "Matrix isolation and ab initio study of the HXeCCH \cdots CO₂ complex," *J. Chem. Phys.*, vol. 127, no. 15, p. 154313, 2007.
- [100] G. K. Moortgat, A. J. Barnes, G. Le Bras, and J. R. Sodeau, *Low-Temperature Chemistry of the Atmosphere*. Berlin, Heidelberg: Springer Berlin Heidelberg, 1994.
- [101] S. P. Willson and L. Andrews, "Matrix Isolation Infrared Spectroscopy," *Low Temp. High Press. Sampl. Tech.*, pp. 1–10, 2002.
- [102] J. E. Espidel and R. K. Harris, "Cryogenic NMR: spectrometer design for studies of matrix-isolated materials," *Magn. Reson. Chem.*, vol. 28, no. Spec. Issue, pp. S15–S19, 1990.
- [103] C. Merten and Y. Xu, "Matrix isolation-vibrational circular dichroism spectroscopy of 3-butyn-2-ol and its binary aggregates," *ChemPhysChem*, vol. 14, no. 1, pp. 213–219, 2013.
- [104] R. Thon, W. Chin, J.-P. Galaup, A. Ouvrard, B. Bourguignon, and C. Crépin, "Vibrational Perturbations of W(CO)₆ Trapped in a Molecular Lattice Probed by Linear and Nonlinear Spectroscopy," *J. Phys. Chem. A*, vol. 117, no. 34, pp. 8145–8156, Aug. 2013.
- [105] N. H. Balshaw, "Practical Cryogenics: an introduction to laboratory cryogenics," no. 1865, p. 96, 2001.
- [106] G. Ventura and L. Risegari, *The art of cryogenics*, First edit. Elsevier Ltd, 2008.
- [107] R. Radebaugh, "Cryocoolers: the state of the art and recent developments.," *J. Phys. Condens. Matter*, vol. 21, no. 16, p. 164219, 2009.
- [108] W. E. Gifford, "The Gifford-McMahon Cycle," *Advances in Cryogenic Engineering*. pp. 1–11, 1966.
- [109] H. O. McMahon and W. E. Gifford, "Closed-cycle helium refrigeration," *Solid. State. Electron.*, vol. 1, no. 4, pp. 273–278, 1960.
- [110] E. D. Becker and G. C. Pimentel, "Spectroscopic Studies of Reactive Molecules by the Matrix Isolation Method," *J. Chem. Phys.*, vol. 25, no. 2, p. 224, 1956.
- [111] "<http://webbook.nist.gov/chemistry/>."
- [112] W. M. Haynes, B. Thomas, and D. R. Lide, Eds., *CRC Handbook of Chemistry and Physics, 96th Edition*, 96th ed. Taylor & Francis, CRC Press, 2006.
- [113] R. Kolos, "Carbon-nitrogen chain molecules in the laboratory and in interstellar medium," Institute of Physical Chemistry of the Polish Academy of Sciences, 2003.
- [114] G. M. Barrow, *Introduction to Molecular Spectroscopy*, Internatio. McGraw-Hill, 1962.
- [115] A. Einstein, "Zur Quantentheorie der Strahlung," *Mitteilungen der Phys. Gesellschaft Zürich*, vol. 18, no. 17, pp. 47–62, 1916.
- [116] A. Yariv, *Quantum Electronics*, 2nd Editio. John Wiley & Sons inc, 1975.
- [117] J. E. Lennard-Jones, "The electronic structure of some diatomic molecules," *Trans. Faraday Soc.*, vol. 25, no.

- 668, pp. 668–686, 1929.
- [118] W. Kutzelnigg, “Friedrich Hund and Chemistry,” *Angew. Chemie Int. Ed. English*, vol. 35, no. 6, pp. 572–586, 1996.
- [119] G. Herzberg, *Molecular spectra and molecular structure: II. Infrared and Raman spectra of polyatomic molecules*, 7th ed. Van Nostrand Company Inc., 1956.
- [120] J. Chalmers and P. Griffiths, *Handbook of vibrational spectroscopy: theory and instrumentation*. Wiley, 2002.
- [121] D. Mayo, F. Miller, and R. Hannah, *Course Notes On The Interpretation Of Infrared And Raman Spectra*. Hoboken, New Jersey: Wiley Interscience, 2003.
- [122] J. R. Ferraro, K. Nakamoto, and C. W. Brown, *Introductory Raman Spectroscopy*. Elsevier Science, 2003.
- [123] E. B. Wilson, J. C. Decius, and P. C. Cross, *MOLECULAR VIBRATIONS: The Theory of Infrared and Raman Vibrational Spectra*, vol. 102, no. 9. McGraw-Hill, 1955.
- [124] A. J. Barnes, W. J. Orville-Thomas, A. Müller, and R. Gaufres, Eds., *Matrix isolation Spectroscopy*. D. Reidel Publishing Company, 1980.
- [125] D. Boal, G. Briggs, H. Hüber, G. A. Ozin, E. A. Robinson, and A. Vander Voet, “Matrix Isolation Laser Raman Spectroscopy in Inorganic Chemistry,” *Nat. Phys. Sci.*, vol. 231, pp. 174–175, 1971.
- [126] M. S. Baird, I. R. Dunkin, N. Hacker, M. Poliakoff, and J. J. Turner, “Cyclopentadienylidene. A matrix isolation study exploiting photolysis with unpolarized and plane-polarized light,” *J. Am. Chem. Soc.*, vol. 103, no. 17, pp. 5190–5, 1981.
- [127] M. E. Jacox and D. E. Milligan, “Matrix isolation study of the vacuum ultraviolet photolysis of allene and methylacetylene. Vibrational and electronic spectra of the species C₃, C₃H, C₃H₂, and C₃H₃,” *Chem. Phys.*, vol. 4, no. 1, pp. 45–61, Apr. 1974.
- [128] M. Bahou, P. Das, Y.-F. Lee, Y.-J. Wu, and Y.-P. Lee, “Infrared spectra of free radicals and protonated species produced in para-hydrogen matrices,” *Phys. Chem. Chem. Phys.*, vol. 16, no. 6, pp. 2200–10, 2014.
- [129] I. F. Silvera, “The solid molecular hydrogens in the condensed phase: Fundamentals and static properties,” *Rev. Mod. Phys.*, vol. 52, no. 2, pp. 393–452, 1980.
- [130] K. Marushkevich, L. Khriachtchev, and M. Räsänen, “High-energy conformer of formic acid in solid neon: Giant difference between the proton tunneling rates of cis monomer and trans-cis dimer,” *J. Chem. Phys.*, vol. 126, no. 24, 2007.
- [131] D. T. Anderson and L. O. Paulson, “High-resolution vibrational spectroscopy of trans-formic acid in solid parahydrogen,” *J. Phys. Chem. A*, vol. 113, no. 9, pp. 1770–1778, 2009.
- [132] M. E. Fajardo and S. Tam, “Rapid vapor deposition of millimeters thick optically transparent parahydrogen solids for matrix isolation spectroscopy,” *J. Chem. Physics*. 3/8/1998, vol. 108, no. 10, p. 4237. 5p. 1 Diagram, 4237.
- [133] L. Khriachtchev, *Physics and Chemistry at Low Temperatures*. 2011.
- [134] M. J. Frisch, G. W. Trucks, H. B. Schlegel, G. E. Scuseria, M. A. Robb, J. R. Cheeseman, G. Scalmani, V. Barone, B. Mennucci, G. A. Petersson, H. Nakatsuji, M. Caricato, X. Li, H. H. P., A. F. Izmaylov, J. Bloino, G. Zheng, D. J. Sonnenb, M. Hada, M. Ehara, K. Toyota, R. Fukuda, J. Hasegawa, M. Ishida, T. Nakajima, Y. Honda, O. Kitao, H. Nakai, T. Vreven, J. Montgomery, J. A., J. E. Peralta, F. Ogliaro, M. Bearpark, J. J. Heyd, E. Brothers, K. N. Kudin, V. N. Staroverov, R. Kobayashi, J. Normand, K. Raghavachari, A. Rendell, J. C. Burant, S. S. Iyengar, J. Tomasi, M. Cossi, N. Rega, J. M. Millam, M. Klene, J. E. Knox, J. B. Cross, V. Bakken, C. Adamo, J. Jaramillo, R. Gomperts, R. E. Stratmann, O. Yazyev, A. J. Austin, R. Cammi, C. Pomelli, J. W. Ochterski, R. L. Martin, K. Morokuma, V. G. Zakrzewski, G. A. Voth, P. Salvador, J. J. Dannenberg, S. Dapprich, A. D. Daniels, O. Farkas, J. B. Foresman, J. V. Ortiz, J. Cioslowski, D. J. Fox, R. D. O. Gaussian 09, M. J. Frisch, G. W. Trucks, H. B. Schlegel, G. E. Scuseria, M. A. Robb, J. R. Cheeseman, G. Scalmani, V. Barone, B. Mennucci, G. A. Petersson, H. Nakatsuji, M. Caricato, X. Li, H. H. P., A. F. Izmaylov, J. Bloino, G. Zheng, D. J. Sonnenb, M. Hada, M. Ehara, K. Toyota, R. Fukuda, J. Hasegawa, M. Ishida, T. Nakajima, Y. Honda, O. Kitao, H. Nakai, T. Vreven, J. Montgomery, J. A., J. E. Peralta, F. Ogliaro, M. Bearpark, J. J. Heyd, E. Brothers, K. N. Kudin, V. N. Staroverov, R. Kobayashi, J. Normand, K. Raghavachari, A.

REFERENCES

- Rendell, J. C. Burant, S. S. Iyengar, J. Tomasi, M. Cossi, N. Rega, J. M. Millam, M. Klene, J. E. Knox, J. B. Cross, V. Bakken, C. Adamo, J. Jaramillo, R. Gomperts, R. E. Stratmann, O. Yazyev, A. J. Austin, R. Cammi, C. Pomelli, J. W. Ochterski, R. L. Martin, K. Morokuma, V. G. Zakrzewski, G. A. Voth, P. Salvador, J. J. Dannenberg, S. Dapprich, A. D. Daniels, O. Farkas, J. B. Foresman, J. V. Ortiz, J. Cioslowski, D. J. Fox, and 2009. Gaussian, Inc., Wallingford CT, "Gaussian 09, Revision D.01." Gaussian, Inc., Wallingford CT, 2009., 2009.
- [135] A. P. Hines, C. M. Dawson, R. H. McKenzie, and G. J. Milburn, "Entanglement and bifurcations in Jahn-Teller models," *Phys. Rev. A - At. Mol. Opt. Phys.*, vol. 70, no. 2, pp. 1–12, 2004.
- [136] G. A. Worth and L. S. Cederbaum, "BEYOND BORN -OPPENHEIMER : Molecular Dynamics Through a Conical Intersection," *Annu Rev. Phys. Chem.*, vol. 55, pp. 127–158, 2004.
- [137] A. Szabo and N. S. Ostlund, "Modern Quantum Chemistry: Introduction to Advanced Electronic Structure Theory," *Introduction to Advanced Electronic Structure Theory*. Genereal Publishing Company, p. 480, 1996.
- [138] C. J. Cramer, *Essentials of Computational Chemistry Theories and Models*, Second edi., vol. 42, no. 2. John Wiley & Sons, Ltd, 2004.
- [139] P. W. Atkins and R. S. Friedman, *Molecular Quantum Mechanics*, 5th ed. Oxford University Press, 2005.
- [140] I. N. Levine, *Quantum Chemistry*, 7th ed. Pearson, 2014.
- [141] S. F. Boys, "Electronic wave functions. I. A general method of calculation for the stationary states of any molecular system," *Proc. R. Soc. London, Ser. A Math. Phys. Eng. Sci.*, vol. 200, pp. 542–554, 1950.
- [142] D. C. Young, *COMPUTATIONAL CHEMISTRY A Practical Guide for Applying Techniques to Real-World Problems*, vol. 9, no. 3. John Wiley & Sons inc, 2001.
- [143] Frank Jensen, "Introduction to Computational Chemistry," pp. 1–630, 2006.
- [144] P. Hohenberg and W. Kohn, "Inhomogeneous electron gas," *Phys. Rev. B*, no. 5, pp. 865–871, 1964.
- [145] W. Kohn and L. J. Sham, "Self-Consistent Equations Including Exchange and Correlation Effects," *Phys. Rev.*, vol. 140, no. 4A, pp. A1133–A1138, 1965.
- [146] V. P. Gupta, *Principles and Applications of Quantum Chemistry*. Elsevier Inc., 2015.
- [147] S. H. Vosko, L. Wilk, and M. Nusair, "Accurate spin-dependent electron liquid correlation energies for local spin density calculations: a critical analysis," *Can. J. Phys.*, vol. 58, no. 8, pp. 1200–1211, 1980.
- [148] C. Lee, W. Yang, and R. G. Parr, "Development of the Colle-Salvetti correlation-energy formula into a functional of the electron density," *Phys. Rev. B*, vol. 37, no. 2, pp. 785–789, Jan. 1988.
- [149] A. D. Becke, "Density-functional thermochemistry. III. The role of exact exchange," *J. Chem. Phys.*, vol. 98, no. 7, p. 5648, 1993.
- [150] P. J. Stephens, F. J. Devlin, C. F. Chabalowski, and M. J. Frisch, "Ab Initio Calculation of Vibrational Absorption and Circular Dichroism Spectra Using Density Functional Force Fields," *J. Phys. Chem.*, vol. 98, no. 45, pp. 11623–11627, 1994.
- [151] Y. Zhao and D. G. Truhlar, "The M06 suite of density functionals for main group thermochemistry, thermochemical kinetics, noncovalent interactions, excited states, and transition elements: Two new functionals and systematic testing of four M06-class functionals and 12 other function," *Theor. Chem. Acc.*, vol. 120, no. 1–3, pp. 215–241, 2008.
- [152] R. F. W. Bader, "A Quantum Theory of Molecular Structure and Its Applcations," *Chem. Rev. (Washington, D. C.)*, vol. 91, p. 893, 1991.
- [153] C. Matta and R. Boyd, Eds., *The quantum theory of atoms in molecules*. Wiley-VCH, 2007.
- [154] B. Silvi and A. Savin, "Classification of Chemical-Bonds Based on Topological Analysis of Electron Localization Functions," *Nature*, vol. 371, no. 6499, pp. 683–686, 1994.
- [155] A. D. Becke and K. E. Edgecombe, "A simple measure of electron localization in atomic and molecular systems,"

- J. Chem. Phys.*, vol. 92, pp. 5397–5403, 1990.
- [156] C. Narth, Z. Maroun, R. A. Boto, R. Chaudret, M.-L. Bonnet, J.-P. Piquemal, and J. Contreras-García, “A complete NCI perspective: From New Bonds to Reactivity,” in *Applications of Topological Methods in Molecular Chemistry*, R. Chauvin, Ed. Springer International, 2016, pp. 491–527.
- [157] E. R. Johnson, S. Keinan, P. Mori-Sanchez, J. Contreras-Garcia, A. Cohen, and W. Yang, “Revealing Noncovalent Interactions,” *J. Am. Chem. Soc.*, vol. 132, no. 18, pp. 6498–6506, 2009.
- [158] R. A. Boto, J. Contreras-García, J. Tierny, and J.-P. Piquemal, “Interpretation of the Reduced Density Gradient,” *Mol. Phys.*, vol. 114, no. 7–8, pp. 1406–1414, 2016.
- [159] R. Chaudret, B. de Courcy, J. Contreras-García, E. Gloaguen, A. Zehnacker-Rentien, M. Mons, and J.-P. Piquemal, “Unraveling non-covalent interactions within flexible biomolecules: from electron density topology to gas phase spectroscopy,” *Phys. Chem. Chem. Phys.*, vol. 16, no. 21, pp. 9876–91, 2014.
- [160] S. D. Schrøder, J. H. Wallberg, J. A. Kroll, Z. Maroun, V. Vaida, and H. G. Kjaergaard, “Intramolecular Hydrogen Bonding in Methyl Lactate,” *J. Phys. Chem. A*, vol. 119, no. 37, pp. 9692–9702, Sep. 2015.
- [161] I. M. Alecu, J. Zheng, Y. Zhao, and D. G. Truhlar, “Computational thermochemistry: Scale factor databases and scale factors for vibrational frequencies obtained from electronic model chemistries,” *J. Chem. Theory Comput.*, vol. 6, no. 9, pp. 2872–2887, 2010.
- [162] V. Barone, “Anharmonic vibrational properties by a fully automated second-order perturbative approach,” *J. Chem. Phys.*, vol. 122, no. 1, p. 14108, Jan. 2005.
- [163] K. K. Irikura, R. D. Johnson, and R. N. Kacker, “Uncertainties in scaling factors for ab initio vibrational frequencies,” *J. Phys. Chem. A*, vol. 109, no. 37, pp. 8430–8437, 2005.
- [164] V. Barone, J. Bloino, C. A. Guido, and F. Lipparini, “A fully automated implementation of VPT2 Infrared intensities,” *Chem. Phys. Lett.*, vol. 496, no. 1–3, pp. 157–161, 2010.
- [165] P. L. Polavarapu, “Ab initio vibrational Raman and Raman optical activity spectra,” *J. Phys. Chem.*, vol. 94, no. 21, pp. 8106–8112, 1990.
- [166] P. L. Polavarapu, *Vibrational Spectra: Principles and Applications with Emphasis on Optical Activity*. Elsevier science B.V., 1998.
- [167] G. Keresztury, S. Holly, G. Besenyey, J. Varga, A. Wang, and J. R. Durig, “Vibrational spectra of monothiocarbamates-II. IR and Raman spectra, vibrational assignment, conformational analysis and ab initio calculations of S-methyl-N,N-dimethylthiocarbamate,” *Spectrochimica Acta Part A: Molecular Spectroscopy*, vol. 49, no. 13–14, pp. 2007–2026, 1993.
- [168] D. Michalska and R. Wysokiński, “The prediction of Raman spectra of platinum(II) anticancer drugs by density functional theory,” *Chem. Phys. Lett.*, vol. 403, no. 1–3, pp. 211–217, 2005.
- [169] D. Michalska, D. C. Bienko, A. J. Abkowitz-Bienko, and Z. Latajka, “Density functional, Hartree-Fock, and MP2 studies on the vibrational spectrum of phenol,” *J. Phys. Chem.*, vol. 100, no. 45, pp. 17786–17790, 1996.
- [170] P. Sinha, S. E. Boesch, C. Gu, R. A. Wheeler, and A. K. Wilson, “Harmonic Vibrational Frequencies: Scaling Factors for HF, B3LYP, and MP2 Methods in Combination with Correlation Consistent Basis Sets,” *J. Phys. Chem. A*, vol. 108, no. 42, pp. 9213–9217, Oct. 2004.
- [171] K. B. Lipkowitz and D. B. Boyd, *Reviews in Computational Chemistry, II*, vol. 3, no. 11. 1997.
- [172] E. G. Lewars, *Computational Chemistry: Introduction to the theory and applications of molecular and quantum mechanics*, Second Edi. Springer, 2011.
- [173] C. J. Cramer and D. G. Truhlar, “A universal approach to solvation modeling,” *Acc. Chem. Res.*, vol. 41, no. 6, 2008.
- [174] P. Piecuch, K. Kowalski, I. S. O. Pimienta, and M. J. Mcguire, *Recent advances in electronic structure theory: Method of moments of coupled-cluster equations and renormalized coupled-cluster approaches*, vol. 21, no. 4. 2010.

REFERENCES

- [175] K. B. Wiberg, R. E. Stratmann, and M. J. Frisch, "A time-dependent density functional theory study of the electronically excited states of formaldehyde, acetaldehyde and acetone," *Chem. Phys. Lett.*, vol. 297, no. November, pp. 60–64, 1998.
- [176] J. B. Foresman and Æ. Frisch, *Exploring chemistry with electronic structure methods: a guide to using Gaussian*, 2nd ed. Gaussian Inc., 1996.
- [177] D. G. Truhlar and B. C. Garrett, "Dynamical Bottlenecks and Semiclassical Tunneling Paths for Chemical Reactions," *Journal de Chimie Physique et de Physico-Chimie Biologique*, vol. 84, pp. 365–369, 1987.
- [178] R. P. Bell, *The tunnel effect in Chemistry*. Boston, MA: University Press, Cambridge, 1980.
- [179] "http://www.chemcraftprog.com." .
- [180] J. Contreras-García, E. R. Johnson, S. Keinan, R. Chaudret, J.-P. Piquemal, D. N. Beratan, and W. Yang, "NCIPLOT: A Program for Plotting Noncovalent Interaction Regions," *J. Chem. Theory Comput.*, vol. 7, no. 3, pp. 625–632, Mar. 2011.
- [181] A. D. Becke, "Density-functional thermochemistry. IV. A new dynamic correlation functional and implications for exact-exchange mixing," *J. Chem. Phys.*, vol. 104, no. 3, pp. 1040–1046, 1996.
- [182] C. Y. Peng, P. Y. Ayala, H. B. Schlegel, and M. J. Frisch, "Using redundant internal coordinates to optimize equilibrium geometries and transition states," *J. Comput. Chem.*, vol. 17, pp. 49–56, 1996.
- [183] H. B. Schlegel, "Optimization of Equilibrium Geometries and Transition Structures," *Adv. Chem. Phys.*, vol. 3, no. 2, pp. 249–286, 2007.
- [184] H. B. Schlegel, "Estimating the Hessian for gradient type geometry optimisations," *Theor. Chem. Acc.*, vol. 66, p. 333, 1984.
- [185] E. Runge and E. K. U. Gross, "Density-functional theory for time-dependent systems," *Phys. Rev. Lett.*, vol. 52, no. 12, pp. 997–1000, 1984.
- [186] P. Kin-Kin Dea, "The Nature of the intramolecular hydrogen bond in the enol tautomer of 2,4-pentanedione," California Institute of Technology, 1972.
- [187] *Catalogue Aldrich Chemie* .
- [188] M. Petitjean, E. Reyès-Pérez, D. Pérez, P. Mirabel, and S. Le Calvé, "Vapor pressure measurements of hydroxyacetaldehyde and hydroxyacetone in the temperature range (273 to 356) K," *J. Chem. Eng. Data*, vol. 55, no. 2, pp. 852–855, 2010.
- [189] M. E. Fajardo, S. Tam, and M. E. DeRose, "Matrix isolation spectroscopy of H₂O, D₂O, and HDO in solid parahydrogen," *J. Mol. Struct.*, vol. 695–696, pp. 111–127, 2004.
- [190] D. Forney, M. E. Jacox, and W. E. Thompson, "The Mid- and Near-Infrared Spectra of Water and Water Dimer Isolated in Solid Neon," *J. Mol. Spectrosc.*, vol. 157, no. 2, pp. 479–493, 1993.
- [191] H. P. Gush, E. J. Allin, H. L. Welsh, and W. F. J. Hare, "The Infrared Fundamental Band of Liquid and Solid Hydrogen," *Can. J. Phys.*, vol. 38, no. 2, pp. 176–193, 1960.
- [192] S. Tam and M. E. Fajardo, "Single and double infrared transitions in rapid-vapor-deposited parahydrogen solids: Application to sample thickness determination and quantitative infrared absorption spectroscopy," *Appl. Spectrosc.*, vol. 55, no. 12, pp. 1634–1644, 2001.
- [193] B. Optics, "Guide for Infrared Spectroscopy Conversion," p. 22, 2009.
- [194] H. Buchenau, E. L. Knuth, J. Northby, J. P. Toennies, and C. Winkler, "Mass spectra and time-of-flight distributions of helium cluster beams," *J. Chem. Phys.*, vol. 92, no. 11, p. 6875, 1990.
- [195] J. A. Northby, "Experimental studies of helium droplets," *J. Chem. Phys.*, vol. 115, no. 22, pp. 10065–10077, 2001.
- [196] J. P. Toennies and A. F. Vilesov, "Superfluid helium droplets: A uniquely cold nanomatrix for molecules and

- molecular complexes," *Angew. Chemie - Int. Ed.*, vol. 43, no. 20, pp. 2622–2648, 2004.
- [197] F. Stienkemeier and K. K. Lehmann, "Spectroscopy and dynamics in helium nanodroplets," *J. Phys. B At. Mol. Opt. Phys.*, vol. 39, no. 8, p. R127, 2006.
- [198] S. Yang and A. M. Ellis, "Helium droplets: a chemistry perspective," *Chem. Soc. Rev.*, vol. 42, pp. 472–484, 2013.
- [199] C. Callegari, K. K. Lehmann, R. Schmied, and G. Scoles, "Helium nanodroplet isolation rovibrational spectroscopy: Methods and recent results," *J. Chem. Phys.*, vol. 115, no. 22, pp. 10090–10110, 2001.
- [200] D. L. Howard, H. G. Kjaergaard, J. Huang, and M. Meuwly, "Infrared and Near-Infrared Spectroscopy of Acetylacetone and Hexafluoroacetylacetone," *J. Phys. Chem. A*, vol. 119, no. 29, pp. 7980–7990, 2015.
- [201] Z. Mielke and L. Sobczyk, "Vibrational Isotope Effects in Hydrogen Bonds," in *Isotope Effects in Chemistry and Biology*, A. Kohen and H. H. Limbach, Eds. Boca Raton: Taylor & Francis, CRC Press, 2005, pp. 281–304.
- [202] N. O. B. Lüttschwager, "Thesis dissertation," Georg-August-Universität Göttingen.
- [203] V. Mohacek-Grosev, K. Furić, and H. Ivanković, "Luminescence and Raman spectra of acetylacetone at low temperatures," *J. Phys. Chem. A*, vol. 111, no. 26, pp. 5820–7, 2007.
- [204] Y. P. Lee, Y. J. Wu, and J. T. Hougen, "Direct spectral evidence of single-axis rotation and ortho-hydrogen-assisted nuclear spin conversion of CH₃ F in solid para-hydrogen," *J. Chem. Phys.*, vol. 129, no. 10, pp. 1–6, 2008.
- [205] S. Coussan, Y. Ferro, A. Trivella, M. Rajzmann, P. Roubin, R. Wieczorek, C. Manca, P. Piecuch, K. Kowalski, M. Włoch, S. A. Kucharski, and M. Musiał, "Experimental and theoretical UV characterizations of acetylacetone and its isomers," *J. Phys. Chem. A*, vol. 110, no. 11, pp. 3920–3926, 2006.
- [206] H. Nakanishi, H. Morita, and S. Nagakura, "Electronic structure and spectra of the keto and enol forms of AA," *Bull. Chem. Soc. Jpn.*, vol. 50, no. 9, pp. 2255–2261, 1977.
- [207] L. Khriachtchev, "Rotational isomers of small molecules in noble-gas solids: From monomers to hydrogen-bonded complexes," *J. Mol. Struct.*, vol. 880, no. 1–3, pp. 14–22, 2008.
- [208] K. Marushkevich, L. Khriachtchev, J. Lundell, a. V. Domanskaya, and M. Räsänen, "Vibrational spectroscopy of trans and cis deuterated formic acid (HCOOD): Anharmonic calculations and experiments in argon and neon matrices," *J. Mol. Spectrosc.*, vol. 259, no. 2, pp. 105–110, 2010.
- [209] M. C. Henry and C. R. Yonker, "FT-IR studies of acetylacetonates in supercritical CO₂ using a capillary cell at pressures up to 3.1 kbar," *Anal. Chem.*, vol. 76, no. 16, pp. 4684–4689, 2004.
- [210] E. M. S. Maçôas, L. Khriachtchev, M. Pettersson, R. Fausto, and M. Räsänen, "Rotational isomerization of small carboxylic acids isolated in argon matrices: tunnelling and quantum yields for the photoinduced processes," *Phys. Chem. Chem. Phys.*, vol. 7, no. 5, pp. 743–749, 2005.
- [211] M. Tsuge, K. Marushkevich, M. Räsänen, and L. Khriachtchev, "Infrared characterization of the HCOOH...CO₂ complexes in solid argon: Stabilization of the higher-energy conformer of formic acid," *J. Phys. Chem. A*, vol. 116, no. 22, pp. 5305–5311, 2012.
- [212] M. Tsuge and L. Khriachtchev, "Tunneling Isomerization of Small Carboxylic Acids and Their Complexes in Solid Matrixes : A Computational Insight," *J. Phys. Chem. A*, vol. 119, pp. 2628–2635, 2014.
- [213] A. Olbert-Majkut, J. Ahokas, M. Pettersson, and J. Lundell, "Visible light-driven chemistry of oxalic acid in solid argon, probed by Raman spectroscopy," *J. Phys. Chem. A*, vol. 117, no. 7, pp. 1492–1502, Feb. 2013.
- [214] A. Domanskaya, K. Marushkevich, L. Khriachtchev, and M. Räsänen, "Spectroscopic study of cis-to-trans tunneling reaction of HCOOD in rare gas matrices," *J. Chem. Phys.*, vol. 130, no. 15, p. 154509, 2009.
- [215] K. A. Manbeck, N. C. Boaz, N. C. Bair, A. M. S. Sanders, and A. L. Marsh, "Substituent effects on keto-enol equilibria using NMR spectroscopy," *J. Chem. Educ.*, vol. 88, no. 10, pp. 1444–1445, 2011.
- [216] A. Nowroozi, H. Roohi, M. S. Sadeghi Ghoogheri, and M. Sheibaninia, "The competition between the intramolecular hydrogen bond and π -electron delocalization in trifluoroacetylacetone-A theoretical study," *Int.*

REFERENCES

- J. Quantum Chem.*, vol. 111, no. 3, pp. 578–585, 2011.
- [217] S. L. Baughcum, R. W. Duerst, W. F. Rowe, Z. Smith, and E. B. Wilson, "Microwave spectroscopic study of malonaldehyde (3-hydroxy-2-propenal). 2. Structure, dipole moment, and tunneling," *Journal of the American Chemical Society*, vol. 103, no. 21, pp. 6296–6303, 1981.
- [218] T. N. Wassermann, D. Luckhaus, S. Coussan, and M. A. Suhm, "Proton tunneling estimates for malonaldehyde vibrations from supersonic jet and matrix quenching experiments.," *Phys. Chem. Chem. Phys.*, vol. 8, no. 20, pp. 2344–2348, 2006.
- [219] N. O. B. Lüttschwager, T. N. Wassermann, S. Coussan, and M. A. Suhm, "Periodic bond breaking and making in the electronic ground state on a sub-picosecond timescale: OH bending spectroscopy of malonaldehyde in the frequency domain at low temperature," *Phys. Chem. Chem. Phys.*, vol. 12, no. 29, p. 8201, 2010.
- [220] N. O. B. Lüttschwager, T. N. Wassermann, S. Coussan, and M. A. Suhm, "Vibrational tuning of the Hydrogen transfer in malonaldehyde – a combined FTIR and Raman jet study," *Mol. Phys.*, vol. 111, no. September, pp. 2211–2227, 2013.
- [221] D. W. Firth, P. F. Barbara, and H. P. Trommsdorff, "Matrix induced localization of proton tunneling in malonaldehyde," *Chem. Phys.*, vol. 136, pp. 349–360, 1989.
- [222] A. Trivella, "PhD. Thesis," Université de Marseille, 2006.
- [223] S. Kondo and Y. Koga, "Infrared absorption intensities of methyl acetylene," *J. Chem. Phys.*, vol. 69, no. 9, p. 4022, 1978.
- [224] C. Gée, M. A. Gaveau, J. M. Mestdagh, M. Osborne, O. Sublemontier, and J. P. Visticot, "Cluster Isolated Chemical Reactions: Evidence for the Formation of Ba2O in Oxidation Reactions of Barium Dimers," *J. Phys. Chem.*, vol. 100, no. 32, pp. 13421–13427, Jan. 1996.
- [225] A. Engdahl and B. Nelander, "The acetylene-water complex. A matrix isolation study," *Chem. Phys. Lett.*, vol. 100, no. 2, pp. 129–132, 1983.
- [226] M. Rezaei, N. Moazzen-Ahmadi, and A. R. W. McKellar, "Infrared spectra of acetylene–water complexes: C2D2–H2O, C2D2–HDO, and C2D2–D2O," *J. Mol. Spectrosc.*, vol. 272, no. 1, pp. 19–22, 2012.
- [227] D. Tzeli, A. Mavridis, and S. S. Xantheas, "A first principles study of the acetylene-water interaction," *J. Chem. Phys.*, vol. 112, no. 14, pp. 6178–6189, 2000.
- [228] K. C. Lopes, R. C. M. U. Araújo, V. H. Rusu, and M. N. Ramos, "An ab initio study of the molecular properties of the propyne-water hydrogen-bonded complex," *J. Mol. Struct.*, vol. 834–836, no. SPEC. ISS., pp. 258–261, 2007.
- [229] S. F. Tayyari, A. Najafi, R. Afzali, S. Emamian, and Y. A. Wang, "Structure and vibrational assignment of the enol form of 1-chloro-1,1-difluoro-pentane-2,4-dione," *J. Mol. Struct.*, vol. 878, no. 1–3, pp. 10–21, 2008.
- [230] M. A. Rios and J. Rodríguez, "An ab initio study of the conformation and intramolecular proton transfer in the enol form of acetylacetone," *J. Mol. Struct. THEOCHEM*, vol. 204, pp. 137–144, Jan. 1990.
- [231] J. J. Dannenberg and R. Rios, "Theoretical Study of the Enolic Forms of Acetylacetone. How Strong Is the Hydrogen Bond?," *J. Phys. Chem.*, vol. 98, no. Copyright (C) 2013 American Chemical Society (ACS). All Rights Reserved., pp. 6714–6718, 1994.
- [232] X.-B. B. Chen, W.-H. H. Fang, and D. L. Phillips, "Theoretical studies of the photochemical dynamics of acetylacetone: Isomerzation, dissociation, and dehydration reactions," *J. Phys. Chem. A*, vol. 110, no. 13, pp. 4434–4441, 2006.
- [233] T. N. Wassermann, "Experimentelle und theoretische Schwingungsspektroskopie an Protonentransfersystemen in der Gasphase," Georg-August-Universität zu Göttingen, 2005.
- [234] S. L. Widicus Weaver, R. a. H. Butler, B. J. Drouin, D. T. Petkie, K. a. Dyl, F. C. De Lucia, and G. a. Blake, "Millimeter-Wave and Vibrational State Assignments for the Rotational Spectrum of Glycolaldehyde," *Astrophys. J. Suppl. Ser.*, vol. 158, no. 2, pp. 188–192, 2005.

- [235] A. McIlroy and D. J. Nesbitt, "High-resolution, slit jet infrared spectroscopy of hydrocarbons: Quantum state specific mode mixing in CH stretch-excited propyne," *J. Chem. Phys.*, vol. 91, no. 1, p. 104, 1989.

Appendix

Theoretical frequency values (and corresponding intensities: **Int**) of double deuterated acetylacetone (AcAcD₂) calculated in the harmonic (**Harm**) and anharmonic (**Anharm**) approximations, with B3LYP functional and 6-311++G(3df,3pd) basis set.

CCC			CTC			CCT		
Harm	Anharm	Int	Harm	Anharm	Int	Harm	Anharm	Int
3142.9	3003.2	9.6	3176.7	3030.2	6.1	3141.2	2996.6	12.1
3137.9	2998.7	9.5	3143.4	3002.3	10.6	3135.9	2995.9	7.6
3090.2	2949.3	4.8	3081.9	2940.2	10.3	3079.2	2940.1	11.0
3088.0	2954.3	6.5	3081.1	2940.5	6.0	3061.5	2922.1	9.7
3038.2	2928.5	7.8	3034.5	2935.5	16.1	3025.8	2946.4	5.4
3034.0	2951.5	2.6	3027.6	2945.7	4.5	3015.2	2966.0	23.5
2373.8	2297.0	1.3	2758.8	2672.1	28.8	2779.7	2680.7	50.7
2200.1	1857.1	259.2	2309.9	2227.6	11.8	2353.6	2276.1	3.1
1663.3	1616.5	262.7	1734.6	1701.4	169.6	1749.4	1713.2	192.5
1560.3	1515.2	374.1	1628.0	1566.1	544.9	1653.1	1614.0	427.4
1477.1	1445.9	6.8	1492.7	1451.0	7.5	1481.6	1451.5	5.6
1476.3	1436.7	86.6	1477.9	1438.8	8.4	1480.8	1453.3	24.1
1472.3	1433.6	9.1	1467.3	1435.8	12.4	1477.5	1440.0	9.8
1464.7	1432.6	38.9	1458.7	1418.0	80.3	1467.5	1436.7	14.9
1418.5	1390.5	27.9	1411.0	1378.4	48.6	1415.4	1401.1	12.2
1403.5	1368.0	11.3	1384.4	1352.1	30.5	1382.4	1349.2	27.0
1384.9	1354.1	53.9	1322.2	1288.8	122.2	1346.0	1313.2	75.1
1303.1	1270.3	125.9	1289.9	1249.6	15.6	1240.5	1197.1	216.3
1120.2	1076.0	52.3	1106.2	1079.6	62.5	1090.1	1064.5	6.8
1062.2	1035.5	1.2	1069.9	1043.6	1.6	1063.2	1037.7	0.6
1047.4	1027.4	34.3	1039.1	1018.4	2.7	1037.9	1015.7	5.0
1047.1	1020.9	6.6	1022.0	999.1	30.0	1008.7	990.4	9.0
1009.4	991.5	9.7	960.3	934.5	145.0	930.4	919.5	28.2
945.7	933.4	24.5	902.0	886.1	14.2	927.0	911.4	14.9
891.9	881.8	16.5	861.8	848.6	20.5	870.5	860.7	58.4
847.7	837.1	0.5	823.3	808.5	0.8	854.5	841.6	16.3
749.7	740.9	38.0	705.3	699.3	19.9	675.0	664.8	8.4
661.0	646.9	0.6	629.9	618.3	37.8	625.9	612.1	13.3
641.5	629.4	14.2	585.1	588.7	0.3	583.8	575.1	5.0
570.5	562.6	16.2	491.0	492.9	2.2	535.9	530.8	0.9
558.4	555.9	0.2	469.0	471.7	11.7	467.1	468.1	15.8
504.7	502.9	10.5	384.3	381.8	3.3	371.4	370.7	4.7
390.6	391.8	2.7	373.1	350.4	48.2	336.9	338.5	0.4
365.7	358.0	7.2	339.7	345.8	1.7	316.6	297.8	42.9
228.1	222.3	3.3	210.7	228.6	3.1	188.6	176.7	2.3
180.5	167.4	0.1	164.9	160.9	0.2	171.4	174.1	3.5
148.4	125.9	0.0	106.2	91.4	1.3	139.0	136.7	2.3
118.2	92.5	1.2	98.7	109.9	0.1	103.8	100.8	0.3
27.9	-92.1	0.1	57.2	59.4	1.5	59.4	56.4	3.8

CTT			TCC			TCT		
Harm	Anharm	Int	Harm	Anharm	Int	Harm	Anharm	Int
3160.0	3019.8	10.8	3145.3	3008.2	7.2	3142.4	3002.5	12.6
3142.9	3001.5	11.4	3134.5	2995.8	5.5	3139.1	2999.5	5.6
3082.1	2942.0	9.0	3084.9	2943.3	6.4	3100.2	2963.2	7.2
3058.6	2920.6	10.4	3063.5	2896.6	7.2	3058.7	2960.2	10.4
3028.5	2946.4	3.6	3036.1	2964.9	11.4	3042.2	2947.4	2.9
3012.0	2925.0	32.3	3005.0	2905.5	8.9	3013.4	2918.1	24.4
2780.2	2684.0	53.4	2767.4	2661.9	51.9	2790.4	2689.2	56.4
2343.8	2264.7	4.3	2359.2	2279.1	0.7	2360.9	2282.4	1.3
1732.2	1694.4	171.4	1716.4	1686.3	232.3	1717.0	1685.3	174.8
1649.0	1603.3	480.5	1648.4	1614.0	397.3	1682.2	1646.3	363.0
1501.6	1448.2	7.4	1495.6	1486.7	10.1	1482.0	1453.6	9.1
1476.8	1439.0	8.2	1486.4	1471.2	11.5	1480.6	1449.9	11.0
1467.0	1434.9	13.0	1479.3	1451.2	35.9	1475.8	1443.0	8.2
1459.7	1427.7	41.3	1473.6	1433.5	7.7	1462.1	1424.2	22.0
1405.5	1373.0	46.1	1421.2	1407.8	33.1	1418.0	1401.2	23.3
1384.9	1352.7	33.7	1377.7	1342.4	67.1	1394.2	1360.3	47.7
1309.9	1275.3	251.1	1353.7	1319.2	101.3	1339.8	1303.9	126.1
1290.2	1258.9	17.0	1234.5	1202.8	67.6	1232.3	1200.4	117.8
1100.7	1078.2	17.7	1116.8	1093.3	41.3	1115.0	1092.3	36.3
1070.4	1043.6	1.2	1065.4	1039.6	0.8	1064.8	1039.9	0.1
1039.1	1017.2	3.2	1038.3	1014.5	4.8	1045.4	1023.9	5.5
1019.5	994.6	35.0	1010.9	990.3	55.2	1012.1	993.2	44.4
954.0	936.6	63.6	989.7	970.3	17.8	982.8	964.6	3.4
916.1	901.1	112.5	939.2	903.8	40.5	921.0	908.7	25.3
850.2	837.7	5.1	832.0	818.6	2.7	861.6	853.1	47.1
819.5	812.8	1.2	768.9	750.5	2.4	777.9	764.0	5.1
720.4	707.1	12.0	702.1	687.1	12.6	705.1	693.7	12.1
630.3	621.8	36.3	590.8	585.2	2.8	582.2	580.5	12.4
584.4	579.9	0.3	585.7	574.7	0.0	571.7	561.8	3.4
493.1	489.0	2.8	534.8	527.7	0.0	531.7	526.7	0.5
457.0	456.9	4.7	525.7	521.4	17.3	518.0	514.2	6.7
393.2	390.5	1.1	381.2	380.2	3.5	374.7	375.3	2.9
341.9	345.4	2.2	368.0	347.7	37.8	340.9	337.6	0.6
299.6	290.6	50.5	339.2	334.0	2.5	278.7	275.2	42.2
212.2	210.6	10.8	245.2	220.6	1.6	197.9	193.5	3.7
167.4	162.4	0.1	211.0	204.1	2.9	193.0	178.8	3.7
133.1	112.9	0.1	178.2	163.5	2.8	176.6	161.7	0.0
101.9	101.1	0.1	135.5	128.6	0.2	142.2	141.0	2.0
62.7	56.9	8.9	71.0	56.8	3.4	66.5	61.4	3.9

APPENDIX

TTC			TTT			Keto		
Harm	Anharm	Int	Harm	Anharm	Int	Harm	Anharm	Int
3205.1	3059.5	2.5	3198.2	3055.0	2.1	3145.4	3000.6	6.2
3139.6	2999.9	10.4	3138.6	2996.9	10.4	3145.2	3000.5	8.8
3097.6	2963.0	7.6	3094.9	2960.3	9.0	3086.7	2948.7	4.5
3086.2	2935.2	5.3	3060.1	2922.2	8.6	3086.5	2948.4	0.1
3042.8	2924.9	11.8	3034.2	2936.7	7.5	3030.6	2923.9	0.7
3036.6	2937.5	5.5	3017.8	2904.1	24.4	3030.5	2926.9	2.3
2761.6	2663.7	32.5	2788.9	2695.5	57.5	2333.5	2255.1	2.1
2307.3	2228.6	8.1	2342.3	2265.3	2.1	2230.7	2199.2	0.8
1706.3	1672.7	194.1	1707.9	1671.1	168.0	1793.8	1753.0	22.0
1655.6	1609.4	417.1	1677.2	1638.0	398.5	1766.2	1735.1	391.2
1494.8	1445.7	1.5	1500.6	1461.8	0.2	1474.5	1434.2	17.7
1486.8	1448.1	46.7	1488.5	1458.1	26.7	1473.6	1429.9	1.0
1473.9	1432.8	13.8	1479.4	1437.7	14.9	1466.5	1427.3	1.3
1468.6	1428.2	2.7	1470.1	1428.7	3.2	1466.2	1424.8	29.5
1420.3	1386.3	23.3	1416.9	1400.9	17.3	1390.0	1354.2	3.4
1388.1	1354.2	31.5	1386.1	1352.2	34.1	1389.8	1356.5	77.2
1326.5	1298.0	169.8	1312.7	1276.9	272.8	1230.0	1189.8	27.9
1272.4	1238.8	16.4	1268.4	1234.7	38.9	1186.8	1150.0	261.5
1135.5	1109.7	137.3	1123.7	1101.1	28.3	1090.8	1082.7	1.8
1063.8	1037.7	1.3	1062.9	1037.4	0.9	1082.1	1057.7	8.7
1044.0	1021.4	2.7	1042.6	1021.8	3.1	1077.8	1054.2	0.2
1022.0	1003.0	4.1	1020.0	1002.6	3.3	1018.2	1000.5	35.3
997.9	980.1	73.7	990.8	976.6	99.2	1008.0	992.8	1.6
910.7	887.2	48.1	919.2	906.0	51.9	942.3	923.1	16.0
824.5	812.7	0.5	815.9	807.2	3.5	797.2	783.0	0.0
772.5	758.1	3.2	764.8	751.6	1.4	795.0	783.4	4.6
731.5	712.8	19.8	747.7	731.7	13.1	758.3	741.1	0.3
584.3	576.5	0.0	579.6	577.1	26.7	740.5	726.1	12.7
578.2	577.3	19.2	577.8	573.4	1.3	627.8	621.5	1.4
540.0	536.9	0.4	525.7	530.8	11.7	520.7	518.8	19.0
483.6	476.8	2.4	486.6	481.7	2.3	492.7	490.6	6.1
395.2	392.9	10.0	402.7	399.1	2.1	479.2	476.2	5.8
369.7	351.9	49.2	321.8	326.5	6.7	358.3	363.7	1.7
321.0	323.8	5.8	260.0	257.3	49.8	318.5	328.3	0.9
230.5	239.1	0.9	236.6	232.9	0.7	162.4	150.8	0.0
226.3	231.0	6.8	227.3	220.2	0.5	161.7	147.4	0.1
173.9	168.1	0.6	180.3	179.5	0.0	142.5	144.1	1.0
82.0	71.5	0.1	110.3	127.6	0.4	56.9	54.4	8.5
49.1	45.6	3.9	48.3	52.6	0.2	46.5	42.7	11.5

Theoretical frequency values (and corresponding intensities: **Int**) of monodeuterated acetylacetone (AcAcCD) calculated in the harmonic (**Harm**) and anharmonic (**Anharm**) approximations, with B3LYP functional and 6-311++G(3df,3pd) basis set.

CCC			CCT			CTC		
Harm	Anharm	Int	Harm	Anharm	Int	Harm	Anharm	Int
3143.0	3004.2	12.2	3817.6	3630.2	79.0	3790.9	3620.1	43.6
3138.0	2997.3	9.5	3141.2	2997.3	12.1	3176.7	3030.1	6.1
3090.2	2947.0	4.8	3135.89	2994.3	7.6	3143.4	3002.4	10.6
3088.0	2958.6	6.5	3079.2	2940.1	11.0	3081.9	2940.3	10.3
3038.3	2941.3	17.7	3061.6	2922.1	9.8	3081.1	2940.6	6.0
3034.3	2934.9	5.3	3025.8	2947.2	5.3	3034.5	2938.9	16.2
3006.5	2351.4	359.2	3015.2	2966.7	22.7	3027.6	2946.2	4.5
2373.8	2296.2	0.8	2353.6	2272.5	3.1	2310.0	2227.2	11.7
1665.7	1608.6	355.3	1751.8	1715.3	174.7	1735.8	1700.0	166.3
1645.8	1603.9	282.7	1667.9	1623.7	415.7	1634.6	1574.7	571.7
1479.6	1446.9	38.0	1481.9	1458.2	14.5	1492.8	1450.9	7.8
1477.1	1447.4	6.7	1481.7	1451.8	5.3	1477.9	1440.3	8.4
1472.3	1429.1	9.6	1477.5	1440.3	9.7	1467.3	1434.5	12.4
1466.8	1427.8	20.6	1467.6	1438.0	15.6	1459.1	1417.2	74.1
1437.4	1397.8	179.8	1415.5	1401.4	10.4	1417.1	1381.7	55.6
1410.9	1365.8	35.2	1382.9	1349.7	37.9	1385.6	1351.7	42.8
1386.2	1358.9	45.3	1347.2	1314.4	59.0	1371.8	1338.7	16.0
1372.5	1289.1	72.6	1300.3	1263.1	287.6	1291.7	1252.9	28.2
1268.4	1232.1	134.8	1195.3	1165.8	71.2	1189.9	1146.0	229.9
1064.6	1041.4	6.0	1063.2	1038.1	0.5	1070.0	1043.4	1.2
1062.3	1039.0	0.7	1057.8	1037.2	3.4	1068.7	1040.1	15.5
1047.1	1024.3	7.9	1038.0	1015.5	4.9	1039.1	1018.3	2.7
1019.1	1001.4	9.6	1008.8	991.3	10.5	1023.0	1006.2	33.9
1006.0	986.2	69.9	927.7	910.9	16.4	948.1	927.1	90.3
947.8	933.0	13.6	875.3	863.1	57.7	864.3	844.9	11.9
911.0	907.3	32.4	855.7	841.4	10.6	827.3	813.3	4.0
848.7	838.9	0.9	675.5	666.5	6.2	707.9	700.1	29.1
671.4	671.0	4.4	631.9	620.9	12.0	631.1	619.5	39.5
647.0	635.6	12.5	591.9	582.3	17.1	588.7	592.0	4.4
579.2	575.5	11.3	537.5	532.4	2.7	499.2	473.8	61.7
558.7	557.2	0.0	483.6	482.9	15.6	489.8	488.2	21.3
512.9	511.1	11.2	415.7	383.7	78.0	480.7	484.7	12.1
391.4	398.9	2.5	372.1	369.7	4.8	396.3	393.4	1.6
373.4	362.9	7.1	340.8	340.6	0.3	340.3	346.5	1.7
231.5	227.7	3.3	191.4	178.6	1.5	212.6	228.0	3.2
180.7	174.3	0.0	173.3	173.6	3.6	166.9	162.6	0.4
148.6	146.3	0.0	139.2	137.2	2.1	106.2	90.4	1.3
118.2	126.9	1.2	103.9	100.2	0.3	98.7	107.1	0.1
27.9	-9.1	0.1	60.4	56.9	3.7	57.6	59.6	1.5

APPENDIX

CTT			TCC			TCT		
Harm	Anharm	Int	Harm	Anharm	Int	Harm	Anharm	Int
3818.6	3635.6	83.7	3803.9	3606.8	86.2	3832.0	3642.2	89.1
3160.0	3020.4	10.4	3145.3	3006.5	7.3	3142.4	2999.2	12.6
3142.9	3001.8	11.5	3134.5	2995.5	5.5	3139.1	3001.3	5.6
3082.1	2942.0	9.0	3084.9	2943.3	6.3	3100.2	2960.4	7.2
3058.6	2920.7	10.5	3063.5	2898.7	7.3	3058.8	2918.3	10.6
3028.5	2947.5	3.6	3036.1	2962.6	11.2	3042.2	2947.7	2.8
3012.0	2924.0	31.0	3004.5	29630	8.9	3013.4	2965.2	23.4
2343.9	2262.6	4.2	2359.2	2275.5	0.7	2360.9	2276.2	1.2
1735.9	1699.4	184.6	1716.9	1682.3	208.7	1718.5	1684.5	114.7
1659.2	1616.9	399.5	1656.8	1618.8	442.5	1695.9	1660.6	405.8
1501.7	1447.3	6.9	1496.3	1491.8	8.7	1482.1	1451.4	8.6
1476.8	1441.7	8.1	1487.6	1472.7	9.2	1481.6	1460.4	6.5
1467.0	1436.1	13.1	1479.5	1451.7	38.4	1475.8	1443.4	8.3
1461.1	1425.1	21.0	1473.7	1433.3	8.1	1462.1	1424.4	21.3
1405.5	1372.6	47.6	1424.4	1402.9	32.2	1418.0	1401.8	22.2
1385.9	1353.1	56.6	1378.6	1344.0	40.2	1394.2	1360.4	47.9
1349.0	1314.0	360.8	1372.1	1337.2	70.5	1340.4	1304.8	140.4
1297.5	1261.5	37.1	1296.2	1264.9	78.7	1288.9	1251.2	148.3
1208.2	1174.9	28.4	1199.9	1170.4	122.9	1216.3	1188.2	90.8
1070.8	1049.0	36.1	1065.5	1040.4	0.6	1064.8	1040.7	0.1
1070.4	1043.6	1.2	1053.5	1029.3	44.6	1061.6	1041.1	7.3
1039.2	1017.1	3.5	1038.3	1014.4	4.5	1045.5	1023.0	5.2
1016.9	996.4	18.8	1002.4	987.2	31.7	1012.2	993.6	45.5
948.5	931.3	127.9	987.7	968.1	9.6	980.8	965.1	9.1
851.7	840.4	9.5	867.2	854.2	15.6	864.9	850.9	40.7
821.1	808.9	3.3	770.7	751.3	2.5	778.5	765.1	4.3
722.5	709.3	7.7	702.1	685.5	12.9	705.2	695.2	12.9
632.3	625.1	38.0	602.2	591.8	2.5	592.9	586.3	9.0
586.9	582.1	2.4	591.3	575.3	2.6	579.4	568.9	11.6
493.8	490.0	5.8	535.1	527.8	0.4	532.1	528.2	1.0
475.7	477.9	4.9	527.0	523.9	17.5	525.8	522.8	8.4
403.9	389.1	93.4	490.6	469.4	68.3	383.4	381.3	2.6
396.6	394.0	1.1	389.2	387.2	3.6	365.3	364.0	80.8
342.5	347.3	2.2	343.3	338.1	1.8	341.6	335.3	0.6
214.4	221.4	10.6	245.4	219.9	1.4	200.1	195.7	3.8
170.2	166.9	0.4	214.0	208.5	2.9	197.0	182.7	1.7
133.1	113.5	0.1	179.0	164.7	2.5	177.1	162.0	0.02
101.9	108.7	0.1	136.3	128.6	0.1	142.5	141.2	1.7
62.7	56.4	8.9	72.1	59.4	3.5	67.2	63.6	4.0

TTC			TTT			Keto		
Harm	Anharm	Int	Harm	Anharm	Int	Harm	Anharm	Int
3794.8	3610.3	49.7	3830.0	3651.6	88.4	3145.4	3000.8	6.3
3205.1	3059.7	2.6	3198.2	3055.5	2.0	3145.3	3000.7	8.7
3139.6	3000.7	10.4	3138.6	2997.0	10.4	3107.9	2970.7	4.3
3097.6	2963.3	7.6	3094.9	2960.3	9.0	3086.7	2948.7	4.3
3086.2	2935.2	5.3	3060.1	2922.2	8.7	3086.5	2948.8	0.2
3042.8	2925.4	11.8	3034.2	2936.7	7.5	3030.6	2923.6	0.7
3036.6	2937.5	5.5	3017.8	2956.4	23.5	3030.4	2923.7	2.2
2307.4	2229.3	7.9	2342.3	2260.0	2.1	2280.4	2211.4	1.3
1706.8	1675.4	173.8	1709.1	1676.5	109.6	1795.9	1772.3	21.5
1662.4	1617.8	460.3	1687.8	1648.9	416.0	1767.3	1730.49	388.9
1494.8	1444.5	1.4	1500.6	1460.5	0.2	1474.5	1430.3	17.7
1487.0	1448.9	45.8	1489.6	1459.8	16.1	1473.9	1432.7	1
1473.9	1431.1	14.2	1479.5	1438.8	14.4	1466.8	1423.7	2
1468.6	1427.8	2.7	1470.2	1428.89	3.5	1466.3	1426.8	27.8
1424.5	1389.7	25.2	1416.9	1401.2	18.7	1390.5	1356.8	5.7
1388.9	1355.4	33.8	1386.9	1352.4	60.5	1390.0	1357.7	76.2
1372.9	1342.0	25.8	1348.1	1309.6	343.9	1326.1	1294.5	19.5
1275.2	1242.2	2.1	1269.8	1236.0	51.2	1261.5	1229.0	23.5
1219.1	1199.3	369	1234.8	1206.4	6.0	1199.3	1164.7	162.6
1072.7	1062.0	4.3	1075.3	1053.6	99.3	1173.2	1144.5	98.3
1063.9	1037.5	1.1	1062.9	1037.9	0.8	1080.5	1056.6	0.8
1044.1	1021.9	2.7	1042.7	1021.7	3.5	1044.6	1020.7	6.1
1022.4	1004.2	3.8	1020.5	1003.0	2.5	1024.9	1006.6	26.6
998.6	984.4	71.2	989.9	977.4	73.0	975.9	956.0	4.3
829.0	816.9	3.1	816.4	806.2	4.7	888.8	874.4	17.1
773.9	759.3	1.9	766.6	751.2	1.2	821.7	809.9	4.5
733.2	714.1	26.6	749.0	733.5	9.7	772.5	756.0	2.5
588.6	578.8	3.9	582.1	576.0	5.4	750.1	734.1	9.2
581.7	581.3	20.9	581.0	578.4	26.5	628.0	618.3	1.5
545.4	541.0	0.8	539.7	540.9	11.0	534.6	533.3	22.7
494.7	466.8	86.6	486.9	482.8	3.6	496.7	494.9	3.3
482.7	474.0	1.2	411.9	406.7	1.6	483.1	479.8	6.6
409.6	405.0	10.1	349.9	351.9	91.9	381.7	388.3	1.7
323.3	326.6	6	322.3	327.5	6.8	320.5	329.9	0.8
230.7	239.5	0.7	237.2	233.2	0.02	162.5	151.2	0.02
228.2	233.2	6.5	229.6	221.9	06	161.7	148.1	0.06
175.3	170.0	0.9	183.1	182.6	0.5	142.9	144.2	1.0
82	72.1	0.1	110.3	128.0	0.4	56.9	54.9	8.5
49.7	48.7	3.9	48.3	52.5	0.2	47.0	44.4	11.7

APPENDIX

Theoretical frequency values (and corresponding intensities: **Int**) of monodeuterated acetylacetonone (AcAcOD) calculated in the harmonic (**Harm**) and anharmonic (**Anharm**) approximations, with B3LYP functional and 6-311++G(3df,3pd) basis set.

CCC			CCT			CTC		
Harm	Anharm	Int	Harm	Anharm	Int	Harm	Anharm	Int
3211.8	3083.3	2.9	3188.7	3063.4	6.5	3176.7	3030.7	6.2
3142.9	3003.3	9.5	3141.2	2996.8	11.7	3143.5	3003.2	12.2
3137.7	2996.2	9.1	3135.5	2992.9	6.8	3129.9	3008.9	16.2
3090.2	2947.6	4.8	3079.2	2940.2	11.0	3081.9	2940.4	10.3
3088.0	2961.8	6.5	3061.5	2922.1	9.7	3081.1	2940.7	6.0
3038.2	2928.5	7.8	3025.8	2946.9	5.3	3034.5	2941.5	16.1
3034.0	2946.4	2.5	3015.2	2878.0	23.4	3027.5	2933.4	4.1
2200.2	1819.3	258.7	2779.7	2680.4	50.7	2758.7	2671.7	28.1
1673.7	1625.5	273.2	1756.7	1720.1	190.7	1742.1	1705.7	168.5
1566.5	1517.1	383.6	1659.9	1621.1	429.1	1634.7	1577.1	556.5
1490.5	1454.2	32.1	1486.8	1464.5	13.1	1492.7	1453.1	7.5
1477.1	1447.7	6.6	1481.7	1451.8	5.7	1477.9	1437.7	8.3
1472.3	1424.4	9.3	1477.5	1440.3	9.8	1469.3	1424.6	11.4
1464.7	1434.0	39.0	1467.8	1437.0	12.7	1460.6	1420.0	89.1
1434.9	1399.8	63.6	1423.3	1392.0	55.4	1434.1	1395.1	39.1
1410.9	1373.4	1.7	1410.7	1380.5	2.7	1393.5	1358.6	19.8
1391.1	1361.4	49.6	1380.9	1348.8	42.9	1382.4	1352.4	15.6
1304.5	1260.7	119.1	1249.0	1212.6	196.7	1296.7	1261.9	50.7
1198.4	1170.2	21.0	1192.4	1167.7	48.4	1187.9	1151.1	137.7
1112.5	1039.3	66.3	1065.7	1039.4	1.6	1071.3	1046.3	0.7
1063.3	1041.8	2.1	1060.3	1039.5	7.0	1056.1	1030.6	3.0
1047.3	1025.0	7.0	1038.7	1017.0	5.8	1039.8	1018.8	3.8
1032.6	1013.7	15.7	995.2	976.8	10.8	1009.3	986.2	40.6
991.3	978.9	33.1	931.5	911.5	29.6	959.3	940.0	131.7
938.5	923.3	3.6	914.1	896.6	2.9	895.7	864.7	33.8
901.9	890.5	20.3	876.8	865.8	82.6	837.4	825.5	2.7
801.8	792.9	7.9	819.5	804.6	20.0	837.3	826.3	32.3
746.6	734.1	50.1	642.5	633.7	0.1	631.0	619.2	38.4
642.7	641.1	14.4	626.8	617.7	13.6	598.7	605.6	0.0
631.7	622.3	6.5	536.2	530.6	1.2	538.5	537.7	0.1
558.7	559.0	1.1	468.5	469.6	15.7	472.9	479.1	12.2
505.3	503.3	10.4	374.4	373.9	5.0	385.2	383.4	3.2
397.1	405.3	2.8	337.5	339.7	0.4	373.6	351.1	49.1
365.8	357.9	7.2	316.8	298.4	42.3	340.8	349.0	1.6
228.8	225.7	3.3	190.0	178.1	2.6	211.5	229.7	3.1
182.3	176.3	0.1	172.1	174.8	3.6	170.0	167.9	0.3
149.4	147.7	0.0	141.0	138.1	2.3	106.3	91.9	1.3
119.4	128.0	1.2	103.8	100.8	0.3	98.7	110.5	0.1
28.0	3.4	0.1	59.9	57.6	3.7	57.5	59.3	1.5

CTT			TCC			TCT		
Harm	Anharm	Int	Harm	Anharm	Int	Harm	Anharm	Int
3175.2	3042.8	4.8	3196.7	3064.5	2.2	3197.6	3064.0	3.1
3160.0	3018.6	10.7	3144.9	3005.2	6.8	3142.4	2999.5	12.7
3142.9	3002.4	11.0	3134.5	2995.6	5.5	3138.8	3001.7	5.3
3082.1	2942.1	9.1	3084.9	2943.3	6.4	3100.2	2960.3	7.2
3058.6	2920.7	10.4	3063.5	2898.1	7.2	3058.7	2918.2	10.4
3028.4	2945.8	3.5	3036.0	2961.4	11.4	3042.2	2948.1	2.9
3011.9	2914.5	32.2	3005.0	2953.9	8.9	3013.4	2885.1	24.3
2780.2	2683.7	53.4	2767.4	2662.4	51.8	2790.4	2689.4	56.4
1741.4	1707.8	175.2	1718.4	1686.4	258.3	1718.6	1689.1	208.6
1654.1	1606.9	485.9	1661.0	1630.2	347.3	1695.6	1658.8	309.2
1501.6	1448.4	7.4	1495.6	1487.4	10.1	1483.2	1465.8	4.1
1476.9	1438.6	8.0	1486.7	1469.0	8.0	1482.0	1449.4	9.3
1468.0	1438.7	9.1	1482.7	1453.6	24.2	1475.8	1444.9	8.2
1460.5	1420.8	49.8	1473.6	1435.3	7.8	1462.2	1423.5	25.0
1421.5	1388.8	102.4	1423.0	1402.0	48.9	1418.6	1400.1	29.4
1389.9	1359.7	45.7	1390.4	1353.7	93.9	1394.6	1360.5	48.1
1381.2	1350.8	12.7	1377.8	1342.9	42.6	1379.5	1342.1	81.3
1293.9	1256.5	40.0	1283.5	1257.7	131.4	1284.2	1255.5	140.0
1177.0	1148.9	157.0	1213.7	1187.6	7.7	1207.3	1175.7	61.2
1071.8	1044.7	0.4	1067.8	1041.7	2.1	1067.3	1042.5	1.1
1055.1	1032.6	60.6	1061.0	1039.9	15.2	1058.9	1040.0	12.7
1040.3	1017.4	4.8	1040.0	1016.3	6.1	1047.7	1026.7	7.2
989.4	969.9	1.9	1002.1	982.5	100.2	1009.2	990.7	42.4
956.9	939.4	64.6	990.3	971.7	19.0	950.9	934.0	6.7
909.3	895.5	77.7	868.5	845.9	7.0	901.5	900.9	65.8
872.3	853.8	24.1	857.1	834.6	17.4	860.4	841.4	20.3
839.4	827.6	8.7	792.8	775.2	3.0	808.7	794.7	13.6
631.5	623.5	37.0	628.3	615.5	1.6	622.5	613.6	0.0
601.0	596.8	0.5	593.4	587.5	3.2	585.8	583.7	13.5
528.2	525.2	2.1	544.7	537.0	0.0	535.1	531.1	1.5
461.5	462.4	5.3	533.1	529.7	18.1	524.4	520.4	6.6
394.2	392.0	1.0	381.2	381.3	3.4	374.8	372.6	2.9
343.3	348.7	2.3	368.3	348.0	37.7	342.1	337.9	0.6
300.4	291.5	49.8	340.4	335.6	2.6	279.0	275.3	41.5
213.1	211.5	10.9	245.2	220.5	1.6	198.6	194.4	3.8
171.6	169.3	0.0	211.8	204.8	3.0	194.5	184.6	4.3
133.2	112.8	0.1	181.1	167.2	2.9	176.6	161.2	0.0
101.9	101.4	0.1	137.1	129.0	0.1	144.2	142.6	2.0
63.1	56.8	9.0	71.2	57.1	3.3	67.0	61.6	3.9

APPENDIX

TTC			TTT			Keto		
Harm	Anharm	Int	Harm	Anharm	Int	Harm	Anharm	Int
3205.1	3060.2	2.6	3198.2	3056.5	2.1	3145.4	3000.8	6.3
3139.6	3001.5	9.9	3174.8	3050.1	2.1	3145.3	3000.7	8.7
3127.3	3001.7	14.4	3138.6	2997.1	10.4	3107.9	2970.7	4.3
3097.6	2963.2	7.6	3094.9	2960.4	9.0	3086.7	2948.7	4.3
3086.2	2935.0	5.3	3060.1	2922.4	8.6	3086.5	2948.8	0.2
3042.7	2925.4	11.7	3034.2	2936.8	7.5	3030.6	2923.6	0.7
3036.6	2937.6	5.6	3017.8	2906.7	24.3	3030.4	2923.7	2.2
2761.6	2664.6	31.9	2788.9	2695.2	57.4	2280.4	2211.4	1.3
1708.8	1677.6	217.4	1709.4	1675.6	193.5	1795.9	1772.3	21.5
1668.2	1628.4	378.5	1689.7	1641.8	364.1	1767.3	1730.5	388.9
1494.8	1448.3	1.5	1500.6	1463.9	0.2	1474.5	1430.3	17.7
1487.9	1450.0	38.4	1489.1	1460.5	23.6	1473.9	1432.7	1.0
1473.9	1432.8	14.0	1479.5	1440.8	15.1	1466.8	1423.7	2.0
1469.1	1428.0	3.0	1470.2	1430.8	4.0	1466.3	1426.8	27.8
1428.1	1393.3	24.6	1421.6	1399.3	26.0	1390.5	1356.8	5.7
1389.8	1356.7	23.3	1387.2	1354.1	25.0	1390.0	1357.7	76.2
1382.1	1351.4	23.5	1371.7	1345.0	77.1	1326.1	1294.5	19.5
1294.1	1264.0	108.7	1290.7	1254.6	78.7	1261.5	1229.0	23.5
1250.8	1221.9	208.9	1230.2	1201.1	229.1	1199.3	1164.7	162.6
1065.4	1041.3	0.3	1064.7	1039.6	0.1	1173.2	1144.5	98.3
1050.0	1026.9	2.6	1047.9	1029.3	45.1	1080.5	1056.6	0.8
1045.9	1023.9	4.9	1045.2	1022.9	6.0	1044.6	1020.7	6.1
1024.8	1005.9	4.6	1022.9	1003.6	0.3	1024.9	1006.6	26.6
960.7	949.1	128.7	932.1	918.5	3.1	975.9	956.0	4.3
878.3	852.0	30.3	910.8	886.7	23.0	888.8	874.4	17.1
867.0	843.9	5.2	890.4	877.2	74.7	821.7	809.9	4.5
789.1	774.2	2.1	781.8	764.5	1.9	772.5	756.0	2.5
588.4	580.3	0.0	585.7	580.6	1.4	750.1	734.1	9.2
582.4	580.0	20.6	584.7	582.5	30.4	628.0	618.3	1.5
545.6	543.5	0.6	531.3	535.1	10.3	534.6	533.3	22.7
532.4	525.2	0.1	524.9	522.6	1.9	496.7	494.9	3.3
395.5	395.1	10.1	403.1	400.5	2.1	483.1	479.8	6.6
370.4	352.9	50.5	322.6	327.7	6.6	381.7	388.3	1.7
321.6	324.7	5.8	260.9	257.8	49.0	320.5	329.9	0.8
230.8	237.2	0.9	236.8	233.6	1.0	162.5	151.2	0.0
227.3	232.5	6.8	228.3	221.9	0.5	161.7	148.1	0.1
178.9	172.9	0.6	184.3	183.6	0.0	142.9	144.2	1.0
82.4	70.9	0.1	110.9	127.9	0.4	56.9	54.9	8.5
49.1	44.3	3.9	48.4	52.5	0.1	47.0	44.4	11.7

Theoretical frequency values (and corresponding intensities: **Int**) of chloroacetylacetone (AcAcCl) calculated in the harmonic (**Harm**) approximation, with M06-2X functional and 6-311++G(3df,3pd) basis set.

CCC		CCT		CTC		CTT		TCC	
Harm	Int								
3187.9	6.7	3883.1	112.4	3785.8	76.2	3899.2	125.6	3903.5	126.8
3183.5	5.0	3207.8	0.5	3186.5	5.5	3186.5	6.4	3180.7	4.6
3138.9	0.3	3185.6	6.6	3181.5	5.7	3157.4	0.1	3173.6	1.6
3137.8	1.4	3139.7	2.2	3155.5	0.3	3150.2	7.5	3142.8	0.8
3076.3	1.5	3111.3	3.7	3137.8	1.8	3139.8	1.5	3112.1	2.2
3073.6	1.3	3073.6	0.4	3087.1	3.0	3074.4	0.1	3079.2	1.7
3060.8	372.0	3055.6	12.7	3072.5	0.2	3067.0	21.0	3040.8	5.6
1727.4	207.3	1824.4	169.2	1799.3	154.8	1800.0	154.4	1808.8	206.7
1652.2	419.0	1694.6	310.2	1641.8	534.5	1674.3	286.2	1668.0	368.3
1498.7	24.4	1495.7	6.0	1481.4	4.7	1490.6	12.1	1508.0	8.5
1480.2	7.0	1480.3	6.1	1479.2	11.9	1477.4	11.1	1506.2	2.1
1475.9	16.2	1479.9	10.8	1473.5	9.8	1468.0	16.3	1489.3	25.9
1465.6	13.9	1470.0	14.6	1468.9	16.3	1461.8	10.8	1480.6	12.4
1434.7	101.5	1420.4	24.0	1420.0	50.9	1420.9	17.8	1424.5	40.6
1407.9	46.2	1396.1	43.0	1399.3	42.8	1399.1	61.4	1384.1	40.1
1393.2	34.3	1360.1	91.1	1387.1	3.6	1361.1	311.7	1382.4	33.6
1366.1	164.6	1294.5	154.6	1321.0	1.4	1318.9	123.7	1282.7	90.9
1302.0	199.8	1229.3	138.3	1258.6	279.6	1234.3	45.6	1216.7	182.0
1081.5	23.0	1061.3	0.5	1059.5	29.2	1067.9	23.2	1063.6	3.3
1058.7	0.0	1052.2	24.8	1059.2	4.0	1052.1	7.8	1058.0	0.9
1049.4	6.1	1042.5	5.5	1051.4	37.3	1047.1	19.9	1041.9	3.1
1046.1	40.3	1026.3	110.2	1041.7	1.5	1037.9	0.1	1028.4	83.4
1011.8	1.8	1001.7	27.1	978.8	22.8	983.9	14.0	966.8	13.5
987.4	84.8	918.3	27.4	925.3	50.7	926.6	106.3	926.4	28.4
933.8	36.5	653.2	24.4	658.8	28.6	662.5	29.0	653.3	6.3
677.5	14.0	646.6	0.3	656.8	50.4	649.4	0.5	649.6	11.7
648.8	0.4	530.1	4.8	599.0	26.0	565.3	30.1	581.0	26.2
554.4	0.7	516.7	9.4	562.6	14.0	562.5	6.1	552.7	4.0
535.8	11.5	466.0	1.5	538.0	36.1	459.0	2.5	481.1	59.3
476.4	3.3	404.5	8.3	451.9	5.6	420.2	88.7	475.6	1.3
449.3	3.6	401.3	90.3	411.4	0.9	408.2	0.7	412.5	2.8
377.6	8.7	380.8	0.8	378.0	1.5	386.9	4.7	357.1	1.9
263.0	0.0	287.4	0.1	271.6	3.1	264.3	0.9	319.5	10.8
248.2	3.8	282.8	3.1	258.8	0.0	258.3	0.8	277.7	0.8
238.4	1.2	222.2	3.7	229.1	2.5	235.1	7.8	265.2	0.1
182.7	0.0	217.1	0.0	199.6	0.0	205.0	0.1	246.3	2.3
167.6	0.1	118.0	1.5	184.9	1.7	189.8	2.9	139.1	0.3
116.6	0.8	85.5	0.3	126.8	0.1	119.5	0.2	94.0	2.7
90.1	3.1	26.5	8.3	46.8	3.8	38.9	7.3	50.0	2.0

APPENDIX

TCT		TTC		TTT		Keto	
Harm	Int	Harm	Int	Harm	Int	Harm	Int
3895.7	124.8	3760.3	86.0	3897.5	115.8	3187.5	3.2
3208.8	0.4	3204.3	1.2	3233.2	1.2	3186.0	2.4
3185.2	5.7	3182.8	3.8	3179.1	4.5	3157.3	3.7
3153.4	2.5	3156.9	3.8	3149.5	4.1	3139.3	0.1
3107.9	4.2	3153.1	2.4	3110.4	5.2	3133.1	0.9
3081.6	1.3	3084.7	3.7	3073.3	3.1	3072.4	0.4
3052.7	13.8	3077.4	1.3	3057.3	14.3	3065.5	0.6
1813.6	184.0	1802.2	195.2	1812.2	190.1	1876.2	71.6
1728.0	243.1	1678.2	416.6	1722.6	222.5	1845.7	275.9
1495.7	7.1	1509.7	14.4	1517.0	4.1	1478.5	11.9
1482.7	9.7	1499.0	12.6	1498.2	13.4	1474.1	9.7
1478.5	2.6	1479.5	3.3	1479.0	0.9	1470.9	10.3
1470.6	15.8	1468.5	14.6	1473.2	17.2	1466.7	18.1
1421.9	56.9	1423.7	40.1	1420.5	17.4	1398.5	35.9
1399.8	31.8	1391.9	19.8	1389.2	29.6	1395.9	47.3
1357.1	96.5	1380.0	29.1	1344.4	424.0	1294.8	24.5
1288.4	63.6	1306.1	11.9	1299.9	29.2	1256.5	29.9
1230.5	131.3	1277.8	312.9	1250.5	15.0	1208.8	118.9
1062.8	0.0	1061.9	12.7	1062.7	5.8	1173.5	70.6
1055.0	57.8	1055.7	8.8	1057.5	7.8	1082.8	1.6
1049.7	4.9	1049.7	8.2	1038.6	12.7	1025.4	1.9
1036.7	80.5	1041.4	2.9	1035.4	13.4	1007.3	16.8
965.0	54.4	975.0	39.4	974.4	76.8	975.6	0.2
937.2	27.7	911.0	35.2	922.5	38.1	893.2	28.3
653.1	1.2	652.5	31.5	651.5	15.3	830.4	7.5
637.8	29.4	639.4	51.0	635.2	17.8	783.2	6.0
568.3	5.7	616.4	24.1	581.9	12.9	629.1	6.5
531.0	4.4	593.8	0.7	569.3	9.9	585.1	29.2
470.5	2.3	545.8	32.6	481.5	5.4	531.2	8.0
409.8	0.3	480.7	4.4	427.3	1.0	480.1	10.8
358.4	1.0	426.9	1.7	377.2	88.4	414.4	0.6
337.9	88.1	337.4	3.7	350.3	3.3	339.4	0.9
293.1	3.8	290.9	0.3	292.9	1.3	236.2	7.0
274.4	0.8	276.8	0.2	268.2	0.2	222.0	1.0
265.7	0.1	258.2	4.0	257.2	1.2	196.6	0.6
244.5	3.8	254.1	1.7	250.6	2.8	169.6	0.2
119.8	2.0	142.2	0.7	130.1	0.8	152.1	1.3
89.0	0.5	108.8	0.6	111.9	1.7	66.2	7.8
47.5	3.0	42.9	3.1	44.4	2.3	56.0	6.9

Theoretical frequency values (and corresponding intensities: **Int**) of deuterated chloroacetylacetone (AcAcCl(D)) calculated in the harmonic (**Harm**) approximation, with M06-2X functional and 6-311++G(3df,3pd) basis set.

CCC		CCT		CTC		CTT		TCC	
Harm	Int								
3187.8	5.1	3207.8	0.5	3186.5	5.5	3186.5	6.4	3180.7	4.6
3183.4	4.0	3185.6	6.6	3181.5	5.7	3157.4	0.1	3173.5	1.4
3138.9	0.3	3139.7	2.2	3155.5	0.3	3150.2	7.9	3142.7	0.8
3137.8	1.4	3111.3	3.7	3137.8	1.8	3139.8	1.5	3112.1	2.1
3076.2	0.5	3073.6	0.4	3087.1	3.0	3074.4	0.1	3079.1	1.7
3073.6	0.0	3055.6	13.6	3072.5	0.3	3067.0	22.5	3041.3	5.1
2242.5	265.0	2827.6	71.7	2753.9	44.4	2839.0	77.7	2839.0	75.4
1725.0	235.4	1823.3	180.0	1798.5	155.4	1797.8	148.2	1808.7	214.6
1562.1	357.5	1678.7	315.2	1632.5	485.2	1661.0	367.9	1661.2	336.0
1498.6	19.0	1495.5	6.5	1479.2	11.9	1489.6	5.5	1506.6	10.2
1480.2	7.0	1479.9	10.9	1479.1	5.3	1477.3	11.1	1504.2	3.5
1475.9	16.2	1478.9	12.3	1473.4	9.8	1467.9	17.5	1487.7	24.1
1464.5	28.7	1470.0	14.5	1468.9	16.2	1461.7	10.1	1480.7	12.4
1432.2	52.1	1420.3	24.1	1416.6	43.3	1420.7	26.4	1420.2	46.5
1407.3	52.7	1395.8	37.7	1398.5	42.5	1398.7	44.4	1382.6	71.2
1392.3	30.7	1358.9	73.8	1353.5	68.4	1349.1	136.0	1365.6	39.8
1308.1	194.0	1246.2	226.8	1308.9	87.1	1301.9	154.3	1241.6	102.3
1156.7	146.1	1097.6	5.6	1102.2	37.6	1091.2	42.2	1116.2	76.2
1056.9	1.8	1061.3	0.5	1058.7	5.1	1056.3	22.0	1057.4	1.4
1049.4	6.2	1042.5	5.5	1051.6	55.7	1052.0	7.2	1041.9	3.4
1048.4	42.1	1028.8	60.4	1041.7	1.3	1037.9	0.1	1032.6	116.1
1024.7	0.1	1002.2	21.5	991.1	82.6	983.9	12.8	999.4	10.8
997.9	7.8	935.9	34.8	976.2	67.2	945.9	34.8	926.8	28.4
925.6	27.2	909.7	69.2	886.4	8.3	914.3	118.4	883.4	2.2
738.6	44.8	646.5	26.9	656.2	50.0	656.1	28.7	653.0	4.6
673.1	15.4	644.5	1.9	650.2	7.5	647.9	1.9	645.2	13.9
631.8	2.0	527.8	1.1	571.8	0.5	558.8	1.2	577.3	23.9
553.0	1.4	505.4	8.8	546.3	14.2	545.6	28.3	547.8	0.0
533.7	10.4	459.5	2.6	450.9	5.5	456.8	1.7	465.3	1.4
465.0	2.5	402.9	8.3	422.7	42.7	406.4	0.5	406.3	3.0
448.1	4.0	377.3	0.8	404.1	1.1	385.0	5.0	385.5	19.9
370.4	9.6	304.2	33.2	375.5	1.5	315.4	42.7	352.5	2.6
261.8	0.0	282.0	3.3	268.9	3.6	259.6	5.0	306.8	16.4
248.2	3.6	278.0	14.0	258.7	0.0	256.9	1.1	273.2	4.0
234.8	1.3	220.1	3.6	228.1	2.3	232.1	7.7	264.5	0.2
182.5	0.0	217.1	0.1	199.7	0.0	205.0	0.1	243.9	2.3
167.0	0.2	117.8	1.5	184.8	1.7	189.8	3.0	139.7	0.3
116.6	0.8	85.5	0.3	123.1	0.1	118.3	0.1	90.6	3.0
89.9	3.0	26.3	8.2	46.7	3.8	38.8	7.3	49.4	1.8

APPENDIX

TCT		TTC		TTT		Keto	
Harm	Int	Harm	Int	Harm	Int	Harm	Int
3208.9	0.4	3204.3	1.2	3233.2	1.2	3187.5	3.1
3185.1	5.6	3182.8	3.8	3179.1	4.5	3186.0	2.5
3153.1	2.5	3156.9	3.8	3149.5	4.1	3139.3	0.1
3107.8	4.2	3153.1	2.4	3110.4	5.3	3133.1	0.7
3081.4	1.3	3084.7	3.9	3073.3	3.1	3072.4	0.4
3052.7	15.1	3077.4	1.3	3057.3	15.2	3065.6	0.6
2836.4	78.4	2735.3	50.0	2838.2	73.0	2323.8	3.4
1813.5	191.0	1802.2	199.6	1812.0	194.3	1874.4	74.1
1713.9	247.5	1668.6	367.4	1710.1	261.1	1845.0	277.9
1495.6	7.6	1509.6	14.6	1516.4	4.4	1478.4	12.2
1480.6	9.7	1498.7	12.2	1497.9	15.5	1473.9	9.3
1477.5	6.1	1479.4	3.1	1478.8	2.0	1470.6	12.0
1468.8	16.0	1467.6	15.7	1473.0	20.2	1466.6	17.0
1421.9	51.6	1420.0	37.7	1420.5	17.7	1397.7	36.3
1399.5	29.2	1391.9	20.1	1389.1	23.4	1395.7	48.2
1353.7	71.7	1347.1	182.1	1330.3	270.4	1241.3	27.9
1235.3	151.0	1301.0	27.3	1284.4	50.0	1197.3	182.8
1109.5	16.9	1111.9	61.0	1098.8	15.3	1083.0	4.1
1062.9	0.0	1059.6	9.5	1059.2	2.7	1072.8	3.3
1049.7	5.1	1052.9	18.2	1049.5	10.8	1049.9	23.0
1035.9	80.7	1041.3	2.8	1036.0	8.5	1002.1	2.3
976.0	7.8	1002.4	97.6	979.7	32.3	962.5	26.4
938.5	5.7	935.7	12.9	922.4	37.1	906.5	10.7
915.8	112.3	893.1	25.0	920.9	87.6	817.7	5.7
652.3	2.3	644.6	10.8	651.1	17.5	771.6	4.6
632.5	34.7	638.2	46.9	628.7	16.8	755.9	5.9
553.5	3.4	585.9	0.4	573.0	5.3	628.8	6.6
528.7	1.4	582.6	1.2	559.1	12.9	582.1	27.5
467.6	2.3	470.1	4.3	478.5	5.0	523.0	6.2
403.2	0.6	432.4	37.4	422.8	1.2	477.9	11.7
356.3	1.1	418.9	7.1	349.9	3.3	413.1	0.6
292.8	0.3	336.6	3.6	297.0	9.2	337.4	0.9
273.8	0.9	289.9	0.3	278.3	30.5	235.4	6.9
255.0	0.2	273.5	0.2	263.9	2.1	220.9	1.1
241.1	3.8	258.0	4.0	255.1	4.4	196.3	0.6
240.0	47.2	253.7	1.9	247.8	6.8	169.5	0.2
119.2	1.9	141.4	0.7	129.7	0.6	151.6	1.3
88.9	0.6	106.8	0.5	111.1	1.6	66.1	7.8
46.3	3.1	42.9	3.1	44.3	2.3	56.0	6.9

Theoretical frequency values (and corresponding intensities: **Int**) of hexafluoroacetylacetone (AcAcF6) calculated in the harmonic (**Harm**) approximation, with M06-2X functional and 6-311++G(3df,3pd) basis set.

CCC		CCT		CTC		CTT		TCC	
Harm	Int								
3456.9	205.6	3849.5	195.8	3856.9	112.5	3847.9	260.9	3865.7	199.3
3269.0	10.7	3252.6	7.8	3193.0	5.7	3222.7	5.4	3244.2	10.5
1807.4	151.1	1876.4	131.7	1879.1	122.3	1872.9	124.2	1850.4	238.6
1691.4	276.2	1759.1	255.7	1716.2	499.6	1740.5	387.0	1735.3	293.1
1501.2	128.0	1474.8	112.3	1483.6	71.5	1453.6	167.1	1492.8	133.6
1417.2	82.0	1394.1	42.8	1404.3	134.4	1405.2	157.1	1403.0	56.0
1345.4	89.0	1334.8	250.8	1331.1	30.9	1331.7	153.4	1340.7	59.5
1310.0	535.7	1287.8	187.9	1280.7	220.3	1286.8	294.3	1315.3	103.3
1279.7	142.9	1282.1	357.3	1270.6	31.4	1280.2	21.2	1280.6	188.4
1271.8	395.5	1272.1	433.9	1263.2	309.2	1268.3	289.5	1252.7	556.0
1247.5	272.3	1210.1	522.0	1241.5	396.0	1245.8	221.4	1241.7	282.7
1222.3	259.4	1209.5	17.7	1206.2	224.2	1210.8	231.2	1197.5	286.9
1146.8	59.6	1150.6	45.0	1189.5	194.0	1170.0	316.6	1168.1	238.8
1119.6	229.6	1081.4	150.5	1079.6	266.3	1073.7	96.9	1071.9	66.2
939.3	11.9	925.4	4.3	905.5	91.3	905.5	123.1	895.2	17.0
848.9	69.5	866.9	43.8	868.1	39.4	889.4	23.5	893.3	43.9
845.0	2.7	835.3	12.5	815.9	4.1	808.7	6.5	793.2	6.8
837.4	25.1	778.3	0.2	767.2	0.1	772.9	5.0	756.7	1.3
769.4	17.6	759.9	7.6	750.4	65.7	751.3	65.4	748.9	13.4
762.8	14.2	725.2	2.3	709.2	0.8	707.3	1.9	734.8	2.6
736.1	12.4	664.3	56.4	645.4	21.3	645.8	7.4	665.2	35.5
671.5	60.9	593.3	20.3	592.3	1.4	591.5	1.1	593.5	0.2
596.5	23.4	577.7	26.8	558.5	17.3	559.0	26.7	565.2	22.6
583.3	13.1	534.7	2.3	532.4	28.9	526.1	9.1	538.8	13.1
534.5	3.4	515.7	0.7	525.2	3.1	516.9	1.2	522.4	0.1
520.6	0.3	444.0	0.2	490.2	64.7	476.0	98.3	471.6	8.3
444.2	0.2	430.3	10.5	449.8	2.0	453.2	2.1	449.6	17.3
437.4	0.5	371.8	81.4	432.1	2.3	432.6	5.0	414.1	27.6
359.7	1.1	336.1	2.1	367.4	4.3	383.8	4.8	364.2	4.7
314.4	4.0	314.4	7.0	323.5	1.5	325.1	5.3	324.1	1.9
312.3	0.0	301.7	12.5	280.7	0.1	281.6	2.0	298.8	7.7
253.9	0.7	232.4	2.1	269.7	5.5	276.7	6.3	269.0	4.4
235.9	1.9	231.1	2.5	242.4	3.1	243.2	0.0	236.3	1.5
217.6	4.1	209.1	3.0	165.0	0.4	166.4	0.2	189.5	3.8
120.9	3.2	108.5	1.1	157.9	2.1	159.0	2.7	139.7	3.4
100.3	1.5	93.3	0.3	114.8	1.1	114.9	0.0	126.8	2.4
90.8	1.2	47.3	2.4	90.8	0.1	95.6	0.0	81.2	2.1
33.6	0.1	31.2	0.0	35.9	0.9	34.9	0.8	42.9	0.6
20.5	0.1	15.9	0.4	18.1	1.0	20.8	0.0	29.8	0.1

APPENDIX

TCT		TTC		TTT		Keto	
Harm	Int	Harm	Int	Harm	Int	Harm	Int
3853.4	211.2	3872.3	107.8	3856.3	188.2	3159.8	3.6
3244.2	8.2	3186.8	4.6	3209.9	7.3	3092.5	3.2
1851.6	220.5	1876.2	197.4	1872.0	206.7	1933.1	2.9
1778.7	178.1	1759.6	228.7	1780.1	146.1	1901.8	352.6
1463.6	178.2	1475.2	109.9	1442.0	215.7	1447.2	14.1
1386.6	86.0	1362.1	37.0	1367.9	15.9	1386.0	52.6
1345.6	16.4	1301.3	189.1	1317.1	193.1	1375.0	64.8
1283.5	389.1	1277.8	399.0	1287.0	335.4	1297.6	55.3
1280.1	7.3	1274.4	108.1	1270.4	220.8	1292.9	320.2
1275.9	473.8	1249.4	77.1	1248.2	164.7	1282.7	109.5
1228.9	287.7	1241.1	99.0	1236.1	186.2	1227.8	262.5
1209.9	255.0	1227.9	404.2	1219.4	177.4	1207.4	130.5
1182.4	271.4	1182.1	53.0	1184.0	304.6	1200.9	189.2
1083.8	54.5	1128.0	427.4	1136.0	115.7	1099.8	218.0
902.1	47.3	872.6	62.1	888.2	90.0	1069.0	86.4
892.3	31.5	830.3	11.4	835.3	7.1	954.2	13.5
798.2	4.1	816.6	4.6	814.1	4.2	837.3	0.4
762.1	0.2	757.3	28.7	759.9	23.0	800.7	1.9
744.3	13.6	700.6	11.6	698.3	11.4	771.0	7.6
724.1	2.1	688.9	14.2	687.0	36.6	691.9	17.3
666.7	28.0	641.1	3.2	649.7	1.1	646.6	20.5
591.9	1.1	597.6	8.8	599.0	9.0	592.0	0.9
566.7	22.1	538.1	3.6	537.1	3.9	561.4	20.4
538.2	3.5	522.4	4.3	518.9	1.6	546.6	11.2
519.7	0.1	508.2	6.6	507.1	3.2	520.7	10.3
462.3	6.9	488.1	19.3	490.2	17.5	506.5	7.9
430.3	9.1	437.7	0.6	439.5	5.0	438.0	5.7
369.4	2.5	411.7	92.1	382.9	0.6	432.5	3.4
342.3	58.6	381.5	2.9	350.2	104.1	360.0	1.7
319.7	11.7	325.7	3.0	328.9	7.8	352.3	0.5
296.4	37.1	274.3	1.7	277.5	1.0	256.6	0.1
258.1	2.8	265.7	4.4	267.3	3.8	240.6	1.3
229.7	2.2	246.5	5.2	248.8	4.2	206.0	12.0
175.3	2.6	226.1	5.8	224.3	7.8	194.7	8.5
125.0	0.1	140.7	0.8	146.4	0.4	107.1	1.1
118.2	0.6	112.4	0.4	116.9	0.5	82.1	1.9
100.4	1.7	84.2	0.3	94.2	0.0	52.3	0.1
35.7	0.4	60.1	0.1	77.3	0.2	29.5	0.3
23.1	0.4	41.9	2.4	43.4	1.6	22.4	0.4

Theoretical frequency values (and corresponding intensities: **Int**) of trifluoroacetylacetone (AcAcF₃(CO)) calculated in the harmonic (**Harm**) approximation, with M06-2X functional and 6-311++G(3df,3pd) basis set.

CCC		CCT		CTC		CTT		TCC	
Harm	Int								
3353.4	234.4	3880.1	118.9	3855.5	76.4	3891.2	131.6	3886.3	165.2
3256.9	1.7	3241.6	2.1	3221.8	5.5	3231.0	2.9	3228.5	0.9
3183.3	4.4	3178.8	2.7	3188.9	5.5	3151.7	9.6	3187.6	3.9
3138.2	0.6	3115.8	2.7	3131.1	1.2	3149.3	0.0	3135.8	1.4
3074.1	0.6	3056.2	7.3	3073.5	4.4	3069.1	12.5	3073.9	2.2
1774.5	175.8	1857.5	159.2	1844.5	147.9	1830.9	145.9	1822.7	292.8
1657.7	598.7	1717.6	537.0	1678.1	731.5	1686.4	535.7	1688.4	538.7
1508.9	37.3	1494.4	4.3	1491.3	9.5	1490.6	6.6	1489.6	6.5
1475.5	8.9	1485.7	8.2	1489.2	37.3	1461.1	12.8	1477.0	8.7
1465.1	129.1	1452.4	71.9	1464.9	32.0	1455.8	120.5	1464.0	109.3
1430.2	15.6	1416.9	5.8	1407.2	81.2	1412.8	1.3	1411.0	24.2
1395.0	22.8	1371.7	42.6	1376.6	134.0	1380.9	254.5	1402.0	59.5
1348.8	255.2	1308.8	259.7	1321.7	10.7	1312.8	96.8	1335.2	31.9
1279.0	177.0	1265.9	316.9	1270.2	212.6	1266.6	230.1	1296.3	306.9
1225.1	169.9	1206.2	17.6	1229.8	118.8	1224.1	117.1	1211.4	185.7
1213.8	263.6	1201.1	261.1	1203.2	261.9	1207.0	259.2	1172.1	260.2
1137.6	177.7	1112.4	161.0	1113.0	224.6	1105.7	124.2	1132.5	105.3
1063.7	3.2	1066.4	2.6	1067.8	1.3	1045.2	5.8	1067.6	3.1
1033.1	6.5	1029.3	6.9	1038.1	39.5	1042.8	35.0	1042.3	25.1
967.5	5.3	941.8	32.8	909.2	108.7	907.3	135.5	960.4	29.2
904.0	77.9	876.3	45.0	876.6	1.4	868.5	15.4	869.4	37.0
889.6	30.4	831.0	37.3	847.3	52.5	860.8	29.0	789.8	7.4
813.7	24.6	782.0	0.4	775.6	0.0	783.5	3.2	754.6	2.0
775.0	14.3	746.2	41.0	749.2	61.2	749.4	61.0	697.0	5.1
749.4	40.6	591.7	3.6	590.8	18.5	592.6	6.1	599.5	5.0
597.7	0.5	586.4	9.3	557.5	14.7	562.4	6.2	594.9	31.0
590.5	8.2	520.8	6.0	527.6	0.9	525.5	10.1	563.8	9.2
528.1	19.0	502.5	24.4	508.3	79.3	510.7	12.2	525.2	3.2
524.4	3.8	443.8	1.9	490.4	6.5	451.5	1.4	482.8	36.2
443.7	1.4	437.3	84.5	452.9	0.9	443.1	92.3	439.0	23.7
394.8	3.9	370.4	4.2	385.1	2.4	387.7	0.0	380.7	4.3
324.6	0.6	322.1	0.6	330.0	1.5	332.3	4.8	336.3	0.6
272.8	0.8	260.9	7.7	266.0	1.2	268.7	2.7	258.4	0.4
251.9	7.0	232.0	2.5	257.7	6.2	249.5	8.1	251.1	5.1
177.7	0.4	187.8	0.0	154.7	3.1	170.7	3.0	180.1	3.7
138.2	0.3	133.0	0.4	143.1	0.5	140.2	0.6	160.4	1.7
134.5	0.7	130.1	1.2	74.0	0.2	122.8	0.0	130.7	0.8
83.2	0.2	52.9	1.3	37.4	0.9	48.5	3.0	82.3	1.3
17.0	1.9	32.9	1.9	23.0	0.7	27.9	0.0	44.7	0.4

APPENDIX

TCT		TTC		TTT		Keto	
Harm	Int	Harm	Int	Harm	Int	Harm	Int
3892.6	131.1	3856.4	70.9	3892.0	129.4	3185.6	2.7
3233.7	1.6	3238.5	1.0	3247.1	2.8	3135.7	0.7
3181.1	2.4	3171.2	5.8	3208.3	2.4	3130.3	1.4
3114.7	2.9	3149.9	2.2	3119.2	3.2	3073.7	2.0
3055.8	7.7	3085.8	1.9	3063.2	11.6	3066.1	1.8
1826.8	270.2	1817.8	282.0	1819.1	305.4	1905.8	118.1
1740.8	375.7	1698.3	507.3	1731.1	360.8	1868.6	215.0
1489.2	1.6	1509.4	15.4	1514.9	8.9	1483.4	14.8
1486.2	8.2	1475.0	15.6	1474.0	9.0	1469.8	13.9
1443.5	109.7	1459.6	13.9	1437.7	108.3	1438.9	27.3
1407.7	21.5	1409.9	19.5	1412.4	20.6	1399.7	35.4
1388.1	87.2	1399.5	11.7	1390.6	80.6	1390.9	17.6
1309.1	169.4	1298.9	284.4	1300.5	13.2	1319.7	263.0
1268.7	278.3	1280.2	194.7	1278.8	443.4	1269.8	190.7
1223.6	252.7	1233.4	35.5	1225.3	214.0	1259.4	27.7
1208.1	53.9	1202.3	232.7	1197.1	229.3	1218.4	218.6
1141.1	178.2	1174.1	334.2	1170.1	114.6	1178.1	37.5
1067.2	2.6	1064.2	7.9	1063.6	5.7	1071.7	63.6
1034.0	10.3	1041.9	31.4	1037.3	4.6	1035.0	45.8
953.9	56.9	910.3	33.6	913.4	55.6	1028.0	41.6
875.8	41.4	881.5	55.5	900.7	50.5	885.9	1.2
795.6	4.9	791.5	8.4	789.9	3.7	827.9	1.2
761.9	0.1	759.8	1.0	764.0	5.7	822.6	0.1
690.6	17.5	691.9	15.4	687.5	28.4	728.2	32.8
592.7	19.6	612.0	2.6	606.0	24.9	625.1	3.1
586.9	2.2	561.5	9.1	551.9	16.9	588.9	1.9
558.3	6.4	545.0	24.5	540.3	10.5	536.2	26.4
531.8	5.6	528.7	10.7	525.8	0.3	513.3	0.9
442.1	2.9	508.4	73.0	454.6	1.7	499.2	6.8
380.7	3.2	451.5	11.8	399.6	6.4	426.8	4.2
370.4	78.9	399.0	6.3	397.2	88.6	375.0	1.1
336.7	0.1	342.9	2.9	342.2	5.8	324.7	1.3
258.5	11.1	268.2	3.9	269.5	0.6	229.5	2.1
221.3	2.5	262.5	3.6	264.3	1.0	208.9	5.5
196.6	0.0	182.2	0.7	183.6	0.9	139.0	0.7
152.4	0.9	162.4	1.7	171.2	1.7	122.1	0.6
137.2	0.8	137.4	0.3	134.9	2.1	63.5	6.0
108.4	0.3	105.1	0.2	90.5	1.6	41.6	2.4
38.7	2.6	38.6	1.3	36.4	0.1	16.2	3.7

Theoretical frequency values (and corresponding intensities: **Int**) of trifluoroacetylacetone (AcAcF₃(OH)) calculated in the harmonic (**Harm**) approximation, with M06-2X functional and 6-311++G(3df,3pd) basis set.

CCC		CCT		CTC		CTT		TCC	
Harm	Int								
3262.4	3.4	3859.2	169.2	3870.1	89.9	3862.4	233.0	3893.1	120.2
3210.9	351.3	3240.4	1.5	3185.2	5.2	3207.6	2.1	3245.0	5.8
3185.9	0.2	3184.1	5.5	3172.0	7.9	3184.9	5.1	3175.2	1.8
3132.1	1.3	3126.4	3.5	3126.5	3.7	3127.2	3.3	3108.7	2.0
3067.7	0.3	3062.6	1.2	3062.6	1.6	3063.3	1.1	3040.0	5.9
1769.0	252.3	1844.2	183.7	1844.2	144.4	1839.4	150.7	1819.6	257.1
1695.8	181.4	1758.7	183.5	1719.1	411.6	1742.2	307.7	1751.4	174.1
1496.4	46.1	1479.8	8.5	1480.6	9.4	1479.5	9.1	1501.3	38.2
1478.1	9.0	1473.8	14.2	1476.8	75.3	1471.5	16.3	1499.9	9.3
1468.7	18.5	1462.4	63.3	1467.3	48.3	1444.9	265.5	1467.6	66.3
1406.1	169.6	1393.3	131.2	1397.5	17.9	1399.5	11.6	1388.0	50.2
1381.1	80.5	1356.4	192.4	1352.1	30.4	1356.2	49.7	1329.6	137.3
1327.7	457.8	1287.5	295.3	1269.8	49.5	1284.3	268.2	1291.8	65.5
1264.0	376.9	1277.7	414.6	1261.7	273.8	1284.2	160.3	1272.4	255.6
1239.3	273.3	1206.9	94.6	1235.5	434.2	1238.5	183.9	1239.8	409.4
1238.5	22.6	1199.6	243.3	1198.6	60.5	1183.0	272.8	1231.7	268.5
1147.7	58.1	1143.4	23.1	1171.7	281.7	1157.1	142.5	1105.3	69.5
1052.0	5.7	1046.2	5.0	1045.5	6.0	1046.4	7.3	1047.0	5.3
1004.9	14.2	996.5	8.9	972.5	69.7	973.1	62.3	1001.8	26.5
938.2	12.4	908.2	12.3	961.6	14.7	955.8	12.7	886.5	24.9
921.2	61.7	859.7	32.0	861.7	26.4	887.6	12.3	880.7	6.9
872.7	6.7	858.7	23.7	810.2	3.1	803.3	5.7	822.7	5.1
833.7	41.3	730.5	5.2	706.7	0.8	704.1	1.7	731.2	0.0
745.2	6.3	728.1	2.8	665.1	41.2	668.8	14.4	729.6	23.7
736.1	13.8	602.9	1.3	598.1	24.4	599.3	41.5	604.6	4.2
607.8	0.0	601.2	0.5	588.3	0.2	590.3	4.5	593.6	2.2
599.4	3.3	559.3	51.6	579.7	12.1	578.0	10.5	542.1	22.2
584.7	49.8	516.4	0.2	528.2	14.8	516.7	2.2	523.3	5.9
524.5	1.4	438.0	7.8	469.2	78.5	445.2	1.1	450.0	1.2
438.2	0.9	344.0	4.4	442.5	0.1	443.9	96.4	430.5	53.9
366.4	4.3	332.9	77.0	372.6	3.7	390.9	6.3	374.3	1.1
308.1	1.1	311.1	5.1	330.6	0.2	334.5	1.3	313.0	3.0
302.0	0.0	288.3	11.2	260.9	1.9	262.6	1.4	310.4	1.2
267.7	2.7	253.4	2.3	238.1	3.9	243.5	7.1	265.9	2.9
154.2	4.2	142.8	0.3	173.5	0.1	173.2	0.8	257.9	16.3
131.5	1.2	140.5	2.3	152.3	0.2	152.2	1.2	162.1	3.3
120.6	0.8	109.4	0.1	139.3	0.0	138.2	0.0	132.7	5.1
96.2	0.9	44.0	8.7	99.2	1.7	102.2	0.6	60.0	0.3
39.4	0.7	19.7	0.0	7.3	0.6	18.8	2.9	40.8	2.7

APPENDIX

TCT		TTC		TTT	
Harm	Int	Harm	Int	Harm	Int
3861.08	176.50	3871.8	95.4	3879.1	215.7
3242.52	4.56	3188.3	1.7	3204.1	3.7
3185.60	5.62	3170.4	6.9	3186.8	2.5
3142.11	1.99	3163.0	1.9	3165.6	1.3
3074.78	0.13	3088.2	0.5	3088.6	0.5
1817.95	250.73	1805.5	215.2	1806.0	223.8
1785.42	98.65	1746.0	226.0	1762.2	154.3
1480.21	10.19	1495.8	7.0	1492.0	8.0
1470.73	63.56	1479.3	12.6	1480.9	21.0
1444.23	95.82	1467.9	94.2	1433.9	182.4
1401.82	46.03	1400.8	37.8	1404.1	59.1
1339.39	41.96	1312.0	43.0	1333.8	121.1
1291.22	218.32	1286.4	355.4	1272.2	182.6
1277.16	182.91	1268.6	24.2	1259.0	63.4
1271.91	443.60	1250.2	210.4	1243.6	254.5
1196.99	280.51	1221.7	261.5	1231.3	386.2
1114.74	11.73	1174.2	334.1	1183.7	125.3
1053.35	6.64	1051.6	8.8	1054.2	10.6
1017.26	31.85	1037.5	8.2	1031.2	0.7
892.99	31.23	886.3	23.8	915.7	14.8
880.32	25.41	879.2	3.2	871.0	16.1
831.52	7.13	794.8	5.1	790.8	3.8
729.20	18.23	704.2	4.2	696.6	2.2
718.88	2.64	655.6	9.5	659.2	7.1
608.22	2.58	618.2	25.7	612.2	43.2
596.55	0.24	585.8	7.4	582.5	3.9
540.12	21.38	540.0	5.2	542.3	4.6
514.98	0.38	520.0	6.7	511.2	2.2
445.44	5.82	468.5	13.1	470.6	11.8
373.18	2.24	446.6	86.4	385.4	4.9
315.54	13.97	378.2	5.5	371.5	27.8
308.60	52.03	353.4	0.3	366.3	69.1
286.03	29.90	263.6	5.2	271.6	0.9
258.99	9.40	256.8	2.8	262.3	2.7
234.41	0.09	220.7	0.1	216.1	0.2
154.48	4.34	174.6	4.4	172.8	4.4
121.79	0.20	156.2	0.2	156.9	0.7
58.70	0.45	73.2	2.1	66.4	3.7
30.2	4.66	15.6	6.4	14.1	2.4

APPENDIX

Theoretical frequency values (and corresponding intensities: **Int**) of chloromalonaldehyde (MaCl) calculated in the harmonic (**Harm**) approximation, with M06-2X functional and 6-311++G(3df,3pd) basis set.

CCC		CCT		CTC		CTT		TCC	
Harm	Int								
3389.3	208.2	3908.9	178.1	3796.2	83.3	3909.5	181.3	3880.5	66.3
3214.8	8.2	3193.2	2.9	3240.1	4.9	3207.4	2.3	3231.9	2.1
3042.9	39.6	2983.8	61.6	2993.7	54.2	2998.3	53.3	2921.0	84.8
1773.4	175.4	1848.7	157.3	1838.0	134.7	1841.0	118.8	1839.2	253.3
1637.3	303.5	1712.2	257.8	1690.6	568.5	1725.7	403.2	1695.6	281.2
1438.2	27.7	1437.7	16.5	1430.6	15.3	1429.5	19.3	1468.8	10.1
1386.4	31.1	1398.6	19.2	1379.0	2.6	1347.3	72.5	1387.3	33.0
1383.4	109.8	1293.5	229.9	1321.7	15.0	1297.1	310.4	1338.2	4.7
1275.9	235.6	1250.7	1.9	1254.3	83.0	1268.4	4.7	1194.9	301.8
1106.2	83.5	1049.7	146.6	1125.8	226.8	1117.4	54.8	1124.9	129.1
1050.5	4.3	1034.9	1.6	1036.6	0.7	1038.5	0.0	1006.1	6.3
1001.5	17.1	948.1	4.7	967.1	13.5	936.5	7.8	976.6	8.5
927.5	44.0	893.6	99.0	780.5	110.6	786.1	74.7	728.4	16.3
865.1	86.9	493.9	2.1	629.2	10.0	630.9	57.9	650.4	28.0
517.2	15.7	455.0	29.3	611.2	93.0	502.1	8.7	512.1	89.4
486.2	6.5	454.7	14.8	457.0	2.9	458.7	0.7	469.1	2.6
381.0	2.1	323.1	79.6	415.3	5.6	372.5	116.9	348.0	3.4
291.3	1.5	291.9	4.2	246.9	7.4	253.1	0.1	257.7	4.8
287.0	3.6	256.7	18.7	245.5	3.5	245.3	4.0	229.0	17.7
240.6	6.7	207.0	2.8	203.1	0.5	191.5	4.7	217.4	7.8
219.3	6.1	119.7	11.2	144.4	10.7	140.3	21.6	156.6	5.6

TCT		TTC		TTT		Keto	
Harm	Int	Harm	Int	Harm	Int	Harm	Int
3922.4	195.7	3784.4	84.1	3910.6	189.2	3135.5	4.2
3204.5	2.8	3227.2	2.5	3193.5	3.9	3009.4	28.1
3020.5	29.1	2962.8	57.1	2952.9	63.8	3002.0	42.7
1835.3	242.3	1841.1	247.9	1846.7	244.4	1892.6	204.5
1736.6	179.4	1715.6	448.3	1750.4	302.0	1866.6	155.5
1444.2	18.3	1439.1	6.1	1441.3	10.0	1419.7	1.8
1375.5	19.8	1381.4	2.5	1362.4	5.1	1400.3	9.4
1301.9	151.3	1325.2	10.0	1298.5	398.9	1280.3	15.7
1213.9	18.5	1249.3	60.6	1243.2	27.8	1217.8	10.4
1124.8	282.5	1182.2	334.5	1178.1	53.4	1109.0	51.5
1028.1	0.8	1023.0	1.5	1020.0	0.3	1068.1	0.6
944.1	8.1	936.3	15.2	901.7	10.2	1018.1	21.9
726.0	60.7	716.5	12.4	710.8	67.3	884.7	6.3
651.0	9.2	660.0	49.1	673.4	21.2	780.0	24.8
469.6	1.8	611.6	88.2	504.9	2.1	619.2	10.8
428.2	1.2	501.5	0.0	500.4	7.7	458.4	9.8
327.5	67.0	438.9	3.5	378.9	113.1	306.3	9.8
247.4	1.2	350.2	12.5	347.1	17.7	287.9	3.3
228.6	64.0	225.9	2.2	215.8	4.5	218.8	18.0
207.0	2.5	207.7	11.1	206.5	1.1	85.5	11.2
162.9	9.8	136.3	5.5	135.8	8.4	70.6	6.8

Synthèse en français

La liaison hydrogène est une interaction stabilisante très importante, qui est présente dans de nombreux systèmes moléculaires, des petits clusters d'eau à la molécule d'ADN. L'étude du cas de la liaison hydrogène intramoléculaire (LHI) est d'un intérêt particulier en raison du rôle important de ce type d'interaction dans les processus de transfert d'hydrogène interne, dans la photodynamique et la conformation structurale. La famille des molécules β -dicarboxyles est un système modèle de LHI unique car il possède relativement peu de degrés de liberté et tous les processus mentionnés précédemment sont clairement présents. L'objectif principal de ce travail est d'étudier le lien entre structure isotopique et électronique des molécules β -dicarboxyles, force de la liaison hydrogène intramoléculaire, sélectivité sur le processus de photoisomérisation et couplage du transfert d'hydrogène avec d'autres mouvements de grande amplitude. Les expériences sont complétées par des calculs de chimie quantique.

Quatre molécules de la famille des β -dicétones (acétylacétone doublement deutérée, 3-chloroacétylacétone, hexafluoroacétylacétone et trifluoroacétylacétone) et une β -dialdéhyde (2-chloromalonaldéhyde) sont étudiées dans des environnements inertes à basse température par spectroscopie électronique et vibrationnelle (FT-IR et Raman). Le néon et le para hydrogène ont été utilisés principalement comme matrices hôtes permettant une analyse spectroscopique claire, à cause de la faible interaction entre ces solides et les molécules piégées à l'intérieur. Les β -dicarboxyles se présentent sous deux formes tautomères: le céto et l'énol, mais ce dernier prédomine en grande partie en phase gazeuse, et par conséquent, dans les échantillons déposés étudiés. Huit différents conformères énoliques peuvent exister, mais celui avec LHI (énol chélaté) est le plus stable. Ces conformères peuvent être divisés en quatre paires dans lesquelles chaque couple partage la même structure squelettique et ne diffère que dans la conformation hydroxyle. Le conformère énolique fermé a toujours été trouvé comme l'espèce la plus stable dans nos expériences, en accord avec les calculs théoriques.

L'influence de l'environnement et de la force de la liaison hydrogène sur des variables spectroscopiques comme la largeur de bande, l'intensité et le déplacement spectral sont discutées. Les résultats expérimentaux permettent de confirmer le classement en terme de LHI déduit des calculs théoriques. Nous avons également trouvé des preuves expérimentales du processus de conversion de spin nucléaire dans la forme énolique fermée de l'acétylacétone doublement deutérée en matrice de para-hydrogène. Ce processus n'a pas été observé dans les autres analogues de l'acétylacétone.

Différents conformères énoliques ouverts ont été produits dans chaque système après excitation par laser UV. Les conformères énoliques ouverts présentent des ordres d'énergie différents pour chaque analogue halogéné en raison de l'existence d'interactions non covalentes spécifiques, comme le révèlent les calculs théoriques effectués avec les logiciels Gaussian 09 et NCI-plot. Néanmoins, dans tous les cas, les conformères produits sont les conformères les plus stables de leurs paires énoliques. Ceci est expliqué par un processus régi par passage tunnel de l'hydrogène hydroxylique, comme observé expérimentalement dans les isotopologues deutérés. A partir des résultats expérimentaux, nous avons proposé un mécanisme général pour expliquer la photo-isomérisation dans ces systèmes.

Par ailleurs, la technique des gouttelettes d'hélium a également été utilisée pour avoir accès à des informations spectroscopiques précieuses (spectres ro-vibrationnels) sur des complexes fortement ou faiblement liés en milieu inerte. Le rôle de l'eau comme espèce donneur ou accepteur de protons dans un complexe peut facilement être modifié par un déséquilibre des forces d'interaction en jeu. Les résultats préliminaires sur le système à liaison hydrogène intermoléculaire propyne-eau dans des gouttelettes d'hélium sont présentés. Les résultats suggèrent que l'eau se comporte comme donneur de protons, contrairement au système acétylène-eau. De plus, la molécule de glycolaldéhyde a été étudiée avec cette technique comme exemple de système LIH.